Winter School on Simulation and Optimization of Extreme Fluids

Modeling, Discretization, Optimization, and Simulation of Fluid-Structure Interaction

Nov 13-14, 2014 at IWR of Heidelberg University

Thomas Wick

Johann Radon Institute for Computational and Applied Mathematics (RICAM)

Linz in Austria

thomas.wick@ricam.oeaw.ac.at

Last update: Monday, November 17, 2014

Foreword

I am very grateful to the organizers of this winter schools; namely Thomas Richter, Boris Vexler, Dominik Meidner, and Rolf Rannacher, for the opportunity to hold this lecture on fluid-structure interaction (FSI) problems at IWR Heidelberg. Still, fluid-structure interaction is one of the most challenging problems that extend into all parts of applied mathematics: modeling and theory, numerical techniques, large-scale high performance computations, sensitivity analysis and optimization. These notes represent a mixture of state-of-the-art research; as well as teaching material of basic techniques that have been well known for a long time now.

Beyond classical fluid-structure modeling; namely coupling incompressible Navier-Stokes equations and three-dimensional elasticity, we make excursions to two related (in the first view: simplified) problems: coupling of Darcy flow with elasticity and coupling flow lubrication approximations to Poisson's problem. Not only does this show the applicability of FSI-techniques in related fields but it does also demonstrate how physics and applications lead to different modeling aspects while possibly neglecting characteristic features of standard FSI.

In order to access, understand, and work with the content of these notes, I suggest as academical requirements classes for numerical methods for ordinary and partial differential equations (ODEs and PDEs). Furthermore, PDE analysis, Sobolev spaces, functional analysis, and concepts in continuum mechanics would be very helpful.

I wish to express my special gratitude to Thomas Richter with whom I have had many discussions on fluid-structure interaction in the last years. Moreover, I have had the pleasure to work and discuss with so many fantastic scientists that contributed indirectly to these notes through joint publications or simply through discussions: they are all listed acknowledgment section.

Before we start let me ask a question and ask for your help: Have you ever written a long text, a thesis or a book? If yes, you remember very well that the first draft(s) have never been your final manuscript and often - in particular after some days - you find again and again errors and spelling mistakes. I promise that I carefully wrote these notes and had more than one look for proof-reading; but since active research is involved, parts of the text are under current development and subject to changes. Please be patient and forgiving with me if you find errors and let me know them such that I can improve future versions of these notes. Thanks a lot!

Thomas Wick[1] [2] [3]

(Linz, Austin, Heidelberg/Warsaw, Siegen)

---

[1] Many thanks to my FSI (**F**rench-**S**ociété-**I**nternational)-ladies for their patience with me.

[2] In addition, I am very grateful to Ulrich Langer for the opportunity to work on these notes during my RICAM-time.

[3] thomas.wick@ricam.oeaw.ac.at

Updates Nov 17, 2014

After lecturing at IWR Heidelberg, I made the following updates motivated by own observations and recommendations by several participants (many, many thanks!!):

- Figure 6;

- More details to illustrate structural damping; e.g., in Figure 10;

- More explanation of variational-monolithic coupling;

- Classification of physics in the fully coupled problems: Problem 5.19 and 5.62

- Many more details in Section 5.6 - almost new section compared to the old version of the script;

- New Section 6.6 with a hopefully simple example how we discretize and linearize.

Thomas Wick
(Nov 17, 2014, Linz)

Contents

1 A Brief Motivation for FSI-Research and Challenges

1.1 Real-world observations, their impact, and principal questions

Fluid-structure interaction (FSI)[4] remains one of the most challenging topics to date, although many publications have appeared with specific emphasize on applications, coupling algorithms, and theory. Classical examples are found in industrial processes, mechanical engineering, aero-elasticity, and biomechanics. Specifically, fluid-structure interactions (FSI) are important to describe flows around elastic structures as for instance in the flutter analysis of airplanes, parachute FSI, or blood flow in the cardiovascular system, possibly with hyperelastic structure models, and heart valve dynamics, see, for example [20, 49–51, 87, 165, 179, 184, 195, 196, 206, 215, 225] (of course, these references are by far not sufficient - if I would list all, we would arrive at > 1000). However, fluid-structure interaction is implicitly contained in many other fields as for example in porous media flow (here fluid-structure interaction is needed on the microscopic level where solid pores interact with the flow; through homogenization, the so-called Biot equations are obtained [35–37, 177]).

Revisiting current research in fluid-structure interaction and closely related fields indicate that nothing else than

<div align="center">

Health and Energy

</div>

constitute the **big picture** of possible applications. Of course both topics are of highest relevance in our human society in order to prepare for future decades and centuries![5]

Let us start with two examples I have been involved in [6]. The first topic is health (specifically the heart) [7]:
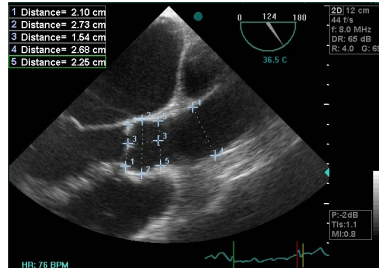
Figure 1: Long axis heart valve. Provided by Jeremi Mizerski [178] (and in collaboration with Rolf Rannacher; my PhD thesis [248]) .

---

[4]In these notes, I use both notations: 'structure' and 'solid'.

[5]Another urgent topic is climate research, for instance.

[6]There are so many interesting topics in FSI research, please forgive me at this point that I only mention two topics I have been working on.

[7]Simulation of the heart is a very difficult topic and I am not claiming that I completely solved this. I rather restricted my focus on the development of adaptive finite element methods.

The second 'big picture' is energy recovery: this includes both conventional resources as well as novel techniques such as geothermal energy[8].
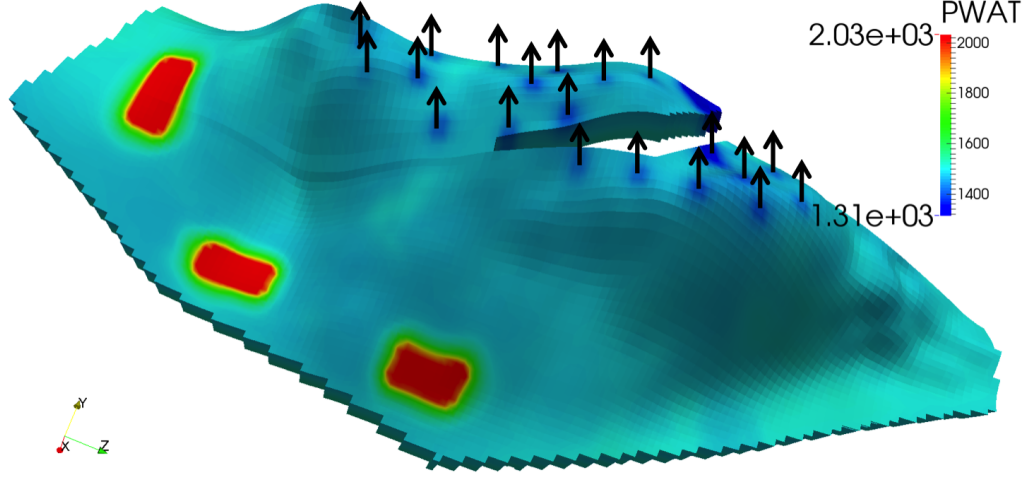
Figure 2: Numerical simulation of reservoir flow with high permeability zones (in red) in subsurface modeling: porous media flow applications in which FSI-techniques are required for microscale modeling as well as coupling of multiphysics equations (in collaboration with Mary F. Wheeler, Andro Mikelić and Gurpreet Singh [176, 257]).

Ideally, the three basic questions we have to ask are:

- What are we doing? (What is the example or application?)

- How are we doing this? (Modeling, solution theory, numerical discretization, simulation, optimization, uncertainty analysis, comparison with experimental data, verification and validation)

- Why are we doing this? (Is there a link to our real-world? What is the impact?)

The circle of research that we are entering is highlighted in Figure 3.

---

[8]Wind energy recovery is also a hot topic in computational fluid-structure interaction.
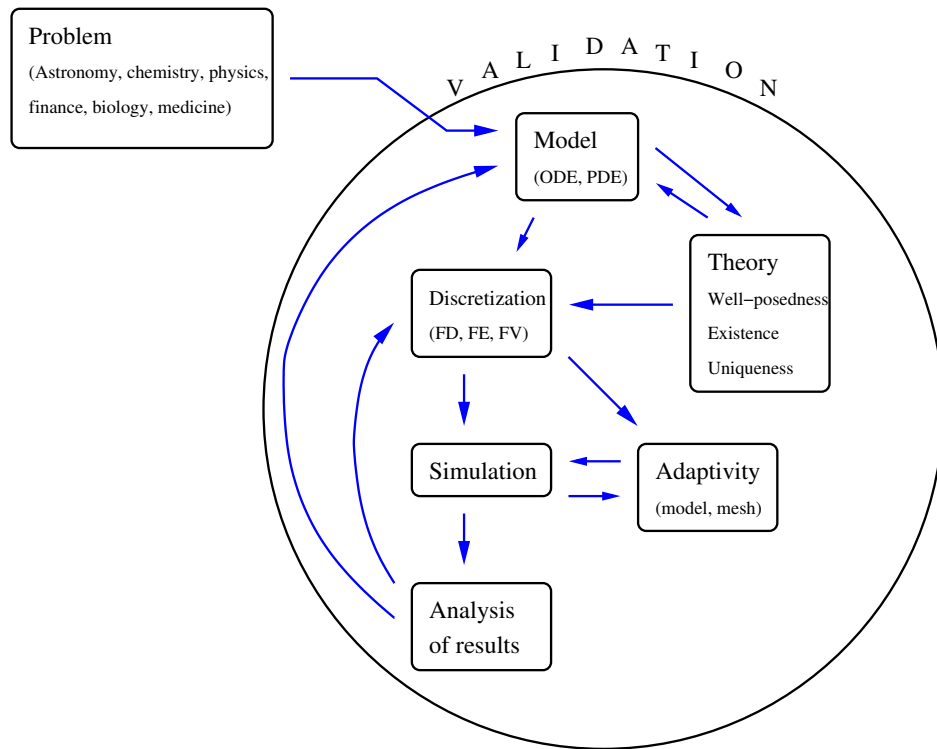
Figure 3: 'The third pillar of science: scientific computing/computational engineering and sciences'. Forward modeling and validation.

Having sufficient trust into our forward model, we can go one step further and think about optimization (i.e., inverse modeling): parameter estimation, optimal control, inverse problems, optimal experimental design.

- Why should we do this?

Well, having the forward model (the state equation) is one part, but often (except in academic examples and simplified situations), material parameters or the geometry are not known, for instance. Or, we are given some output but do not know the state that caused this output (inverse problems). Or, we want to control the PDE into a certain solution/state (optimal control). As sketch of the abstract optimization process is provided in Figure 4.
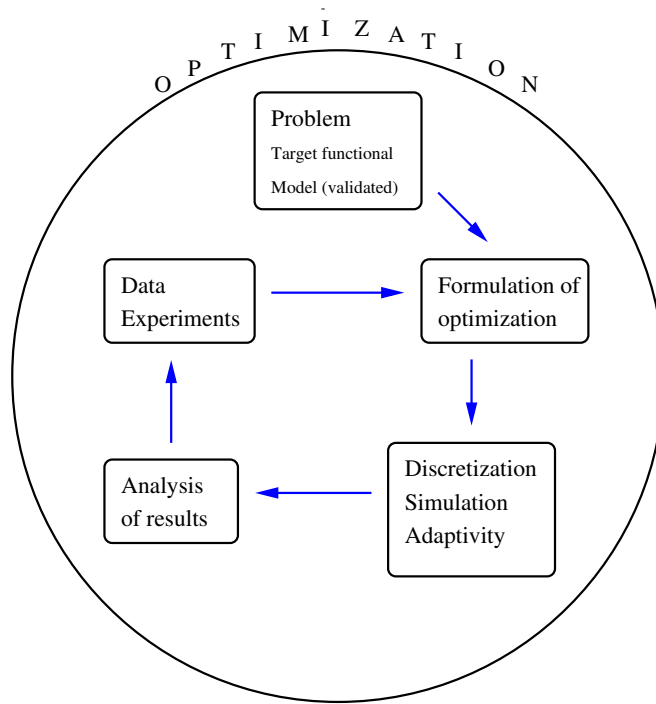
Figure 4: 'The third pillar of science: scientific computing/computational engineering and sciences'. Optimization.

1.2 The challenges of FSI from a mathematical perspective

After identification of possible topics that FSI-research is associated with, it remains the question:

- Why is applied-mathematical FSI difficult?

Challenge 1.1. *The answers are:*

- *Dealing and coupling of different classes of PDEs: elliptic, parabolic, hyperbolic that require different mathematical analysis and numerical tools;*

- *Multidomain character and interface coupling conditions;*

- *Combining different coordinate systems.*

Warning 1.2. *On the first view, it seems natural to consider large problems as I advertised at the beginning. And of course we should go for it. And it seems straightforward to add more and more equations to capture all physics and perform correct modeling. However, this is neither accessible from the theoretical point of view nor due to computational cost. Consider the simple example of an aircraft with Reynolds number 10^8. A direct numerical simulation (DNS) that captures the smallest scales of order $O(Re^{9/4})$, would lead to a mesh with 10^{18} mesh points. This is simply infeasible with todays supercomputers [214] [9]. Consequently, we have to find approximations with less computational cost. This is one reason, why we also touch topics such as Reynold's lubrication approximation and discuss reduced modeling.*

1.3 Conclusions and outline of these notes

I try to provide a mixture of basic techniques and sophisticated algorithms and examples. Not only do we study these aspects in terms of classical fluid-structure interaction but we do also glance on special situations (porous media - fluid-structure modeling on the microscale; and lubrication approximations). The main parts concentrate on continuum mechanics and forward modeling of fluid-structure interaction. Later, we also extend to sensitivity analysis including dual-weighted residual a posteriori error estimation and PDE-based optimization with flow and fluid-structure interaction and provide corresponding algorithmic details. For basics on PDE-based optimization and numerical optimization, we refer reader to [136, 186, 236, 241] and the many references provided therein.

Hopefully, everybody will identify himself with some parts of these notes and learn something new.

---

[9]This note is inspired by a talk given by Johan Jansson at IWH Heidelberg, Nov 2014.

2 Notation and Spaces

Throughout these lecture notes, we use standard function spaces [76, 260]. Let $\Omega \subseteq \mathbb{R}^d, d \in \{2, 3\}$ be a bounded domain with boundary $\partial\Omega$. We generally assume the boundary to be Lipschitzian. A precise definition is given in [1, 119]. The outer unit normal vector to $\partial\Omega$ is denoted by n.

We denote by $\Omega := \Omega(t) \subset \mathbb{R}^d, d = 2, 3$, the domain of the fluid-structure interaction problem. This domain consists of two time-dependent subdomains $\Omega_f(t)$ and $\Omega_s(t)$. The interface between both domain is denoted by $\Gamma_i(t) = \partial\Omega_f(t) \cap \partial\Omega_s(t)$. The initial (or later reference) domains are denoted by $\widehat{\Omega}_f$ and $\widehat{\Omega}_s$, respectively, with the interface $\widehat{\Gamma}_i = \partial\widehat{\Omega}_f \cap \partial\widehat{\Omega}_s$. Furthermore, we denote the outer boundary by $\partial\widehat{\Omega} = \widehat{\Gamma} = \widehat{\Gamma}_D \cup \widehat{\Gamma}_N$ where $\widehat{\Gamma}_D$ and $\widehat{\Gamma}_N$ denote Dirichlet and Neumann boundaries, respectively. For the convenience of the reader and when we expect no confusion, we omit the explicit time-dependence and we use $\Omega := \Omega(t)$ to indicate time-dependent domains. Throughout these notes, we indicate with 'f' and 's' suffixes, fluid and structure related terms, respectively.

Function spaces on fixed domains

We adopt standard notation for the usual Lebesgue and Sobolev spaces [1, 260]. Let $X \subset \mathbb{R}^d, d = 2, 3$ be a time-independent domain. For instance, we later use $X := \widehat{\Omega}_f$ or $X := \widehat{\Omega}_s$. We indicate by $L^p(X), 1 \le p \le \infty$ the standard Lebesgue space that consists of measurable functions u, which are Lebesgue-integrable to the p-th power. The set $L^p(X)$ forms a Banach space with the norm $\|u\|_{L^p(X)}$.

$$\|u\|_{L^p(X)} := \left(\int_X |u(x)|^p \, \mathrm{d}x \right)^{\frac{1}{p}}, \quad 1 \le p < \infty, \tag{1}$$

$$\|u\|_{L^\infty(X)} := \mathrm{ess} \sup |u(x)|. \tag{2}$$

We obtain the Hilbert space $L^2(X)$ for $p = 2$, equipped with the inner product

$$(u, v)_{L^2(X)} := \int_X u(x)v(x) \, \mathrm{d}x.$$

The Sobolev space $W^{m,p}(X), m \in \mathbb{N}, 1 \le p \le \infty$ is the space of functions in $L^p(X)$ that have distributional derivatives of order up to m, which belong to $L^p(X)$. This space is equipped with the norm

$$\|u\|_{W^{m,p}(X)} := \left(\sum_{|\alpha| \le m} \|D^\alpha u\|_{L^p(X)}^p \right)^{\frac{1}{p}}, \quad 1 \le p < \infty,$$

$$\|u\|_{W^{m,\infty}(X)} := \max_{|\alpha| \le m} \|D^\alpha u\|_{L^\infty(X)}.$$

The symbol $\alpha = (\alpha_1, \ldots, \alpha_d) \in \mathbb{N}^d$ denotes a multi-index with the properties

$$|\alpha| := \sum_{j=1}^d \alpha_j, \quad D^\alpha := \frac{\partial^{|\alpha|}}{\partial x_1^{\alpha_1} \cdots \partial x_d^{\alpha_d}}.$$

For $p = 2, H^m(X) := W^{m,2}(X)$ is a Hilbert space equipped with the norm with the inner product

$$(u, v)_{H^m(X)} := \sum_{|\alpha| \leq m} (D^\alpha u, D^\alpha v)_{L^2(X)},$$

and the norm $|| \cdot ||_{H^m(X)}$ [260]. semi-norms

$$|u|_{W^{m,p}(X)} := \left(\sum_{|\alpha|=m} \|D^\alpha u\|_{L^p(X)}^p \right)^{\frac{1}{p}}, \quad 1 \leq p < \infty,$$

$$|u|_{W^{m,\infty}(X)} := \max_{|\alpha|=m} \|D^\alpha u\|_{L^\infty(X)}.$$

Finally, we indicate the subspace $W^{m,p}(X)$ of functions with zero trace on ∂X by $W_0^{m,p}(X)$. Specifically, we define $H_0^1(X) = \{u \in H^1(X) : u = 0 \text{ on } \Gamma_D \subset \partial X\}$. We use frequently the short notation

$$\hat{V}_X := H^1(X), \quad \hat{V}_X^0 := H_0^1(X),$$

and

$$\hat{L}_X := L^2(X), \quad \hat{L}_X^0 := L^2(X)/\mathbb{R}.$$

Specifically, we introduce the trial and the test space of the velocity variables in the fluid domain,

$$\hat{V}_{f,\hat{v}}^0 := \{\hat{v}_f \in H_0^1(\widehat{\Omega}_f) : \hat{v}_f = \hat{v}_s \text{ on } \widehat{\Gamma}_i\}.$$

Moreover, we introduce the trial and the test spaces for the artificial displacement (for mesh moving using ALE[10]) in the fluid domain,

$$\hat{V}_{f,\hat{u}}^0 := \{\hat{u}_f \in H_0^1(\widehat{\Omega}_f) : \hat{u}_f = \hat{u}_s \text{ on } \widehat{\Gamma}_i\},$$

$$\hat{V}_{f,\hat{u},\widehat{\Gamma}_i}^0 := \{\hat{\psi}_f \in H_0^1(\widehat{\Omega}_f) : \hat{\psi}_f = \hat{\psi}_s \text{ on } \widehat{\Gamma}_i \subset \partial X\}.$$

The dual space of $H_0^m(X)$ is denoted by $H^{-m}(X)$. We indicate the duality pairing between $H^{-m}(X)$ and $H_0^m(X)$ by

$$\langle f, u \rangle, \quad f \in H^{-m}(X), \quad u \in H_0^m(X).$$

The dual space is a Banach space with the norm

$$\|f\|_{H^{-m}(X)} := \sup_{\varphi \in H_0^m(X)} \frac{\langle f, \varphi \rangle}{|\varphi|_{H^m(X)}}.$$

For the definition of space-time functions, let $I := (0, T)$ with $0 < T < \infty$ a bounded time interval. Let,

$$v(x, t), \quad \text{with } (x, t) \in X \times I$$

---

[10]Definition later.

13

be such a function. For any Banach space X and $1 \leq p \leq \infty$, the set $L^p(I, X)$ denotes the space of L^p-integrable functions v from I into X. This is a Banach space with the norm

$$\|v\|_{L^p(I,X)} := \left(\int_I \|v(t)\|_X^p \, \mathrm{d}t \right)^{\frac{1}{p}}, \quad 1 \leq p < \infty,$$

$$\|v\|_{L^\infty(I,X)} := \operatorname{ess\,sup}_{t \in I} \|v(t)\|_X.$$

Moreover, we also need the space

$$H^1(I, X) = \left\{ v \in L^2(I, X) \mid \partial_t v \in L^2(I, X) \right\}.$$

Detailed derivation of these spaces by means of the Bochner integral can be found in [66, 260].

Let γ be an open regular, i.e., Lipschitz continuous, and measurable subset of ∂X. We denote with $H^{1/2}(\gamma)$ the space of functions defined on γ that are traces of functions in $H^1(X)$ [110]. Furthermore, we recall the Korn [56]

$$\|\nabla u\|^2 \leq C_K(X) \|D(u)\|^2 \quad \forall u \in H^1(X)^d$$

and the Poincaré inequality [110]

$$\|u\|_{L^2(X)}^2 \leq C_P(X) \|\nabla u\|_{L^2(X)}^2 \quad \forall u \in H_0^1(X)^d,$$

with a positive constant $C_P(X)$ depending on the domain X. We also remind the trace inequality [260]

$$\|u\|_{L^2(\partial X)} \leq C_T(X) \|u\|_{H^1(X)} \quad \forall u \in H^1(X)^d,$$

with a positive constant $C_T(X)$ depending on the domain X. For Korn's inequality [43, 56], let $\hat{u}_s \in H^1(\widehat{\Omega}_s)$ and $\hat{\epsilon} = \frac{1}{2}(\widehat{\nabla}\hat{u}_s + \widehat{\nabla}\hat{u}_s^T) \in L^2(\widehat{\Omega}_s)$. Then,

$$\|\hat{u}_s\|_{H^1(\widehat{\Omega}_s)} \leq C_K \left(|\hat{u}_s|_{L^2(\widehat{\Omega}_s)}^2 + |\hat{\epsilon}|_{L^2(\widehat{\Omega}_s)}^2 \right)^{1/2} \quad \forall \hat{u}_s \in H^1(\widehat{\Omega}_s),$$

and some constant C_K.

Function spaces on moving domains

For the stability analysis of our equations, it is convenient to work in time-dependent domains. Thus, we introduce (on a moving domain Ω):

$$V := \{ v : \Omega \times I \to \mathbb{R}^d : v \circ \hat{\mathcal{A}} = \hat{v}, \ \hat{v} \in [H^1(\widehat{\Omega})]^d \},$$

$$L := \{ p : \Omega \times I \to \mathbb{R} : p \circ \hat{\mathcal{A}} = \hat{p}, \ \hat{p} \in [L^2(\widehat{\Omega})] \},$$

where $\hat{\mathcal{A}} : \widehat{\Omega} \to \Omega$ denotes the ALE transformation that is explained below. The admissibility of the spaces is given by the relations

$$V \subseteq [H^1(\Omega)]^d, \quad \text{and} \quad L \subseteq [L^2(\Omega)].$$

This relation was proven by Formaggia and Nobile [85] and is recalled in Section 5.3.3. A deeper discussion of fluid-structure interaction in moving domains can be found in Formaggia et al. [87] (chapter 3) and the many references cited therein.

Convention for vector-valued functions

For the corresponding spaces of the d-dimensional vector-valued functions, we bear the notation $L^p(X)^d$, $H^1(X)^d$, etc. in mind, equipped with the usual product norm. The scalar products and corresponding norms are defined in an analogous way as those for scalar functions. We expect that the reader is familiar with the Navier-Stokes equations and structural mechanics in d-dimensions. Consequently, we do not differentiate between one-dimensional and d-dimensional spaces and the corresponding solution variables.

Notational conventions

For the reader's convenience, we often use

$$(\cdot, \cdot)_X := (\cdot, \cdot)_{L^2(X)} \quad \text{and} \quad || \cdot ||_X := || \cdot ||_{L^2(X)},$$

where $X = \Omega_f, \Omega_s$ or the corresponding spaces in the fixed reference domains $\widehat{X} = \widehat{\Omega}_f, \widehat{\Omega}_s$. Furthermore, in time-dependent spaces in which we need explicitly the dependence on time, we use

$$(\cdot, \cdot)_{X^n} := (\cdot, \cdot)_{L^2(X^n)} \quad \text{and} \quad || \cdot ||_{X^n} := || \cdot ||_{L^2(X^n)}.$$

In other cases, we denote explicitly the used scalar product and the induced norm, for instance,

$$(\cdot, \cdot)_{H^1(X^n)} \quad \text{and} \quad || \cdot ||_{H^1(X^n)}.$$

Gauss' divergence theorem, green's theorem, integration by parts

Proposition 2.1 (Gauss' divergence theorem - special version). *Let $\Omega \subset \mathbb{R}^n, n = 1, 2, 3$ be a cuboid and $\mathbf{A} = (A_1, A_2, A_3)$ a continuously differentiable vector field in a neighborhood of $\overline{\Omega}$. Then,*

$$\int_\Omega div\mathbf{A} \, dx = \int_{\partial\Omega} \mathbf{A} \cdot \mathbf{n} \, ds. \tag{3}$$

The outer normal of $\partial\Omega$ is given by n.

Proposition 2.2 (Green's theorem). *Let $u \in C^2(\overline{\Omega})$ and $v \in C^1(\overline{\Omega})$. Then,*

$$\int_\Omega v\Delta u \, dx = -\int_\Omega \nabla v \cdot \nabla u + \int_{\partial\Omega} v\partial_n u \, ds. \tag{4}$$

Proposition 2.3 (Partial integration). *Let $\sigma, u, v \in C^2(\overline{\Omega})$. Then,*

$$\int_\Omega v\, div(\sigma\, \boldsymbol{grad}u) \, dx = -\int_\Omega \sigma\nabla v \cdot \nabla u \, dx + \int_{\partial\Omega} v\sigma\partial_n u \, ds.$$

15

More notation

We use standard notation from functional analysis and finite elements theory. The colon operator denotes a scalar product between two matrices (tensors):

$$\sigma : e$$

means in 2d:

$$\begin{pmatrix} \sigma_1 & \sigma_2 \\ \sigma_3 & \sigma_4 \end{pmatrix} : \begin{pmatrix} e_1 & e_2 \\ e_3 & e_4 \end{pmatrix} = \sigma_1 e_1 + \sigma_2 e_2 + \sigma_3 e_3 + \sigma_4 e_4.$$

The 'dot' operator means a scalar product between two vectors:

$$u \cdot v = \begin{pmatrix} u_1 \\ u_2 \end{pmatrix} \cdot \begin{pmatrix} v_1 \\ v_2 \end{pmatrix} = u_1 v_1 + u_2 v_2.$$

When the multiplication is between two scalar-valued functions $u = u_1$ and $v = v_1$ then, no punctutation operator is used: $uv = u_1 v_1$. The gradient and divergence operators are used according to the 'nabla'-operator notation:

The gradient of a single-valued function $v := v(x, y)$ reads:

$$\nabla v = \begin{pmatrix} \partial_x v \\ \partial_y v \end{pmatrix}.$$

The divergence does only makes sense for vector-valued functions $(v_1(x, y), v_2(x, y)$:

$$\operatorname{div} v := \nabla \cdot v := \nabla \cdot \begin{pmatrix} v_1 \\ v_2 \end{pmatrix} = \partial_x v_1 + \partial_y v_2.$$

3 Partial Differential Equations

Let us start with some definitions:

Definition 3.1 (PDE [76]). *A partial differential equation (PDE) is an equation involving an unknown function with at least two variables and certain of its partial derivatives.* ⋄

Definition 3.2 (Coupled system of PDEs). *A coupled system of PDEs is a collection of at least two PDEs that interact through parameters, right-hand side forces or interface terms.* ⋄

Unfortunately[11], there is no general theory for studying PDEs and consequently, there is no common framework to approximate and compute these PDEs on a computer.

Apart from important PDE-analysis questions (which are discussed in standard textbooks such as [76, 260]) regarding to well-posedness, strong and weak solutions and their regularity, the **principal difficulty in fluid-structure interaction** is that we intend to couple three (perhaps the most important) classes of PDEs together:

- Second-order and fourth-order elliptic equations: the mesh motion equation (using ALE-FSI);

- Second-order parabolic equations: Navier-Stokes fluid flow (if we assume moderate Reynolds numbers);

- Second-order hyperbolic equations: elasto-dynamic solid equation.

Fourth-order problems in this respect seem a bit fancy; however they are indeed important in solid and fluid mechanics:

Remark 3.3 (Fourth-order equations in solid mechanics). *Fourth-order equations are well known in solid mechanics since they include bending moments, e.g., Kirchhoff plates [43].*

Remark 3.4 (Fourth-order problems in fluid mechanics). *To derive Galerkin FEM methods for fluid problems, sometimes the derivation is made via the so-called streamline formulation. Here the intermediate step includes an explicit respresentation of the vorticity [200].*

Remark 3.5 (Homework). *Please recall and make yourself familiar about the characteristics of each of these classes (e.g., existence and uniqueness, maximum principle, regularity).* ⋄

---

[11]Maybe *fortunately* because otherwise there would be nothing else remaining to do.

4 Basic Principles of Continuum Mechanics

Continuum mechanics is a key tool to describe physical phenomena of a macroscopic system without taking into account knowledge on detailed compositions of internal structures. Many classical important fields are covered by these concepts such as hydrodynamics and fluid mechanics, solid mechanics, or heat phenomena. Of course there are limitations when we consider phenomena on micro- or nanoscales in which other models such a particle representations are more appropriate to be used.

Befor we begin, one important remark: continuum mechanics is obvisously linked to physics and one might think that the mathematical impact is rather limited. This is **not** the case for fluid-structure modeling! We encounter most of the presented concepts again in Section 5. It is worth to careful study the present section.

4.1 Kinematics; including Eulerian and Lagrangian modeling

In kinematics, we study the motion and deformation of bodies. All phenomena that we consider are described in an open subset of the three-dimensional space.

To study kinematics we introduce two different coordinate systems: Lagrangian coordinates $\hat{x}$ (also called reference frame or material coordinates) and Eulerian coordinates x (the current domain or spatial domain). In the Lagrangian coordinate system, a specific material point and its deformation (i.e., its evolution in time) are observed (see in Figure 4.1 the bold black line). In contrast, using Eulerian coordinates, we observe a fixed point in space and observe what is happening at this spatial point while time is evolving. It might be occupied by different materials while time advances (imagine a river; here you do not identify the single water particle but the general flow pattern). To make it more clear: please think of Heidelberg's old town Hauptstrasse when there is Christmas market or any other day in the year. Imagine you observe people walking there: do you follow a specific person (that would be Lagrangian modeling) or do you look at the general flow of people (Eulerian point of view).

Remark 4.1. *From Figure 4.1 we already identify the principle difficulty in formulating a common coordinate system when the underlying physics are described in Lagrangian **and** Eulerian coordinates. Shall we 'move' the Eulerian system according to $h(x)$ or shall we find any other presentation of $h(x)$ that fits with an Eulerian description. One powerful possibility that we consider in detail in Section 5.3 is the arbitrary Lagrangian-Eulerian (ALE) framework in which the Eulerian system fits with $h(x)$ and is moved.* ⋄
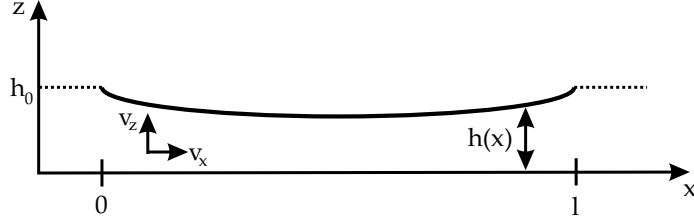
Figure 5: The membrane (bold black line) with deflection $h(x)$ is computed in Lagrangian coordinates; whereas a possible fluid represented by v_x and v_z components between in $[0, l] \times [0, h(x)]$ is considered in Eulerian coordinates. This figure already demonstrates the principle difficulty when coupling Lagrangian and Eulerian coordinates since both systems interacts with each other.

Furthermore, we need a so-called *reference* configuration $\widehat{\Omega} \subset \mathbb{R}^d$ (or undeformed configuration), which is open and connected. Depending on the application there are different possibilities of reference configurations; in particular when working with stress-free or pre-stressed configurations [139] (imagine a book that is just placed on a table or a hot sausage that you slice in order to peel off the skin).

The time-evolution of a material point $\hat{x} \in \widehat{\Omega}$ is described by the mapping:

$$t \mapsto x(t, \hat{x}).$$

For the following, let us introduce the following notation to describe (physical) variables:

- Lagrangian coordinates: $\hat{f}(t, \hat{x})$.

- Eulerian coordinates: $f(t, x)$.

The deformation is defined as

Definition 4.2 (Deformation field). *A deformation of $\widehat{\Omega}$ is a smooth one-to-one mapping*

$$\widehat{T} : \widehat{\Omega} \to \Omega \quad \text{with } (t, \hat{x}) \mapsto (t, x) = (t, \widehat{T}(t, \hat{x})).$$

This mapping associates each point $\hat{x} \in \widehat{\Omega}$ (of a reference domain) to a new position $x \in \Omega$ (of the physical domain). $\diamond$

The displacement field is defined as

Definition 4.3 (Material/Lagrangian description of the displacement field).

$$\hat{u} : (t, \hat{x}) \to \hat{u}(t, \hat{x}) = x(t, \hat{x}) - \hat{x}$$

and it relates a particle's position in the reference configuration $\hat{x}$ to its corresponding position in the current configuration x at time t. $\diamond$

In the spatial description, we have

Definition 4.4 (Spatial/Eulerian description of the displacement field)**.**

$$u(t, x) = x - \hat{x}(x, t).$$

This is formulated in terms of the current displacement, which results from its original position $\hat{x}$ plus the displacement for that position. $\diamond$

It holds

Definition 4.5 (Identification of function values)**.**

$$f(t, x(t, \hat{x})) = \hat{f}(t, \hat{x}).$$

$\diamond$

With the help of the chain rule, we then obtain

Definition 4.6 (Total/Material derivative)**.**

$$D_t f(t, x) = \partial_t f(t, x) + \nabla f(t, x) \cdot v(t, x).$$

$\diamond$

The material derivative describes the change of an Eulerian variable f at a fixed material point $\hat{x}$ that is at time t at point x and travels with the velocity $v(t, x)$.

4.1.1 Deformation gradient $\widehat{F}$ and Jacobian of the deformation $\hat{J}$

In this section, we introduce two key quantities that are required to transform and formulate equations in different coordinate systems. Specifically, we introduce concepts to study the changes of size and shape of a body that is moved from the reference configuration $\widehat{\Omega}$ to the current domain Ω.

For simplicity, let a body occupies $\widehat{\Omega}$ at time $t = 0$. It is described by its position vector $\hat{x} = (\hat{x}_1, \hat{x}_2, \hat{x}_3)$ in a Cartesian coordinate system with the orthonormal basis $(\hat{e}_1, \hat{e}_2, \hat{e}_3)$. At time t the body has evolved (and possibly changed its size and shape) and occupies the current domain Ω. Here, the position vector is $x_i(t, \hat{x}_j)$. Consequently:

$$\hat{x} = \hat{x}_i \hat{e}_i, \quad x = x_i(t, \hat{x}_j) \hat{e}_i$$

(using Einstein's sum convention).

In order to define the deformation gradient, let us consider an infinitesimal material vector $d\hat{x}$ in $\widehat{\Omega}$ that displaces the material particle at $\hat{x}$ such that the new position is $\hat{x} + d\hat{x}$. In the current domain, the previous operation yields $x + dx$.

- The key purpose of the deformation gradient $\widehat{F}$ is to link dx and $d\hat{x}$.

$\widehat{F}$ is a key principle in continuum mechanics and a primary measure of deformation with nine components for all times. It transports any material vector $d\hat{x}$ to dx onto the current (deformed) configuration.

Definition 4.7 (Deformation gradient $\widehat{F}$)**.**

$$dx = \widehat{F} \cdot d\hat{x},$$

with $\widehat{F} = \widehat{\nabla}x$, i.e, $\widehat{F}_{ij} = \frac{\partial x_i}{\partial \hat{x}_j}$. $\diamond$

Its inverse and transpose are defined correspondingly:

$$d\hat{x} = \widehat{F}^{-1} \cdot dx, \quad dx = d\hat{x} \cdot \widehat{F}^T.$$
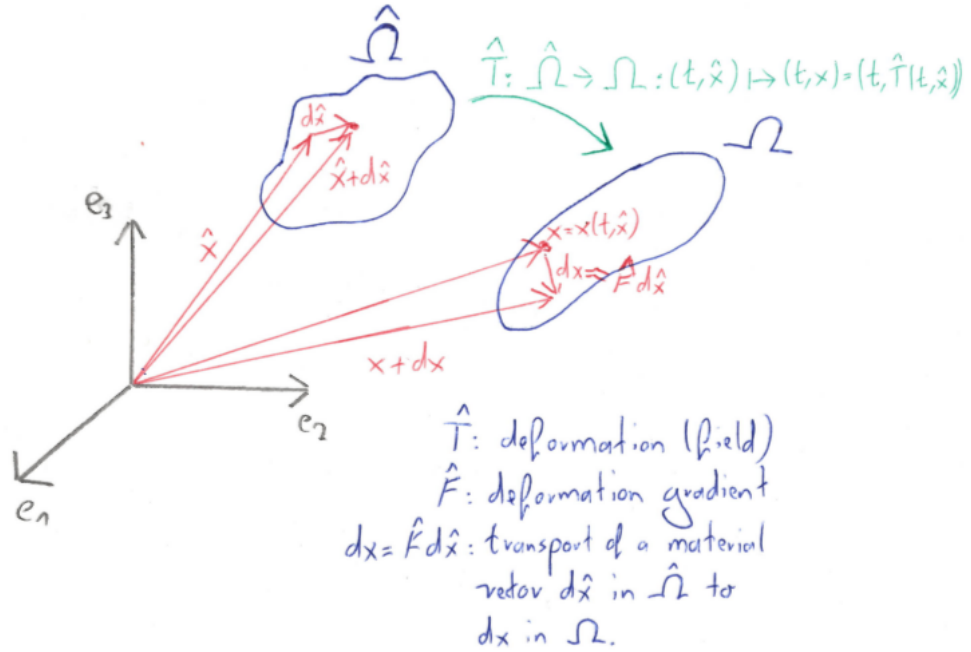
Figure 6: Transport of materials vectors, transformation $\widehat{T}$, and deformation gradient $\widehat{F}$.

Relation of deformation gradient and displacements
We are now prepared to relate $\widehat{F}$ and the displacement $\hat{u}(t, \hat{x})$. Recall from Definition 4.3

$$x = \hat{x} + \hat{u}.$$

Definition 4.8 (Deformation and deformation gradient)**.**

$$\widehat{T} = id + \hat{u}.$$

The deformation gradient $\widehat{F}$ can be expressed in terms of $\hat{u}$ as follows:

$$\widehat{F} = \nabla \widehat{T} = \hat{I} + \widehat{\nabla} \hat{u}.$$

With the help of the deformation, $\widehat{T}$, we can represent the deformed configuration as $\Omega = \widehat{T}(\widehat{\Omega})$.

Although we have Definition 4.5, such a relation does not hold for derivatives. Here we have (see also Figure 6):

$$\nabla f = \widehat{\nabla} \hat{f} \, \widehat{F}^{-1}.$$

Determinant of deformation

The determinant of the deformation gradient (mathematically speaking we would call it as the functional determinant) is defined as

Definition 4.9.

$$\hat{J} := det(\widehat{F}) > 0,$$

which is used to relate volume changes between infinitesimal reference and current domains:

$$d\Omega = \hat{J} d\widehat{\Omega}. \tag{5}$$

$\diamond$

Extending Relation (5) to the whole domain, we can compute the volume change:

$$|\Omega| = \int_{\Omega} 1 \, dx = \int_{\widehat{\Omega}} \hat{J}(t, \hat{x}) \, d\hat{x}, \tag{6}$$

which further yields (employing the Eulerian development formula $\partial_t \hat{J}(t, \hat{x}) = \nabla \cdot v(t, x) \hat{J}(t, \hat{x})$)

$$\frac{d}{dt} |\Omega| = \int_{\Omega} \nabla \cdot v(t, x) \, dx.$$

Consequently, $\hat{J}$ characterizes the volume ratio and is called in r-adaptive methods, the *adaptation factor* (Section 5.5). Physically, we do not allow for negative volumes $\hat{J} < 0$ (which is mathematically still allowed). Furthermore, $\hat{J} = 0$ would mean that $\widehat{F}$ is not invertible and has serious consequences in fluid-structure interaction modeling using the ALE approach causing the approach to fail. Consequently, we shall control $\hat{J}$ such that is stays positive during a numerical computation.

If a body does not move, we have $\widehat{F} = \hat{I}$ and it follows $\hat{J} = 1$. On the other hand, a motion is called isochoric when $\hat{J} = 1$ with possibly $\widehat{F} \neq \hat{I}$.

Nanson's formula

This formula is required to transform normal vectors between both coordinate systems. Let $ds := ds n$ and $d\hat{s} := d\hat{s}\hat{n}$ be vector elements of infinitesimally small areas and n and $\hat{n}$ the corresponding normal vectors. Then,

Definition 4.10 (Nanson's formula)**.**

$$ds = \hat{J} \widehat{F}^{-T} d\hat{s}.$$

$\diamond$

4.1.2 Reynolds' transport theorem - differentiation under the integral sign

Proposition 4.11 (Reynolds' transport theorem)**.** *Let* $(t, \hat{x}) \mapsto x(t, \hat{x})$ *be given under some assumptions (details see [74]). Furthermore, let the functions* $(t, x) \mapsto \partial_t x(t, \hat{x})$ *and* $(t, x) \mapsto f(t, x)$ *be continuously differentiable. Then,*

$$\frac{d}{dt} \int_\Omega f(t, x)\, dx = \int_\Omega \left[\partial_t f(t, x) + \nabla \cdot (f(t, x) \cdot v(t, x)) \right]\, dx.$$

4.1.3 Strain tensor

There are various definitions for strain tensors [139]. Let us introduce the most important concepts for these lecture notes:

Definition 4.12 (Right Cauchy-Green tensor $\widehat{C}$)**.**

$$\widehat{C} = \widehat{F}^T \widehat{F},$$

which is symmetric and positive definite for all $\hat{x} \in \widehat{\Omega}$. $\diamond$

Definition 4.13 (Green-Lagrange strain tensor $\widehat{E}$)**.**

$$\widehat{E} = \frac{1}{2}(\widehat{F}^T \widehat{F} - \hat{I}),$$

which is again symmetric and positive definite for all $\hat{x} \in \widehat{\Omega}$ *since* $\widehat{C}$ *and of course,* $\hat{I}$ *have these properties.* $\diamond$

Geometrically speaking, the strain tensors measure the changes, caused by the deformation, both in lengths and angels of two material vectors.

Performing geometric linearization, we often work with the linearized Green-Lagrange strain tensor

Definition 4.14 (Linearized Green-Lagrange strain tensor $\widehat{E}_{lin}$)**.**

$$\widehat{E}_{lin} = \frac{1}{2}(\widehat{\nabla}\hat{u} + \widehat{\nabla}\hat{u}^T).$$

$\diamond$

4.2 Balance principles and conservation equations

The equations in continuum mechanics are based on the fundamental physical principles:

- Mass

- Momentum

- Angular momentum

- Energy

4.2.1 Conservation of mass - the continuity equation

Let $\rho(t, x)$ be the mass density in Eulerian coordinates.

Definition 4.15 (Conservation of mass).

$$\frac{d}{dt} \int_\Omega \rho(t, x)\, dx = 0.$$

◇

Applying Reynolds' transport theorem, we get the integral formulation

$$\int_\Omega \left[\partial_t \rho(t, x) + \nabla \cdot (\rho(t, x) v(t, x)) \right]\, dx = 0.$$

This equation must hold for each sub-domain of Ω. If ρ and v are sufficiently smooth, we get the differential formulation

$$\partial_t \rho + \nabla \cdot (\rho v) = 0.$$

Remark 4.16 (Homework). *Make yourself clear how we come from the integral formulation to the differential form.* ◇

Remark 4.17. *When changes in density are time-independent, we have*

$$\nabla \cdot (\rho v) = 0.$$

If the density is also spatially constant, we get

$$\nabla \cdot v = 0.$$

◇

4.2.2 Conservation of momentum

Let $f : \Omega \to \mathbb{R}^d$ be a given force density acting on the volume; and let $g : \partial\Omega \to \mathbb{R}^d$ a surface-related force (traction force).

Newton's second law states:
$$\frac{d}{dt}(mv) = F,$$

where F is the force that acts on the mass.

In continuum mechanics Newton's second law reads:

$$\frac{d}{dt} \int_\Omega \rho v\, dx = \int_\Omega \rho f\, dx + \int_{\partial\Omega} g\, ds.$$

Employing again Reynolds' transport theorem yields:

$$\int_\Omega \left[\partial_t(\rho v) + \nabla \cdot (\rho v v) \right]\, dx = \int_\Omega \rho f\, dx + \int_{\partial\Omega} g\, ds.$$

Applying Cauchy's existence [43, 55] of the stress tensor,

$$g = \sigma \cdot n,$$

further allows to write (and using Gauss' divergence theorem)

$$\int_{\partial\Omega} g \, ds = \int_{\partial\Omega} \sigma \cdot n \, ds = \int_{\Omega} \nabla \cdot \sigma \, dx.$$

After some calculations, we finally obtain:

$$\rho \partial_t v + \rho (v \cdot \nabla) v - \nabla \cdot \sigma = \rho f.$$

4.2.3 Conservation of angular momentum

Proposition 4.18. *Let all parameters and data ρ, v, f, g be sufficiently smooth. If conservation of momentum and angular momentum are satisfied, then Cauchy's stress tensor σ is symmetric.*

Remark 4.19. *In formulating the Navier-Stokes equations, you often find a non-symmetric formulation. We strongly emphasize that such a simplification is related to the specific setting. In general, you must use the symmetric stress tensor.*

4.2.4 Conservation of energy

The conservation of energy reads:

$$\frac{d}{dt} \int_{\Omega} \rho (\frac{1}{2} |v|^2 + u) \, dx = \int_{\Omega} \rho f \cdot v \, dx + \int_{\partial\Omega} \sigma n \cdot v \, ds - \int_{\partial\Omega} g \cdot n \, ds + \int_{\Omega} \rho h \, dx$$

This leads into,
$$\rho \partial_t u + \rho v \cdot \nabla u - \sigma : Dv + \nabla \cdot g - \rho h = 0.$$

Here, u is related to the inner energy, v to the kinetic energy, f and σn right hand side source terms, and g and h are related to heat energy terms.

4.3 Incompressible, isothermal equations with constant density

If there are no variations in density and temperature, we obtain the following equations for conservation of momentum and mass balance:

$$\rho \partial_t v + \rho (v \cdot \nabla) v - \nabla \cdot \sigma = \rho f,$$
$$\nabla \cdot v = 0.$$

The specification of the stress tensor σ follows in Section 4.4.

4.4 Constitutive laws

The Cauchy stress tensor is not yet specified in Section 4.3 and hence the previous equations do hold for all materials; specifically they do not distinguish between fluids, solids, or gas. These properties are fixed by *constitutive* laws that are obtained from measurements, for instance.

We provide two examples for constitutive laws:

- Friction-free fluid flow. Here, only pressure forces are taken into account. The stress tensor reads:
$$\sigma = -pI.$$

- Viscous flow with inner friction:
$$\sigma = -pI + \mu(\nabla v + \nabla v^T) + \lambda \nabla \cdot vI,$$

  where λ and μ are volume and shear viscosity, respectively. In the case of incompressible materials, i.e., $\nabla \cdot v = 0$, this relationship reduces to
$$\sigma = -pI + \mu(\nabla v + \nabla v^T).$$

Remark 4.20. *In Navier-Stokes formulations, you often find the non-symmetric version*
$$\sigma = -pI + \mu \nabla v.$$

$\diamond$

4.5 Incompressible, isothermal Navier-Stokes equations

$$\rho \partial_t v + \rho(v \cdot \nabla)v - \nabla \cdot \sigma = \rho f,$$
$$\nabla \cdot v = 0,$$

where
$$\sigma = -pI + \mu(\nabla v + \nabla v^T).$$

Here, $\mu = \rho \nu$ is the dynamic viscosity, whereas ν is the so-called kinematic viscosity.

We have not yet talked about boundary conditions, which are crucial to all equations presented so far. Depending on them and suitable right hand side data, we might obtain existence of a unique solution; for details we refer to [227].

For the full 3d Navier-Stokes equations, the complete proof for smooth solutions is still missing and one of the Millennium prices. Concretely, one has to establish existence and smoothness of solutions in $\mathbb{R}^3$ [78]. This problem is also open for the Euler equations ($\nu = 0$). The 2d solution has been established in [164].

4.6 Modeling thin fluid films: the lubrication equation

In many applications, the Navier-Stokes equations are reduced to a linear velocity-pressure relationship (Darcy) or further to a lower-dimensional lubrication equation, the so-called Reynolds' lubrication equation. This approximation is used when the geometry width (or height) is small compared to the length. In addition, we assume that the Reynolds number is small; otherwise advection effects would play a major role.

Definition 4.21. *(Reynolds number)*
For the characteristic data of a fluid; namely, velocity and length, we define

$$Re = \frac{UL}{\nu},$$

where $\nu = \frac{\mu}{\varrho}$ is the kinematic velocity as previously used. ⋄

For fluids with high viscosity, friction terms dominate compared to inertia forces. Consequently, we neglect the convection term $v \cdot \nabla v$.

Example 4.22. *Small Reynolds numbers appear in the following situations for instance:*

- *Transport of microscopic elements (here L is very small),*

- *Deformation/Transport of geological structures such as ice glaciers,*

- *Fluids with high viscosity such as honey.*

Of course, these examples come from different applications, but they all have in common that the Reynolds number is small and for the solution (in theory as well as numerics), we can employ similar tools. These facts were discovered by Reynolds in 1883.

In the following, we assume no volume forces. Possible forces which can be represented by a potential can be inserted in the term ∇p. Furthermore, we assume a quasi-stationary velocity field, namely $\frac{\partial v}{\partial t} \approx 0$. Then, we obtain the linear Stokes equations:

$$0 = -\nabla p + \eta \Delta v,$$

together with suitable boundary conditions, they have a unique solution [227].

4.6.0.1 Derivation of Reynolds' equation in 1D The mathematical tools behind the following calculations is a dimensional analysis. Our derivation is based on a two-dimensional setting and the resulting PDE will be dependent only on x. The extension to three dimensions is straightforward. Let us begin with a thin fluid film that is placed on a fixed piece (i.e., a table). With thin, we mean $h(x) \ll l$ (height much smaller than length).
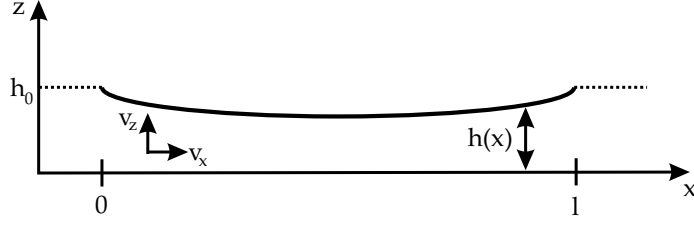
Figure 7: Lubrication film with height $h(x)$ and velocity components v_x and v_z

We start from the Stokes equations:

$$\nabla p = \eta \Delta v \quad \Leftrightarrow \quad \frac{\partial}{\partial x_i} p = \eta \frac{\partial^2 v_i}{\partial x_l^2} \quad \text{for } i = x, y.$$

Since the film is thin, we omit pressure variations in z-direction. Similarly, we take only velocity variations in x-direction such that we obtain

$$-\frac{dp}{dx} + \eta \left(\frac{\partial^2 v_x}{\partial x^2} + \frac{\partial^2 v_x}{\partial z^2} \right) = 0 \quad \text{with } v_x = v_x(x, z). \tag{7}$$

Changes of the velocity in x-direction are much smaller than in z-direction and we can assume:

$$\left| \frac{\partial^2 v_x}{\partial x^2} \right| \ll \left| \frac{\partial^2 v_x}{\partial z^2} \right|.$$

Consequently, (7) can be written as

$$-\frac{dp}{dx} + \eta \frac{\partial^2 v_x}{\partial z^2} = 0.$$

We assume a viscous fluid with no-slip boundary conditions

$$v_x(x, 0) = v_x(x, h) = 0, \quad \text{both boundaries are fixed.}$$

Or,

$$v_x(x, 0) = u_0 \quad \text{and} \quad v_x(x, h) = u_h, \quad h = h(x).$$

if the lower or upper boundary move with the horizontal velocity u_0 i.e.,. u_h:

Proposition 4.23 (Velocity profile of a thin film in 1D)**.** *The evolution of a fluid characterized by a thin film is given by:*

$$v_x = -\frac{1}{2\eta} \frac{dp}{dx} z(h - z) - u_0 \left(\frac{z}{h} - 1 \right) + \frac{z}{h} u_h, \quad h = h(x), \, v_x = v_x(x, z),$$

with the no-slip boundary conditions:

$$v_x(x, 0) = u_0 \quad \text{and} \quad v_x(x, h) = u_h.$$

28

Proof. Two times integration leads to the velocity field of the thin film

$$-\frac{dp}{dx} + \eta\frac{\partial^2 v_x}{\partial z^2} = 0$$

$$\Rightarrow \quad -\frac{dp}{dx}z + \eta\frac{\partial v_x}{\partial z} + C_1 = 0, \quad C_1 = \text{const}$$

$$\Rightarrow \quad -\frac{dp}{dx}\frac{1}{2}z^2 + \eta v_x + C_1 z + C_2 = 0, \quad C_1, C_2 = \text{const.}$$

Applying the boundary conditions leads to

$$i) \quad v_x(x,0) = u_0 \quad \Rightarrow \eta u_0 + C_2 = 0 \quad \Rightarrow C_2 = -\eta u_0$$

$$ii) \quad v_x(x,h) = u_h \quad \Rightarrow -\frac{dp}{dx}\frac{1}{2}h^2 + \eta u_h + C_1 h - \eta u_0 = 0$$

$$\Rightarrow C_1 = \frac{1}{h}\left(\frac{dp}{dx}\frac{1}{2}h^2 + \eta(u_0 - u_h)\right).$$

Inserting

$$0 = -\frac{dp}{dx}\frac{1}{2}z^2 + \eta v_x + z\frac{1}{h}\left(\frac{dp}{dx}\frac{1}{2}h^2 + \eta(u_0 - u_h)\right) - \eta u_0$$

$$\Leftrightarrow \quad 0 = \frac{1}{2}\frac{dp}{dx}z^2 + \frac{1}{2}\frac{dp}{dx}zh + \eta v_x + \frac{z}{h}\eta(u_0 - u_h) - \eta u_0$$

$$\Leftrightarrow \quad 0 = \frac{1}{2\eta}\frac{dp}{dx}(zh - z^2) + v_x + \frac{z}{h}u_0 - u_0 - \frac{z}{h}u_h$$

$$\Leftrightarrow \quad v_x = -\frac{1}{2\eta}\frac{dp}{dx}z(h - z) - u_0(\frac{z}{h} - 1) + \frac{z}{h}u_h.$$

$$\square$$

In order to obtain the pressure, we begin with the mass balance equation

$$\text{div } v = 0 \quad \Leftrightarrow \quad \frac{\partial v_x}{\partial x} + \frac{\partial v_z}{\partial z} = 0.$$

Integrating of the height $h = h(x)$ yields:

$$\int_0^h \frac{\partial v_x}{\partial x}\,dz + [v_z]_0^h = 0. \tag{8}$$

Using differentiation of parametric integrals gives us:

$$\int_{g(x)}^{h(x)} \frac{\partial}{\partial x}f(x,z)\,dz = \frac{d}{dx}\int_{g(x)}^{h(x)} f(x,z)\,dz - \frac{\partial h}{\partial x}f(x,h(x)) + \frac{\partial g}{\partial x}f(x,g(x)).$$

29

For (8), we obtain the implications:

$$\frac{d}{dx} \int_0^h v_x \, dz - \frac{dh}{dx} v_x(x, h) + [v_z]_0^h = 0$$

$$\Rightarrow \quad \frac{d}{dx} \int_0^h \left(-\frac{1}{2\eta}\frac{dp}{dx} z(h-z) - u_0(\frac{z}{h} - 1) + \frac{z}{h}u_h \right) dz - \frac{dh}{dx} u_h + [v_z]_0^h = 0$$

$$\Rightarrow \quad \frac{d}{dx} \left[-\frac{1}{2\eta}\frac{dp}{dx}\left(\frac{1}{2}z^2 h - \frac{1}{3}z^3 \right) - u_0\left(\frac{1}{2h}z^2 - z \right) + \frac{1}{2h}z^2 u_h \right]_0^h - \frac{dh}{dx} u_h + [v_z]_0^h = 0$$

$$\Rightarrow \quad \frac{d}{dx}\left(-\frac{1}{2\eta}\frac{dp}{dx}\left(\frac{1}{2}h^3 - \frac{1}{3}h^3 \right) - u_0(\frac{h}{2} - h) + u_h\frac{h}{2} \right) - \frac{dh}{dx} u_h + [v_z]_0^h = 0.$$

By composing all terms, we obtain the Reynolds equation for a viscous thin film between moving boundaries:

$$\frac{d}{dx}\left(-\frac{1}{12\eta}\frac{dp}{dx}h^3 + \frac{1}{2}h(u_0 + u_h) \right) - \frac{dh}{dx}u_h + [v_z]_0^h = 0. \tag{9}$$

We get:

Proposition 4.24 (Pressure distribution of a thin film in 1D). *Let the top boundary $z = h(x)$ be moving with a velocity $v_z(x, h) =: v_z$; the lower boundary at $h = 0$ is fixed for simplicity. Then,*

$$-\frac{d}{dx}\left(\frac{h^3}{12\eta}\frac{dp}{dx} \right) = v_z.$$

Appropriate Neumann boundary conditions are:

$$\frac{dp(0)}{dx} = \Delta p_1 \quad and \quad \frac{dp(1)}{dx} = \Delta p_2.$$

In two-dimensions, we have

Proposition 4.25 (Pressure distribution of a thin film in 2D). *Let the top boundary $z = h(x)$ be moving with a velocity $v_z(x, h) =: v_z$; the lower boundary at $h = 0$ is fixed for simplicity. Then,*

$$-\nabla \cdot \left(\frac{h^3}{12\eta}\nabla p \right) = v_z, \quad h = h(x, y).$$

Neumann boundary conditions are given by

$$i) \quad \frac{\partial p}{\partial x} = \Delta p_1 \quad on \ \Gamma_1 \quad and \quad \frac{\partial p}{\partial x} = \Delta p_2 \quad on \ \Gamma_3,$$

$$ii) \quad \frac{\partial p}{\partial y} = \Delta p_3 \quad on \ \Gamma_2 \quad and \quad \frac{\partial p}{\partial y} = \Delta p_4 \quad on \ \Gamma_4.$$

Remark 4.26 (Existence of the pressure lubrication equation). *We emphasize that the pressure lubrication problem is of elliptic type. Here, Neumann conditions on all boundary parts require a compatibility condition (e.g., [43]) in order to establish existence of the problem. This is equivalent to saying that the pressure solution is only determined up to a constant.* ⋄

4.7 Modeling solids

In these lecture notes, we mainly concentrate on elastic deformations for solid modeling. Specifically, this means that a body under deformation goes back into its initial configuration if forces are removed. So, we work in the linear regime sketched in Figure 4.7 [12].

When the body does not go back into its initial configuration and a deformed settings remains, we work in an elasto-plastic regime with plastic deformations.

There are huge contributions to hyperelastic materials. We aim to provide a brief overview of basics concepts that help us throughout these lecture notes. For detailed considerations, we refer to [38, 56, 139, 146].
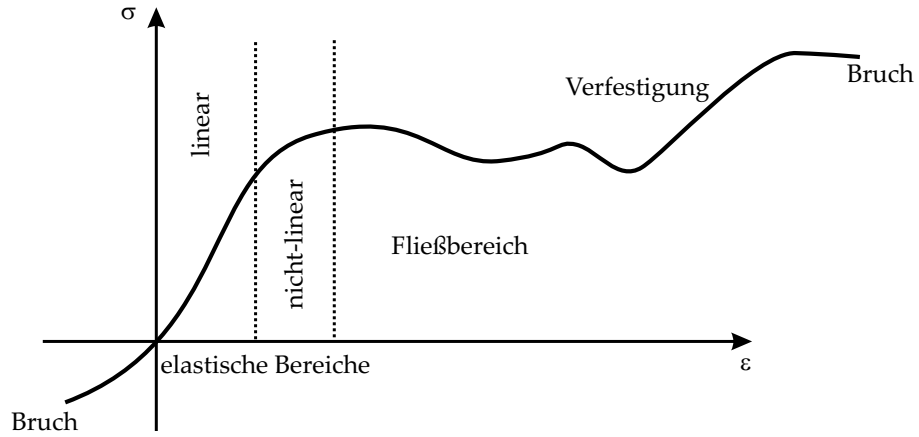
Figure 8: The stress-strain diagram. Here, σ is the stress and ε is the strain.

Typically and in contrast to fluid problems, elasticity is described in Lagrangian coordinates. One reason is related to history-dependent materials. Using Lagrangian coordinates, it facilitates treatment of such laws because each mesh point represents at all times the same material point (for example stress-update procedures in nonlinear elasticity or plasticity). However, it is nevertheless possible to obtain such information in an Eulerian framework; for a discussion, we refer the reader to [38] (chapter 5). Lagrangian coordinates describe a material point $\hat{x}$ in the reference configuration $\widehat{\Omega}$,

---

[12]I took this figure from my Master thesis that was written in German. Bruch = break, damage; Bereich = region; Fließ= flow; Verfestigung = hardening; nicht = non.

which is usually the configuration without outer forces (remember in contrast to pre-stressed configurations [139]).

Since we intend to compute the solution (deformation and stress) in Lagrangian coordinates, but the Cauchy's stress tensor is formulated in the Eulerian framework, we need to transform this tensor back to the reference configuration. This operation is achieved with the so-called Piola-Kirchhoff stress tensor:

Definition 4.27 (First Piola stress tensor)**.**

$$\widehat{\Pi} = \hat{J}\widehat{\sigma}_s \widehat{F}^{-T}.$$

where $\widehat{\sigma}_s$ is Cauchy's stress tensor. ⋄

With its help, we are able to transform the solid equations from Ω to $\widehat{\Omega}$. We notice that $\widehat{\Pi}$ is in general not symmetric although $\widehat{\sigma}_s$ has this property. However, this is often advantageous and consequently we define a second stress tensor in the reference domain:

Definition 4.28 (Second Piola stress tensor)**.**

$$\widehat{\Sigma} = \widehat{F}^{-1}\widehat{\Pi} = \hat{J}\widehat{F}^{-1}\widehat{\sigma}_s \widehat{F}^{-T} \quad \Leftrightarrow \quad \widehat{F}\widehat{\Sigma} = \widehat{\Pi} = \hat{J}\widehat{\sigma}_s \widehat{F}^{-T}. \tag{10}$$

⋄

We are now prepared to formulate the equations for elasticity. As we previously learned, without specifying constitutive laws the conservation equations do hold for all aggregation states. We recall the conservation of momentum:

$$\frac{d}{dt}\int_{\Omega} \hat{\rho}\partial_t u \, dx = \int_{\Omega} \hat{f} \, dx + \int_{\partial\Omega} \sigma n ds.$$

Here, the density $\hat{\rho}$ and the volume force $\hat{f}$ are related to the reference configuration. Further calculation (using Gauss' divergence theorem and Reynolds transport theorem) yields

$$\int_{\Omega} \left(\hat{\rho}\partial_t^2 u - \nabla \cdot \sigma \right) dx = \int_{\Omega} \hat{f} \, dx. \tag{11}$$

We notice that the convective term in Reynolds' theorem vanishes since we work in a Lagrangian setting. For sufficiently smooth functions and since (11) holds for each subdomain of Ω, we can write the differential form of the elasto-dynamics equations:

$$\hat{\rho}\partial_t^2 u - \nabla \cdot \sigma = \hat{f}. \tag{12}$$

Remark 4.29 (A mixed formulation)**.** *We notice that you can split the solid equation into a first order system:*

$$\hat{\rho}\partial_t v - \nabla \cdot \sigma = \hat{f},$$
$$\hat{\rho}(\partial_t u - v) = 0.$$

In fact in Section 5 and 6, we go with this mixed formulation. Reasons are of numerical nature and are explained in [12]. We notice that standard temporal solid discretization is based on the so-called Newmark scheme [143, 261, 262]. ⋄

In order to specify the properties of a specific material, we again need a constitutive law for the stress tensor. We already discussed the linearized strain tensor if we deal with small strains. In addition, we need a relationship between the stress and strain (we refer to Figure 4.7). Often, Hooke's law is consulted, which reads:

Definition 4.30 (Linear stress-strain relationship/Hooke's law).

$$\sigma_{ij} = \sum_{k,l=1}^{d} a_{ijkl} E_{kl}^{lin} \quad for\ i,j = 1, \ldots, d.$$

$\diamond$

The tensor $(a_{ijkl})_{ijkl}^{d} \in \mathbb{R}^d \times \mathbb{R}^d \times \mathbb{R}^d \times \mathbb{R}^d$ has 81 components in $3d$. Using symmetry arguments and further assumptions (e.g. isotropy), we arrive at

Definition 4.31 (St. Venant-Kirchhoff-Material).

$$\widehat{\sigma}(\hat{u}) = 2\mu\widehat{E} + \lambda tr(\widehat{E})\hat{I},$$

with the Lamé constants μ and λ. $\diamond$

Remark 4.32. *We notice that this material law has limitations for problems that involve large strains.* $\diamond$

Remark 4.33 (Hyperelastic materials). *There is a huge body of literature concerned with general laws of hyperelasticity [38, 56, 139, 146] from which the St. Venant-Kirchhoff material is a special case. A material is called hyperelastic, and therefore path-independent, when the applied work during a deformation process does only depend on the initial state and the final configuration. In this case, there exists a potential, the stored strain energy function or elastic potential per unit undeformed volume [139].* $\diamond$

Remark 4.34 (Incompressible materials: neo-Hookean, Mooney-Rivlin).

$$
\begin{aligned}
\widehat{\sigma}_s(\hat{u}) &:= -\hat{p}_s\hat{I} + \mu_s\hat{F}\hat{F}^{-T}, \\
\widehat{\sigma}_s(\hat{u}) &:= -\hat{p}_s\hat{I} + \mu_s\hat{F}\hat{F}^{-T} + \mu_2\hat{F}^{-T}\hat{F}^{-1},
\end{aligned}
\tag{13}
$$

with the coefficients μ_s and μ_2 . $\diamond$

Often, the elasticity of structures is characterized by the Poisson ratio ν_s ($\nu_s < \frac{1}{2}$ for compressible materials) and the Young modulus E_Y. The relationship to the Lamé coefficients μ_s and λ_s is given by:

$$\nu_s = \frac{\lambda_s}{2(\lambda_s + \mu_s)}, \qquad E_Y = \frac{\mu_s(\lambda_s + 2\mu_s)}{(\lambda_s + \mu_s)}, \tag{14}$$

$$\mu_s = \frac{E_Y}{2(1 + \nu_s)}, \qquad \lambda_s = \frac{\nu_s E_Y}{(1 + \nu_s)(1 - 2\nu_s)}. \tag{15}$$

Let us finally derive the relationship between incompressible fluids and solids. Recall:

$$\nabla \cdot v = 0 \text{ for fluids} \quad \hat{J} = 1 \text{ for solids} .$$

Since they represent the same physical mechanism; namely mass conservation, they should be the same! We calculate:

$$|\Omega| = \int_{\widehat{\Omega}} \hat{J} \, d\hat{x}$$
$$\Rightarrow \frac{d}{dt} |\Omega| = \int_{\Omega} \nabla \cdot v \, dx.$$

4.8 Summary: Equations for modeling fluids and solids

4.8.0.2 Fluid equations

In a Newtonian incompressible fluid, it holds:

$$\sigma_f := \sigma_f(v_f, p_f) = -p_f I + 2\rho_f \nu_f D(v_f), \quad D(v_f) := \frac{1}{2}(\nabla v_f + \nabla v_f^T) \qquad (16)$$

with the velocity v_f, the pressure p_f, the identity matrix I, the density ρ_f, and the (kinematic) viscosity ν_f.

Using the equations for momentum and continuity together with the Cauchy stress tensor, we obtain the incompressible, isothermal Navier-Stokes Equations:

$$\rho_f \partial_t v_f + \rho_f (v_f \cdot \nabla) v_f - 2\text{div}(\rho_f \nu_f D(v_f)) + \nabla p_f = \rho_f f, \quad \text{in } \Omega_f, t \in I, \qquad (17)$$
$$\text{div } v_f = 0, \quad \text{in } \Omega_f, t \in I. \qquad (18)$$

These equations are supplemented by appropriate boundary conditions. The first type are Dirichlet conditions (a prescribed velocity):

$$v_f = g \quad \text{on } \Gamma_{f,D} \subset \partial \Omega_f,$$

with a given function $g : \Gamma_{f,D} \times I \to \mathbb{R}^d$. Such a Dirichlet condition is seen in the velocity domain on the interface Γ_i in the case of a fluid-structure interaction setting, i.e.,

$$v_f = v_s \quad \text{on } \Gamma_i.$$

The second natural type are Neumann boundary conditions (applied stresses):

$$\sigma_f n_f = [-p_f I + 2\rho_f \nu_f D(v_f)] \, n_f = h \quad \text{on } \Gamma_{f,N} \subset \partial \Omega_f,$$

with a given vector-valued function $h = h(x,t)$. This condition is mostly used for the outflow boundary (*do-nothing condition* [134]). However, the do-nothing condition implies a constant pressure on this boundary that is not physiological in bio-medical applications [88, 197]. Recent advances considering stability and well-posedness of settings including the do-nothing conditions have been obtained in [42]. In particular, the authors propose a modification, the *directional do-nothing condition*, that is necessary when out- and inflow on one boundary part is involved.
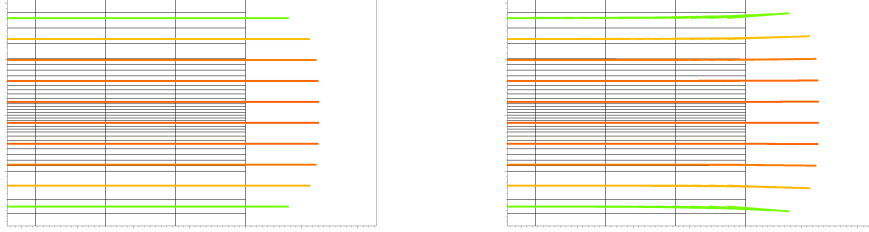
Figure 9: Impact of the correction term on the outflow boundary using the do-nothing [134] condition. In order to get the 'correct' outflow profile using the symmetric stress tensor, you need to subtract the symmetric part $\rho_f \nu_f \nabla v^T n_f$ on the outflow boundary. Otherwise you get non-physical curved streamlines as displayed in the right figure. Further examples and serious consequences are shown in [42].

4.8.0.3 Regularity of fluid equations In the following, we formulate time-dependent functions in the Bochner spaces [260].

Problem 4.35 ([227], p. 190). *Let $\hat{f}_f$ and $\hat{v}_f^0$ be given by*

$$\hat{f}_f \in L^2(I; H^{-1}(\widehat{\Omega}_f)), \quad v_f^0 \in \hat{L}(\widehat{\Omega}_f).$$

Find: $\hat{v}_f \in L^2(I; H^1(\widehat{\Omega}_f))$ such that the standard Navier-Stokes equations (as defined, e.g., by Temam [227]) are solved with the initial data $\hat{v}_f(0) = \hat{v}_f^0$.

Theorem 3.1 in [227] shows that at least one solution to the previous defined problem exists, i.e., it holds

$$\hat{v}_f \in L^2(I, H^1(\widehat{\Omega}_f)).$$

The main consequence for fluid-structure interaction is that $\hat{v}_f \in H^{1/2}(\widehat{\Gamma}_i)$.

4.8.0.4 Solid equations For elasto-dynamics, we have:

$$\hat{\rho}_s \partial_t^2 \hat{u}_s - \widehat{\mathrm{div}}(\widehat{F}\widehat{\Sigma}) = \hat{\rho}_s \hat{f}, \quad \text{in } \widehat{\Omega}_s, \, t \in I. \tag{19}$$

This second-order (in time) equation is supplemented by appropriate initial conditions and boundary conditions. As for the fluid equations, we prescribe Dirichlet boundary conditions (fixing the displacements):

$$\hat{u}_s = \hat{g} \quad \text{on } \widehat{\Gamma}_{s,D} \subset \partial\widehat{\Omega}_s,$$

where $\hat{g}$ is a given function. We can also employ Neumann boundary condition (surface stresses):

$$\widehat{F}\widehat{\Sigma}\hat{n}_s = \hat{J}\hat{\sigma}_s\widehat{F}^{-T}\hat{n}_s = \hat{h} \quad \text{on } \widehat{\Gamma}_{s,N} \subset \partial\widehat{\Omega}_s,$$

in which $\hat{h}$ is a given vector-valued function. Such a condition is seen from the structure side on the interface in case of a fluid-structure interaction problem, i.e.,

$$\widehat{F}\widehat{\Sigma}\hat{n}_s = -\hat{J}\hat{\sigma}_f\widehat{F}^{-T}\hat{n}_f \quad \text{on } \widehat{\Gamma}_i.$$

4.8.0.5 Regularity of the solid equations Before we consider the regularity of the solid equations, we extend the previously-derived equations. For mathematical and physical reasons, it might be desirable to introduce damping terms.

Example 4.36 (Physical reason for damping terms). *As example, consider the harmonic oscillator, vibrations or simply a pendular that we let oscillating (remember your physics classes). This pendular will stop at a finite time - otherwise we would have created the famous perpetual motion machine. Correct physical modeling of this process, consequently, requires introducing damping terms (i.e., friction terms).* ⋄

Example 4.37 (Mathematical point of view). *Damping terms introduce higher regularity into the solid solutions. We see later that this is important in the mathematical analysis of fluid-structure interaction.* ⋄

The modified structure problem including damping terms reads:

$$\hat{\rho}_s\partial_t^2\hat{u}_s - \widehat{\text{div}}(\widehat{F}\widehat{\Sigma}(\hat{u}_s)) + \gamma_w\partial_t\hat{u}_s - \gamma_s\partial_t\widehat{\text{div}}(\hat{\epsilon}(\hat{u}_s)) = \hat{\rho}_s\hat{f}_s \quad \text{in } \widehat{\Omega}_s, \, t \in I, \qquad (20)$$

with $\gamma_s, \gamma_w \geq 0$. The first damping term is referred to as *weak damping* whereas the second damping term is called *strong damping*. Using strong damping, the full operator is used for damping, leading to an additional condition on the interface (because of integration by parts) that has to be considered for the coupling with fluids. Assuming that temporal and spatial differentiation can be changed, we obtain for strong damping:

$$-\gamma_s\partial_t\widehat{\text{div}}(\hat{\epsilon}(\hat{u}_s)) = -\gamma_s\widehat{\text{div}}(\hat{\epsilon}(\partial_t\hat{u}_s)) = -\gamma_s\widehat{\text{div}}(\hat{\epsilon}(\hat{v}_s)), \quad \text{with } \hat{v}_s = \partial_t\hat{u}_s.$$

The change of temporal and spatial differentiation is invalid for nonlinear strong damping, where we could have been used the full nonlinear operator, i.e.,

$$-\gamma_s\partial_t\widehat{\text{div}}(\widehat{F}\widehat{\Sigma}(\hat{u}_s)) \not\approx -\gamma_s\widehat{\text{div}}(\widehat{F}\widehat{\Sigma}(\hat{v}_s)). \qquad (21)$$

Such damping strategies have been employed in computational fluid-structure interaction as a perfectly-matched layer (PML) [30] approach to absorb outgoing elastic waves in elastic-wall-fluid-flap simulations [249] as illustrated in Figure 10.
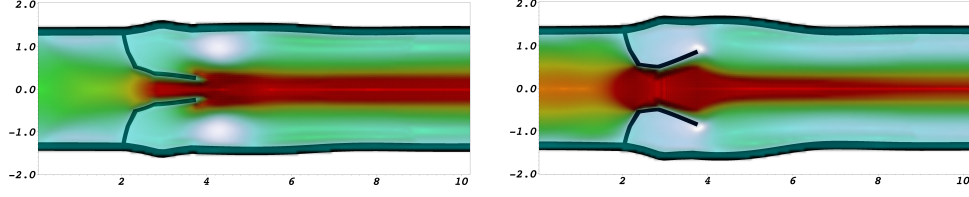
Figure 10: Damped elastic equations are employed in $x \geq 6$ as a PML-approach to absorb outgoing elastic waves in the elastic walls.

Next, we pose a standard mixed formulation of the structure equations,

$$\hat{\rho}_s \partial_t \hat{v}_s - \widehat{\mathrm{div}}(\widehat{F}\widehat{\Sigma}(\hat{u}_s)) + \gamma_w \hat{v}_s - \gamma_s \widehat{\mathrm{div}}(\hat{\epsilon}(\hat{v}_s)) = \hat{\rho}_s \hat{f}_s \quad \text{in } \widehat{\Omega}_s,\, t \in I, \tag{22}$$

$$\hat{\rho}_s(\partial_t \hat{u}_s - \hat{v}_s) = 0 \quad \text{in } \widehat{\Omega}_s,\, t \in I, \tag{23}$$

where $\hat{\epsilon}(\hat{v}_s)$ is defined by

$$\hat{\epsilon}(\hat{v}_s) = \frac{1}{2}(\widehat{\nabla}\hat{v}_s + \widehat{\nabla}\hat{v}_s^T). \tag{24}$$

The modified structure problem (23) reduces to the original problem (19) when the damping parameters are set to $\gamma_w = \gamma_s = 0$.

Remark 4.38. *Using strong damping requires modification of the continuity of normal stresses at the FSI-interface.*

Remark 4.39 (Alternative to obtain higher regularity)**.** *Similar to elliptic and parabolic equations if we assume higher regularity on data and the domain, we obtain higher regularity on the solid solution. For details, I refer to PDE analysis textbooks, e.g., Section 7.2 in [76].*

Remark 4.40 (Mixture of boundary conditions)**.** *Having Dirichlet and Neumann boundary conditions requires that the closures of both boundary parts do not intersect in order to keep the regularity of the solution [56], p. 298.* ◇

Problem 4.41 ([120], p. 351)**.** *Let $\hat{f}_s \in L^2(I, L^2(\widehat{\Omega}_s))$. Find*

$$\hat{u}_s \in L^2(I, H_0^1(\widehat{\Omega}_s)) \quad \text{and} \quad \hat{v}_s = d_t \hat{u}_s \in L^2(I, L^2(\widehat{\Omega}_s)),$$

such that the hyperbolic structure equations

$$d_t^2 \hat{u}_s - \Delta \hat{u}_s = \hat{f}_s \quad \text{in } I \times \widehat{\Omega}_s,$$

$$\hat{u}_s = 0 \quad \text{on } I \times \partial\widehat{\Omega}_s,$$

are solved with the initial data $\hat{u}_s(0) = \hat{u}_s^0$ and $\hat{v}_s(0) = \hat{v}_s^0$.

37

In Grossmann and Roos [120], Theorem 5.6 tells us that this problem has a unique solution. The regularity of that solution is given by

$$\hat{u}_s \in L^2(I, H_0^1(\widehat{\Omega}_s)) \quad \text{and} \quad \hat{v}_s = d_t \hat{u}_s \in L^2(I, L^2(\widehat{\Omega}_s)).$$

Consequently, we cannot expect $\hat{v}_s \in H^{1/2}(\widehat{\Omega}_s)$. Thus, condition (32) is only formally valid. For this reason, we assumed a priori enough regularity of the hyperbolic structure equations. This was also observed (and resolved) in theoretically-oriented articles with focus on proofs of existence of fluid-structure interaction problems [7, 61, 62, 147] [13].

The lack of solid-regularity can be resolved by using a vanishing viscosity approach (that act on the velocity variables) to the structure equations. This coincides with the terms introduced in Equation (20).

To analyze the regularity of structural deformations in more detail, we consider the following hyperbolic equation with weak and linear strong damping.

Problem 4.42 ([103])**.** *Let $\hat{f}_s$ be sufficient regular. Let $\gamma_s \geq 0$ and $\gamma_w > -\gamma_s \lambda_1$, where λ_1 is the first eigenvalue of the $-\Delta$ operator under homogeneous Dirichlet boundary conditions. Find*

$$\hat{u}_s \in L^2(I, H_0^1(\widehat{\Omega}_s)) \quad \text{and} \quad \hat{v}_s = d_t \hat{u}_s \in L^2(I, L^2(\widehat{\Omega}_s)),$$

such that the hyperbolic structure equations with weak and strong damping

$$d_t^2 \hat{u}_s - \Delta \hat{u}_s + \gamma_w d_t \hat{u}_s - \gamma_s d_t \Delta \hat{u}_s = \hat{f}_s \quad in \ I \times \widehat{\Omega}_s,$$
$$\hat{u}_s = 0 \quad on \ I \times \partial\widehat{\Omega}_s,$$

are solved with the initial data $\hat{u}_s(0) = \hat{u}_s^0$ and $\hat{v}_s(0) = \hat{v}_s^0$.

For example, in the work from Gazzola and Squassina [103], the first statement on p. 189 explains that this problem has a unique solution. In particular, the regularity of $\hat{v}_s$ is given by

$$\hat{v}_s = d_t \hat{u}_s \in L^2(I, H_0^1(\widehat{\Omega}_s)),$$

for arbitrary $\gamma_s > 0$; hence, $\hat{v}_s \in H^{1/2}(\widehat{\Gamma}_i)$. Thus, linear strong damping provides more regularity of the solution, specifically for $\hat{v}_s$, such that the coupling condition (32) holds true. We finally notice that we only consider regularity properties of linear structure equations. Thus, typical nonlinearities of the structural operators are neglected.

---

[13] In this sense, we would like to point to two other important contributions analyzing FSI from the theoretical point of view: [226] investigate time-dependent FSI flow-elastic-shell coupling with small displacements; and [117] existence of a stationary FSI problem formulated in ALE coordinates.

5 Fluid-Structure Modeling

In Section 4, we have prepared ourselves with modeling of physics in terms of conservation laws and partial differential equations. In this section, we shall couple these equations into one common framework. The principal challenges are listed in Challenge 1.1. We discuss different coupling algorithms and concentrate on two of them on which I have been working in the last few years.

The procedure of FSI-coupling is as follows: Let us say, we are given fluid equations in Eulerian coordinates and solid equations in a Lagrangian framework. The first questions we need to pose are:

- How to we couple or combine the coordinate systems?

- Once we decided for a technique, we further ask ourselves which amount of information needs to be transferred to the other problem; i.e, do we need weak or strong coupling? This question might be posed from an application viewpoint but also from a mathematical perspective (as example to the latter aspect: a consistent Galerkin formulation for gradient-based sensitivity analysis would require a monolithic coupling).

This information guides us through the discretization and the solution algorithm. We particularly focus on consistent variational-monolithic coupling.

5.1 Techniques for coupling fluids and solids

In this first subsection, we provide an overview of possible coupling techniques.

5.1.1 Choosing frameworks for the coupled fluid-solid system

- **Immersed boundary (IB) method:**
  References [131, 194].
  This method was specifically designed for applications in hemodynamics and heart valve simulations. It keeps the Eulerian and Lagrangian coordinate systems and the coupling is achieved by a Dirac delta function that can be seen as a momentum forcing source term of the fluid equations. Consequently, the discretization uses two different meshes. Temporal discretization can be carried out with finite difference schemes such as first-order backward Euler or higher-order Runge-Kutta. Closely related is the immersed finite element method [265].

- **Immersed structural potential method:**
  References: [107].
  As the name indicates, this method is related to the IB method. Since numerical diffusion is a challenge in the original IB-method the current method mainly tries to reduce these errors. In addition, it allows to employ state-of-the-art fiber-reinforced solid models.

- **Fictious domain method (FD):**
  References: [8, 111–113].
  As in immersed boundary methods, two meshes (possibly nonmatching) are used and the kinematic coupling condition is imposed with Lagrange multipliers and possibly with mortar coupling. Again, the fluid is treated in the Eulerian framework and the solid in Lagrangian coordinates.

- **Arbitrary Lagrangian-Eulerian (ALE):**
  References: [28, 68, 90, 137, 145, 187].
  The ALE method is perhaps the oldest approach. Here, Eulerian and Lagrangian frameworks are combined without changing the mesh topology. One needs to solve or prescribe the mesh movement of the fluid mesh. Difficult for large deformations if no remeshing is used. The key advantage is that the interface aligns with mesh edges and interface-terms such as traction forces can be computed with high accuracy.

- **Fixed mesh ALE (FM-ALE):**
  References: [58].
  Here, an ALE approach is used in which at each time step, the problem is projected on a fixed background mesh. In other words: in each time step remeshing is performed. The method was in particular developed for solid mechanics with large strains in which the elements stretch.

- **Universal mesh method:**
  References: [102].
  This method has similarities to the FM-ALE method and tries again to combine advantages from Eulerian and Lagrangian representations. In particular, large deformations are possible. The key difference to FM-ALE is that during temporal integration element splitting as in FM-ALE is avoided.

- **Hybrid level-set/front-tracking approach:**
  References: [17].
  The idea behind this approach is similar to the universal mesh method: roughly-speaking, Eulerian and Lagrangian frameworks are combined. A level-set approach (interface-capturing) method is used to detect the interface, then the mesh nodes are shifted in order to align the interface with mesh edges.

- **Fully Eulerian FSI:**
  References: [69, 207].
  This approach belongs to the fixed-mesh approaches but in contrast to IB and FD methods, solid mechanics is formulated in terms of Eulerian coordinates. Therefore, the coupled system can be computed on a single mesh. Coupling is achieved by a variational monolithic formulation. As in the previous methods, the interface is first captured (here with the initial-point set method rather than a level-set approach). For the cut-cells a locally modified FEM method has been proposed and is currently under further development [91, 206].

- **Discontinuous Galerkin (DG):**
  References: [79, 123, 124, 126, 245].
  A specific proposed a method is by [245] in which again the fluid is kept in Eulerian coordinates and the solid is modeled in a Lagrangian setting. This specific formulation is closely related to the IB method. Application to standard ALE schemes is straightforward and performed in [123, 124]. In [79, 126], compressible Navier-Stokes equations in ALE form are coupled with solid mechanics.

- **XFEM /GFEM fixed-grid approach, Eulerian-Lagrangian coupling with level-sets, mortar coupling**
  References: [106, 132, 166, 244].
  The key idea is to compute the fluid in an Eulerian framework and to couple it to the Lagrangian structure. The interface (again) cuts the mesh cells and is not anymore aligned with mesh faces. In order to represent jumps of the velocity, pressure and stress fields, the extended/generalized finite element (XFEM/GFEM) scheme is used. Recently, it has been shown that both approaches are equivalent [96]. The approach is that the shape functions are enriched by using additional degrees of freedom together with special enrichment functions that are designed according to the solution form (its characteristics are generally known). Mortar coupling [106] and mortar with domain decomposition [132] allow for non-matching meshes on the interface. A Lagrange multiplier is introduced to satisfy the coupling conditions.

- **Isogeometric analysis (IGA):**
  References: [19, 144].
  In IGA, the test and ansatz functions are not anymore polynomials but splines: e.g., non-uniform rational B-Splines. The main purpose of IGA is to combine geometry representation and discretization. In particular, higher order discretization require less degrees of freedom (for example for C^1 implementations) as a standard finite element model.

- **Deforming spatial domain/stabilized space-time (DSD/SST):**
  References: [228, 229]:
  This method is an interface-tracking method and moves the mesh similar to an ALE approach. The problem is written in terms of a space-time discretization rather than splitting into spatial Galerkin finite elements combined with finite differences in time (Rothe method or the other way around method of lines).

- **Lattice Boltzmann (LBM):**
  References: [162, 163].
  Lattice Boltzmann methods have been introduced for computational fluid dynamics simulations. Rather than using continuum mechanics equations, the fluid is represented by particles on a so-called lattice mesh. Has been successfully applied for fluid-structure interaction.

- **The particle finite element method (PFEM):**
  References: [190].

The PFEM method is based on a particle representation in which both continua (fluid and solid) are modeled in Lagrangian coordinates. The nodes (the particles) are connected in order to build a mesh that serves as computational domain. The resulting triangulation can be used for a finite element discretization. The method is capable to treat large deformations and free surface problems (e.g. water waves). Again, this approach has been successfully applied for fluid-structure interaction.

In addition to the primer coupling techniques, we briefly mention examples of hybrid techniques that couple two of the primal techniques in different parts of the domain:

- IB-Lattice Boltzmann for solving fluid-particle interaction problems [80];

- FD-ALE: [125, 215];

- Fluid-solid interface-tracking/interface-capturing technique (MITICT - FSITICT) [3, 232];

- Coupling of fully-Eulerian/ALE (EALE) - FSITICT [253, 254].

5.1.2 Combining the underlying frameworks: FSI coupling algorithms

The key question we have to pose is:

- Shall the energy balance on the interface be satisfied? That means, do we satisfy

$$v_f = v_s,$$
$$\sigma_f n = \sigma_s n,$$

  after temporal discretization?

The answers can be roughly divided into the following concepts [82]:

- Strongly-coupled (or implicit) schemes preserve the coupling conditions after time discretization. Monolithic methods are strongly-coupled by construction or partitioned approaches with several subiterations between both subsystems.

- Weakly-coupled (or loosely, explicit, staggered) schemes do not 'exactly' satisfy the coupling conditions in each time step. Partitioned approaches with few subiterations are weakly-coupled. Famous examples where these algorithms have been applied are problems in aero-elasticity.

- Semi-implicit schemes [5, 6, 83] are a comprise of the previous two schemes with respect to computational cost and stability.

- Coupling via an optimization algorithm [155] [14].

---

[14]In fact this approach is quite recent with satisfactory results for artery applications with small displacements. Performance w.r.t. to larger displacements (e.g., FSI benchmarks [142]) have not yet been performed.

Remark 5.1 (Added-mass effect [54, 243]). *In several studies it has been shown that weakly-coupled schemes introduce instabilities when both densities such as in hemodynamic problems are of similar order; consequently, strongly-coupled schemes are required. Various stabilization techniques have been investigated to make weakly-coupled schemes stable [52, 83, 98, 170, 243].* ⋄

5.1.3 Regularity of interface coupling in fluid-structure

Apart from practical aspects, there are some theoretical findings that should be taken into account:

- The regularity gap between $v_f \in H^1$ and $v_s \in L^2$. Might be overcome by backward difference discretization of v_s [155]. Or by a viscosity method by adding additional viscous terms to the structure equation [61, 62, 147]. Basically, if we add structural damping (might be also physically taking place; and refer to our discussion in Section 4.8.0.5), we obtain higher spatial regularity for v_s.

5.2 Lagrangian, Eulerian, ALE

As we learned Section 4, Eulerian and Lagrangian approaches are the classical ways to describe problems in continuum mechanics. The so-called arbitrary-Eulerian-Lagrangian (ALE) approach is an intermediate method to overcome some of the shortcomings of the Eulerian and Lagrangian frameworks as we described above. Despite possible drawbacks (mesh degeneration for large deformations; mesh tangling, mesh racing), we focus on this approach in the following sections. The reasons are:

- It is one of the oldest and possibly (still) most widely-used algorithms.

- It is an interface-tracking approach in which the interface is aligned with mesh edges at all times and allows for accurate measurements of, for example, traction forces.

- It combines Lagrangian and Eulerian coordinate systems and we naturally learn to work with transformation rules, which are (partially) indispensable for other (but younger) approaches.

- Implemented correctly (which I always assume), it is an efficient, robust, and accurate method in terms of a single consistent variational form and therefore allows for trustable extensions towards sensitivity analysis and optimization [15] as discussed in Section 7. In this respect, our view in these lecture notes is more directed to classical numerical topics (such as convergence studies, stability, and error estimation) rather than real-world applications.

Let us recapitulate:

---

[15] This does not mean that the other approaches are not capable of doing this, but first we have to trust our forward solver before we can go with adjoint formulations.

43

- Lagrangian methods: mainly designed for problems in structural mechanics, allows easy tracking of surfaces and interfaces between different materials, also appropriate for materials with history dependent constitutive relations (such as plasticity); but has difficulties for problems with large mesh deformations;

- Eulerian methods: used in fluid mechanics, the mesh is fixed and the body moves with respect to the mesh, consequently, mesh deformations do not appear here; but the interface is allowed to cut through cells, which requires adapted discretization techniques in order to keep accuracy and robustness,

- ALE methods: The mesh can be moved (in the extreme case as in an Lagrangian setting; on the other extreme: it is not moved at all and we recover an Eulerian approach), this flexibility is the major advantage and specifically for fluid-structure interaction it leads to moving meshes around the interface and fixed mesh far away (see Figure 11).

Generally-speaking the ALE approach tries to conserve mesh regularity and equidistribution (the optimal mesh geometry) of mesh vertices while keeping the mesh topology. Essentially, we shall control size, shape, and orientation of mesh cells. The location of new vertices or the velocity of mesh points is usually determined by solving an additional partial differential equation: the moving mesh equation. In addition, a scalar (or vector) valued monitor function is used to determine the optimal mesh vertices distribution. From the mathematical viewpoint, the ALE-transformation maps one domain into another and are therefore linked to geometry aspects. Furthermore, they have common features with differential geometry (i.e., optimal transport) and mean curvature flows.

5.3 ALE-FSI

In the present chapter, we discuss fluid-structure interaction problems in ALE coordinates. The ALE mapping is defined by solving an additional partial differential equation, for which we present three possibilities. With the help of this mapping, we realize the fluid mesh motion. Next, the coupled framework is described in a coupled fashion, leading to a variationally-coupled monolithic representation of fluid-structure interaction. Our terminology to describe the monolithic approach is based on [69–71, 140, 141, 207].

Firstly, we need to define the ALE transformation:

Definition 5.2. *The ALE mapping is defined in terms of the fluid mesh displacement $\hat{u}_f$ such that*

$$\hat{\mathcal{A}}(\hat{x},t) : \widehat{\Omega}_f \times I \to \Omega_f, \quad \text{with } \hat{\mathcal{A}}(\hat{x},t) = \hat{x} + \hat{u}(\hat{x},t). \tag{25}$$

It is specified through the deformation gradient and its determinant

$$\widehat{F} := \widehat{\nabla}\hat{\mathcal{A}} = \hat{I} + \widehat{\nabla}\hat{u}, \quad \hat{J} := det(\widehat{F}). \tag{26}$$

Furthermore, function values in Eulerian and Lagrangian coordinates are identified by

$$u(x) =: \hat{u}(\hat{x}), \quad \text{with } x = \hat{\mathcal{A}}(\hat{x},t). \tag{27}$$

44

The mesh velocity is defined by $w := \partial_t \hat{\mathcal{A}}$. ⋄

To formulate FSI in ALE coordinates, there are two possible ways presented in the literature:

- ALE_{dm}: We compute the fluid equations on the deformed configuration Ω and move the mesh explicitly.

- ALE_{fx}: All fluid equations are transformed onto the fixed reference configuration $\widehat{\Omega}$. In our work, we prefer this second possibility.

5.3.1 The ALE time derivative

The derivation of both approaches follows the same rules that we sketch in the following. Let us briefly explain the relations between different time derivatives for different frameworks (such as the Lagrangian, the Eulerian, and the ALE frameworks). In a Lagrangian setting, the total and the partial derivatives coincide:

$$d_t \hat{f}(\hat{x}, t) = \partial_t \hat{f}(\hat{x}, t).$$

In an Eulerian framework, we find the following standard relation between the *material time-derivative* (the total time derivative) $d_t f$ and the partial time derivative $\partial_t f$:

$$d_t f(x, t) = v \cdot \nabla f + \partial_t f(x, t),$$

where the additional term $v \cdot \nabla f$ is referred to as a transport term. In an analogous fashion, we extend this concept to define the *ALE time-derivative*

$$\hat{\partial}_t f(x, t) := \partial_t|_{\hat{\mathcal{A}}} f(x, t) = w \cdot \nabla f + \partial_t f(x, t), \tag{28}$$

where the transport term appears due to the motion of the computational domain. In a Lagrangian description, we have $w = 0$. In contrast, it holds $w = v$ in an Eulerian framework. The ALE time-derivative has important ramifications for the numerical discretization of ALE equations; for a deeper discussion, we refer to [87], p. 88.
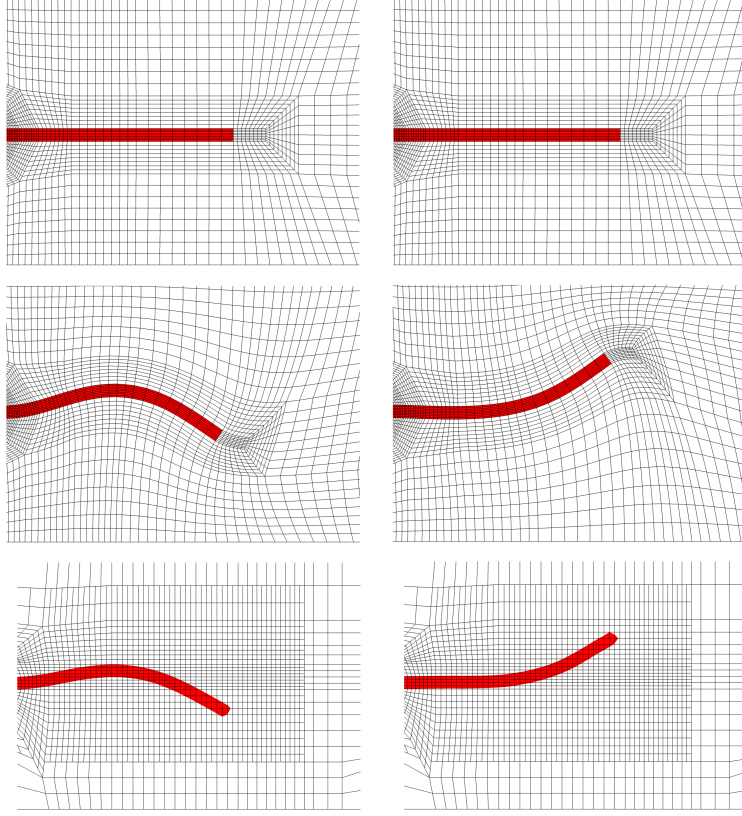
Figure 11: Comparison of cell occupation and computational domains for two time steps between the ALE$_{fx}$ (top and middle) and Eulerian (bottom) method. In ALE$_{fx}$, all computations are done in the same fixed reference domain $\widehat{\Omega}$ (top). In particular, a specific cell remains all times the same material (here, an elastic structure in red), i.e., Ω_f and Ω_s are time-independent. The mesh movement is hidden in the transformation $\vec{F}$ and J. The physical (current) ALE domain $\Omega(t)$ including the mesh movement is displayed in the middle. In contrast, the computation with the Eulerian approach is performed on a fixed (time-independent) mesh Ω_E (bottom). However, the two sub-domains for the structure and the fluid $\Omega_{s,E}$ and $\Omega_{f,E}$ change in each time step because the material id of a cell might change since the elastic structure (red) moves freely through the mesh. Figures partially taken from [253].

46

5.3.2 Navier-Stokes in ALE coordinates

Inserting now the ALE time derivative into the Navier-Stokes equations, we obtain:

Problem 5.3 (ALE$_{dm}$ fluid problem). *Find*
$\{v_f, p_f\} \in \{v_f^D + V_f^0\} \times L_f^0$ *such that the initial data satisfy* $v_f(0) = v_f^0$, *and for almost all time steps* $t \in I$ *holds:*

$$\rho_f(\hat{\partial}_t v_f, \psi^v)_{\Omega_f} + \rho_f\big((v_f - w) \cdot \nabla v_f, \psi^v\big)_{\Omega_f}$$
$$+ (\sigma_f, \nabla\psi^v)_{\Omega_f} - \langle \sigma_f n_f, \nabla\psi^v \rangle_{\Gamma_{f,N} \cup \Gamma_i} - \rho_f(f, \psi^v)_{\Omega_f} = 0 \quad \forall \psi^v \in V_f^0, \qquad (29)$$
$$(div\, v_f, \psi^p)_{\Omega_f} = 0 \quad \forall \psi^p \in L_f^0,$$

with the Cauchy stress tensor

$$\sigma_f = -p_f I + 2\rho_f \nu_f D(v_f) = -p_f I + \rho_f \nu_f (\nabla v_f + \nabla v_f^T),$$

and a correction term on the outflow boundary ([134]):

$$g := -\rho_f \nu_f \nabla v_f^T \quad on\ \Gamma_{f,N} = \Gamma_{out}.$$

This is now the place in which ALE$_{fx}$ and ALE$_{dm}$ differ. Working with ALE$_{dm}$, we keep the above equations and solve these equations on the current domain Ω with appropriate discretization of the ALE time derivatives[16]:

$$\hat{\partial}_t v_f = \frac{1}{k}(v_f^n - v_f^{n-1} \circ \hat{\mathcal{A}}^{n-1} \circ (\hat{\mathcal{A}}^n)^{-1}).$$

Here, we work with an ALE map $\hat{\mathcal{A}}$ which is defined from the previous time step t_{n-1} to the the present time step t_n. Thus, the reference configuration at time step t_n is denoted by Ω^n. Moreover, $v^n \in \Omega^n$ is used as an approximation to $v(t_n)$, which is transported from Ω^n to any other configuration Ω^l (for $l \neq n$) through the ALE map ([183]):

$$\hat{\mathcal{A}}_{n,l} = \hat{\mathcal{A}}_l \circ \hat{\mathcal{A}}_n^{-1}.$$

On the other hand, in ALE$_{fx}$, we use the fundamental theorem of calculus [154] in higher dimensions, and we obtain the Navier-Stokes equations on a fixed domain. This formulation introduces additional geometric nonlinearities in the equations (rather than in terms of the mesh) and they are formulated in terms of $\widehat{F}$ and $\hat{J}$.

Remark 5.4. *Reading the literature, it seems that more people use ALE$_{dm}$ to formulate fluid-structure interaction problems. Of course, the equations look much nicer than introducing all transformation rules. However, we want to emphasize that in our taste, the ALE$_{fx}$ approach is a more consistent way since all equations are formulated on the same domain $\widehat{\Omega}$ leading to a consistent variational-monolithic coupling scheme. From the computational viewpoint it is maybe just a matter of taste.* ⋄

---

[16]Many thanks to my present colleague Huidong Yang for fruitful discussions!

Proposition 5.5 (A claim without rigorous proof). *ALE_{fx} and ALE_{dm} are equivalent methods.*

Let us know work with ALE_{fx} and explain things in more detail. The boundary of $\widehat{\Omega}_f$ is divided into three non-overlapping parts $\partial\widehat{\Omega}_f = \widehat{\Gamma}_{f,D} \cup \widehat{\Gamma}_{f,N} \cup \widehat{\Gamma}_i$, where $\widehat{\Gamma}_i$ denotes later the interface and it coincides with $\widehat{\Gamma}_{f,N}$ in the case of pure fluid problems. We prescribe

$$\hat{u} = \hat{u}_D, \quad \text{and} \quad \hat{v} = \hat{v}_D \quad \text{on } \widehat{\Gamma}_{f,D},$$

$$\hat{J}\widehat{\sigma}_f \widehat{F}^{-T}\hat{n}_f = \hat{g} \quad \text{on } \widehat{\Gamma}_{f,N}.$$

Let $\hat{v}_f^D$ a suitable extension of Dirichlet inflow data. Then, the variational form in $\widehat{\Omega}_f$ reads:

Problem 5.6 (ALE_{fx} fluid problem). *Find*
$\{\hat{v}_f, \hat{p}_f\} \in \{\hat{v}_f^D + \hat{V}_f^0\} \times \hat{L}_f^0$ such that the initial data $\hat{v}_f(0) = \hat{v}_f^0$ are satisfied, and for almost all time steps $t \in I$ holds:

$$\hat{\rho}_f(\hat{J}\partial_t\hat{v}_f, \hat{\psi}^v)_{\widehat{\Omega}_f} + \hat{\rho}_f(\hat{J}\widehat{F}^{-1}(\hat{v}_f - \hat{w}) \cdot \widehat{\nabla}\hat{v}_f, \hat{\psi}^v)_{\widehat{\Omega}_f} + (\hat{J}\widehat{\sigma}_f\widehat{F}^{-T}, \widehat{\nabla}\hat{\psi}^v)_{\widehat{\Omega}_f}$$

$$= \langle \hat{J}\hat{g}_f\widehat{F}^{-T}\hat{n}_f, \hat{\psi}^v \rangle_{\widehat{\Gamma}_{f,N}} + \langle \hat{J}\widehat{\sigma}_f\widehat{F}^{-T}\hat{n}_f, \hat{\psi}^v \rangle_{\widehat{\Gamma}_i} + \hat{\rho}_f(\hat{J}\hat{f}_f, \hat{\psi}^v)_{\widehat{\Omega}_f},$$

$$(\widehat{div}(\hat{J}\widehat{F}^{-1}\hat{v}_f), \hat{\psi}^p)_{\widehat{\Omega}_f} = 0,$$

for all $\hat{\psi}^v \in \hat{V}_f^0$ and $\hat{\psi}^p \in \hat{L}_f^0$, and with the transformed Cauchy stress tensor

$$\widehat{\sigma}_f = -\hat{p}_f\hat{I} + 2\hat{\rho}_f\nu_f\widehat{D}(\hat{v}_f) = -\hat{p}_f\hat{I} + 2\hat{\rho}_f\nu_f(\widehat{\nabla}\hat{v}_f\widehat{F}^{-1} + \widehat{F}^{-T}\widehat{\nabla}\hat{v}_f^T). \tag{30}$$

As before, $\hat{g}_f$ accounts for (possible) Neumann data, for instance, a correction term for the do-nothing outflow condition (see Figure 4.8.0.2 if this correction term is not applied):

$$\hat{g}_f = -\hat{\rho}_f\nu_f\widehat{F}^{-T}\widehat{\nabla}\hat{v}_f^T \quad \text{on } \widehat{\Gamma}_{f,N} = \widehat{\Gamma}_{\text{out}}. \tag{31}$$

Remark 5.7 (At all times). *We use from time to time the notation <u>for all times</u> or <u>for almost all time steps</u>. Please notice that this is a mathematical persnicketiness[17] on the continuous level. As alternative, we could have used the notation $L^2(I, X)$ for time-dependent Sobolev spaces. Of course, on the discretized level, we compute at each (discrete) timestep a solution to our problem. ◇*

Remark 5.8 (Variational-monolithic coupling; see also Section 5.3.6). *Coupling fluid flows with structural deformations along an interface $\widehat{\Gamma}_i$ requires the fulfillment of two coupling conditions. Fluid flows require a Dirichlet condition on $\widehat{\Gamma}_i$, i.e., the continuity of the velocities is strongly enforced in the corresponding Sobolev spaces. The structural problem is driven by the normal stresses that act on $\widehat{\Gamma}_i$ caused by the fluid. These normal stresses are achieved with the boundary term:*

$$\langle \hat{J}\widehat{\sigma}_f\widehat{F}^{-T}\hat{n}_f, \hat{\psi}^v \rangle_{\widehat{\Gamma}_i} \quad \text{on } \widehat{\Gamma}_i.$$

◇

---

[17]Spitzfindigkeit

Remark 5.9. *Finally, we note that the do-nothing conditions implicitly normalizes the pressure by*

$$\int_{\widehat{\Gamma}_{out}} \hat{p} \, d\hat{s} = 0.$$

In such a case, it is sufficient to work with the space $\hat{L}_f$ instead of $\hat{L}_f^0$. ⋄

5.3.3 On the regularity of the ALE mapping

Because we work with both moving spaces and fixed spaces for fluid flows, we recall the findings of [183], which provide the regularity conditions of the ALE mapping.

Problem 5.10. *The ALE mapping $\hat{\mathcal{A}}$ has to be defined such that $\hat{v} \in H^1(\widehat{\Omega})$ if and only if $v = \hat{v} \circ \hat{\mathcal{A}}^{-1} \in H^1(\Omega)$.*

Using classical function spaces, a sufficient condition is that $\hat{\mathcal{A}}$ is a C^1-diffeomorphism:

$$\hat{\mathcal{A}} \in C^1(\overline{\widehat{\Omega}}), \quad \hat{\mathcal{A}}^{-1} \in C^1(\overline{\Omega}),$$

and

$$\widehat{F} \in L^\infty(\widehat{\Omega}), \quad F \in L^\infty(\Omega).$$

This requirement must be weakened because classical function spaces are inappropriate when approximate solutions with help of a Galerkin finite element scheme are computed.

Proposition 5.11. *Let $\widehat{\Omega}$ be a bounded domain with $C^{1,1}$-boundary (see, e.g., [260]). Let $\hat{\mathcal{A}}$ be invertible in the closure of $\widehat{\Omega}$ and there holds for each $t \in I$ the two conditions*

- *$\Omega = \hat{\mathcal{A}}(\widehat{\Omega})$ is bounded and $\partial\Omega$ is Lipschitz-continuous.*

- *Let $\hat{\mathcal{A}} \in W^{1,\infty}(\widehat{\Omega})$ and $\hat{\mathcal{A}}^{-1} \in W^{1,\infty}(\Omega)$.*

Then, $v \in H^1(\Omega)$ if and only if $\hat{v} = v \circ \hat{\mathcal{A}} \in H^1(\widehat{\Omega})$. Moreover, the corresponding norms are equivalent.

For a proof of this Lemma, we refer to [183].

Remark 5.12 (Accessing the ALE mapping regularity). *As previously explained, as quantity to measure the ALE regularity, we can consult the determinant $\hat{J}$ of the deformation gradient. In particular, $\hat{J} > 0$ if $\|\hat{u}_f\|_{W^{2,p}(\widehat{\Omega}_f;\mathbb{R}^d)}$ is sufficiently small and we see that this implies $\widehat{\mathcal{A}}$ and $\widehat{\mathcal{A}}^{-1} \in W^{1,\infty}(\widehat{\Omega};\mathbb{R}^{d\times d})$. Furthermore, the more we bound the adaptation factor $\hat{J}$ away from zero, the better the regularity. In other words, all mesh motion models aim to control $\hat{J}$ and try to bound this quantity away from zero. Here, it is clear from the theoretical standpoint (and numerical tests (see Figures 13 and 14 and 15) confirm the theory) that biharmonic mesh motion leads to higher regularity than harmonic or linear-elastic models.* ⋄

5.3.4 Interface coupling conditions

In this section, we state the interface coupling conditions for fluid-structure interaction. The coupling of the fluid with the structure equations must satisfy three conditions: continuity of velocities, continuity of normal stresses, and geometrical coupling. In the main part of this section, we focus our attention on formulations for defining the ALE mapping $\hat{\mathcal{A}}$.

5.3.4.1 Physical conditions: continuity of velocity and stress The velocity field must be continuous on the interface (which is a Dirichlet-like condition seen from the fluid side). Sufficient regularity for the structure velocity is taken as assumption, such that this velocity can be given to the fluid problem. In detail, we have

$$v_f = w = v_s \quad \text{on } \Gamma_i. \tag{32}$$

To complete the structure problem, we must enforce the balance of the normal stresses on the interface:

$$\hat{J}\hat{\sigma}_f \widehat{F}^{-T}\hat{n}_f + \widehat{F}\widehat{\Sigma}\hat{n}_s + \gamma_s \hat{\epsilon}(\hat{v}_s)\hat{n}_s = 0 \quad \text{on } \widehat{\Gamma}_i. \tag{33}$$

This condition corresponds to a Neumann-like boundary condition for the structure subsystem.

Remark 5.13. *Condition* (33) *is formulated for a general solid equation including strong damping. Removing the term* $\gamma_s \hat{\epsilon}(\hat{v}_s)\hat{n}_s$ *brings you to the standard formulation that you find in the literature.* ⋄

5.3.4.2 Geometric coupling (the third condition) For fluid-structure interaction based on the 'arbitrary Lagrangian-Eulerian' framework (ALE), the choice of appropriate fluid mesh movement is important. In general, an additional elasticity equation is solved [51, 221, 233]. For moderate deformations, one can pose an auxiliary Laplace problem [48, 68, 259] that is known as harmonic mesh motion. More advanced equations from linear elasticity (including Jacobi-based stiffening) are also available [213, 233]. Thirdly, we also use (for mesh moving) the fourth-order biharmonic equation that others have studied for fluid flows in ALE coordinates [130]. It was also shown there, that using the biharmonic model provides greater freedom in the choice of boundary and interface conditions. In general, the biharmonic mesh motion model leads to a smoother mesh (and larger deformations of the structure) compared to the mesh motion models based on second order partial differential equations [250]. Although the mesh behavior of the harmonic and the biharmonic mesh motion models were analyzed in [130] for different applications, we upgrade these concepts to fluid-structure interaction problems. Quantitative comparisons are shown in the Figures 14 and 15 (taken from [250]).

In the discrete setting of the coupled problem, the moving fluid domain follows the motion of the interface (it is therefore a geometrical coupling):

$$\hat{u}_f = \hat{u}_s \quad \text{on } \widehat{\Gamma}_i, \tag{34}$$

from which we obtain immediately $\hat{w} = \hat{v}_s$ with temporal differentiation.

We define the ALE mapping in terms of the displacement variable, such that we obtain

$$\hat{u}(\hat{x}) = \hat{\mathcal{A}}(\hat{x}) - \hat{x}.$$

Inside the fluid domain $\widehat{\Omega}_f$ this operation is arbitrary and it is described by means of a partial differential equation, such that we produce a smooth evolution of the fluid mesh. In the following, we discuss the three possible partial differential equations in detail, which can be used for fluid mesh moving. In two dimensional configurations, the mesh moves in x- and y-direction, which allows us to find a vector-valued artificial displacement variable

$$\hat{u}_f := (\hat{u}_f^{(1)}, \hat{u}_f^{(2)}, \hat{u}_f^{(3)}) := (\hat{u}_f^{(x)}, \hat{u}_f^{(y)}, \hat{u}_f^{(z)}).$$

We need the single components of $\hat{u}_f$ below to apply different types of boundary conditions to the biharmonic mesh motion model. In the following, the formal description of the first two mesh motion models coincides and only differ in the definition of the stress tensors $\widehat{\sigma}_{\text{mesh}}$.

5.3.5 Mesh motion models

5.3.5.1 Mesh motion with a harmonic model The simplest model is based on the harmonic equation, which reads in strong formulation:

$$-\widehat{\text{div}}(\hat{\sigma}_{\text{mesh}}) = 0, \quad \hat{u}_f = \hat{u}_s \text{ on } \widehat{\Gamma}_i, \quad \hat{u}_f = 0 \text{ on } \partial\widehat{\Omega}_f \setminus \widehat{\Gamma}_i, \tag{35}$$

with

$$\widehat{\sigma}_{\text{mesh}} = \alpha_u \widehat{\nabla} \hat{u}_f.$$

The monitor function $\alpha_u := \alpha_u(\hat{x})$ (for a solid equation, we would just call it diffusion parameter) is chosen such that a good fluid mesh quality is guaranteed. The oldest idea steems from [259]. As second idea, we can choose

$$\alpha_u(\hat{x}) = a + b\exp(-c\hat{d}), \tag{36}$$

with certain constants $a, b, c > 0$. The Euclidian distance of a point $\hat{x}$ to the interface $\widehat{\Gamma}_i$ is denoted by $\hat{d} = |\hat{x} - \widehat{\Gamma}_i|$. Another, even simpler, strategy was proposed by Tezduyar et al. [233], which was further developed by Stein et al. [221]. They propose to choose as monitor function:

$$\alpha_u(\hat{x}) = \hat{J}^{-1}. \tag{37}$$

This choice works well because mesh cell distortion appears in the vicinity of $\widehat{\Gamma}_i$. That means $\hat{J} \searrow 0$ near $\widehat{\Gamma}_i$, and consequently $\alpha_u(\hat{x}) \gg 0$ near $\widehat{\Gamma}_i$. By reason that high diffusion causes low mesh movement, the quality of the fluid mesh is maintained. For a comparison of different choices of $\alpha_u := \alpha_u(\hat{x})$, we refer to [250].

Remark 5.14. *Using model (37) leads to a nonlinear equation for $\widehat{\sigma}_{mesh}$ since $\hat{u}$ is used to define $\hat{J}$.* ⋄

5.3.5.2 Mesh motion with a linear elastic model The equation of linear elasticity is formally based on the well-known momentum equations from structural mechanics as introduced previously. In a steady-state regime, we obtain the following equation defining a static equilibrium:

$$-\widehat{\mathrm{div}}(\widehat{\sigma}_{\mathrm{mesh}}) = 0, \quad \hat{u}_f = \hat{u}_s \text{ on } \widehat{\Gamma}_i, \quad \hat{u}_f = 0 \text{ on } \partial\widehat{\Omega}_f \setminus \widehat{\Gamma}_i,$$

where $\widehat{\sigma}_{\mathrm{mesh}}$ is formally equivalent to the STVK constitutive tensor in Equation (4.31). It is given by

$$\widehat{\sigma}_{\mathrm{mesh}} := \alpha_\lambda (\mathrm{tr}\,\widehat{E}_{lin})\hat{I} + 2\alpha_\mu \widehat{E}_{lin}, \tag{38}$$

where $\widehat{E}_{lin}$ was defined in Definition 4.14. The mesh monitor parameters $\alpha_\lambda := \alpha_\lambda(\hat{x})$ and $\alpha_\mu := \alpha_\mu(\hat{x})$ are chosen in a way, such that a good fluid mesh quality is guaranteed. By virtue of (14), we compute α_λ and α_μ from the Young modulus E_Y and the Poisson ration ν_s. Therefore, we choose E_Y according to (36) or (37). Further, we choose a negative Poisson ratio (recall that $\nu_s \in (-1, 0.5]$). Materials with negative Poisson ratio belongs to auxetic materials and they become thinner in the perpendicular direction, when they are compressed. This is a useful property for the evolution of the fluid mesh. We refer the reader again to [221] (and references cited therein) for other choices of α_λ and α_μ.

5.3.5.3 Mesh motion with a biharmonic model Using the biharmonic mesh model provides much more freedom in choosing boundary conditions [57, 130]. In these notes, solving the biharmonic equation is introduced as a third possible fluid mesh deformation:

$$\widehat{\Delta}^2 \hat{u}_f = 0 \quad \text{in } \widehat{\Omega}_f, \quad \hat{u}_f = \hat{u}_s \text{ and } \partial\hat{u}_f = \partial\hat{u}_s \quad \text{on } \widehat{\Gamma}_i, \quad \hat{u}_f = \partial\hat{u}_f = 0 \quad \text{on } \partial\widehat{\Omega}_f.$$

This model is considered in a mixed formulation in the sense of Ciarlet [57]. As before, an artificial material parameter is used to control the mesh motion. Then, we deduce

$$\hat{\eta}_f = -\alpha_u \hat{\Delta}\hat{u}_f \quad \text{and} \quad -\alpha_u \hat{\Delta}\hat{\eta}_f = 0. \tag{39}$$

It is more convenient to consider the single component functions $\hat{u}_f^{(1)}$, $\hat{u}_f^{(2)}$ and $\hat{u}_f^{(3)}$,

$$\hat{\eta}_f^{(1)} = -\alpha_u \hat{\Delta}\hat{u}_f^{(1)} \quad \text{and} \quad -\alpha_u \hat{\Delta}\hat{\eta}_f^{(1)} = 0, \tag{40}$$

$$\hat{\eta}_f^{(2)} = -\alpha_u \hat{\Delta}\hat{u}_f^{(2)} \quad \text{and} \quad -\alpha_u \hat{\Delta}\hat{\eta}_f^{(2)} = 0, \tag{41}$$

$$\hat{\eta}_f^{(3)} = -\alpha_u \hat{\Delta}\hat{u}_f^{(3)} \quad \text{and} \quad -\alpha_u \hat{\Delta}\hat{\eta}_f^{(3)} = 0. \tag{42}$$

We utilize two types of boundary conditions. First, we pose the *first type of boundary conditions* (that corresponds to conditions of a clamped plate)

$$\hat{u}_f^{(k)} = \partial_n \hat{u}_f^{(k)} = 0 \quad \text{on } \partial\widehat{\Omega}_f \setminus \widehat{\Gamma}_i, \quad \text{for } k = 1, 2, 3. \tag{43}$$

Second, we are concerned with a mixture of boundary conditions

$$\hat{u}_f^{(1)} = \partial_n \hat{u}_f^{(1)} = 0 \quad \text{and} \quad \hat{\eta}_f^{(1)} = \partial_n \hat{\eta}_f^{(1)} = 0 \quad \text{on } \widehat{\Gamma}_{\text{in}} \cup \widehat{\Gamma}_{\text{out}}, \tag{44}$$

$$\hat{u}_f^{(2)} = \partial_n \hat{u}_f^{(2)} = 0 \quad \text{and} \quad \hat{\eta}_f^{(2)} = \partial_n \hat{\eta}_f^{(2)} = 0 \quad \text{on } \widehat{\Gamma}_{\text{wall}}, \quad \text{on } \widehat{\Gamma}_{\text{in}} \cup \widehat{\Gamma}_{\text{out}}, \tag{45}$$

$$\hat{u}_f^{(3)} = \partial_n \hat{u}_f^{(3)} = 0 \quad \text{and} \quad \hat{\eta}_f^{(3)} = \partial_n \hat{\eta}_f^{(3)} = 0 \quad \text{on } \widehat{\Gamma}_{\text{wall}}. \tag{46}$$

which we call *second type of boundary conditions*. In particular, the conditions

$$\hat{\eta}_f^{(k)} = \partial_n \hat{\eta}_f^{(k)} = 0 \quad \text{on } \widehat{\Gamma}_{\text{in}} \cup \widehat{\Gamma}_{\text{out}}, \quad \text{for } k = 1, 2, 3, \tag{47}$$

mean, that a plate is left free along this boundary part. Using biharmonic mesh motion, we also must enforce two conditions on the interface:

$$\hat{u}_f = \hat{u}_s \quad \text{and} \quad \partial_n \hat{u}_f = \partial_n \hat{u}_s \quad \text{on } \widehat{\Gamma}_i.$$

Remark 5.15. *Using the second type of boundary conditions in a rectangular domain where the coordinate axes match the Cartesian coordinate system, leads to mesh movement only in the tangential direction. This effect reduces mesh cell distortion because only the perpendicular directions of $\hat{u}_f$ and $\hat{\eta}_f$ are constrained to zero at the different parts of $\partial \widehat{\Omega}$. The effects of these boundary conditions are examined in Figure 13 ⋄*

Remark 5.16 (Mixed system on non-convex domains). *It has been shown in [266], that the solutions of the biharmonic problem do not correspond (in general) to the mixed system if the problem is considered on a non-convex domain. This is exactly the case in our situations. However, we emphasize that the mesh motion problem is an artificial problem and we are not interested in its accurate physical solution but rather in a reasonable approximation in order to move the mesh. ⋄*

Remark 5.17 (Tolerance of the numerical solution). *We notice again that the moving mesh equations are auxiliary equations to move the mesh. This means in particular, we are still mainly interested in the solution of the physical equations (fluid and solid). Consequently, for the numerical solution of the mesh moving equations a much lower tolerance can be employed for the nonlinear and/or linear solver. ⋄*
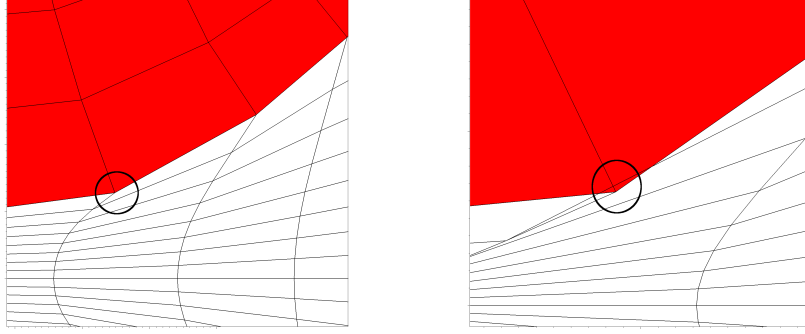
Figure 12: Mesh tangling/degeneration in which the inner angle 180 degree opening (left) and mesh racing in which solid mesh cells (in red) intersect illegally with fluid cells (in white) - right figure.
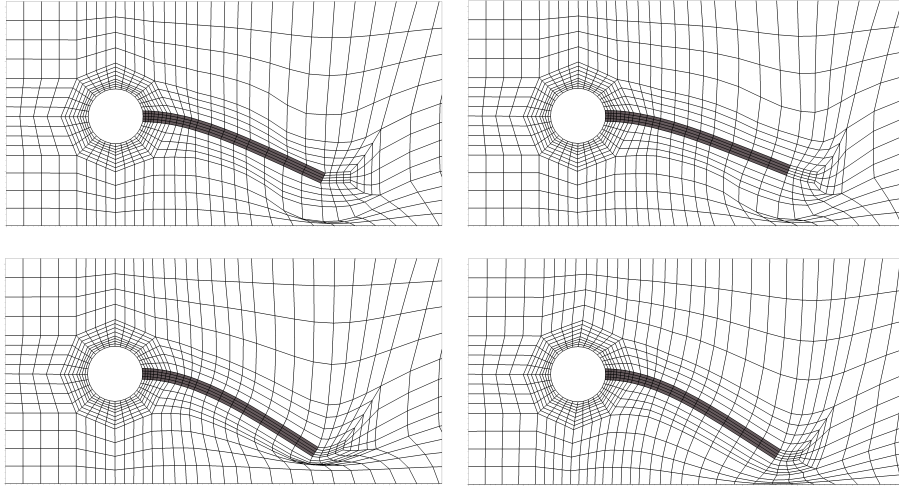
Figure 13: CSM 4 test [250] with harmonic and linear-elastic mesh motion models on top. Both models lead to mesh distortion close to the lower boundary. At the bottom, meshes using biharmonic mesh motion are displayed, which perform significantly better near the tip of the beam. In addition, we observe node-clustering that is a typical result of mesh motion.
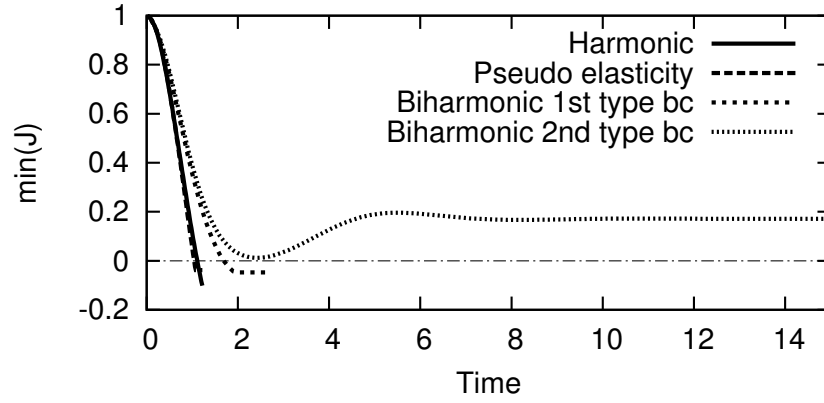
Figure 14: Function plots of $\min(\hat{J})$ for the mesh motion models of the CSM 4 test. Degeneration of mesh cells corresponds to negative values of $\hat{J}$, arising in the first three models.
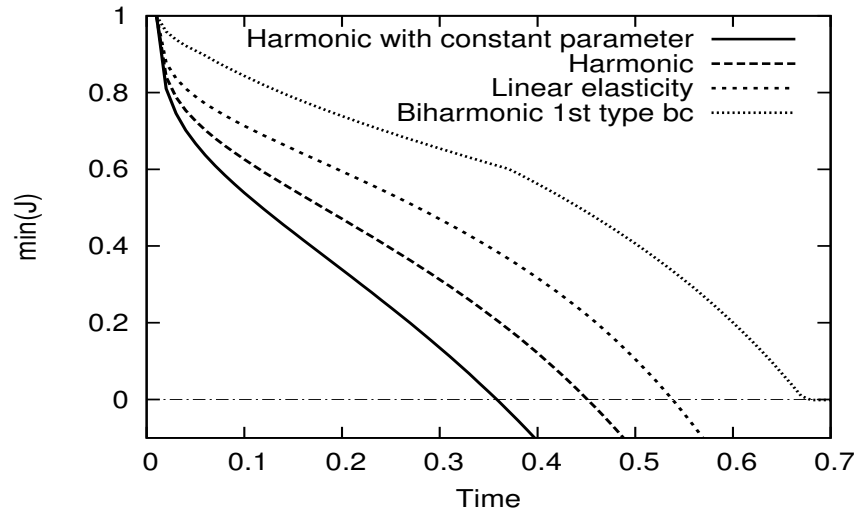
Figure 15: Function plots of $\min(\hat{J})$ for the mesh motion models of the membrane on fluid test (proposed in [18] and re-computed in [250]). Degeneration of mesh cells corresponds to negative values of $\hat{J}$, arising in the first three models.

5.3.6 Variational-monolithic coupling

Before we state the coupled FSI problem, let us briefly recapitulate our philosophy for coupling. In these notes, we aim for a consistent variational-monolithic coupling scheme in which we need all equations defined in the same domain; therefore, ALE_{fx} was introduced. In variational monolithic coupling, Neumann-like interface conditions, like the continuity of normal stresses are fulfilled exactly in a weak sense on the continuous level:

$$\langle \hat{J}\hat{\sigma}_f \widehat{F}^{-T} \hat{n}_f, \varphi \rangle + \langle \widehat{F}\widehat{\Sigma}\hat{n}_s, \varphi \rangle + \langle \gamma_s \hat{\epsilon}(\hat{v}_s)\hat{n}_s, \varphi \rangle = 0 \quad \forall \varphi \in V. \tag{48}$$

The continuity of flow conditions,

$$v_f = v_s,$$

are incorporated directly in the Sobolev spaces as usually done for Dirichlet conditions.

Remark 5.18. *We use the same coupling idea for the fully Eulerian approach described in Section 5.6. Again: this is possible since all equations are defined in the same domain; there it is Ω.*

5.3.7 A variational-monolithic FSI-formulation using ALE_{fx}

With the previous preparations at hand, in this section, we define the monolithically coupled fluid-structure interaction problems employing the ALE_{fx} approach. Thus, we define the setting in a fixed domain and formulate the equations in a fashion that can be used in a straightforward way for the implementation. The coupled strong problem (with the fluid equations defined in a moving domain Ω) can be formulated as illustrated previously, see [87], p. 120-121, and [19]. The corresponding weak formulations have also been derived elsewhere [19, 180].

The definitions of the fully coupled problems include three types of nonlinearities that are divided into two groups. The physical nonlinearities includes the convection term for the fluid and the nonlinear structure model, whereas the additional nonlinearity induced by the ALE transformation is a so-called geometric nonlinearity.

Then, the weak form reads:

Problem 5.19 (ALE_{fx} FSI with harmonic and linear-elastic mesh motion)**.** *Find* $\{\hat{v}_f, \hat{v}_s, \hat{u}_f, \hat{u}_s, \hat{p}_f, \hat{p}_s\} \in \{\hat{v}_f^D + \hat{V}_{f,\hat{v}}^0\} \times \hat{L}_s \times \{\hat{u}_f^D + \hat{V}_{f,\hat{u}}^0\} \times \{\hat{u}_s^D + \hat{V}_s^0\} \times \hat{L}_f^0 \times \hat{L}_s^0$, *such that* $\hat{v}_f(0) = \hat{v}_f^0$, $\hat{v}_s(0) = \hat{v}_s^0$, $\hat{u}_f(0) = \hat{u}_f^0$, *and* $\hat{u}_s(0) = \hat{u}_s^0$ *are satisfied, and for almost*

all time steps $t \in I$ holds:

Fluid momentum $\begin{cases} (\hat{J}\hat{\rho}_f \partial_t \hat{v}_f, \hat{\psi}^v)_{\widehat{\Omega}_f} + (\hat{\rho}_f \hat{J}(\widehat{F}^{-1}(\hat{v}_f - \hat{w}) \cdot \widehat{\nabla})\hat{v}_f), \hat{\psi}^v)_{\widehat{\Omega}_f} \\ + (\hat{J}\hat{\sigma}_f \widehat{F}^{-T}, \widehat{\nabla}\hat{\psi}^v)_{\widehat{\Omega}_f} - \langle \hat{g}_f, \hat{\psi}^v \rangle_{\widehat{\Gamma}_N} - (\hat{\rho}_f \hat{J}\hat{f}_f, \hat{\psi}^v)_{\widehat{\Omega}_f} \quad = 0 \quad \forall \hat{\psi}^v \in \hat{V}^0_{f, \widehat{\Gamma}_i}, \end{cases}$

Solid momentum, 1st eq. $\begin{cases} (\hat{\rho}_s \partial_t \hat{v}_s, \hat{\psi}^v)_{\widehat{\Omega}_s} + (\widehat{F}\widehat{\Sigma}, \widehat{\nabla}\hat{\psi}^v)_{\widehat{\Omega}_s} \\ + \gamma_w(\hat{v}_s, \hat{\psi}^v)_{\widehat{\Omega}_s} + \gamma_s(\hat{\epsilon}(\hat{v}_s), \widehat{\nabla}\hat{\psi}^v)_{\widehat{\Omega}_s} - (\hat{\rho}_s \hat{f}_s, \hat{\psi}^v)_{\widehat{\Omega}_s} \quad = 0 \quad \forall \hat{\psi}^v \in \hat{V}^0_s, \end{cases}$

Fluid mesh motion $\begin{cases} (\hat{\sigma}_{mesh}, \widehat{\nabla}\hat{\psi}^u)_{\widehat{\Omega}_f} \quad = 0 \quad \forall \hat{\psi}^u \in \hat{V}^0_{f, \hat{u}, \widehat{\Gamma}_i}, \end{cases}$

Solid momentum, 2nd eq. $\begin{cases} \hat{\rho}_s(\partial_t \hat{u}_s - \hat{v}_s, \hat{\psi}^u)_{\widehat{\Omega}_s} \quad = 0 \quad \forall \hat{\psi}^u \in \hat{L}_s, \end{cases}$

Fluid mass conservation $\begin{cases} (\widehat{div}(\hat{J}\widehat{F}^{-1}\hat{v}_f), \hat{\psi}^p)_{\widehat{\Omega}_f} \quad = 0 \quad \forall \hat{\psi}^p \in \hat{L}^0_f, \end{cases}$

Solid mass conservation $\begin{cases} (\hat{P}_s, \hat{\psi}^p)_{\widehat{\Omega}_s} \quad = 0 \quad \forall \hat{\psi}^p \in \hat{L}^0_s, \end{cases}$

with $\hat{\rho}_f$, $\hat{\rho}_s$, ν_f, μ_s, λ_s, $\widehat{F}$, and $\hat{J}$ as defined before. The stress tensors $\hat{\sigma}_f$, $\widehat{\Sigma}$, and $\hat{\sigma}_{mesh}$ are defined in the Equations (30), (13), (4.31), and in (35) and (38), respectively. The pressure-related quantity in the last equation is determined by $\hat{P}_s = \hat{J} - 1$ (volume conserving), using incompressible materials, such as the INH or the IMR material. In the case of the STVK material, the last term is not present.

Recall that we use the mixed form of the wave equation, for this reason we have a decomposition of the momentum equation into two subequations.

Next, we state the monolithic setting for fluid-structure interaction with a biharmonic mesh motion model utilizing the first type of boundary conditions:

Problem 5.20 (ALE$_{fx}$ FSI with biharmonic mesh motion). *Find*
$\{\hat{v}_f, \hat{v}_s, \hat{u}_f, \hat{u}_s, \hat{\eta}_f, \hat{\eta}_s, \hat{p}_f, \hat{p}_s\} \in \{\hat{v}_f^D + \hat{V}_{f,\hat{v}}^0\} \times \hat{L}_s \times \{\hat{u}_f^D + \hat{V}_{f,\hat{u}}^0\} \times \{\hat{u}_s^D + \hat{V}_s^0\} \times \hat{V}_f \times$
$\hat{V}_s \times \hat{L}_f^0 \times \hat{L}_s^0$, *such that* $\hat{v}_f(0) = \hat{v}_f^0$, $\hat{v}_s(0) = \hat{v}_s^0$, $\hat{u}_f(0) = \hat{u}_f^0$, $\hat{u}_s(0) = \hat{u}_s^0$ *are satisfied,*
for almost all time steps $t \in I$, *and*

$$(\hat{J}\hat{\rho}_f \partial_t \hat{v}_f, \hat{\psi}^v)_{\widehat{\Omega}_f} + (\hat{\rho}_f \hat{J}(\widehat{F}^{-1}(\hat{v}_f - \hat{w}) \cdot \widehat{\nabla})\hat{v}_f), \hat{\psi}^v)_{\widehat{\Omega}_f}$$
$$+(\hat{J}\hat{\sigma}_f \widehat{F}^{-T}, \widehat{\nabla}\hat{\psi}^v)_{\widehat{\Omega}_f} - \langle \hat{g}_f, \hat{\psi}^v \rangle_{\widehat{\Gamma}_N} - (\hat{\rho}_f \hat{J}\hat{f}_f, \hat{\psi}^v)_{\widehat{\Omega}_f} = 0 \quad \forall \hat{\psi}^v \in \hat{V}_{f,\widehat{\Gamma}_i}^0,$$
$$(\hat{\rho}_s \partial_t \hat{v}_f, \hat{\psi}^v)_{\widehat{\Omega}_s} + (\widehat{F}\widehat{\Sigma}, \widehat{\nabla}\hat{\psi}^v)_{\widehat{\Omega}_s}$$
$$+\gamma_w(\hat{v}_s, \hat{\psi}^v)_{\widehat{\Omega}_s} + \gamma_s(\hat{\epsilon}(\hat{v}_s), \widehat{\nabla}\hat{\psi}^v)_{\widehat{\Omega}_s} - (\hat{\rho}_s \hat{f}_s, \hat{\psi}^v)_{\widehat{\Omega}_s} = 0 \quad \forall \hat{\psi}^v \in \hat{V}_s^0,$$
$$(\alpha_u \hat{\eta}_f, \hat{\psi}^\eta)_{\widehat{\Omega}_f} - (\alpha_u \widehat{\nabla}\hat{u}_f, \widehat{\nabla}\hat{\psi}^\eta)_{\widehat{\Omega}_f} = 0 \quad \forall \hat{\psi}^\eta \in \hat{V}_f,$$
$$(\alpha_u \hat{\eta}_s, \hat{\psi}^\eta)_{\widehat{\Omega}_s} - (\alpha_u \widehat{\nabla}\hat{u}_s, \widehat{\nabla}\hat{\psi}^\eta)_{\widehat{\Omega}_s} = 0 \quad \forall \hat{\psi}^\eta \in \hat{V}_s,$$
$$(\alpha_u \widehat{\nabla}\hat{\eta}_f, \widehat{\nabla}\hat{\psi}^u)_{\widehat{\Omega}_f} = 0 \quad \forall \hat{\psi}^u \in \hat{V}_{f,\hat{u},\widehat{\Gamma}_i}^0,$$
$$\hat{\rho}_s(\partial_t \hat{u}_s - \hat{v}_s, \hat{\psi}^u)_{\widehat{\Omega}_s} = 0 \quad \forall \hat{\psi}^u \in \hat{L}_s,$$
$$(\widehat{div}(\hat{J}\widehat{F}^{-1}\hat{v}_f), \hat{\psi}^p)_{\widehat{\Omega}_f} = 0 \quad \forall \hat{\psi}^p \in \hat{L}_f^0,$$
$$(\hat{P}_s, \hat{\psi}^p)_{\widehat{\Omega}_s} = 0 \quad \forall \hat{\psi}^p \in \hat{L}_s^0,$$

*with all quantities as defined in Problem 5.19 and the monitor parameter α_u defined
in* (39).

Remark 5.21. *The monolithic variational formulation for the second type of boundary
conditions is formally equivalent as demonstrated in Problem 5.20. Only the definition
of the function spaces for trial and test functions of the displacement variables $\hat{u}$ and
$\hat{\eta}$ changes.* ◇

For later purposes (basically Chapter 7), we also state a stationary version of the
coupled equations:

Problem 5.22 (Stationary FSI with harmonic and linear-elastic mesh motion). *Find*
$\{\hat{v}_f, \hat{u}_f, \hat{u}_s, \hat{p}_f, \hat{p}_s\} \in \{\hat{v}_f^D + \hat{V}_{f,\hat{v}}^0\} \times \{\hat{u}_f^D + \hat{V}_{f,\hat{u}}^0\} \times \{\hat{u}_s^D + \hat{V}_s^0\} \times \hat{L}_f$, *such that*

$$(\hat{\rho}_f \hat{J}(\widehat{F}^{-1}\hat{v}_f \cdot \widehat{\nabla})\hat{v}_f), \hat{\psi}^v)_{\widehat{\Omega}_f}$$
$$+(\hat{J}\hat{\sigma}_f \widehat{F}^{-T}, \widehat{\nabla}\hat{\psi}^v)_{\widehat{\Omega}_f} - \langle \hat{g}_f, \hat{\psi}^v \rangle_{\widehat{\Gamma}_N} - (\hat{\rho}_f \hat{J}\hat{f}_f, \hat{\psi}^v)_{\widehat{\Omega}_f} = 0 \quad \forall \hat{\psi}^v \in \hat{V}_{f,\hat{v}}^0,$$
$$(\widehat{F}\widehat{\Sigma}, \widehat{\nabla}\hat{\psi}^v)_{\widehat{\Omega}_s} - (\hat{\rho}_s \hat{f}_s, \hat{\psi}^v)_{\widehat{\Omega}_s} = 0 \quad \forall \hat{\psi}^v \in \hat{V}_s^0,$$
$$(\hat{\sigma}_{mesh}, \widehat{\nabla}\hat{\psi}^u)_{\widehat{\Omega}_f} = 0 \quad \forall \hat{\psi}^u \in \hat{V}_{f,\hat{u},\widehat{\Gamma}_i}^0,$$
$$(\widehat{div}(\hat{J}\widehat{F}^{-1}\hat{v}_f), \hat{\psi}^p)_{\widehat{\Omega}_f} = 0 \quad \forall \hat{\psi}^p \in \hat{L}_f^0,$$

with all quantities as defined in Problem 5.19.

Problem 5.22 offers further insight of key differences between stationary and non-
stationary fluid-structure interactions. We do not search any longer for a velocity

solution $\hat{v}_s$ in the structure because it is zero in a stationary setting. Consequently, the damping terms vanish because they are defined by means of $\hat{v}_s$. Likewise, the fluid domain velocity $\hat{w}$ vanishes too.

The weak continuity of the normal stresses of Equation (33) that is required on $\widehat{\Gamma}_i$ becomes an implicit condition computing nonstationary fluid-structure interactions:

$$(\hat{J}\widehat{\sigma}_f \widehat{F}^{-T}\hat{n}_f, \hat{\psi}^v)_{\widehat{\Omega}_f} + (\widehat{F}\widehat{\Sigma}\hat{n}_s, \hat{\psi}^v)_{\widehat{\Omega}_s} + \gamma_s(\hat{\epsilon}(\hat{v}_s)\hat{n}_s, \hat{\psi}^v)_{\widehat{\Omega}_s} = 0 \quad \forall \hat{\psi}^v \in \hat{V}^0.$$

In stationary settings, we deal with

$$(\hat{J}\widehat{\sigma}_f \widehat{F}^{-T}\hat{n}_f, \hat{\psi}^v)_{\widehat{\Omega}_f} + (\widehat{F}\widehat{\Sigma}\hat{n}_s, \hat{\psi}^v)_{\widehat{\Omega}_s} = 0 \quad \forall \hat{\psi}^v \in \hat{V}^0.$$

Remark 5.23 (Discretizing solid's stress tensor in terms of velocities)**.** *An alternative way (and this seems more natural in fluid-structure interaction, see, e.g., [138]) is to take the time derivative on solid's stress tensor, e.g.,*

$$\partial_t \widehat{\sigma}_s(\hat{u}_s) = \partial_t(2\mu \widehat{E}_{lin}(\hat{u}) + \lambda tr(\widehat{E}(\hat{u}))\hat{I}) = 2\mu \widehat{E}_{lin}(\hat{v}) + \lambda tr(\widehat{E}(\hat{v}))\hat{I}.$$

This has the advantage that both stress tensors can be formally combined into one global stress tensor $\widehat{\sigma} = \chi_f \widehat{\sigma}_f + \chi_s \widehat{\sigma}_s$. To the best of my knowledge it is not yet clear which formulation (our or the the unified one) is preferrable from computational cost point of view. ◇

5.3.8 A partitioned approach using ALE$_{fx}$

In this partitioned coupling algorithm, we solve subsequently for three problems:

- The fluid mesh (mesh motion problem);
- Solving the fluid problem in $\widehat{\Omega}$;
- Solving the solid problem.

Then, the weak form reads:

Problem 5.24 (Partioned FSI with harmonic and linear-elastic mesh motion)**.** *Given the initial conditions $\hat{v}_f(0) = \hat{v}_f^0$, $\hat{v}_s(0) = \hat{v}_s^0$, $\hat{u}_f(0) = \hat{u}_f^0$, we compute for almost all time steps $t \in I$ the following problems.*

- *Find $\{\hat{u}_f\} \in \{\hat{u}_f^D + \hat{V}_{f,\hat{u}}^0\}$,*

$$(\widehat{\sigma}_{mesh}, \widehat{\nabla}\hat{\psi}^u)_{\widehat{\Omega}_f} = 0 \quad \forall \hat{\psi}^u \in \hat{V}_{f,\hat{u},\widehat{\Gamma}_i}^0,$$

- *Find $\{\hat{v}_f, \hat{p}_f\} \in \{\hat{v}_f^D + \hat{V}_{f,\hat{v}}^0\} \times \hat{L}_f^0$,*

$$(\hat{J}\hat{\rho}_f \partial_t \hat{v}_f, \hat{\psi}^v)_{\widehat{\Omega}_f} + (\hat{\rho}_f \hat{J}(\widehat{F}^{-1}(\hat{v}_f - \hat{w}) \cdot \widehat{\nabla})\hat{v}_f, \hat{\psi}^v)_{\widehat{\Omega}_f}$$
$$+ (\hat{J}\widehat{\sigma}_f \widehat{F}^{-T}, \widehat{\nabla}\hat{\psi}^v)_{\widehat{\Omega}_f} - \langle \hat{g}_f, \hat{\psi}^v \rangle_{\widehat{\Gamma}_N} - (\hat{\rho}_f \hat{J}\hat{f}_f, \hat{\psi}^v)_{\widehat{\Omega}_f} = 0 \quad \forall \hat{\psi}^v \in \hat{V}_{f,\widehat{\Gamma}_i}^0,$$
$$(\widehat{div}(\hat{J}\widehat{F}^{-1}\hat{v}_f), \hat{\psi}^p)_{\widehat{\Omega}_f} = 0 \quad \forall \hat{\psi}^p \in \hat{L}_f^0,$$

59

- *Find $\{\hat{v}_s, \hat{u}_s\} \in \hat{L}_s \times \{\hat{u}_s^D + \hat{V}_s^0\}$,*

$$(\hat{\rho}_s \partial_t \hat{v}_s, \hat{\psi}^v)_{\widehat{\Omega}_s} + (\widehat{F}\widehat{\Sigma}, \widehat{\nabla}\hat{\psi}^v)_{\widehat{\Omega}_s}$$
$$+\gamma_w(\hat{v}_s, \hat{\psi}^v)_{\widehat{\Omega}_s} + \gamma_s(\hat{\epsilon}(\hat{v}_s), \widehat{\nabla}\hat{\psi}^v)_{\widehat{\Omega}_s} - (\hat{\rho}_s \hat{f}_s, \hat{\psi}^v)_{\widehat{\Omega}_s} = 0 \quad \forall \hat{\psi}^v \in \hat{V}_s^0,$$
$$\hat{\rho}_s(\partial_t \hat{u}_s - \hat{v}_s, \hat{\psi}^u)_{\widehat{\Omega}_s} = 0 \quad \forall \hat{\psi}^u \in \hat{L}_s,$$

with $\hat{\rho}_f$, $\hat{\rho}_s$, ν_f, μ_s, λ_s, $\widehat{F}$, and $\hat{J}$ as defined before. The stress tensors $\hat{\sigma}_f$, $\widehat{\Sigma}$, and $\hat{\sigma}_{mesh}$ are defined in the Equations (30), (13), (4.31), and in (35) and (38), respectively.

5.3.9 A partitioned approach using ALE$_{dm}$

We solve in the same order as in Section 5.3.8 but now the fluid equations on the current (deformed) domain Ω.

The weak form reads:

Problem 5.25 (Partitioned FSI with harmonic and linear-elastic mesh motion). *Given the initial conditions $v_f(0) = v_f^0$, $\hat{v}_s(0) = \hat{v}_s^0$, we compute for almost all time steps $t \in I$ the following problems.*

- *Find $\{\hat{u}_f\} \in \{\hat{u}_f^D + \hat{V}_{f,\hat{u}}^0\}$,*

$$(\hat{\sigma}_{mesh}, \widehat{\nabla}\hat{\psi}^u)_{\widehat{\Omega}_f} = 0 \quad \forall \hat{\psi}^u \in \hat{V}_{f,\hat{u},\widehat{\Gamma}_i}^0,$$

- *Find $\{v_f, p_f\} \in \{v_f^D + V_{f,v}^0\} \times L_f^0$,*

$$(\rho_f \hat{\partial}_t v_f, \psi^v)_{\Omega_f} + (\rho_f(v_f - w) \cdot \nabla) v_f, \psi^v)_{\Omega_f}$$
$$+(\sigma_f, \nabla\psi^v)_{\Omega_f} - \langle g_f, \psi^v \rangle_{\Gamma_N} - (\rho_f f_f, \psi^v)_{\Omega_f} = 0 \quad \forall \psi^v \in V_{f,\Gamma_i}^0,$$
$$(div(\hat{v}_f), \psi^p)_{\Omega_f} = 0 \quad \forall \psi^p \in L_f^0,$$

- *Find $\{\hat{v}_s, \hat{u}_s\} \in \hat{L}_s \times \{\hat{u}_s^D + \hat{V}_s^0\}$,*

$$(\hat{\rho}_s \partial_t \hat{v}_s, \hat{\psi}^v)_{\widehat{\Omega}_s} + (\widehat{F}\widehat{\Sigma}, \widehat{\nabla}\hat{\psi}^v)_{\widehat{\Omega}_s}$$
$$+\gamma_w(\hat{v}_s, \hat{\psi}^v)_{\widehat{\Omega}_s} + \gamma_s(\hat{\epsilon}(\hat{v}_s), \widehat{\nabla}\hat{\psi}^v)_{\widehat{\Omega}_s} - (\hat{\rho}_s \hat{f}_s, \hat{\psi}^v)_{\widehat{\Omega}_s} = 0 \quad \forall \hat{\psi}^v \in \hat{V}_s^0,$$
$$\hat{\rho}_s(\partial_t \hat{u}_s - \hat{v}_s, \hat{\psi}^u)_{\widehat{\Omega}_s} = 0 \quad \forall \hat{\psi}^u \in \hat{L}_s,$$

with $\hat{\rho}_f$, $\hat{\rho}_s$, ν_f, μ_s, λ_s, $\widehat{F}$, and $\hat{J}$ as defined before. The stress tensors $\hat{\sigma}_f$, $\widehat{\Sigma}$, and $\hat{\sigma}_{mesh}$ are defined in the Equations (30), (13), (4.31), and in (35) and (38), respectively.

Remark 5.26 (Iteration loop / Fix point iteration)**.** *In the implementation, we add iteration indices k to all equations and produce sequences of solutions*

$$
\begin{aligned}
&u_f^1, u_f^2, u_f^3, \ldots && \textit{Mesh motion} \\
&v_f^1, v_f^2, v_f^3, \ldots && \textit{Fluid} \\
&p_f^1, p_f^2, p_f^3, \ldots && \textit{Fluid} \\
&\hat{v}_s^1, \hat{v}_s^2, \hat{v}_s^3, \ldots && \textit{Solid} \\
&\hat{u}_s^1, \hat{u}_s^2, \hat{u}_s^3, \ldots && \textit{Solid.}
\end{aligned}
$$

A loosely-coupled scheme would terminate (or be forced to stop) after a few iterations. A strongly-coupled algorithms solves up to a tolerance and based a stopping criterion that is based on the Steklov-Operator, i.e., find $\hat{u}$ on $\widehat{\Gamma}_i$ such that the stress condition $\widehat{\sigma}_f \hat{n}_f = \widehat{\sigma}_s \hat{n}_s$ is satisfied. ⋄

Remark 5.27 (Solution of the mesh motion problem)**.** *In the partitioned approach different solution techniques can be easily employed to solve the three subproblems (mesh, fluid, solid). Here, we emphasize that the mesh motion equation is purely artificial without physical relevance and it can be solved without satisfying a low tolerance. So, its solution can be achieved in a fast way.* ⋄

Remark 5.28 (Decoupling in time)**.** *In the partitioned approach it is obvious (under the condition that certain relationships and additional information are known) that we can decouple in time. For instance, we have seen in [209] that the FSI-benchmark requires smaller time steps than the pure fluid benchmark. An open question is if we could use a partitioned solver in which we solve the fluid equations and mesh motion problem only at every 10th time step.* ⋄

5.3.10 Monolithic and partitioned (fixed-stress) approaches for Darcy flow-elasticity coupling

In this section, we consider a first special case of fluid-solid coupling: the Biot-Lamé-Navier system. The Biot system [35–37] is a standard model in poroelasticity and is a multi-scale problem which is identified on the micro-scale as a fluid-structure interaction problem (details on the interface law are found in Mikelić and Wheeler [177]). Through homogenization, the Biot system is derived for the macro-scale level. This system is specifically suited for applications in subsurface modeling for the poroelastic part, the so-called pay-zone. On the other hand, surrounding rock (the non-pay zone) is modeled with the help of linear elasticity [56]. Therefore, the final configuration belongs to a multiphysics problem in non-overlapping domains in which we again need to specify appropriate interface coupling conditions.

Compared to *classical* FSI modeling, we deal with the following simplifications:

- The Biot problem averages the fluid-solid coupling and we do not have anymore the typical multi-domain structure with interface conditions between fluid and solid.

- The resulting system is quasi-stationary with a time-derivative only in the pressure (fluid) equation.

- The resulting system is geometrically-linearized and all equations are formulated in a common framework without ALE-transformation rules.

Remark 5.29 (Identification of Eulerian and Lagrangian frameworks)**.** *The last point of linearization is based on mainly two assumptions: the hypothesis of small perturbations [60]:*

- *$||\nabla u|| \ll 1$. Then, the Lagrangian and Eulerian methods coincide up to a first-order approximation.*

- *Small displacements u for the skeleton particles:*

$$||u/L|| \ll 1$$

where L is the characteristic length of the pore structure. This second hypothesis allows to identify the reference configuration $\widehat{\Omega}$ with the current domain Ω and additionally, i.e,

$$\hat{x} \approx x, \quad \hat{f}(\hat{x}) \approx f(x), \quad \widehat{\Omega} \approx \Omega.$$

$\diamond$

Remark 5.30 (Darcy's momentum conservation law)**.** *The Darcy flow equations (representing the momentum equations) arise as an intermediate step while averaging the Stokes equations to get the lubrication equation. Darcy [65] derived this law empirically and the mathematical argument can be obtained through homogenization of Stokes' equations [29]. It holds:*

$$v_B = -\frac{1}{\eta_f} K (\nabla p_B - \rho_f g),$$

which gives a linear relationship between the velocity and the pressure gradient. $\diamond$

Problem 5.31. *Find the pressure p_B and displacement u_B such that*

$$\partial_t (c_B p_B + \alpha_B \nabla \cdot u_B) - \frac{1}{\eta_f} \nabla \cdot K(\nabla p_B - \rho_f g) = q \quad in \ \Omega_B \times I,$$

$$-\nabla \cdot \big(\sigma_B(u)\big) + \alpha_B \nabla p_B = f_B \quad in \ \Omega_B \times I,$$

with

$$\sigma_B(u_B) := \mu_B (\nabla u_B + \nabla u_B^T) + \lambda_B \nabla \cdot u_B I,$$

and the coefficients $c_B \geq 0$, the Biot-Willis constant $\alpha_B \in [0,1]$, (in fact, this constant relates to the amount of coupling between the flow part and the elastic part) and the permeability tensor K, fluid's viscosity and its density η_f and ρ_f, gravity g and a volume source term q (i.e., usually fluid injection). In the second equation, the Lamé coefficients are denoted by $\lambda_B > 0$ and $\mu_B > 0$ and f_B is a volume force.

Usually a non-pay zone is described in terms of linear elasticity: Find a displacement u_S such that

$$-\nabla \cdot \big(\sigma_S(u_S)\big) = f_S \quad \text{in } \Omega_S \times I,$$

with

$$\sigma_S(u_S) := \mu_S(\nabla u_S + \nabla u_S^T) + \lambda_S \nabla \cdot u_S I,$$

with the Lamé coefficients μ_S and λ_S and a volume force f_S. On the boundary $\partial\Omega_S := \Gamma_D \cup \Gamma_N$, the conditions

$$u_S = \bar{u}_S \quad \text{on } \Gamma_D, \quad \sigma_S(u_S)n_S = \bar{t}_S \quad \text{on } \Gamma_N,$$

are prescribed with given $\bar{u}_S$ and $\bar{t}_S$.

It finally remains to describe the interface conditions on Γ_i between the two sub-systems:

$$
\begin{aligned}
u_B &= u_S, \\
\sigma_B(u_B)n_B - \sigma_S(u_S)n_S &= \alpha p_B n_B, \\
-\frac{1}{\eta_f} K(\nabla p_B - \rho_f g) \cdot n_S &= 0.
\end{aligned}
\tag{49}
$$

It is important to notice that the second condition in (49), requires careful implementation on the interface. Furthermore, this condition shows in fact similarities to standard fluid-structure interaction coupling conditions.

Let d be the dimension and $V_P := \{\phi^p \in H^1(\Omega_B) | f = p^D \text{ on } \Gamma_p\}$ and $V_S := \{\phi^u \in [H^1(\Omega_B \cup \Omega_S)]^d | g = u^D \text{ on } \Gamma_u\}$ be Hilbert spaces and p^D and u^D extensions of Dirichlet data.

The definition of a weak formulation follows standard argumentation and leads to the system:

Problem 5.32 (Biot-Lamé-Navier Problem)**.** *Find* $\{p, u\} \in \{p^D + V_P\} \times \{u^D + V_S\}$, *such that* $u(0) = u^0$ *and* $p(0) = p^0$, *for almost all times* $t \in I$, *and*

$$
\begin{aligned}
c_B(\partial_t p, \phi^p) + \alpha_B(\nabla \cdot u, \phi^p) + \frac{K}{\nu_F}(\nabla p, \nabla \phi^p) \qquad\qquad\qquad\quad \\
-\rho_F(g, \phi^p) - (q, \phi^p) = 0 \quad \forall \phi^p \in V_P, \\
(\sigma_B, \nabla \phi^u) - \alpha_B(pI, \nabla \phi^u) - (f_B, \phi^u) = 0 \quad \forall \phi^u \in V_S, \\
(\sigma_S, \nabla \phi^u) - (f_S, \phi^u) = 0 \quad \forall \phi^u \in V_S.
\end{aligned}
$$

The corresponding partitioned approach (fixed-stress splitting) reads:

Problem 5.33 (Fixed-stress split of the Biot system)**.** *For* $l = 1, 2, 3, \ldots$, *find* p^l *such that*

$$
\begin{aligned}
\big(c_B + \frac{\alpha^2}{3\lambda + 2\mu}\big)\big(\frac{p^l - p^{n-1}}{\Delta t}, \phi^p\big) + \big(K_{eff}(\nabla p - \rho^0 g), \nabla \phi^p\big) \\
- (q, \phi^p) + \alpha\big(\frac{\nabla \cdot u^{l-1} - \nabla \cdot u^{n-1}}{\Delta t}, \phi^p\big) - \frac{\alpha^2}{3\lambda + 2\mu}\big(\frac{p^{l-1} - p^{n-1}}{\Delta t}, \phi^p\big), \\
= 0 \quad \forall \phi \in V_P.
\end{aligned}
$$

Then, we solve for the displacements u^l such that:

$$\left(\sigma_B, e(\phi^u)\right) = (\alpha p^l, \operatorname{div} \phi^u) + (f_B, \phi^u) \quad \forall \phi^u \in V_S.$$

The iteration is completed if

$$\max\{\|u^l - u^{l-1}\|, \|p^l - p^{l-1}\|\} < TOL_{FS}.$$

5.3.10.1 Numerical results for Mandel's problem We briefly test a specific implementation (the reader is invited to visit DOpElib [116] `Examples/PDE/InstatPDE/Example6` in order to examine and run the example. There, the well-known Mandel's problem [173] is considered, which is an acknowledged benchmark in subsurface modeling. In the second example, the augmented Mandel problem [109] is used as verification.

Example 5.34. *To enhance your imagination, a physical example is that of a sponge that you press: First the fluid pressure will slightly increase due to the sudden application of traction forces on the outer boundary. Then, the pressure reduces (finally to zero) because the fluid is pushed out of the pores.*

The configuration and parameters are taken from [99, 121, 168, 169]. The domain is $[0, 100m] \times [0, 20m]$. As parameters, we choose: $M_B = 2.5 * 10^{12} Pa, c_B = 1/M_B Pa^{-1}, \alpha_B = 1.0, \nu_F = 1.0 * 10^{-3} m^2/s, K_B = 100 md, \rho_F = 1.0 kg/m^3, \bar{t} = F = 1.0 * 10^7 N$. As elasticity parameters in Biot's model, we use $\rho_S = 1.0 kg/m^3, \mu_S = 1.0e + 8, \nu_S = 0.2$. The time step is chosen as $k = 1000s$. The final time is $5 * 10^6 s$ (corresponds to computing 5000 time steps). The initial mesh is 4-times globally refined corresponding to 256 cells and 2467 degrees of freedom (with the Taylor Hood element).
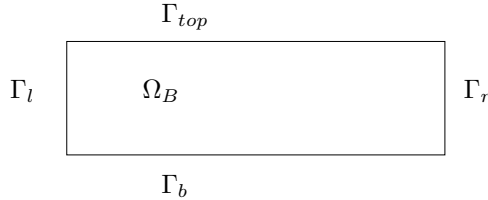

Figure 16: Configuration of Mandel's problem.

As boundary conditions, we choose:

$$\sigma_B n - \alpha_B p_B n = \bar{t} - \alpha_B p_B n \quad \text{on } \Gamma_{top},$$
$$p = 0 \quad \text{on } \Gamma_r,$$
$$u_y = 0 \quad \text{on } \Gamma_b,$$
$$u_x = 0 \quad \text{on } \Gamma_l.$$

For different time steps $t_1 = 1 * 10^3, t_2 = 5 * 10^3, t_3 = 1 * 10^4, t_4 = 1 * 10^5, t_5 = 5 * 10^5$ and $t_{10} = 5 * 10^6 [s]$ (the numeration of time steps is taken from [99]) the solution of the pressure and the x-displacement evaluated on the x-axis is shown in Figure 17. These values coincides with the literature values displayed in [99, 121, 168, 169]. In particular, the well-known Mandel Creyer effect (non-monotonic pressure behavior over time) is identified.
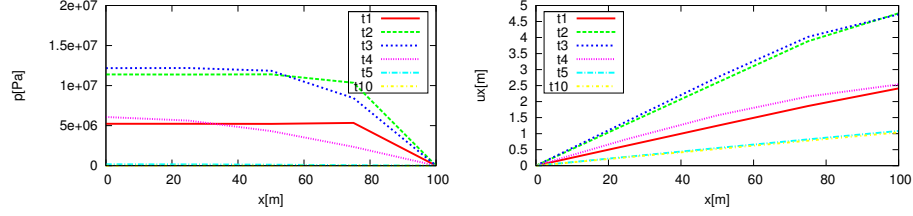

Figure 17: Mandel's problem: Pressure trace and x-displacement on the x-axis.

Next, we test another configuration that is closer to that application. Specifically, we deal now with a problem in non-overlapping domains. The configuration is inspired by Girault et al. [109]. We use the same Biot-region parameters as in the previous example. In addition, we use in the pure elastic zone the same Lamé coefficients, such that $\mu_B = \mu_S$ and $\lambda_B = \lambda_S$. We consider this as a new benchmark configuration that is prototypical for reservoir simulations with some overburden. (In the same manner, an underburdon could have been added in addition. This leads, however, to no additional difficulties). The computational domain is enlarged in height such that $[0, 100m] \times [0, 40m]$ and is sketched in Figure 18.
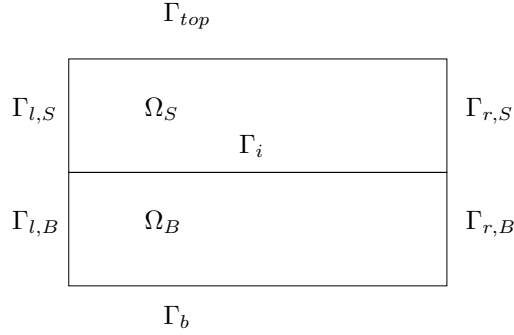

Figure 18: Configuration of augmented Mandel's problem.

65

As boundary conditions, we choose:

$$\sigma_B n = \bar{t} \quad \text{on } \Gamma_{top},$$
$$\sigma_B n = 0 \quad \text{on } \Gamma_{r,S},$$
$$p = 0 \quad \text{on } \Gamma_{r,B},$$
$$u_y = 0 \quad \text{on } \Gamma_b,$$
$$u_x = 0 \quad \text{on } \Gamma_{l,B} \cup \Gamma_{l,S}.$$

The augmented Mandel problem shows also the well-known Mandel Creyer effect as illustrated in Figure 19. Here, it is important to carefully implement the interface conditions on Γ_i. Otherwise the results are not correct from physical point of view. Graphical solutions of the surfaces of pressure distribution is shown in Figure 20. Here, we detect the typical pressure behavior on the x-axis.
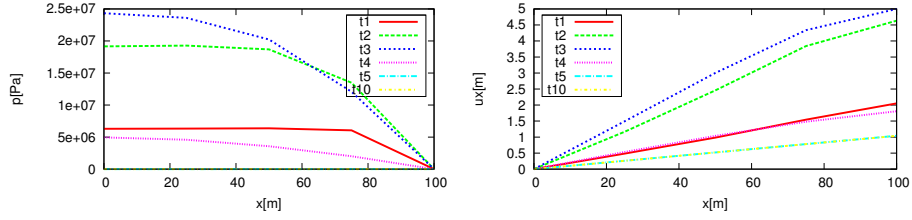

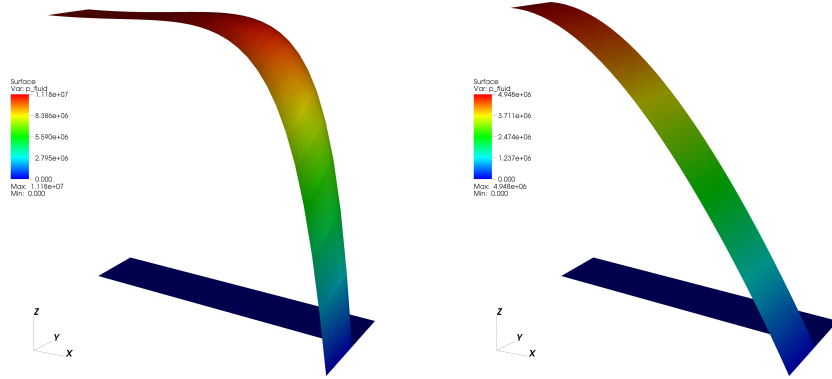Figure 19: Augmented Mandel's problem: Pressure trace and x-displacement on the x-axis.

Figure 20: Augmented Mandel's problem: Pressure surface for two time steps t_1 and t_4.

5.3.11 A rate-dependent partitioned scheme; coupling the membrane equation with Reynolds lubrication model

5.3.11.1 Modeling In this part, we present another partitioned approach (from [247]) that offers some interesting features:

- Coupling of the most simplest equations for fluids (Reynolds lubrication equation) and solids (second order membrane - Laplace - equation). As in the previous section, all equations are linearized and are formulated in a common setting without ALE-transformation rules (please consult Remark 5.29).

- Formulation of the stationary solid equation in terms of a rate-dependent algorithm; well-known from solving plasticity problems [72, 203, 220].

- However, despite from being simple: the lubrication equation is widely used in different fields (see also in these notes; reaction-induced boundary movement or fluid-filled fractures) and rate-dependent algorithms are of utter importance for non-trivial solid models such as just mentioned before for example plasticity.

Let us first simplify the solid equations. By omitting acceleration effects in (12), we arrive at

$$-\widehat{\nabla} \cdot \widehat{\sigma}_s = \hat{f} \quad \text{in } \widehat{\Omega}.$$

The Reynolds equation has been presented in Proposition 4.25. For completeness, in an ALE setting it reads:

Proposition 5.35 (Reynolds lubrication equation in ALE coordinates). *Let the top boundary $\hat{z} = \hat{h}(x)$ be moving with a velocity $\hat{v}_z(x, h) =: v_z$; the lower boundary at $\hat{h} = 0$ is fixed for simplicity. Then,*

$$\nabla \cdot \left(\frac{\hat{h}^3}{12\eta} \hat{J} \widehat{\nabla} \hat{p} \widehat{F}^{-T} \right) = -\hat{v}_z, \quad \hat{h} = \hat{h}(\hat{x}, \hat{y}).$$

Neumann boundary conditions are given by

$$i) \quad \frac{\partial \hat{p}}{\partial x} = \Delta \hat{p}_1 \quad \text{on } \Gamma_1 \quad \text{and} \quad \frac{\partial \hat{p}}{\partial x} = \Delta p_2 \quad \text{on } \Gamma_3,$$

$$ii) \quad \frac{\partial \hat{p}}{\partial y} = \Delta \hat{p}_3 \quad \text{on } \Gamma_2 \quad \text{and} \quad \frac{\partial \hat{p}}{\partial y} = \Delta \hat{p}_4 \quad \text{on } \Gamma_4.$$

In the following, we provide more details on the derivation of the membrane equation.
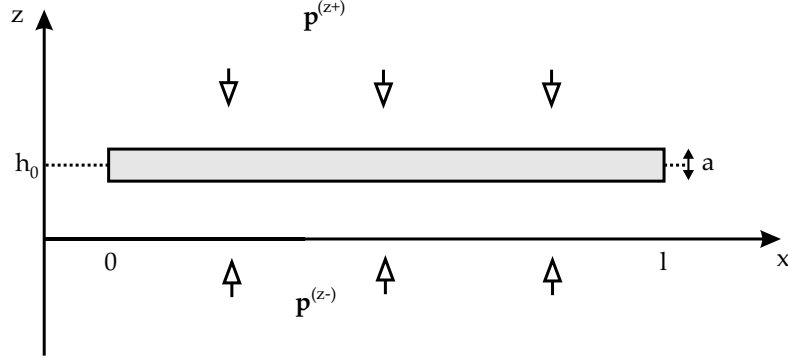
Figure 21: Fixed membrane with length l and thickness a.

The fixed membrane is a special case of the plate equation [43]. Our membrane has length l and thickness a with $a \ll l$

$$0 \leq x, y \leq l \quad \text{and} \quad h_0 - \frac{a}{2} \leq z \leq h_0 + \frac{a}{2}.$$

Lemma 5.36 (Fixed membrane in 2D). *A thin plate with thickness a and length l is subject to forces $p^{(z+)}$ and $p^{(z-)}$ orthogonal to the middle plane. Then,*

$$\frac{\partial^2 z}{\partial x^2} + \frac{\partial^2 z}{\partial y^2} = -\frac{p^{(z+)} - p^{(z-)}}{\mu a} \quad in \ \Omega = [0, l]^2 \tag{50}$$

The non-homogeneous (time-dependent) Dirichlet conditions are $z = h_0$ on $\partial\Omega$.

Remark 5.37. *Bending moments are neglected in the membrane equation. In order to include them, one has to use the fourth-order biharmonic plate equation [43].* ⋄

5.3.11.2 Coupling and variational form The task consists in coupling Reynolds' equation with the membrane equation. However, due to our (over)simplifications, the membrane equation delivers a displacement u (here z) but the lubrication equation requires as input a velocity $\hat{v}_z$. The key trick is now to re-formulate the stationary membrane equation in terms of a quasi-stationary rate-dependent formulation. We follow [72, 203] and introduce a *time* (although these are only rate-increments). We first write the second order membrane problem in terms of a mixed setting using $\Delta z = \operatorname{div}\nabla z$ such that

$$\Delta z = \operatorname{div}\nabla z = \operatorname{div}\sigma \overset{!}{=} -\frac{p^{(z+)} - p_{rey}}{\mu a} =: -\tilde{f} \quad \text{with } \sigma = \nabla z.$$

In classical formulation, the mixed form would read:

$$\text{div}\sigma = -\tilde{f} \quad \text{in } \Omega, \tag{51}$$

$$\sigma = \nabla z \quad \text{in } \Omega, \tag{52}$$

$$z = h_0 \quad \text{on } \partial\Omega. \tag{53}$$

For time discretization, as done in the previous sections, we introduce a time interval $I := [0, T]$ with fixed $N \in \mathbb{N}$ such that we have the time points $t_0, \ldots, t_N$:

$$0 = t_0 < t_1 < \ldots < t_{N-1} < t_N = T.$$

The incremental velocity v_z^n ($n \in \mathbb{N}$) is derived with help of the middle Equation (51). Formal transformation $\sigma(x) \to \sigma(x, t)$ introduces time-dependence of the system and gives us

$$\partial_t \sigma = \partial_t \nabla z = \nabla \partial_t z = \nabla \dot{z} = \nabla v_z = \nabla v_z.$$

In short notation

$$\dot{\sigma} = \nabla v_z.$$

We approximate $\dot{\sigma}$ with a difference quotient for two subsequent time steps t^{n-1} and t^n:

$$\dot{\sigma} \approx \frac{\sigma^{t^n} - \sigma^{t^{n-1}}}{t^n - t^{n-1}} = \nabla v_z^{t^n}, \quad n = 1, 2, \ldots, N.$$

Using $\sigma^{t^n} =: \sigma^n$ and $\nabla v_z^{t^n} =: \nabla_z^n$ yields

$$\dot{\sigma} \approx \frac{\sigma^n - \sigma^{n-1}}{dt^n} = \nabla v_z^n, \quad n = 1, 2, \ldots, N.$$

The function $v_z^n \in V$ is the so-called incremental displacement velocity. To compute the current σ^n, we have

$$\sigma^n = \sigma^{n-1} + dt^n \nabla v_z^n, \quad n = 1, 2, 3, \ldots. \tag{54}$$

We are now prepared to derive a variational formulation. Inserting (54) into the first equation of (51) gives

$$-\text{div}\sigma^n = \tilde{f}^n,$$

and Green's formula

$$\int_\Omega u \, \text{div}\varphi \, dx = -\int_\Omega \nabla u \cdot \varphi \, dx + \int_{\partial\Omega} u\varphi \, ds,$$

and multiplication with a test function $\varphi \in H_0^1(\Omega)$ yields:

$$-\int_\Omega \text{div}\sigma^n \, \varphi \, dx = \int_\Omega \tilde{f}^n \varphi \, dx$$

$$\Leftrightarrow \quad \int_\Omega \sigma^n \cdot \nabla\varphi \, dx - \underbrace{\int_{\partial\Omega} \sigma^n \varphi \, ds}_{=0 \text{ wg. } \varphi \in H_0^1(\Omega)} = \int_\Omega \tilde{f}^n \varphi \, dx.$$

Furthermore,

$$(\sigma^n, \nabla\varphi)_0 = (\sigma^{n-1} + dt^n \nabla v_z^n, \nabla\varphi)_0 = (\sigma^{n-1}, \nabla\varphi)_0 + dt^n(\nabla v_z^n, \nabla\varphi)_0.$$

Additional calculations and the right hand side bring us to

$$dt^n(\nabla v_z^n, \nabla\varphi)_0 = (\tilde{f}^n, \varphi)_0 - (\sigma^{n-1}, \nabla\varphi)_0.$$

Then, the problem reads

Problem 5.38.

$$Find\ v_z^n \in H_0^1(\Omega): \quad dt^n a(v_z^n, \varphi) = l(\varphi) \quad \forall \varphi \in H_0^1(\Omega)$$

With the help if v_z^n, we can now calculate z^n and the stress update σ^n:

- *Displacement:*

$$z^n = z^{n-1} + dt^n v_z^n$$

  with initial value $z^0 = h_0$ (no deflection of the membrane).

- *Stress update:*

$$\sigma^n = \sigma^{n-1} + dt^n \nabla v_z^n \tag{55}$$

  with initial value $\sigma^0 = 0$.

The following results simplifies practical aspects of the implementation:

Proposition 5.39 (Stress recursion σ^n). *For equal-distant time steps dt^n, it holds*

$$\sigma^n = \sigma^0 + dt^n \nabla \left(\sum_{k=1}^{n} v_z^k \right) \quad for\ all\ n \in \mathbb{N}. \tag{56}$$

Proof. The proof is carried out using an induction argument. Begin with (induction start): $n = 1$:

$$\sigma^1 = \sigma^0 + dt^1 \nabla v_z^n.$$

The induction assumption is given by (56). We show now the induction step $n \to n+1$. With (55), we have

$$\sigma^{n+1} = \sigma^n + dt^{n+1} \nabla v_z^{n+1}.$$

Using $dt^n = dt^{n+1}$, and (56) and linearity of the differential operator $\nabla(\cdot)$ yields

$$\sigma^{n+1} = \sigma^0 + dt^n \nabla \left(\sum_{k=1}^{n} v_z^k \right) + dt^n \nabla v_z^{n+1}$$

$$= \sigma + dt^{n+1} \left[\nabla \left(\sum_{k=1}^{n} v_z^k \right) + \nabla v_z^{n+1} \right]$$

$$= \sigma^0 + dt^{n+1} \nabla \left(\sum_{k=1}^{n+1} v_z^k \right).$$

$\square$

The following statement is the main result:

Proposition 5.40 (Weak form of the coupled rate-dependent membrane equation).
For all functions $p^{(z+)}, p_{rey} \in L^2(\Omega)$ and $\sigma^{n-1} \in L^2(\Omega)^d$ of the right hand side, there exists in each pseudo-time step $n = 1, 2, \ldots,$ a unique weak solution $v_z^n \in H_0^1(\Omega)$ with

$$dt^n a(v_z^n, \varphi) = l(\varphi) \quad \forall \varphi \in H_0^1(\Omega) \tag{57}$$

where

$$l(\varphi) = \left(\frac{p^{(z+)}}{\mu a}, \varphi\right)_0 - \left(\frac{p_{rey}}{\mu a}, \varphi\right)_0 - (\sigma^{n-1}, \nabla\varphi)_0.$$

Proof. Let μ, a be constant and let the time interval dt^n be constant as well. Let the previous stress $\sigma^{n-1} \in L^2(\Omega)^d$. Using the Lax-Milgram theorem, and setting

$$l(\varphi) = \left(\frac{p^{(z+)}}{\mu a}, \varphi\right)_0 - \left(\frac{p_{rey}}{\mu a}, \varphi\right)_0 - (\sigma^{n-1}, \nabla\varphi)_0.$$

we obtain a unique solution. □

In the following, we present a partitioned coupling algorithm to solve the coupled Reynolds-membrane problem. The time rates are sufficiently small such that they are negligible compared to the finite element discretization error.

Algorithm 5.41 (Rate-dependent Reynolds-membrane coupling)**.**

A) $\sigma^0 = 0$, $z^0 = h_0$, $f^0 = \dfrac{p^{(z+)}}{\mu a}$, $p_{rey}^0 = 0$;

B) for $n = 1, 2, \ldots$
$\{$

$\qquad dt^n := t^n - t^{n-1}$;

$\qquad f^{n,0} := f^{n-1} - \dfrac{p_{rey}^{n-1}}{\mu a}$;

$\qquad z^{n,0} := z^{n-1}$;

$\qquad k = 1$;

$\qquad do$

$\qquad \{$

$\qquad\qquad$ *Solve structure:*

$\qquad\qquad dt^n a(v_z^{n,k-1}, \varphi) = (f^{n,k-1}, \varphi)_0 - (\sigma^{n-1}, \nabla\varphi)_0$;

$\qquad\qquad \rightarrow v_z^{n,k-1}$

$\qquad\qquad$ *Update displacements:*

$\qquad\qquad z^{n,k} = z^{n,0} + dt^n v_z^{n,k-1}$;

$\qquad\qquad$ *Solve fluid:*

$\qquad\qquad a(p_{rey}^{n,k-1}, \varphi) = (v_z^{n,k-1}, \varphi)_0 + (\varphi, g)_{0,\Gamma}$;

$\qquad\qquad \rightarrow p_{rey}^{n,k-1}$

$\qquad\qquad D_k = \left| \dfrac{z^{n,k} - z^{n,k-1}}{z^{n,k}} \right|$;

$\qquad\qquad k{+}{+}$;

$\qquad \} \, while(D_k > D)$;

$\qquad v^n := v^{n,k_\varepsilon}$;

$\qquad p_{rey}^n := p_{rey}^{n,k_\varepsilon}$;

$\qquad$ *updates:*

$\qquad$ *i)* $z^n = z^{n-1} + dt^n v^n$;

$\qquad$ *ii)* $\sigma^n = \sigma^{n-1} + dt^n \nabla v^n$;

$\qquad$ *iii)* $f^n = f^{n-1} + dt^n f^0$;

$\}$

5.3.11.3 Numerical tests

5.3.11.3.1 Computations with constant pressure $p^{(z+)}$ This section presents the findings that have been obtained using the algorithmic advances from Section 5.3.11. The configuration is sketched in Figure 22 and the parameters are provided in Table 1.
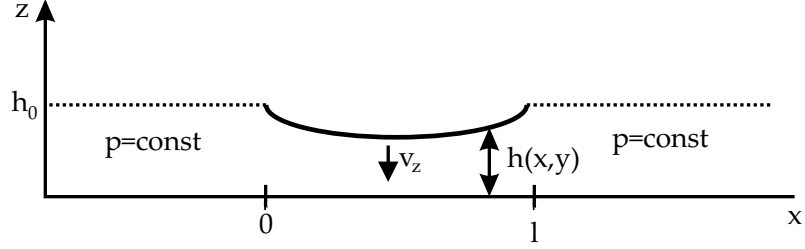
Figure 22: Configuration of membrane-lubrication coupling: the top boundary is moved with a velocity $v_z = v_z(x, h)$.

Table 1: Parameters of the membrane-lubrication coupling.

Parameter	Value	Dimension
l (length of interval)	1	m
h_0	$5 * 10^{-4}$	m
$p^{(z+)}$	$1 * 10^5$	N/m
μ	$4.0 * 10^{10}$	N/m^2
a	$2.5 * 10^{-3}$	m

The initial force is given by

$$f^0 = -\frac{p^{(z+)}}{\mu a} = -\frac{10^5}{10^{11}} = -0.001.$$

The pressure normalization is achieved by the condition:

$$\int_\Omega p\, dx = 0.$$
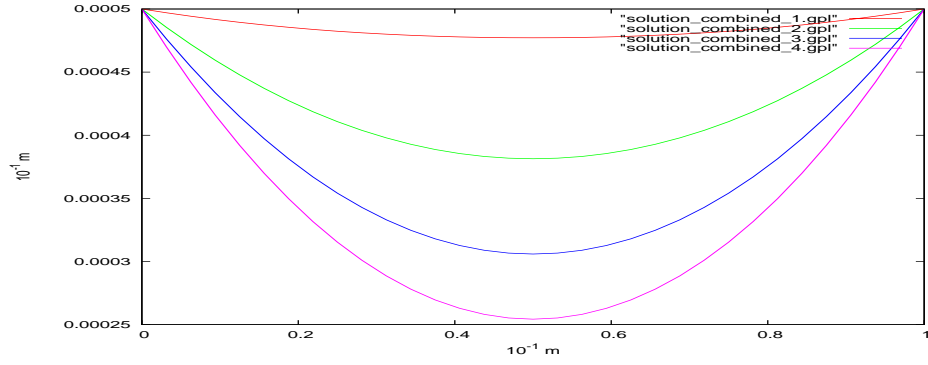
Figure 23: Deformation of the membrane at the time steps $n = 1, 2, 3, 4$ using the constant initial force $f^0 = -0.001$
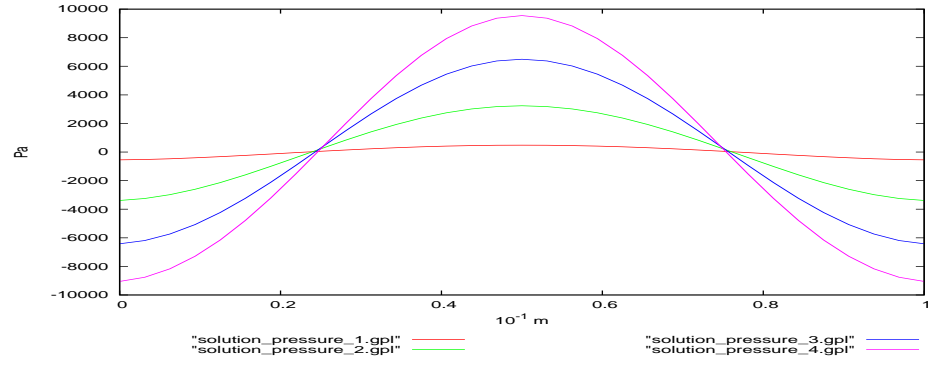
Figure 24: Pressure distribution at time steps obtained $n = 1, 2, 3, 4$ by solving Reynolds' lubrication equation.

Since the membrane deflection has its maximal displacement in the middle of the interval, the highest pressure is obviously also observed here. We notice that the homogeneous Neumann pressure conditions are clearly observed.

5.3.11.3.2 Long-term evolution We extend the previous example and compute $n = 80$ time steps in order to observe a quasi-stationary limit.
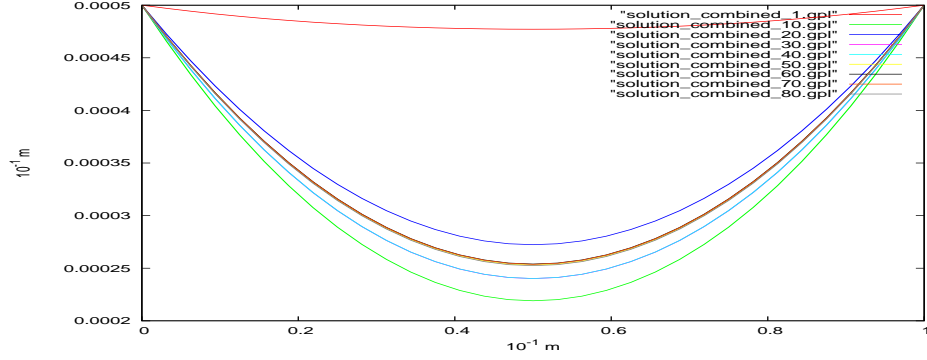
Figure 25: Membrane deformation at the time steps $n = 1, 10, 20, 30, 40, 50, 60, 70, 80$ using the initial force $f^0 = -0.001$.

We observe an oscillating behavior (physically absolutely plausible!) before the membrane reaches its final state. The absolute minimum is $2.5 * 10^{-5} m$. Similar behavior can be seen for the pressure distribution.

Figure 26: Pressure distribution at time steps $n = 1, 10, 20, 30, 40, 50, 60, 70, 80$.

5.3.11.3.3 L^2 **error estimates in 1D** We complement the computational results by
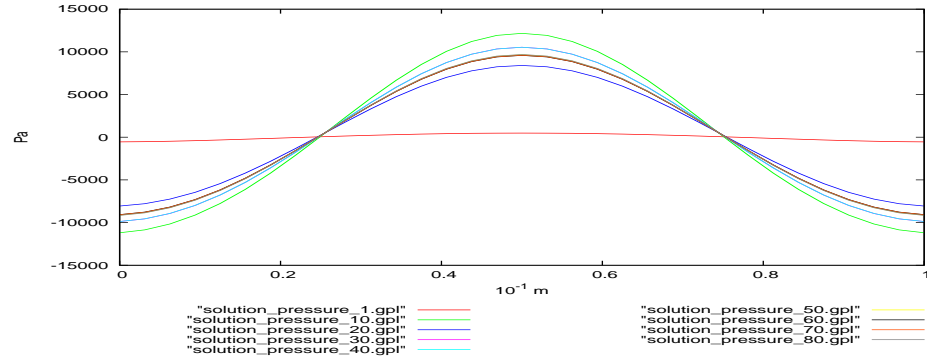some basics from numerical analysis: order of convergence of the numerical solution
with respect to a manufactured solution. In order to relax a bit, let us do this in 1d
and as simple as possible.

Algorithm 5.42. *Let the following problem be given:*

$$-z'' = f \quad in \ \Omega$$
$$z = 0 \quad on \ \Gamma = \{0, 1\}$$

i) *Provide z for which the boundary conditions are fulfilled For example $z(x) =
x(x - 1)$ on the left hand side.*

ii) *Determine $f(x) = -z''$. Here, $f(x) = -1$.*

iii) *Compute u_h.*

iv) *Compare u and u_h in appropriate norms (for example energy norm and/or L^2
norm).*

Example 5.43. *Take*

$$-z'' = \frac{p^{(z+)}}{\mu a} = -0.001 \quad in \ \Omega = (0, 1),$$

with $z(0) = z(1) = 5 * 10^{-4}$. The corresponding manufactured solution reads

$$z(x) = 5 * 10^{-4}(x^2 - x + 1).$$

We know from our numerical methods for PDEs class:

$$||u - u_h||_0 = \mathcal{O}(h^2).$$

Here, we obtain

Cells	DOFs	L^2-error
2	3	$3.282 * 10^{-5}$
4	5	$5.702 * 10^{-6}$
8	9	$1.426 * 10^{-6}$
16	17	$3.566 * 10^{-7}$
32	33	$8.915 * 10^{-8}$
64	65	$2.229 * 10^{-8}$
128	129	$5.572 * 10^{-9}$
256	257	$1.393 * 10^{-9}$

Here, we clearly see $O(h^2)$ convergence.

5.3.12 ALE-FSI techniques using Nitsche's method for moving boundary problems in precipitation-dissolution processes (reactive flow)

In this section, we discuss a second example involving Reynolds' lubrication approximation. Indeed, the setting is quite similar to the previous section:

- a thin channel with boundary movement.

The differences are:

- the boundary movement is now given by chemical reactions (that cause time-dependent displacements) rather than a volume force; consequently, we are dealing with a moving boundary problem (rather than a classical FSI problem) that will be solved with FSI-techniques.

- We formulate a monolithic solution algorithm in which the boundary movement is taken into account by Nitsche's trick.

- Regarding the results, we numerically compute Navier-Stokes in 2D and compare this solution (i.e., its characteristic behavior) to a manufactured upscaled lubrication solution in 1D. The question is: Can we represent the flow by a (cheaper) lower-dimensional equation?

Remark 5.44. *In fact, this example shows how useful it is to learn FSI-techniques. We solve another physical problem but we can adopt our experiences from FSI modeling.* ◇

With regard to the physical model, the chemical reactions represent precipitation-dissolution reactions taking place at the boundaries of the channel resulting in boundary movements act as a precursor to the clogging process. The resulting problem is a coupled flow-reactive transport process in a time-dependent geometry that is solved with the ALE_{fx} approach (for related studies for flow interacting with surfactants, we refer for example to [100, 101]).

The geometry description in which the flow and transport processes take place is given by:

$$
\begin{aligned}
\Omega(t) &:= \{(x,y) \in \mathbb{R}^2 \mid 0 \leq x \leq 1, \; -(\varepsilon - d(x,t)) \leq y \leq (\varepsilon - d(x,t))\}, \\
\Gamma(t) &:= \{(x,y) \in \mathbb{R}^2 \mid 0 \leq x \leq 1, \; y \in \{-(\varepsilon - d(x,t)), (\varepsilon - d(x,t))\}\}, \\
\Gamma_\mathrm{i}(t) &:= \{(x,y) \in \mathbb{R}^2 \mid x = 0, \; -(\varepsilon - d(0,t)) \leq y \leq (\varepsilon - d(0,t))\}, \\
\Gamma_\mathrm{o}(t) &:= \{(x,y) \in \mathbb{R}^2 \mid x = 1, \; -(\varepsilon - d(1,t)) \leq y \leq (\varepsilon - d(1,t))\}.
\end{aligned}
$$

Due to the reactions at the boundaries, Ω and the boundaries Γ's are time-dependent.

The flow and transport of the solutes (the ions) are described by the following system of equations. The transport equation and reaction laws read [153]:

$$
\begin{aligned}
\partial_t c - \nabla \cdot (D\nabla c - vc) &= 0, & \text{in} \quad & \Omega(t) \times (0,T), \\
\rho_s \partial_t d &= f(c, \rho_s d)\sqrt{1 + (\partial_x d)^2}, & \text{on} \quad & \Gamma(t) \times (0,T), \\
f(c, \rho_s d) &= r(c) - w, & \text{on} \quad & \Gamma(t) \times (0,T).
\end{aligned}
\tag{58}
$$

Here, the unknowns are: $c(x, y, t)$, concentration of the charged ions, $d(x, t)$ free and moving boundary resulting due to reactions, and $v(x, y, t)$ the flow field. The known physical parameters are: $D > 0$, diffusion constant, ρ_s, the density of ions in the precipitate. $(58)_1$ describes the transport of solutes due to convection and molecular diffusion processes, whereas $(58)_2$ describes the movement of the boundary due to reaction term f. According to $(58)_3$, the reaction rate f is imposed by the following structure:

$$f(c, \rho_s d) = r(c) - w, \tag{59}$$

where $r(\cdot)$ describes the precipitation part whereas w models the dissolution process. Additionally, we assume that $r(\cdot) : \mathbb{R} \to [0, \infty)$, is monotone and locally Lipschitz continuous in $\mathbb{R}$. The usual mass-action kinetics laws governing the precipitation process satisfy this assumption. For the dissolution process, the rate law is given as

$$w \in H(d), \quad \text{where} \quad H(d) = \begin{cases} \{0\}, & \text{if} \quad d < 0, \\ [0, 1], & \text{if} \quad d = 0, \\ \{1\}, & \text{if} \quad d > 0. \end{cases} \tag{60}$$

Remark 5.45. *The flow equations are given by the incompressible, isothermal Navier-Stokes equations.* ⋄

The flow and transport equations are complemented by the initial and boundary conditions. The initial conditions read:

$$c(x, y, 0) = c_o, \qquad d(x, 0) = d_o. \tag{61}$$

The boundary conditions read:

$$
\begin{array}{llllll}
c & = & c_b, & p(0, y, t) & = & 1, & \text{on} & \Gamma_i(t) \times (0, T), \\
\partial_x c & = & 0, & p(L, y, t) & = & 0, & \text{on} & \Gamma_o(t) \times (0, T), \\
v & = & 0, \quad \nu \cdot (-D \nabla c) \sqrt{1 + (\partial_x d)^2} & = & \partial_t d(\rho_s - c) & \text{on} & \Gamma(t) \times (0, T).
\end{array}
\tag{62}
$$

As stated above, at the inlet and outlet, we prescribe the pressures and further impose that the flow takes place normal to the boundaries.

5.3.12.1 Towards clogging: a 1D averaged lubrication model for fluid flow   Similarly to Section 5.3.11, an upscaled model is obtained by integrating the Navier-Stokes equations in the z-direction. We consider a sequence of problems depending upon the thickness of strip ε and using formal asymptotic expansions, the unknowns are assumed to be of the form

$$z^\varepsilon = z_0 + \varepsilon z_1 + O(\varepsilon^2),$$

78

with z^ε denoting any of $c^\varepsilon, d^\varepsilon, v^\varepsilon$. Following the procedure in [188], the following upscaled equations are derived

$$\partial_x v_0 = 0, \qquad v_0 - \frac{(1-d_0)^3}{3\mu}\partial_x P_0 \;=\; 0,$$

$$\partial_t \big((1-d_0)c_0\big) + \partial_t(\rho_s d_0) \;=\; \partial_x\big(D(1-d_0)\partial_x c_0\big) - \partial_x(v_0 c_0), \qquad (63)$$

$$\partial_t d_0 - f(u_0, \rho_s d_0) \;=\; 0.$$

As our interest is in the case of closing of the channel, the above system of equations degenerates as $d_0 \to 1$.

Remark 5.46. *For more information, we would like to refer the reader to [156, 157], where all details are given. The discretization is realized with the multiphysics template [256] based on the finite element software deal.II [13].* $\diamond$
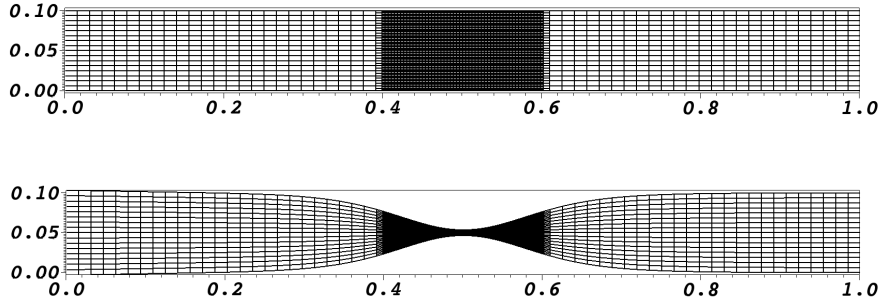
Figure 27: Initial (and also the reference) mesh and the deformed mesh at end time step $T = 14$. Local mesh refinement with hanging nodes is used in the middle of the channel.

When the channel starts getting narrower, the flow profile alters because of changing geometry. However, as the channel starts getting clogged (as observed in Figure 27), the flow is expected to decrease and eventually, the channel should be closed. For the upscaled model, following calculations show that the flow becomes zero as the channel closes. Using $(63)_1$

$$\partial_x\big(\frac{(1-d_0)^3}{3\mu}\partial_x P_0\big) = 0, \text{ leading to } \frac{(1-d_0)^3}{3\mu}\partial_x P_0 = C,$$

and hence,

$$P_0(x,t) = \int_x^1 \frac{C}{(1-d_0(\xi,t))^3}\,d\xi,$$

79

where C is obtained by using the boundary conditions for P_0,

$$v_0(t) = C(t) = \left\{ \int_0^1 \frac{1}{(1 - d_0(\xi, t))^3} d\xi \right\}^{-1}. \tag{64}$$

Now considering (64), formally, one sees that the integral is dominated by the regions where $1 - d_0$ is small and the flow $v_0(t)$ decreases as $(1 - d_0)^3$. Hence, wherever locally $d_0 \to 1$, we get that the flow in the channel tends to zero, allowing us to conclude that in the limit (clogging), the flow becomes zero. Since the 2D model is quite complicated, an analytical treatment is rather difficult. We resort to numerical computations to study this process in Section 5.3.12.5.

5.3.12.2 A variational-monolithic formulation By summarizing the previous sub-problems into one common setting, we derive the framework for the coupled three-field system:

Problem 5.47 (Variational ALE fluid reaction-diffusion moving-boundary problem). *Find* $\{\hat{v}, \hat{p}, \hat{c}, \hat{u}\} \in \{\hat{v}^D + \hat{\mathcal{V}}_f\} \times \hat{\mathcal{L}}_f \times \{\hat{c}^D + \hat{\mathcal{V}}_c\} \times \hat{\mathcal{V}}_c$ *such that for almost times* t:

$$
\begin{aligned}
(\hat{J}\hat{\rho}_f(\partial_t \hat{v} + (\hat{F}^{-1}(\hat{v} - \hat{w}) \cdot \hat{\nabla})\hat{v}), \hat{\psi}^v)_{\hat{\Omega}} & \\
+ (\hat{J}\hat{\sigma}_f \hat{F}^{-T}, \hat{\nabla}\hat{\psi}^v)_{\hat{\Omega}} - \langle \hat{g}_f, \hat{\psi}^v \rangle_{\hat{\Gamma}_N} &= 0 \quad \forall \hat{\psi}^v \in \hat{V}_f, \\
(\widehat{div}(\hat{J}\hat{F}^{-1}\hat{v}), \hat{\psi}^p)_{\hat{\Omega}} &= 0 \quad \forall \hat{\psi}^p \in \hat{L}_f, \\
(\hat{J}\partial_t \hat{c}, \hat{\psi}^c) + (\hat{J}\hat{\sigma}_c \hat{F}^{-T}, \hat{\nabla}\hat{\psi}^c)_{\hat{\Omega}} + (\hat{J}\hat{v}\hat{c}\hat{F}^{-T}, \hat{\nabla}\hat{\psi}^c)_{\hat{\Omega}} & \\
- \langle \hat{J}\hat{g}_c \hat{F}^{-T}, \hat{\psi}^c \rangle_{\hat{\Gamma}_N} - (\hat{J}f_c, \hat{\psi}^c)_{\hat{\Omega}} &= 0 \quad \forall \hat{\psi}^c \in \hat{V}_c, \\
\alpha(\widehat{\nabla}\hat{u}, \widehat{\nabla}\hat{\psi}^u) &= 0 \quad \forall \hat{\psi}^u \in \hat{V}_u.
\end{aligned}
$$

The boundary conditions for the last equation are described in detail in Section 5.3.12.3. Let us note that the above formulation though presented here for the particular description of reaction rates, can be easily adapted to more general or different reaction rates. Even though we have not assumed any reactions taking place in the fluid domain, it is of no particular difficulty to adapt the model to include such rates. Similarly, for the system of reactions, analogous models can be provided. For closely related models of this type, we refer to [174, 189, 246].

Remark 5.48 (Possible extension to classical FSI). *By introducing the full displacement variable in the whole domain rather than just a boundary movement offers the possibility to easily extend the problem to full elasticity. Such a setting might be solving a fluid reaction-diffusion problem in a thin strip in some pay-zone with surrounding elasticity which is the elastic part of a porous medium. This will be explored and discussed elsewhere. However, a satisfactory understanding of the reaction on the elastic properties is still an open question in the community [64], although some suggestions exist [149].* ⋄

5.3.12.3 Nitsche's idea for boundary conditions and wall movement   We comment below how we prescribe the boundary movement on $\Gamma_{\text{top,bottom}}$. Recall, that the 'structure' part is one dimension lower and we need a technique which allows us to describe the variable explicitly. Here, we make use of Nitsche's method [182] and give the normal displacements u_ν weakly to the problem. Starting from the continuous level, we recall:

$$\rho_s v_\nu = \rho_s \partial_t u_\nu := r(c) - H(u) \quad \text{on } \widehat{\Gamma}_{\text{top,bottom}}.$$

This is discretized by a backward difference quotient for the (uniform) time step size $k := k^n := t^{n+1} - t^n$:

$$u_\nu^n - u_\nu^{n-1} = \frac{k}{\rho_s}[r(c^n) - H(u^{n-1})] \quad \text{on } \widehat{\Gamma}_{\text{top,bottom}}.$$

The new displacement for time index n is then obtained by

$$u_\nu^n = u_\nu^{n-1} + \frac{k}{\rho_s}[r(c^n) - H(u^{n-1})] \quad \text{on } \widehat{\Gamma}_{\text{top,bottom}}. \tag{65}$$

In Problem 5.47, the boundary movement is then given (without 'hats') in weak form:

$$(\nabla \hat{u}, \widehat{\nabla}\hat{\psi}^u) + \frac{\alpha_N}{h}\int_{\widehat{\Gamma}_{\text{top,bottom}}} \hat{u}\hat{\psi}^u\, ds - \int_{\widehat{\Gamma}_{\text{top,bottom}}} \widehat{\nabla}\hat{u} \cdot \hat{\nu}\hat{\psi}^u\, ds - \int_{\widehat{\Gamma}_{\text{top,bottom}}} \widehat{\nabla}\hat{\psi}^u \cdot \hat{\nu}\hat{u}\, ds,$$

where h describes as usually the cell diameter and α_N Nitsche's parameter. The last two integrals are required for the consistency of the method [122, 182]. In fact, this is a very elegant way to obtain a monolithically-coupled problem. For the moving boundary, we use the information from the previous time step which brings explicit flavor into the formulation.

   With that, the above semi-linear form (122) is complemented by Nitsche's terms:

$$\begin{aligned}
\hat{A}_h(\hat{U})(\hat{\Psi}) := \hat{A}(\hat{U})(\hat{\Psi}) &+ \frac{\alpha_N}{h}\langle \hat{u}, \hat{\psi}^u\rangle_{\hat{\Gamma}_{\text{top,bottom}}} \\
&- \langle \widehat{\nabla}\hat{u} \cdot \hat{n}\hat{\psi}^u\rangle_{\hat{\Gamma}_{\text{top,bottom}}} - \langle \widehat{\nabla}\hat{\psi}^u \cdot \hat{n}\hat{u}\rangle_{\hat{\Gamma}_{\text{top,bottom}}}.
\end{aligned} \tag{66}$$

5.3.12.4 Numerical convergence tests of line-integrated concentration   We fix $x = 0.25$ and consider the line-integrated concentration $c_x = c(x = 0.25, y, t)$, with $d_x = d(x = 0.25, t)$

$$\bar{c}_x(t) = \int_{-d_x(t)}^{d_x(t)} c_x(y, t)dy \quad \text{on the mesh levels 2,3,4,5,}$$

and note that $\bar{c}_x$ is a function of time only. We then study the evolution of $\bar{c}_x$ for the spatial mesh hierarchy. Here, we measure the error

$$J(c_h - c_{exact}) = J(c_h) - J(c_{exact}) = \bar{c}_x - \bar{c}_{exact},$$

where c_{exact} is computed on the finest mesh level by

$$\bar{c}_{exact}(t) = \int_{-d_x(t)}^{d_x(t)} c_x(y, t) dy \quad \text{on mesh level 5.}$$
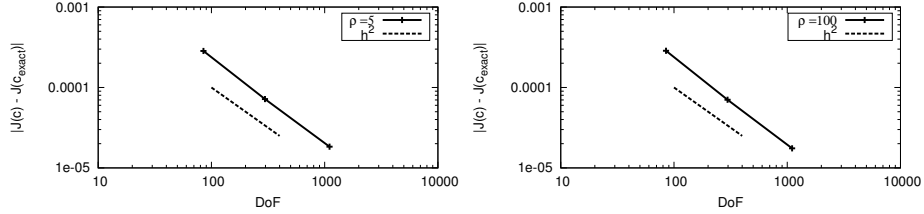

Figure 28: Example 1: test b), quantitative convergence tests of the line-integrated concentration at $x = 0.25$ using global refinement on three different mesh levels. The fourth mesh level is used as 'exact' solution. Displayed are $\rho_s = 5$ (left) and $\rho_s = 100$ (right). Taken from [157].

5.3.12.5 Comparing 2D numerical solution with 1D manufactured model
We conduct numerical tests using the full 2D model and study the pressure and flow profiles.
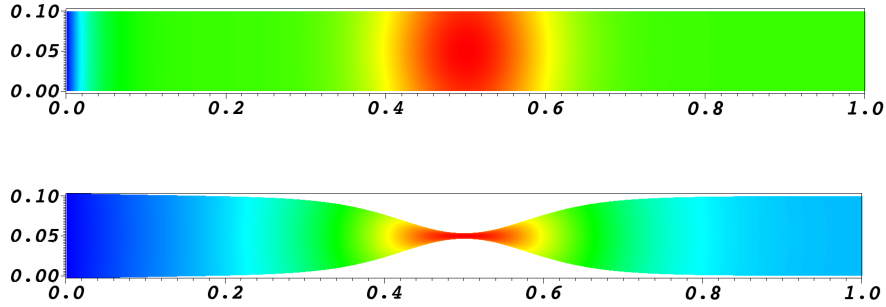
Figure 29: Results of the 2D numerical simulation: Concentration at the first time step and the end time step $T = 14$. At the initial time, the concentration is $c = 1$ in the whole channel. Starting the simulation, $c = 0$ is applied at the inlet boundary (blue) and the source term f increases the concentration in the middle (red).

These 2D tests are based on the second numerical example presented in [157]. Specifically, we have a right-hand side force function (representing an analytical expression for a point source)

$$f(x, y) = a \exp(-b(x - x_m)^2 - c(y - y_m)^2),$$

82

where $a = 1000, b = c = 100$ and $x_m = 0.5, y_m = 0.05$, representing a source with maximum strength at (x_m, y_m) and having an exponential decay and causing the precipitation in the middle of the thin channel $\Omega := [0, 1] \times [0, 0.1]$. All material parameters and geometry information are described in the previously mentioned article [157]. In contrast, the flow is now driven by pressure difference such that we have $p = 1$ on the inflow (left boundary) and $p = 0$ at the right (outflow) boundary. The initial concentration is $c = 1$ for all $x \in \Omega$. In addition, we prescribe $c = 0$ at the left boundary. The goal of our present study is now different from [157]. We are specifically interested in the pressure behavior along the x-axis and the validity of approximating the behavior through the lower-dimensional lubrication equation $(63)_1$.
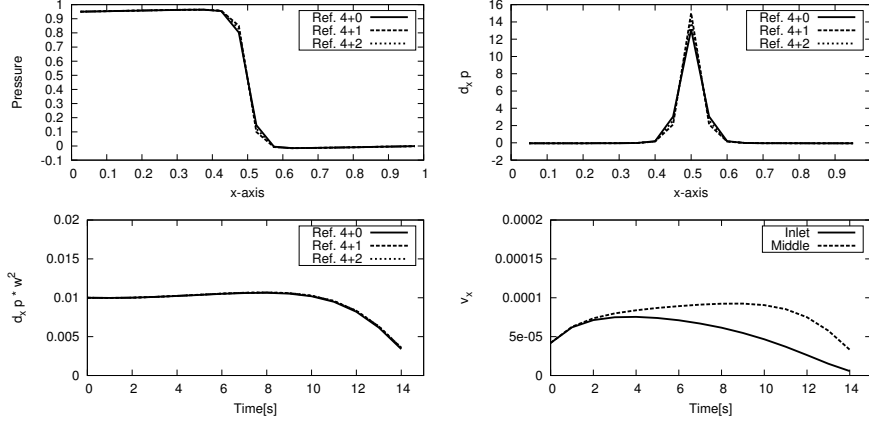

Figure 30: Results of the 2D numerical simulation: Profiles at final time $T = 14$ for the pressure, its gradient, and the key observation quantity $\partial_x p w^2$ shown in the first three figures. Each of the quantities of interest is computed on a sequence of three locally refined meshes to have numerical evidence of convergence. In the final figure, the velocity component in normal flow direction integrated over the cross section is shown on the finest mesh for the inlet and the middle (narrow part of the channel).

Figure 30 shows the pressure and the pressure gradient at $T = 14$ when the channel has closed by ≈ 92 percent. Furthermore, the two bottom figures show $w^2 \partial_x p$ (w is the width of flow domain) and the v_x velocity with respect to time. The choice of this scaling w^2 is motivated by considering $(63)_1$; since the total flow follows the cubic law, the average flow obeys a square law. For the 2D model, achieving the limit is not possible since the mesh will degenerate as the channel is closed. (This drawback in the numerics is investigated in terms of a standard fluid-structure interaction framework in [93–95]). However, the amount of channel constriction is pretty close to the process of clogging. The profile shows that the pressure gradients are blowing up as the channel gets smaller. However, when this is weighted with $2(\varepsilon - d)^2$, that is with square of the opening width of the channel, the resulting quantity goes to zero. This quantity is

proportional to the flow and showing similar behavior as displayed in Figure 30. This suggests that the flow strength vanishes as the channel progressively gets clogged. This is consistent with the case of upscaled model. Figure 29 displays the plot of concentration for two different times.

5.4 FSI techniques on microscopic and macroscopic levels: the Biot system and fluid-filled fracture propagation - towards multiscale problems

When you read the title (Biot plus fracture) of this section, you do not immediately think on fluid-structure interaction. And you are right! We go again away from the very classical point of view. Looking more closely, we however identify parts in which FSI knowledge helps us enormously.

Let us pose some homework rather than explaining everything in detail [18].

One of the key topics are fractures such as in mechanical engineering, subsurface modeling, energy recovery (by far not only oil but more important also heat exchangers in the earth mantle) and also hemodynamics.

Imagine now you are given the task to model fluid-filled fracture propagation in poroelasticity as sketched in Figure 31.
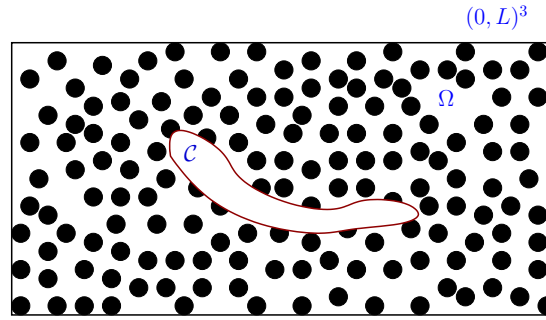
Figure 31: A crack $\mathcal{C}$ embedded in a porous medium. Here, the dimensions of the crack are assumed to be much larger than the pore scale size (black dots) of the porous medium.

What do we need?

- A model for poroelasticity (solid-fluid coupling);

- A model for fracture propagation;

- A model for fluid flow in the fracture.

Possibly (and very likely), we need:

---

[18]In a future version of these notes, we will complement this section with appropriate answers.

- Knowledge on techniques for moving domains, boundaries and interfaces (the fracture is moving!);

- Coupling of different equations from multiphysics via volume terms and interface laws;

- Transformations between different coordinate systems;

- Developing algorithmic schemes in which order we couple and solve the equations;

- Developing of nonlinear and linear solvers.

Remark 5.49. *If we would go into detail (in a future version of these notes, we will do this), then we also need to know how to model and discretize variational inequalities [151, 152, 234].* ⋄

5.5 A larger perspective: Connecting ALE schemes and r-adaptivity (moving mesh methods)

It is interesting to notice that ALE-schemes can be connected to a larger class of mesh-adaption procedures that are known as r-adaptivity methods (a nice overview is provided in [48]). In particular, they are used to improve the finite element discretization accuracy, which is known as r-adaptivity (beyond usual h and p adaptivity). This is slightly different from moving boundary problems, since here, as in fluid-structure interaction, you *must* move the mesh according to the interface. Whereas in other applications it is a powerful method that complements other techniques to improve the accuracy of the solution.

In extension to our explanations in Section 5.2, moving mesh methods can be decomposed into two different sub-classes:

- Location-based methods: the new mesh points are directly obtained from the solution of the auxiliary PDE. Typically, such methods cluster mesh points (see Figure 34).

- Velocity-based methods: the auxiliary PDE computes a mesh-velocity that is then integrated in order to obtain new mesh points. It is clear that such methods are prone to mesh tangling since we work in a Lagrangian-based setting for solving fluid flows and consequently, if we transport the mesh in a setting with high fluid vorticity, mesh faces might intersect. (see, e.g., Figure 12).

Remark 5.50 (Mesh moving in non-convex domains). *In fluid-structure interaction, there is the inherent problem that the moving mesh equations must be solved in non-convex domains, which might lead to additional complications due to re-entrant corners. For a brief discussion, we refer to [73]. However, we observed in several numerical tests [250] that biharmonic mesh motion offers interesting features, and very smooth meshes in non-convex domains. We recall that the second equation is related to the bending moment (in solid mechanics) or the vorticity in fluid dynamics.* ⋄

Since the ALE method can be identified as a moving mesh method, the following theorem from measure theory builds the ground of mesh moving and equidistribution:

Theorem 5.51 (Radon-Nikodym). *Let $\hat{\mathcal{A}}$ be an invertible mapping that maps $\hat{A} \subset \widehat{\Omega}$ to $\hat{\mathcal{A}}(A) \subset \Omega$. The Borel measure is $\nu(\hat{\mathcal{A}}(A)) = |A|$, where $|\cdot|$ denotes the Lebuesgue measure. If ν is a well-defined Borel measure on Ω, then there exists a non-negative function $\alpha : \Omega \to \mathbb{R}$ such that*

$$\nu(\hat{\mathcal{A}}(A)) = \int_{\hat{\mathcal{A}}(A)} M(x)\,dx,$$

for any $\hat{\mathcal{A}}(A) \subset \Omega$. Additionally, M is unique up to a Lebuesgue measure zero.

This theorem ensures that for any invertible mapping $\hat{\mathcal{A}}$, we can find a unique function M such that

$$\int_A dx = \int_{\hat{\mathcal{A}}(A)} M(x)\,dx.$$

The function M is usually called a monitor function that should be large when mesh points are required to be clustered or mesh tangling is likely to occur.

Example 5.52. *The simplest and oldest example is Winslow's method [259]. Another example is given by setting*

$$\alpha = \frac{1}{M} = \frac{1}{\hat{J}}$$

as done by employing Jacobi-based stiffening. We refer to Figure 34 for visualization.

Remark 5.53 (Vector-valued monitor functions)**.** *We notice that the concept of the monitor function is straightforward to apply to matrix-valued monitor functions [48].* ◇

Remark 5.54 (Viewpoint of energy minimization)**.** *The mesh motion equations can be interpreted as the Euler-Lagrange equations of a corresponding energy functional. With this step, mesh moving strategies can be embedded into calculus of variations. As simplest example, we may write harmonic mesh motion as*

$$min\ I(\hat{x}),$$

with

$$I(\hat{x}) = \int_{\widehat{\Omega}} \alpha |\widehat{\nabla} \hat{u}|^2\, d\hat{x}.$$

◇

Remark 5.55 (Extension to time-dependent mesh motion equations)**.** *One might think that a time-dependent mesh motion model would produce more reliable results since fluid-structure interaction is itself time-dependent. Carrying out several numerical tests by using a heat-type equation,*

$$\partial_t \hat{u} - \widehat{\nabla} \cdot (\alpha \widehat{\nabla} \hat{u}) = 0, \quad in\ \widehat{\Omega}_f,$$

or

$$\partial_t \hat{u} - \widehat{\nabla} \cdot \widehat{\sigma}_{mesh} = 0, \quad in\ \widehat{\Omega}_f,$$

we never could produce better results than with a pure stationary method as described in the previous sections. ◇

5.6 Fully Eulerian FSI

5.6.1 Explanation of the approach

The characteristic features of this approach are [69, 71, 207]:

- Formulating both fluid and solid equations in Eulerian coordinates using variational-monolithic coupling resulting in a single semi-linear form;

- Using a single mesh for both equations;

- Accessing the current shape of the solid by an initial point set (IPS) function [69] that maps to the initial domain;

- Implicit usage of a level-set advection function that is automatically included in the solid equation as second equation of a first-order-in-time mixed formulation;

The necessity for this approach (or any other fixed-mesh interface-capturing approach) are explained by the following Figure 32.
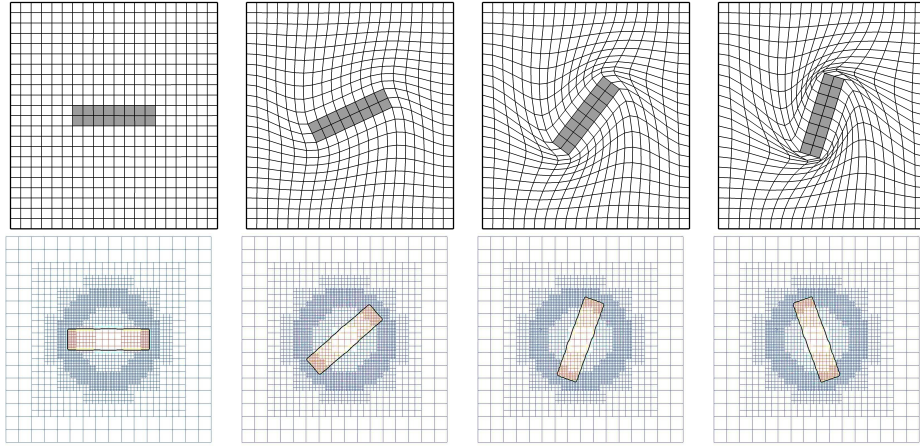
Figure 32: Rotational flow around an unmounted obstacle at different time steps. Top row: moving mesh interface-tracking (ALE) computation without remeshing. Bottom row: fixed-mesh interface-capturing (fully Eulerian) approach (taken from [209]).

Let us briefly recapitulate the necessary ingredients to transform variables, vectors, and tensors from Eulerian to Lagrangian systems and vice versa.

First, we define the inverse transformation required for the fully Eulerian framework, which is, however, only required in the structure domain Ω_s:

$$\mathcal{A}(x,t) : \Omega_s \times I \to \widehat{\Omega}_s, \quad \text{with } \mathcal{A}(x,t) = x - u_s(x,t). \tag{67}$$

Simple calculation yields [69]:

$$\mathcal{A}(\hat{\mathcal{A}}(\hat{x},t),t) = \hat{x}. \tag{68}$$

Spatial differentiation of (68) brings us

$$(I - \nabla u_s) \underbrace{(\hat{I} + \widehat{\nabla} \hat{u}_s)}_{=\widehat{F}_s} = \hat{I}, \tag{69}$$

where I and $\hat{I}$ denote the identity matrices. The following relations between the ALE deformation gradient and its Eulerian counterpart can be inferred from the previous calculations:

$$\widehat{F}_s = (\hat{I} + \widehat{\nabla} \hat{u}_s) = (I - \nabla u_s)^{-1} =: F_s^{-1}, \tag{70}$$

$$\hat{J}_s = \det(\widehat{F}_s) = \det(F_s^{-1}) =: J_s^{-1}. \tag{71}$$

Summarizing, we obtain the deformation gradient and its determinant in Eulerian coordinates:

$$F_s = (I - \nabla u_s), \quad J_s := \det(F_s). \tag{72}$$

Remark 5.56. *In the same way, we define F_f and J_f in the fluid part.* ◇

Remark 5.57. *In the following, we use the short hand notation F and J because it is clear from the context whether we work with F_s and J_s or F_f and J_f, respectively.* ◇

With the help of these relations, we recapitulate the Green-Lagrange tensors in both coordinate systems:

$$E := \frac{1}{2}(F^{-T}F^{-1} - I), \quad \widehat{E} := \frac{1}{2}(\widehat{F}^T \widehat{F} - \hat{I}). \tag{73}$$

With the previously definitions, we recall the constitutive stress tensors in the respective frameworks:

$$\sigma_f := \sigma_f(v_f, p_f) = -p_f I + 2\rho_f \nu_f(\nabla v_f + \nabla v_f^T), \tag{74}$$

$$\widehat{\sigma}_f := \widehat{\sigma}_f(\hat{v}_f, \hat{p}_f) = -\hat{p}_f \hat{I} + 2\hat{\rho}_f \nu_f(\widehat{\nabla} \hat{v}_f \widehat{F}^{-1} + \widehat{F}^{-T} \widehat{\nabla} \hat{v}_f^T), \tag{75}$$

with the velocity v_f, the pressure p_f, the density ρ_f, and the (kinematic) viscosity ν_f and their respective 'hat' coordinates for the definition in the ALE framework. For elastic structures, we use the laws based on the Saint Venant-Kirchhoff (STVK) material:

$$\sigma_s := \sigma_s(u_s) = J F^{-1}(\lambda_s(\operatorname{tr} E)I + 2\mu_s E)F^{-T}, \tag{76}$$

$$\widehat{\sigma}_s := \widehat{\sigma}_s(\hat{u}_s) = \hat{J}^{-1} \widehat{F}(\lambda_s(\operatorname{tr} \widehat{E})\hat{I} + 2\mu_s \widehat{E})\widehat{F}^T, \tag{77}$$

in which the material is characterized by the Lamé coefficients λ_s and μ_s.

It remains to recall the concept of time-derivatives in both frameworks. As before, let $x = x(\hat{x}, t)$, where $\hat{x}$ denotes the initial position of the point x. The velocity v is defined as the total time derivative of the point's position:

$$v(x, t) = d_t x(\hat{x}, t). \tag{78}$$

In Lagrangian coordinates, the total time derivative of a function $\hat{u}(\hat{x}, t) := u(x(\hat{x}, t), t)$ is determined by

$$d_t \hat{u}(\hat{x}, t) = \partial_t \hat{u}(\hat{x}, t) + \hat{\nabla} \hat{u}(\hat{x}, t) d_t \hat{x} = \partial_t \hat{u}(\hat{x}, t), \tag{79}$$

or short

$$d_t \hat{u} = \partial_t \hat{u}, \tag{80}$$

because $d_t \hat{x} = 0$ in the Lagrangian system. In contrast, the total time derivative of a function $u(x, t)$ in the Eulerian framework reads:

$$\begin{aligned} d_t u(x, t) &= \partial_t u(x, t) + \nabla u(x, t) d_t x \\ &= \partial_t u(x, t) + \nabla u(x, t) v(x, t) \\ &= \partial_t u(x, t) + v(x, t) \cdot \nabla u(x, t). \end{aligned} \tag{81}$$

Or short:

$$d_t u = \partial_t u + v \cdot \nabla u. \tag{82}$$

The convection term $v \cdot \nabla u$ denotes the key difference between time derivatives in both frameworks and plays an important role when formulating the governing elasticity equations in Eulerian coordinates.

5.6.2 Comparing variational-monolithic ALE and fully Eulerian FSI

There are striking similarities between our concepts for ALE_{fx} and fully Eulerian FSI using variational-monolithic coupling:

- ALE: $\hat{\mathcal{A}}(\hat{x}, t) : \widehat{\Omega}_f \times I \to \Omega_f$;

- Fully Eulerian: $\mathcal{A}(x, t) : \Omega_s \times I \to \widehat{\Omega}_s$.

Both mappings are exactly the opposite operations (see also Figure 33 as further illustration) and therefore, all principal quantities such as the deformation gradient can be transformed into the other approach. To show these relationships between both frameworks and related computations was the purpose of [207].

5.6.3 IPS - initial point set

Finally, we introduce the initial point set (IPS) [69] for the fully Eulerian framework. This equation is defined on the continuous level (like a level-set function) and is used (after discretization) to map each structure point to its initial position:

Problem 5.58. *Find u such that*

$$\partial_t u - w + (w \cdot \nabla) u = 0, \tag{83}$$

The initial and boundary conditions are given by

$$\begin{aligned} u(x, 0) &= 0, \quad x \in \Omega_E, \\ u(x, t) &= 0, \quad x \in \partial \Omega_E, \, t \in I. \end{aligned}$$
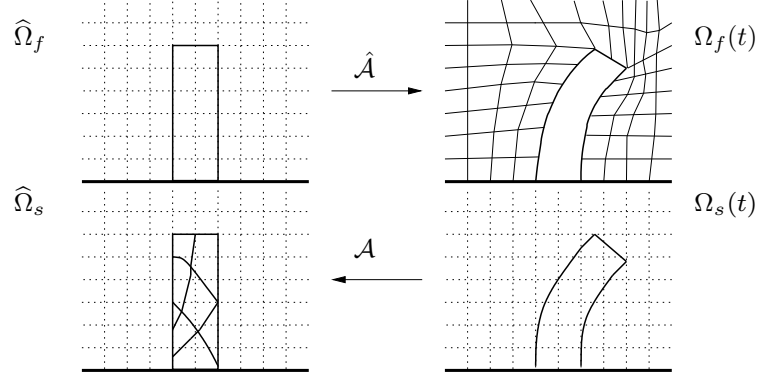
Figure 33: Transformation in ALE$_{fx}$ and fully Eulerian frameworks in order to move the fluid on Ω_f or to detect the solid in $\widehat{\Omega}_s$. To recall: in ALE$_{fx}$ all computations are performed in $\widehat{\Omega}$. In contrast using the fully Eulerian framework all equations are computed in Ω.

Then, the value of u is transported with the velocity w to its initial position at time zero.

Remark 5.59. *The IPS-function is (like level-set) a Hamilton-Jacobi-type equation that requires special techniques for its theory [76] and often for its computation [181, 191, 219]. In fact, it is a pure advection equation that always requires stabilization techniques.*

Remark 5.60 (Difference of the IPS-function and a level-set-function)**.** *Using the IPS-function, the position of the interface is determined by structural mechanics. In contrast, a level-set-function is given by the local fluid velocity normal to the interface. In addition, the IPS-function is already included in the physical model by splitting the second-order-in-time wave equation into a mixed system [12]. Here, the second equation represents the IPS-function. Finally, the IPS-function preserves corners and edges as demonstrated in [70].* ◇

5.6.4 Practical aspects of solid localization

In order to detect the solid in each time step, we use the very definition of $\mathcal{A} := x - u$ and define and indicator function that localizes the solid in $\widehat{\Omega}_s$ (according to the IPS-function). To this end, we define characteristic functions in Ω_f and Ω_s by

$$\chi_s := \begin{cases} 0, & x - u \in \widehat{\Omega}_f, \\ 1, & x - u \in \widehat{\Omega}_s \cup \widehat{\Gamma}_i, \end{cases} \quad \text{and} \quad \chi_f = 1 - \chi_s. \tag{84}$$

How does this operation work? Well, in each point (cell corner or quadrature point), i.e., $x \in \Omega_s$, we subtract the displacement u. If the result $x - u$ belongs to the solid

configuration in the initial setting $\widehat{\Omega}_s = \Omega_s(0)$, then $\chi_s = 1$ (otherwise $\chi_s = 0$). However, if you notice carefully, in a fully implicit way, the displacement is an unknown solution variable itself. Here, we do (for simplification) the following: The characteristic function $\chi_{f,s}$ for the evaluation of the new domain depends on the solution u^n of previous time step (and not on the present unknown solution $u := u^{n+1}$). This circumvents the evaluation of the directional derivatives of $\chi_{f,s}$, but, on the other hand, it introduces an explicit flavor such that the time steps have to be chosen sufficiently small. Consequently, the interface deforms moderately during two time steps u^n and $u := u^{n+1}$. Then,

$$\chi_f(x) = \hat{\chi}_f(x - u) \approx \hat{\chi}_f(x - u^n),$$

should be a good approximation. To ensure that the two domains Ω^{n+1} and Ω^n are sufficiently close such that the previous assumptions may be taken, the time steps k are chosen adaptively and they are used to control to nonlinear solution process. With this explicit usage, an additional nonlinearity at the interface is prevented because the evaluation of the derivatives of the characteristic functions is circumvented:

$$\chi'_f(\delta u; x) \approx \hat{\chi}'_f(\delta u; x - u^n) \Rightarrow \chi'_f(\delta u; x) = 0.$$

5.6.5 Variational-monolithic fully Eulerian FSI - the complete system

As for fluid flows, let v_s^D and u_s^D be suitable extensions of Dirichlet inflow data. Then:

Problem 5.61 (Structure models in Eulerian coordinates). *Find*
$\{v_s, u_s, p_s\} \in L_s \times \{u_s^D + V_s^0\} \times L_s^0$, *such that* $v_s(0) = v_s^0$ *and* $u_s(0) = u_s^0$ *are satisfied, and for almost all time steps* $t \in I$ *holds:*

$$(\rho_s J \partial_t v_s, \psi^v)_{\Omega_s} + (\rho_s J (v_s \cdot \nabla) v_s, \psi^v)_{\Omega_s}$$
$$+ (\sigma_s, \nabla \psi^v)_{\Omega_s} - \langle \sigma_s n_s, \psi^v \rangle_{\Gamma_i \cup \Gamma_N} - (\rho_s J f_s, \psi^v)_{\Omega_s} = 0 \quad \forall \psi^v \in V_s^0,$$
$$\rho_s (\partial_t u_s + (v_s \cdot \nabla) u_s - v_s, \psi^u)_{\Omega_s} = 0 \quad \forall \psi^u \in L_s,$$
$$(J - 1, \psi^p)_{\Omega_s} = 0 \quad \forall \psi^p \in L_s^0,$$

where ρ_s *denotes the structure density,* n_s *the outer normal vector on* Γ_i *and* Γ_N, *respectively. The Cauchy stress tensors for the material models are given by*

$$\sigma_s^{INH} := -p_s I + \mu_s (F^{-1} F^{-T} - I),$$
$$\sigma_s^{STVK} := J F^{-1} (\lambda_s (trE) I + 2\mu_s E) F^{-T}, \tag{85}$$

with the Lamé coefficients λ_s *and* μ_s. *External volume forces are described by the term* f_s. *Using the STVK material, the third equation becomes redundant and the compressibility is related to the Poisson ratio* ν_s *(*$\nu_s < \frac{1}{2}$*).*

Formulating a fully coupled system in Eulerian coordinates results in the innocent problem:

Problem 5.62 (Variational-monolithic FSI in Eulerian coordinates - the mathematical version). *Find*
$\{v_f, v_s, u_s, p_f, p_s\} \in \{v_f^D + V_f^0\} \times L_s \times \{u_s^D + V_s^0\} \times L_f^0 \times L_s^0$, *such that* $v_f(0) = v_s^0$,
$v_s(0) = v_s^0$, $u_s(0) = u_s^0$ *are satisfied, and for almost all time steps* $t \in I$ *holds:*

$$\text{Fluid momentum} \begin{cases} (\chi_f \rho_f \partial_t v_f, \psi_f^v) + (\chi_f \rho_f (v_f \cdot \nabla) v_f, \psi_f^v) \\ + (\chi_f \sigma_f, \nabla \psi_f^v) - (g, \psi_f^v) - (\chi_f \rho_f f_f, \psi_f^v) \quad = 0 \quad \forall \psi_f^v \in V_f^0, \end{cases}$$

$$\text{Solid momentum, 1st eq.} \begin{cases} (\chi_s J \rho_s \partial_t v_s, \psi_s^v) + (\chi_s J \rho_s (v_s \cdot \nabla) v_s, \psi_s^v) \\ + (\chi_s \sigma_s, \nabla \psi_s^v) - (\chi_s J \rho_s f_s, \psi_s^v) \quad\quad\quad = 0 \quad \forall \psi_s^v \in V_s^0, \end{cases}$$

$$\text{Solid momentum, 2nd eq.; IPS} \begin{cases} \chi_s \rho_s (\partial_t u_s + (v_s \cdot \nabla) u_s - v_s, \psi_s^u) \quad = 0 \quad \forall \psi^u \in L_s, \end{cases}$$

$$\text{Fluid mass conservation} \begin{cases} (\chi_f div\, v_f, \psi_f^p) \quad = 0 \quad \forall \psi_f^p \in L_f, \end{cases}$$

$$\text{Solid mass conservation} \begin{cases} (\chi_s P_s, \psi_s^p)_{\Omega_s} \quad = 0 \quad \forall \psi^p \in L_s^0. \end{cases}$$

A crucial point in computing fully nonstationary processes is the decoupling of the fluid v_f and the structure velocity v_s. Using the previous formulation, the fluid velocity disturbs in computations over long time intervals and this leads to oscillations at the interface. To prevent this, analogously to Dunne [69], an additional velocity variable is introduced, satisfying[19]

$$w = v_s \quad \text{in } \Omega_s \cup \Gamma_i,$$
$$\Delta w = 0 \quad \text{in } \Omega_f.$$

As second step, we extend u_s and w_s to the fluid domain for computational reasons[20] Then a possible computational stable framework is given by [255]:

Problem 5.63 (Variational-monolithic FSI in Eulerian coordinates - a computational version). *Find*
$\{v_f, v_s, w_f, w_s, u_f, u_s, p_f, p_s\} \in \{v_f^D + V_f^0\} \times L_s \times \{w_f^D + V_f^0\} \times L_s \times \{u_f^D + V_s^0\} \times \{u_s^D + V_s^0\} \times L_f^0 \times L_s^0$, *such that* $v_f(0) = v_s^0$, $w_f(0) = w_s^0$, $u_f(0) = u_f^0$, $v_s(0) = v_s^0$,

---

[19] This might be overcome by techniques currently investigated in [91].
[20] This second step is of course not mandatory!

$w_f(0) = w_s^0$, $u_s(0) = u_s^0$ *are satisfied, and for almost all time steps $t \in I$ holds:*

$$(\chi_f \rho_f \partial_t v_f, \psi_f^v) + (\chi_f \rho_f (v_f \cdot \nabla) v_f, \psi_f^v)$$
$$+ (\chi_f \sigma_f, \nabla \psi_f^v) - (g, \psi_f^v) - (\chi_f \rho_f f_f, \psi_f^v) = 0 \quad \forall \psi_f^v \in V_f^0,$$
$$(\chi_s J \rho_s \partial_t v_s, \psi_s^v) + (\chi_s J \rho_s (v_s \cdot \nabla) v_s, \psi_s^v)$$
$$+ (\chi_s \sigma_s, \nabla \psi_s^v) - (\chi_s J \rho_s f_s, \psi_s^v) = 0 \quad \forall \psi_s^v \in V_s^0,$$
$$\chi_f(\alpha_w \nabla w_f, \nabla \psi_f^w) = 0 \quad \forall \psi^w \in V_f^0,$$
$$\chi_s(v_s - w_s, \psi_f^w) = 0 \quad \forall \psi^w \in L_s,$$
$$\chi_f \rho_f (\partial_t u_f + (w_f \cdot \nabla) u_f - w_f, \psi_f^u) = 0 \quad \forall \psi^w \in L_f,$$
$$\chi_s \rho_s (\partial_t u_s + (w_s \cdot \nabla) u_s - w_s, \psi_s^u) = 0 \quad \forall \psi^u \in L_s,$$
$$(\chi_f \, div \, v_f, \psi_f^p) = 0 \quad \forall \psi_f^p \in L_f,$$
$$(\chi_s P_s, \psi_s^p)_{\Omega_s} = 0 \quad \forall \psi^p \in L_s^0.$$

with a monitor parameter α_w.

For fully nonstationary simulations, it is important to consider the following three convection terms which make their corresponding equations from pure hyperbolic type:

$$J\rho_s \partial_t v_s + J\rho_s (v_s \cdot \nabla) v_s \quad \text{(1st structure equation)},$$
$$\partial_t u_f + (w_f \cdot \nabla) u_f \quad \text{(3rd fluid equation)}, \tag{86}$$
$$\partial_t u_s + (w_s \cdot \nabla) u_s \quad \text{(3rd structure equation)}.$$

These equations require stabilization for their numerical treatment.

Remark 5.64 (Mass/Volume conservation). *We shall give a brief account to mass conservation because this is a well-known difficulty and often asked when using interface-capturing techniques. This is strongly-related to the signed distance function property, which needs to remain valid for long-time computations. For numerical validations, we refer the reader to [204, 255].* ⋄

Remark 5.65 (Signed distance function property). *Even though reinitialization is not necessary in this framework, it is often being asked. In fact, although the interface-capturing-function is initialized as a signed distance function, it is not for sure it remains so. However, it many situations it is preferable to have a signed distance function throughout the numerical simulation. The reasons are that velocity extension methods can be employed successfully, a possibly given thickness of the interface remains valid, and finally, that the level-set function behaves well near the interface [219]. To ensure the signed-distance property, the interface-capturing-function needs to be reinitialized. For various methods and explication, we refer the reader to the level-set literature. For explicit usage of reinitialization in terms of fully Eulerian fluid-structure interaction, we refer to [127].* ⋄

5.6.6 Summary of features

- The two major drawbacks are cut-cells (interface is not aligned to mesh faces) and convective behavior.

- Detailed comparisons and code-validation with two different software packages (each contains ALE and fully Eulerian codes) have been performed [69, 93, 94, 204, 207, 255]. Further important studies confirming correct modeling are [161, 222].

- On the other hand, we achieve large structural deformations as displayed in Figure 32.
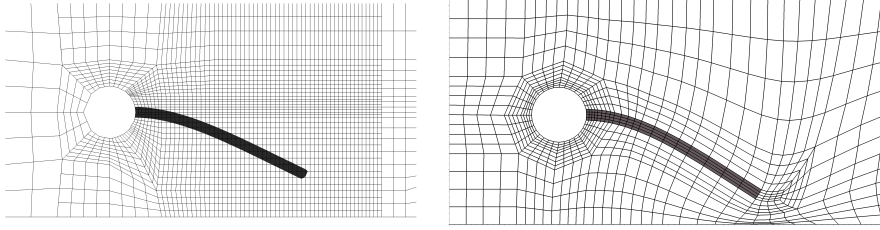

Figure 34: CSM 4 test in fully Eulerian (at left) and ALE coordinates (at right) with biharmonic mesh motion model without any remeshing. The results are taken from [255].

Using an unfitted finite element method and convection-stabilization [255], we obtain similar results to ALE method for the most difficult FSI2-benchmark problem (so, the method is able reproduce benchmark results!). However, for stability and robustness reasons, a locally modified FEM method has been proposed recently [91] that keeps the connectivity of the system matrix and reproduces full convergence order in the energy norm (see also XFEM/GFEM [9]). Furthermore, the improvement of time integration is currently in development [92].
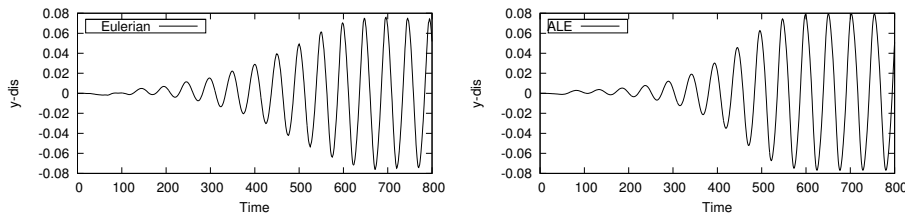

Figure 35: [255]: Comparison of the transient oscillation of the fully Eulerian and the ALE approach for the FSI 2 benchmark.
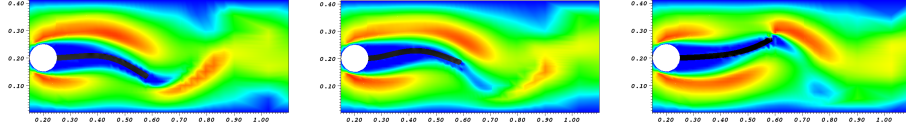
Figure 36: [255]: Dynamics of the FSI 2 benchmark: x-velocity profile to different time steps $t = 7.22, 7.32, 7.42$.

Remark 5.66 (References). *Although being a young and recent method, interesting studies using a fully-Eulerian approach have been obtained in [59, 69, 70, 93–95, 127, 161, 204, 207, 222–224, 255, 267].* ◇

5.7 Coupling of ALE and Eulerian FSI

Let us finally make a brief excursion to a coupled moving mesh/fixed-mesh method:

- Coupling ALE coordinates with the fully Eulerian framework.

To organize a fully monolithically-coupled formulation, the computational domain $\widehat{\Omega}$ is split into an ALE subdomain and an Eulerian subdomain, i.e., $\widehat{\Omega} = \widehat{\Omega}_A \cup \Omega_E$.

We propose the following EALE framework [253, 254] for computing fully nonstationary processes:

Problem 5.67 (Variational fluid-structure interaction in EALE coordinates with an additional velocity). *Find the following variables:*

- *Velocities* $\{v_f, \hat{v}_f, v_s, \hat{v}_s\} \in \{v_f^D + V_{f,v}^0\} \times \{\hat{v}_f^D + \hat{V}_{f,\hat{v}}^0\} \times \{v_s^D + V_{s,v}^0\} \times \hat{L}_s$ *with* $v_f(0) = v_f^0, \hat{v}_f(0) = \hat{v}_f^0, v_s(0) = v_s^0$ *and* $\hat{v}_s(0) = \hat{v}_s^0$,

- *Additional velocities* $\{w_f, w_s\} \in \{w_f^D + V_{f,w}^0\} \times \{w_s^D + V_{s,w}^0\}$ *with* $w_f(0) = w_f^0$ *and* $w_s(0) = w_s^0$,

- *Displacements* $\{u_f, \hat{u}_f, u_s, \hat{u}_s\} \in \{u_f^D + V_{f,u}^0\} \times \{\hat{u}_f^D + \hat{V}_{f,\hat{u}}^0\} \times \{u_s^D + V_{s,u}^0\} \times \{\hat{u}_s^D + \hat{V}_{s,\hat{u}}^0\}$ *with* $u_f(0) = u_f^0, \hat{u}_f(0) = \hat{u}_f^0, u_s(0) = u_s^0$ *and* $\hat{u}_s(0) = \hat{u}_s^0$,

- *Pressures* $\{p_f, \hat{p}_f\} \in L_f^0 \times \hat{L}_f^0$,

such that for $t \in I$ and $\alpha_w > 0$ holds:

$$(\chi_f \rho_f \partial_t v_f, \psi_f^v) + (\chi_f \rho_f (v_f \cdot \nabla) v_f, \psi_f^v) \tag{87}$$

$$+(\chi_f \sigma_f, \nabla \psi_f^v) - \langle \chi_f g_f n_f, \psi_f^v \rangle - (\chi_f \rho_f f_f, \psi_f^v) \tag{88}$$

$$= 0 \quad \forall \psi_f^v \in V_{f,v}^0, \tag{89}$$

$$(\hat{\chi}_f \hat{J} \hat{\rho}_f \partial_t \hat{v}_f, \hat{\psi}_f^v) + \hat{\chi}_f (\hat{\rho}_f \hat{J} (\widehat{F}^{-1} (\hat{v}_f - \partial_t \hat{\mathcal{A}}) \cdot \widehat{\nabla}) \hat{v}_f), \hat{\psi}_f^v) \tag{90}$$

$$+(\hat{\chi}_f \hat{J} \hat{\sigma}_f \widehat{F}^{-T}, \widehat{\nabla} \hat{\psi}_f^v) - \langle \hat{\chi}_f \hat{g}_f \hat{n}_f, \hat{\psi}_f^v \rangle - (\hat{\chi}_f \hat{\rho}_f \hat{J} \hat{f}_f, \hat{\psi}_f^v) \tag{91}$$

$$= 0 \quad \forall \hat{\psi}_f^v \in \hat{V}_{f,\hat{v}}^0, \tag{92}$$

$$\tag{93}$$

$$(\chi_s J \rho_s \partial_t v_s, \psi_s^v) + (\chi_s J \rho_s (v_s \cdot \nabla) v_s, \psi_s^v) \tag{94}$$

$$+(\chi_s \sigma_s, \nabla \psi_s^v) - (\chi_s J \rho_s f_s, \psi_s^v) \tag{95}$$

$$= 0 \quad \forall \psi_s^v \in V_s^0, \tag{96}$$

$$(\hat{\chi}_s \hat{\rho}_s \partial_t \hat{v}_s, \hat{\psi}_s^v) + (\hat{\chi}_s \hat{J} \hat{\sigma}_s \widehat{F}^{-T}, \widehat{\nabla} \hat{\psi}_s^v) - (\hat{\chi}_s \hat{\rho}_s \hat{f}_s, \hat{\psi}_s^v) \tag{97}$$

$$= 0 \quad \forall \hat{\psi}_s^v \in \hat{V}_s^0, \tag{98}$$

$$\tag{99}$$

$$\chi_f \rho_f (\partial_t u_f + (w_f \cdot \nabla) u_f - w_f, \psi_f^u) = 0 \quad \forall \psi_f^u \in V_f^0, \tag{100}$$

$$(\hat{\chi}_f \hat{\sigma}_{mesh}, \widehat{\nabla} \hat{\psi}_f^u) = 0 \quad \forall \hat{\psi}_f^u \in \hat{V}_{f,\hat{u},\widehat{\Gamma}_{i,A}}^0, \tag{101}$$

$$\tag{102}$$

$$\chi_s \rho_s (\partial_t u_s + (w_s \cdot \nabla) u_s - w_s, \psi_s^u) = 0 \quad \forall \psi_s^u \in V_s^0, \tag{103}$$

$$\hat{\chi}_s \hat{\rho}_s (\partial_t \hat{u}_s - \hat{v}_s, \hat{\psi}_s^u) = 0 \quad \forall \hat{\psi}_s^u \in \hat{L}_s, \tag{104}$$

$$\tag{105}$$

$$\chi_f (\alpha_w \nabla w_f, \nabla \psi_f^w) = 0 \quad \forall \psi^w \in V_f^0, \tag{106}$$

$$- \tag{107}$$

$$\tag{108}$$

$$\chi_s (v_s - w_s, \psi_f^w) = 0 \quad \forall \psi^w \in L_s, \tag{109}$$

$$- \tag{110}$$

$$\tag{111}$$

$$(\chi_f \, div \, v_f, \psi_f^p) = 0 \quad \forall \psi_f^p \in L_f^0, \tag{112}$$

$$(\hat{\chi}_f \, \widehat{div} \, (\hat{J} \widehat{F}^{-1} \hat{v}_f), \hat{\psi}_f^p) = 0 \quad \forall \hat{\psi}_f^p \in \hat{L}_f^0, \tag{113}$$

$$\tag{114}$$

Let us understand the meaning of all the twelve equations in Problem 5.67, which is divided into seven parts. In part I, Equation (89) and (92) are the Navier-Stokes equations described in Eulerian coordinates and in the ALE framework. Then, in part II and IV, the first order solid system is used. Consequently, the first equations (Eulerian and secondly in Lagrangian coordinates) are given here in part II. We notice in the Eulerian structure that we deal with an additional (nonstandard) convection

term in Equation (96) due to the transformation from the Lagrangian system. In the third part, we find transformations related to the fluid problems. Here, the first Equation (100) comes from the IPS whereas the second Equation (101) is the well-known moving-mesh PDE for ALE problems. Next, in part IV, the second equations of the elasticity system are given (therefore, related to part II). The next two parts V and VI, Equation (106) and (109), define the additional velocity variable w, which is only required in the Eulerian domain. Finally, the incompressibility condition of the fluid is expressed in part VII.

In Problem 5.67, the characteristic functions in $\widehat{\Omega}_{f,A}$ and $\widehat{\Omega}_{s,A}$ are defined as

$$\hat{\chi}_f := \begin{cases} 1, & \hat{x} \in \widehat{\Omega}_{f,A}, \\ 0, & \hat{x} \in \widehat{\Omega}_{s,A} \cup \widehat{\Gamma}_{i,A}, \end{cases} \quad \text{and} \quad \hat{\chi}_s := 1 - \hat{\chi}_f. \tag{115}$$

Specifically, the cells that belong to the ALE domain are simply marked in the fixed reference configuration because it is clear where the fluid and the structure are located thanks to the interface-tracking character of ALE. However, in the Eulerian domain it is a bit more complicated to identify the structure. Here, the characteristic functions in Ω_f and Ω_s are defined as

$$\chi_f := \begin{cases} 1, & x - u \in \widehat{\Omega}_{f,E}, \\ 0, & x - u \in \widehat{\Omega}_{s,E} \cup \widehat{\Gamma}_{i,E}, \end{cases} \quad \text{and} \quad \chi_s = 1 - \chi_f. \tag{116}$$

Details are provided elsewhere [255].

Remark 5.68 (Coupling conditions for coupling ALE with Eulerian)**.** *The coupling conditions to couple the ALE framework with the fully Eulerian framework on the EALE-interface are given by*

$$\hat{u}_{f,A} = u_{f,E} = 0, \tag{117}$$

$$\partial_n \hat{u}_{f,A} = \partial_n u_{f,E} = 0, \tag{118}$$

$$\widehat{\sigma}_{f,A} \hat{n}_{f,A} = \sigma_{f,E} n_{f,E}. \tag{119}$$

A deeper discussion is provided in [251]. ◇

6 Discretization and Solution of Nonlinear Problems in the ALE$_{fx}$ framework

In this part, we focus on

- Time discretization based on finite differences: first-order backward Euler, second order Crank-Nicolson, second-order shifted Crank-Nicolson, second-order Fractional-Step-θ;

- Spatial discretization based on inf-sup stable Galerkin finite elements;

- Newton's method with simple line search backtracking;

- Solution of the linear equations;

- To discuss a 'simple' problem showing that our approach is easy to realize with pre-understanding of a class such as numerical methods for partial differential equations;

- Pointing to some code pieces that have been used for numerical simulations presented in these notes.

We concentrate on descriptions for the ALE$_{fx}$ setting. The other formulations can be formulated in similar ways; however we notice that fully Eulerian time discretization is a bit tricky since the interface moves between two time steps and test functions might correspond to *the other continuum*. Details are outlined in [92, 209].

6.1 Time

In the domain $\widehat{\Omega}$ and the time interval $I = [0, T]$, we consider the fluid-structure interaction Problem 5.19 with harmonic or linear-elastic mesh motion in an abstract setting (the biharmonic problem is straightforward): Find $\hat{U} = \{\hat{v}_f, \hat{v}_s, \hat{u}_f, \hat{u}_s, \hat{p}_f, \hat{p}_s\} \in \widehat{X}_D^0$, where $\widehat{X}_D^0 := \{\hat{v}_f^D + \hat{V}_{f,\hat{v}}^0\} \times \hat{L}_f \times \{\hat{u}_f^D + \hat{V}_{f,\hat{u}}^0\} \times \{\hat{u}_s^D + \hat{V}_s^0\} \times \hat{L}_f^0 \times \hat{L}_s^0$, such that

$$\int_0^T \hat{A}(\hat{U})(\hat{\Psi}) \, dt = \int_0^T \widehat{F}(\hat{\Psi}) \, dt \quad \forall \hat{\Psi} \in \widehat{X}, \tag{120}$$

where $\hat{\Psi} = \{\hat{\psi}_f^v, \hat{\psi}_s^v, \hat{\psi}_f^u, \hat{\psi}_s^u, \hat{\psi}_f^p, \hat{\psi}_s^p\}$ and $\widehat{X} = \hat{V}_{f,\hat{v}}^0 \times \hat{L}_f \times \hat{V}_{f,\hat{u},\widehat{\Gamma}_i}^0 \times \hat{V}_s^0 \times \hat{L}_f^0 \times \hat{L}_s^0$. The time integral is defined in an abstract sense such that the equation holds for *almost all time steps*.

Problem 6.1 (Semi-linear form of FSI using harmonic mesh motion). *Using the harmonic mesh motion model leads to the following expressions of $\hat{A}(\hat{U})(\hat{\Psi})$ and $\widehat{F}(\hat{\Psi})$:*

$$\widehat{F}(\hat{\Psi}) = (\hat{\rho}_s \hat{f}_s, \hat{\psi}_s^v)_{\widehat{\Omega}_s}, \tag{121}$$

and

$$\hat{A}(\hat{U})(\hat{\Psi}) = (\hat{J}\hat{\rho}_f \partial_t \hat{v}_f, \hat{\psi}_f^v)_{\widehat{\Omega}_f} + (\hat{\rho}_f \hat{J}(\widehat{F}^{-1}\hat{v}_f \cdot \widehat{\nabla})\hat{v}_f), \hat{\psi}_f^v)_{\widehat{\Omega}_f} \tag{122}$$

$$- (\hat{\rho}_f \hat{J}(\widehat{F}^{-1}\hat{w} \cdot \widehat{\nabla})\hat{v}_f), \hat{\psi}_f^v)_{\widehat{\Omega}_f} - \langle \hat{g}_f, \hat{\psi}_f^v\rangle_{\widehat{\Gamma}_N} - (\hat{\rho}_f \hat{J}\hat{f}_f, \hat{\psi}_f^v)_{\widehat{\Omega}_f} \tag{123}$$

$$+ (\hat{J}\hat{\sigma}_f \widehat{F}^{-T}, \widehat{\nabla}\hat{\psi}_f^v)_{\widehat{\Omega}_f} + (\hat{\rho}_s \partial_t \hat{v}_s, \hat{\psi}_s^v)_{\widehat{\Omega}_s} + (\widehat{F}\widehat{\Sigma}, \widehat{\nabla}\hat{\psi}_s^v)_{\widehat{\Omega}_s} \tag{124}$$

$$+ (\hat{\rho}_s \partial_t \hat{u}_s, \hat{\psi}_s^u)_{\widehat{\Omega}_s} - (\hat{\rho}_s \hat{v}_s, \hat{\psi}_s^u)_{\widehat{\Omega}_s} + (\alpha_u \widehat{\nabla}\hat{u}_f, \widehat{\nabla}\hat{\psi}_f^u)_{\widehat{\Omega}_f} \tag{125}$$

$$+ \gamma_w(\hat{v}_s, \hat{\psi}_s^v)_{\widehat{\Omega}_s} + \gamma_s(\hat{\epsilon}(\hat{v}_s), \widehat{\nabla}\hat{\psi}_s^v)_{\widehat{\Omega}_s} \tag{126}$$

$$+ (\widehat{div}(\hat{J}\widehat{F}^{-1}\hat{v}_f), \hat{\psi}_f^p)_{\widehat{\Omega}_f} + (\hat{P}_s, \hat{\psi}_s^p)_{\widehat{\Omega}_s}. \tag{127}$$

The fluid convection term in (122) *is decomposed into two parts for later purposes.*

6.1.1 Basic concepts and considerations for temporal discretization

Before we begin, let us briefly recapitulate some basics from our lecture numerical methods for ordinary differential equations. A classical scheme for problems with a stationary limit is the (implicit) backward Euler scheme (BE), which is strongly A-stable (but only from first order) and dissipative. It is used in numerical Examples, where a stationary limit must be achieved. In contrast, the (implicit) Crank-Nicolson scheme is of second order, A-stable, and has very little dissipation but suffers from case-to-case instabilities caused by rough initial and/or boundary data. These properties are due to weak stability (it is not *strongly* A-stable). A variant of the Crank-Nicolson scheme is called *shifted* Crank-Nicolson scheme, is analyzed in Rannacher et al. [133, 199], which allows for global stability of the solution. These time-stepping schemes are addressed in more detail below. The third scheme summarizes the advantages of the other two and is known as the Fractional-Step-θ scheme for computing unsteady-state simulations [114]. Roughly-speaking it consists of summarizing three Crank-Nicolson steps and has therefore the same accuracy and compuational cost as the Crank-Nicolson scheme. However, it is more robust, i.e., it is strongly A-stable, and therefore well-suited for computing solutions with rough data and long-term computations for problems on fixed meshes. This property also holds for ALE-transformed fluid equations, which is demonstrated in a numerical test below. We also refer the reader to a modification of the Fractional-Step-θ scheme [240].

Definition 6.2 (A-stability). *To summarize:*

- *A-stable (Crank-Nicolson)*

- *strictly A-stable (shifted Crank-Nicolson)*

- *strongly A-stable (backward Euler and Fractional-step-θ)*

$\diamond$

We briefly explain the derivation of One-Step-θ schemes (see, e.g., [237, 240]) for the heat equation. Let

$$\partial_t u - \Delta u = f,$$

be given. Time discretization yields:

$$\frac{u - u^{n-1}}{\delta t} - \theta \Delta u - (1-\theta)\Delta u^{n-1} = \theta f + (1-\theta)f^{n-1}.$$

Thus,

$$u - \delta t \theta \Delta u = u^{n-1} + \delta t(1-\theta)\Delta u^{n-1} + \delta t \theta f + \delta t(1-\theta)f^{n-1}.$$

6.1.1.1 Time stability of second-order hyperbolic equations In fluid-structure interaction, the solid equation is of hyperbolic type and satisfies an energy conservation law on the continuous level. That means that our time-discretization scheme should reproduce this property. We recall findings (neglecting the damping terms) from the theory [12, 31, 120]:

- *Stability in the L^2-norm:* the One-Step-θ scheme (139) is unconditionally stable, i.e., there is no time step restriction on k if and only if $\theta \in [\frac{1}{2}, 1]$.

- *Energy conservation:* the one-step-θ scheme (139) preserves energy only for the choice $\theta = \frac{1}{2}$. For $\theta > \frac{1}{2}$ (e.g., the implicit Euler scheme for the choice $\theta = 1$) the scheme dissipates energy.

Consequently, the Crank-Nicolson scheme is an optimal time-stepping scheme for hyperbolic equations. Possible restrictions with respect to the time-step size are weaker for hyperbolic problems than for parabolic differential equations [120]. This finding leads us to the assumption that the fluid problem has stronger influence on stability aspects than the structural problem.

Remark 6.3. *The last statement is in contradiction to our numerical observations made in [209].* ⋄

To bring it to the point: issues of numerical stability of the coupled problem are of utter importance, as it consists of a combined consideration of two different types of equations:

- the incompressible Navier-Stokes equations which is of parabolic type and that comes with smoothing properties; and the hyperelastic solid equation of hyperbolic type, which requires good conservation properties with very little numerical dissipation.

By these considerations, the Crank-Nicolson scheme and its variants like shifted versions [133, 172, 199] or the fractional step theta scheme [45, 240], appear to be ideal candidates that further show second order accuracy.
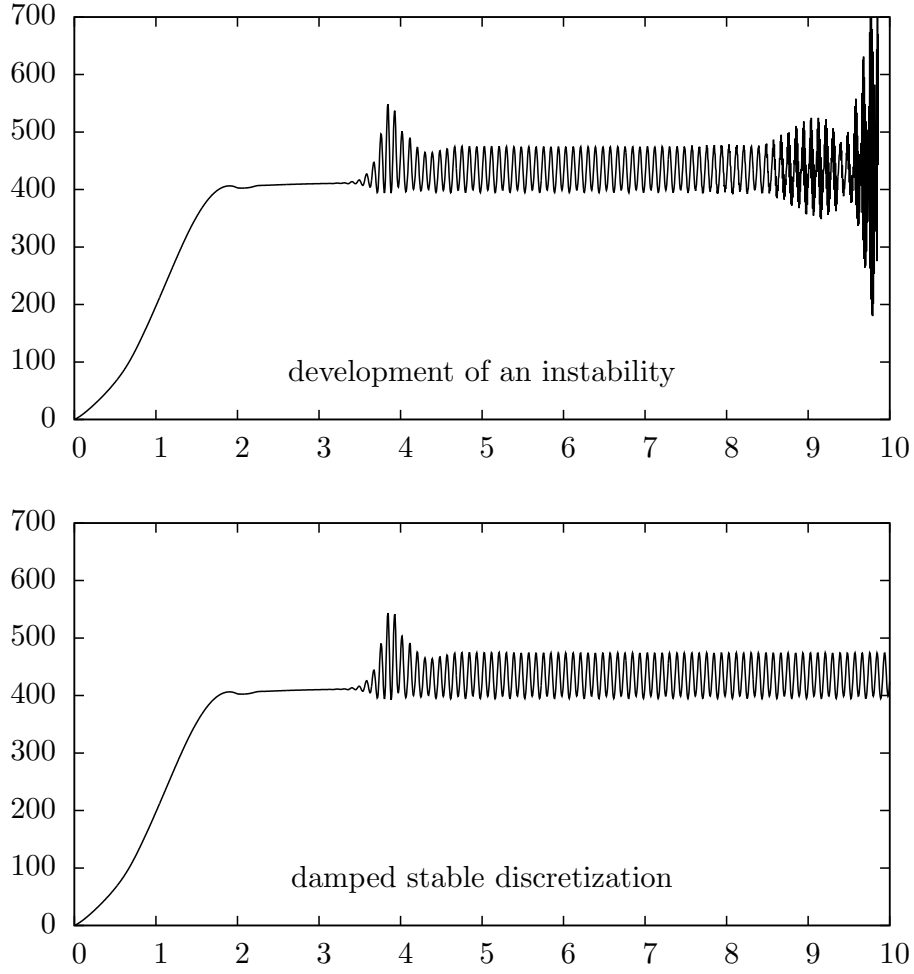
Figure 37: Simulation for $k = 0.005$. Top: undamped Crank-Nicolson scheme develops an instability after $T = 8.5$. Bottom: implicitely shifted scheme produces a stable solution on $I = [0, 10]$ (taken from [209]).

6.1.1.2 Consequences of energy conservation in pipes/tubes/arteries with moving elastic walls Let us briefly illustrate practical consequences associated with hyperbolic (non-damping) solid equations. Assuming we have *optimal* conservation properties using a Crank-Nicolson-type scheme for temporal discretization. As we mentioned in the introduction, hemodynamical applications are often subject of research. Here, blood flows in a veine or artery. Due to its enormous computational cost, we can not simulate the whole circulatory system and we need to *cut* the computational domain.

Blood flow is a pulsating fluid and introduces waves and in particular these waves can be observed in the arterial wall (see a snapshot at time t^* in Figure 38). Using standard Dirichlet or Neumann conditions on the structural boundary conditions (inlet and outlet), elastic waves are reflected. This is non-physical behavior and is subject of present research [49, 89, 105, 183]. Our conclusion that is inferred from these observations is that correct numerical discretization does not necessarily result in the correct physical answer.
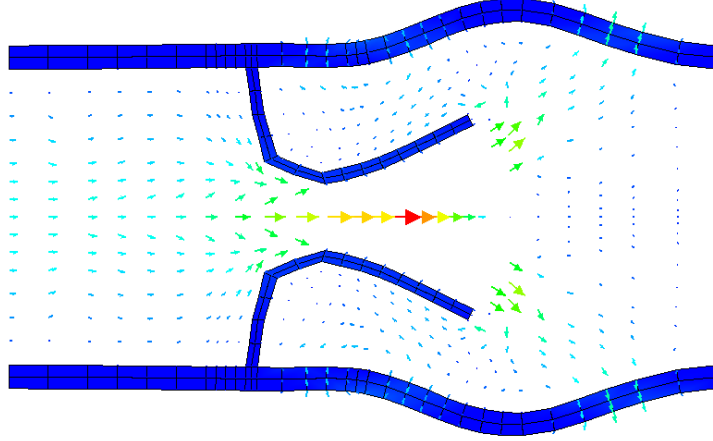

Figure 38: Snapshot at time step t^* of flapping simulation with moving elastic boundaries.

6.1.2 Temporal discretization of fluid-structure interaction

The abstract problem (120) can either be treated by a full time-space Galerkin formulation, which was investigated previously for fluid problems in Besier et al. [33, 34, 218]. Alternatively, the Rothe method can be used in cases where the time discretization is based on finite difference schemes.

To sum-up: After semi-discretization in time, we obtain a sequence of generalized steady-state fluid-structure interaction problems that are completed by appropriate boundary values at every time step. Let us now go into detail and let

$$I = \{0\} \cup I_1 \cup \ldots \cup I_N$$

be a partition of the time interval $I = [0, T]$ into half open subintervals $I_n := (t_{n-1}, t_n]$ of (time step) size $k_n := t_n - t_{n-1}$ with

$$0 = t_0 < \cdots < t_N = T.$$

103

We (formally) define the following semi-linear forms and group them into four categories: time equation terms (including the time derivatives), implicit terms (e.g., the incompressibility of the fluid), pressure terms, and all remaining terms (stress terms, convection, damping, etc.):

$$\hat{A}_T(\hat{U})(\hat{\Psi}) = (\hat{J}\hat{\rho}_f\partial_t\hat{v}_f, \hat{\psi}_f^v)_{\widehat{\Omega}_f} - (\rho_f\hat{J}(\widehat{F}^{-1}\hat{w}\cdot\widehat{\nabla})\hat{v}_f), \hat{\psi}_f^v)_{\widehat{\Omega}_f} \tag{128}$$

$$+ (\hat{\rho}_s\partial_t\hat{v}_s, \hat{\psi}_s^v)_{\widehat{\Omega}_s} + (\hat{\rho}_s\partial_t\hat{u}_s, \hat{\psi}_s^u)_{\widehat{\Omega}_s}, \tag{129}$$

$$\hat{A}_I(\hat{U})(\hat{\Psi}) = (\alpha_u\widehat{\nabla}\hat{u}_f, \widehat{\nabla}\hat{\psi}_f^u)_{\widehat{\Omega}_f} \tag{130}$$

$$+ (\widehat{\operatorname{div}}(\hat{J}\widehat{F}^{-1}\hat{v}_f), \hat{\psi}_f^p)_{\widehat{\Omega}_f} + (\hat{P}_s, \hat{\psi}_s^p)_{\widehat{\Omega}_s}, \tag{131}$$

$$\hat{A}_E(\hat{U})(\hat{\Psi}) = (\hat{\rho}_f\hat{J}(\widehat{F}^{-1}\hat{v}_f\cdot\widehat{\nabla})\hat{v}_f), \hat{\psi}_f^v)_{\widehat{\Omega}_f} + (\hat{J}\hat{\sigma}_{f,vu}\widehat{F}^{-T}, \widehat{\nabla}\hat{\psi}_f^v)_{\widehat{\Omega}_f} \tag{132}$$

$$+ (\widehat{F}\widehat{\Sigma}, \widehat{\nabla}\hat{\psi}_s^v)_{\widehat{\Omega}_s} + \gamma_w(\hat{v}_s, \hat{\psi}_s^v)_{\widehat{\Omega}_s} + \gamma_s(\hat{\epsilon}(\hat{v}_s), \widehat{\nabla}\hat{\psi}_s^v)_{\widehat{\Omega}_s} - (\hat{\rho}_s\hat{v}_s, \hat{\psi}_s^u)_{\widehat{\Omega}_s}, \tag{133}$$

$$\hat{A}_P(\hat{U})(\hat{\Psi}) = (\hat{J}\hat{\sigma}_{f,p}\widehat{F}^{-T}, \widehat{\nabla}\hat{\psi}_f^v)_{\widehat{\Omega}_f} + (\hat{J}\hat{\sigma}_{s,p}\widehat{F}^{-T}, \widehat{\nabla}\hat{\psi}_s^v)_{\widehat{\Omega}_s}, \tag{134}$$

where the reduced stress tensors $\hat{\sigma}_{f,vu}$, $\hat{\sigma}_{f,p}$, and $\hat{\sigma}_{s,p}$ are defined as:

$$\hat{\sigma}_{f,p} = -\hat{p}_f\hat{I}, \quad \hat{\sigma}_{f,vu} = \rho_f\nu_f(\widehat{\nabla}\hat{v}_f\widehat{F}^{-1} + \widehat{F}^{-T}\widehat{\nabla}\hat{v}_f^T), \tag{135}$$

$$\hat{\sigma}_{s,p} = -\hat{p}_s\hat{I}, \quad \text{(if we deal with the INH or IMR material),} \tag{136}$$

and $\widehat{\Sigma}$ denotes as usual the structure tensor of the INH, IMR, or STVK material. The time derivative in $\hat{A}_T(\hat{U})(\hat{\Psi})$ is approximated by a backward difference quotient. For the time step $t_n \in I$ for $n = 1, 2, \ldots, N$ ($N \in \mathbb{R}$), we compute $\hat{v}_i := \hat{v}_i^n, \hat{u}_i := \hat{u}_i^n$ ($i = f, s$) via

$$\hat{A}_T(\hat{U}^{n,k})(\hat{\Psi}) \approx \frac{1}{k}\big(\hat{\rho}_f\hat{J}^{n,\theta}(\hat{v}_f - \hat{v}_f^{n-1}), \hat{\psi}^v\big)_{\widehat{\Omega}_f} - \frac{1}{k}\big(\hat{\rho}_f(\hat{J}\widehat{F}^{-1}(\hat{u}_f - \hat{u}_f^{n-1})\cdot\widehat{\nabla})\hat{v}_f, \hat{\psi}^v\big)_{\widehat{\Omega}_f} \tag{137}$$

$$+ \frac{1}{k}\big(\hat{\rho}_s(\hat{v}_s - \hat{v}_s^{n-1}), \hat{\psi}^v\big)_{\widehat{\Omega}_s} + \big(\hat{u}_s - \hat{u}_s^{n-1}, \hat{\psi}^u\big)_{\widehat{\Omega}_s}, \tag{138}$$

where we introduce a parameter θ, which is clarified below. Furthermore, we use

$$\hat{J}^{n,\theta} = \theta\hat{J}^n + (1-\theta)\hat{J}^{n-1},$$

and $\hat{u}_i^n := \hat{u}_i(t_n)$, $\hat{v}_i^n := \hat{v}_i(t_n)$, and $\hat{J} := \hat{J}^n := \hat{J}(t_n)$. The former time step is given by $\hat{v}_i^{n-1}$, etc. for $i = f, s$.

6.1.2.1 The One-Step-θ scheme Let the previous time step solution $\hat{U}^{n-1} = \{\hat{v}_f^{n-1}, \hat{v}_s^{n-1}, \hat{u}_f^{n-1}, \hat{u}_s^{n-1}, \hat{p}_f^{n-1}, \hat{p}_s^{n-1}\}$ and the time step $k := k_n = t_n - t_{n-1}$ be given.
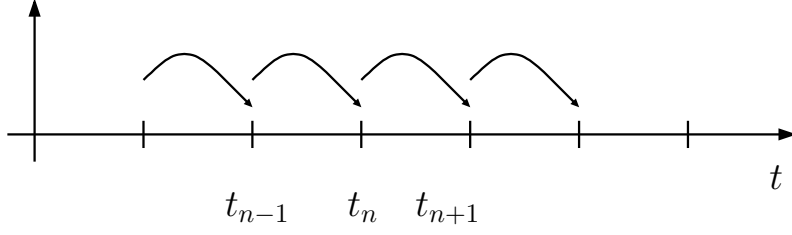
Figure 39: Time step computation using One-Step-θ schemes.

Find $\hat{U}^n = \{\hat{v}_f^n, \hat{v}_s^n, \hat{u}_f^n, \hat{u}_s^n, \hat{p}_f^n, \hat{p}_s^n\}$ such that

$$\hat{A}_T(\hat{U}^{n,k})(\hat{\Psi}) + \theta\hat{A}_E(\hat{U}^n)(\hat{\Psi}) \tag{139}$$

$$+\hat{A}_P(\hat{U}^n)(\hat{\Psi}) + \hat{A}_I(\hat{U}^n)(\hat{\Psi}) = -(1-\theta)\hat{A}_E(\hat{U}^{n-1})(\hat{\Psi}) \tag{140}$$

$$+ \theta\widehat{F}^n(\hat{\Psi}) + (1-\theta)\widehat{F}^{n-1}(\hat{\Psi}), \tag{141}$$

where $\widehat{F}^n(\hat{\Psi}) = (\hat{\rho}_s\hat{f}_s^n, \hat{\psi}_s^v)_{\widehat{\Omega}_s}$ with $\hat{f}_s^n := \hat{f}_s(t_n)$. The concrete scheme depends on the choice of the parameter θ. Specifically, we get the backward Euler scheme for $\theta = 1$, the Crank-Nicolson scheme for $\theta = \frac{1}{2}$, and the shifted Crank-Nicolson for $\theta = \frac{1}{2} + k_n$ [133, 199]. We notice that for problems with large time steps ($k \geq 0.5$), we need to normalize/non-dimensionalize the equations in order to get the characteristic time step size that can be used for the shifted variant. Otherwise, you have $\theta > 1$, we is senseless. As alternative, one can use the Rannacher time-stepping by adding backward Euler steps on a regular basis [198].

6.1.2.2 The Fractional-Step-θ scheme We choose $\theta = 1 - \frac{\sqrt{2}}{2}, \theta' = 1 - 2\theta$, and $\alpha = \frac{1-2\theta}{1-\theta}, \beta = 1 - \alpha$. The time step is split into three consecutive sub-time steps. Let $\hat{U}^{n-1} = \{\hat{v}_f^{n-1}, \hat{v}_s^{n-1}, \hat{u}_f^{n-1}, \hat{u}_s^{n-1}, \hat{p}_f^{n-1}, \hat{p}_s^{n-1}\}$ and the time step $k := k_n = t_n - t_{n-1}$ be given.
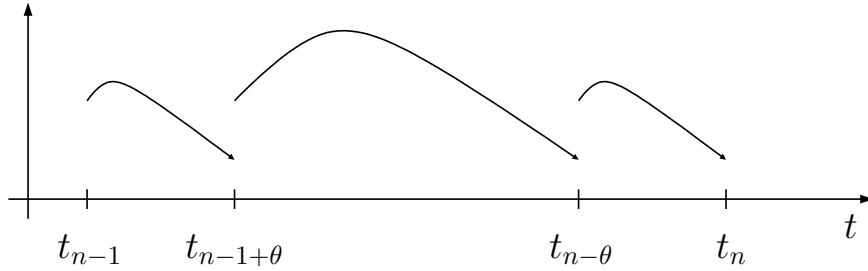

Figure 40: Time step computation using the Fractional-Step-θ scheme.

Find $\hat{U}^n = \{\hat{v}_f^n, \hat{v}_s^n, \hat{u}_f^n, \hat{u}_s^n, \hat{p}_f^n, \hat{p}_s^n\}$ such that

$$\hat{A}_T(\hat{U}^{n-1+\theta,k})(\hat{\Psi}) + \alpha\theta\hat{A}_E(\hat{U}^{n-1+\theta})(\hat{\Psi}) \tag{142}$$

$$+\theta\hat{A}_P(\hat{U}^{n-1+\theta})(\hat{\Psi}) + \hat{A}_I(\hat{U}^{n-1+\theta})(\hat{\Psi}) = -\beta\theta\hat{A}_E(\hat{U}^{n-1})(\hat{\Psi}) + \theta\hat{F}^{n-1}(\hat{\Psi}), \tag{143}$$

$$\tag{144}$$

$$\hat{A}_T(\hat{U}^{n-\theta,k})(\hat{\Psi}) + \alpha\theta\hat{A}_E(\hat{U}^{n-\theta})(\hat{\Psi}) \tag{145}$$

$$+\theta'\hat{A}_P(\hat{U}^{n-\theta})(\hat{\Psi}) + \hat{A}_I(\hat{U}^{n-\theta})(\hat{\Psi}) = -\alpha\theta'\hat{A}_E(\hat{U}^{n-1+\theta})(\hat{\Psi}) + \theta'\hat{F}^{n-\theta}(\hat{\Psi}), \tag{146}$$

$$\tag{147}$$

$$\hat{A}_T(\hat{U}^{n,k})(\hat{\Psi}) + \alpha\theta\hat{A}_E(\hat{U}^n)(\hat{\Psi}) \tag{148}$$

$$+\theta\hat{A}_P(\hat{U}^n)(\hat{\Psi}) + \hat{A}_I(\hat{U}^n)(\hat{\Psi}) = -\beta\theta\hat{A}_E(\hat{U}^{n-1})(\hat{\Psi}) + \theta\hat{F}^{n-\theta}(\hat{\Psi}). \tag{149}$$

With the help of the previous considerations, we formulate a statement for the time-discretized equations:

Problem 6.4. *Let the semi-linear form $\hat{A}(\cdot)(\cdot)$ be formulated in terms of the previous arrangement, such that*

$$\hat{A}(\hat{U})(\hat{\Psi}) := \hat{A}_T(\hat{U})(\hat{\Psi}) + \hat{A}_I(\hat{U})(\hat{\Psi}) + \hat{A}_E(\hat{U})(\hat{\Psi}) + \hat{A}_P(\hat{U})(\hat{\Psi}).$$

After time discretization, let the time derivatives are approximated with

$$\hat{A}_T(\hat{U})(\hat{\Psi}) \approx \hat{A}_T(\hat{U}^{n,k})(\hat{\Psi}),$$

such that the time-discretized semi-linear form reads

$$\hat{A}(\hat{U}^n)(\hat{\Psi}) := \hat{A}_T(\hat{U}^{n,k})(\hat{\Psi}) + \hat{A}_I(\hat{U}^n)(\hat{\Psi}) + \hat{A}_E(\hat{U}^n)(\hat{\Psi}) + \hat{A}_P(\hat{U}^n)(\hat{\Psi}).$$

Then, we aim to find $\hat{U}^n = \{\hat{v}_f^n, \hat{v}_s^n, \hat{u}_f^n, \hat{u}_s^n, \hat{p}_f^n, \hat{p}_s^n\} \in \widehat{X}_D^0$, where $\widehat{X}_D^0 := \{\hat{v}_f^D + \hat{V}_{f,\hat{v}}^0\} \times \hat{L}_s \times \{\hat{u}_f^D + \hat{V}_{f,\hat{u}}^0\} \times \{\hat{u}_s^D + \hat{V}_s^0\} \times \hat{L}_f^0 \times \hat{L}_s^0$ and $\widehat{X} = \hat{V}_{f,\hat{v}}^0 \times \hat{L}_s \times \hat{V}_{f,\hat{u},\widehat{\Gamma}_i}^0 \times \hat{V}_s^0 \times \hat{L}_f^0 \times \hat{L}_s^0$, for all $n = 1, 2, \ldots, N$ such that

$$\hat{A}(\hat{U}^n)(\hat{\Psi}) = \widehat{F}(\hat{\Psi}) \quad \forall\hat{\Psi} \in \widehat{X},$$

where this equation is treated with one specific time-stepping scheme as introduced previously.

Remark 6.5 (Newmark scheme [143, 261, 262] for temporal solid discretization)**.** *We notice that the standard discretization for solid equations is based on the so-called Newmark scheme, which avoids splitting into a first-order mixed system. The relation to special cases of One-Step-θ schemes (in particular Crank-Nicolson) is discussed in [12].* ◇

Remark 6.6 (Geometrical conservation law)**.** *Using the ALE_{dm} scheme for time discretization, there have been studies [77, 85, 86, 183] that convergence is influenced by the discretization of the mesh motion velocity and also depends if ALE conservative schemes are used. Such studies are open questions for ALE_{fx} schemes. Several examples and ideas are presented in [183], p. 71.* ◇

6.1.3 Numerical observations for long-term FSI computations

In this section, we are interested in the following:

- The detection of instabilities (or even the blow-up of solutions in finite time) for the ordinary (i.e., unstabilized) Crank-Nicolson scheme. If we observe any, we are able to resolve them by the choice of a sufficiently small time step.

- Finally, we compare the standard second-order time-stepping schemes for the simulation of nonstationary fluid flows/fluid-structure interactions such as the Crank-Nicolson scheme, the shifted Crank-Nicolson scheme, and the Fractional-Step-θ scheme.

The following conclusions were obtained by studying the fluid-structure interaction benchmark test FSI 2 [142]. To detect numerical artefacts is a delicate task, therefore, we study (qualitative) convergence with respect to space and time on three different (globally-refined) mesh levels with $1914, 7176$ and 27744 degrees of freedom using the Q_2^c/P_1^{dc} element (which is introduced in the next section). Moreover, we use three different time levels with the time steps $k = 0.01, 0.005$ and 0.001. It is sufficient to study the results for the drag evaluation because we observed the same qualitative behavior for all the four quantities of interest (the x- and the y-displacement, the drag, and the lift).

Observation 1

We observed in our computations that there are only minor differences in the drag evaluation computed with the unstabilized Crank-Nicolson scheme using the different ALE convection term discretizations defined in the problems above. Specifically, we observed unstable behavior (blow-up) for computations over long-term intervals, as illustrated in Figure 41. Naturally, we expected this behavior from our previous numerical analysis.

Observation 2

As expected, the shifted Crank-Nicolson scheme and the Fractional-Step-θ scheme showed no stability problems in long-term computations, even for the large time step $k = 0.01$ (see the top of Figure 42). This result indicates that the instabilities induced by the ALE convection term have minor consequences, and our observation is in agreement with the statement in [86]. Furthermore, all time-stepping schemes are stable over the entire time interval for a sufficiently small time step $k = 0.001$; (see the bottom Figure 42).
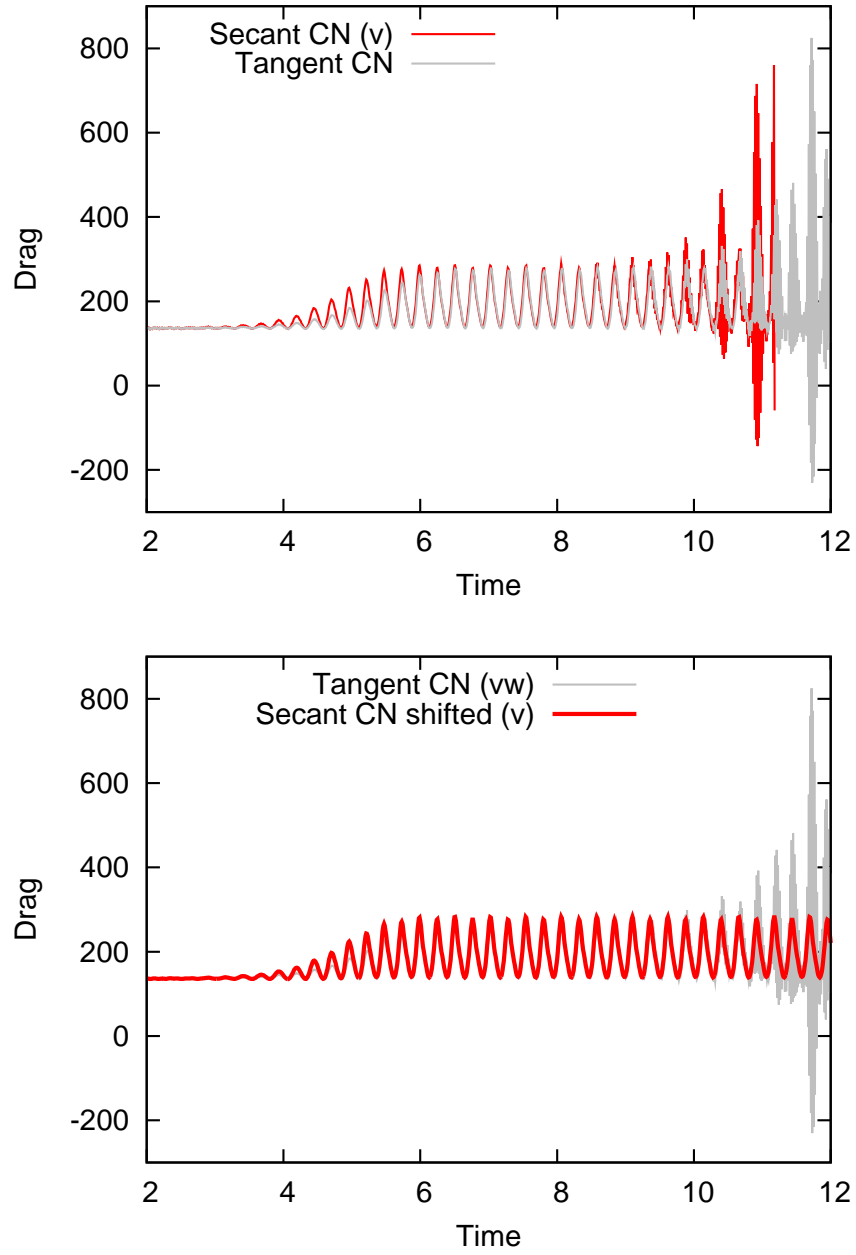
Figure 41: Blow-up (using the time step $k = 0.01$) of the unstabilized Crank-Nicolson schemes (secant and tangent) whereas the shifted Crank-Nicolson schemes is stable throughout the whole time interval. We notice that the secant Crank-Nicolson scheme exhibits the instabilities earlier than the tangent version. The unit of the time axis is s, whereas the drag unit is $kg/m\,s^2$.

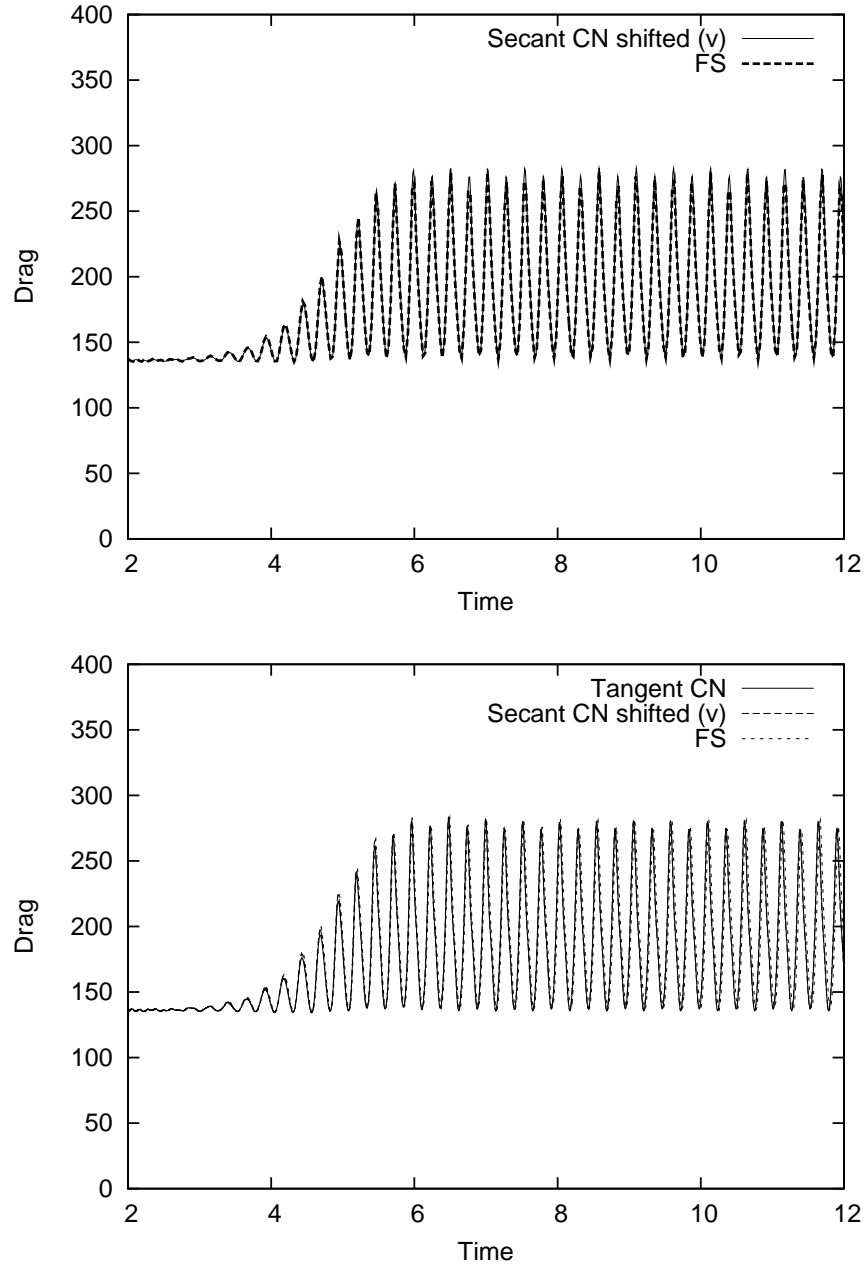Figure 42: Top: stable solution (using the large time step $k = 0.01$) computed with the shifted Crank-Nicolson and the Fractional-Step-θ scheme. Recall the blow-up of the unstabilized Crank-Nicolson scheme in this case. Bottom: using the smaller time step $k = 0.001$ yields stable solutions for any time-stepping scheme. The unit of the time axis is s, whereas the drag unit is $kg/m\,s^2$.

109

6.1.4 Time stability

In the following, we consider the stability of the monolithically coupled problem.

Theorem 6.7. *Let the fluid-structure interaction problem be coupled via an implicit solution algorithm and let both subproblems be time-discretized with the second order Crank-Nicolson scheme. The coupled problem is assumed to be isolated, i.e., $v_f^{n+1} = 0$ on $\partial\Omega_f \setminus \Gamma_i$ and $\widehat{F}\widehat{\Sigma}(\hat{u}_s^{n+1})\hat{n}_s = 0$ on $\partial\widehat{\Omega}_s \setminus \widehat{\Gamma}_i$. Further, in the case of strong damping $\gamma_w > 0$, let $\hat{\epsilon}(\hat{v}_s^{n+1})\hat{n}_s = 0$ on $\partial\widehat{\Omega}_s \setminus \widehat{\Gamma}_i$. Then,*

$$
\begin{aligned}
&\rho_f||v_f^{n+1}||_{\Omega_f^{n+1}}^2 + \hat{\rho}_s||\hat{v}_s^{n+1}||_{\widehat{\Omega}_s}^2 + \int_{\widehat{\Omega}_s} W\big(\widehat{F}(\hat{u}_s^{n+1})\big)\,\mathrm{d}x \\
&\quad + k\rho_f\nu_f||D(v_f^{n+1} + v_f^n)||_{\Omega_f^{n+1}}^2 + \frac{k\rho_f}{4}\int_{\Omega_f^{n+1}} \nabla \cdot w^{n+1}|v_f^{n+1} + v_f^n|^2\,\mathrm{d}x \\
&\quad + \frac{k\gamma_w}{2}||\hat{v}_s^{n+1}||_{\widehat{\Omega}_s}^2 + \frac{k\gamma_s}{2}||\hat{\epsilon}(\hat{v}_s^{n+1})||_E^2 \\
&\leq \rho_f||v_f^n||_{\Omega_f^{n+1}}^2 + \rho_s||\hat{v}_s^n||_{\widehat{\Omega}_s}^2 + \int_{\widehat{\Omega}_s} W(\widehat{F}(\hat{u}_s^n))\,\mathrm{d}x \\
&\quad + \frac{k\gamma_w}{2}||\hat{v}_s^n||_{\widehat{\Omega}_s}^2 + \frac{k\gamma_s}{2}||\hat{\epsilon}(\hat{v}_s^n)||_E^2.
\end{aligned}
$$

Proof. The proof can be found in [248]. $\qquad\square$

6.2 Space

The time-discretized equations are the starting point for a finite element Galerkin discretization method in space.

6.2.1 Galerkin approximations

Our goal is to approximate the weak solutions by using finite-dimensional subspaces. So far, the equations still contain the continuous spatial spaces $\hat{V}, \hat{V}^0$ and $\hat{L}^0$. In the following, we discuss the spatial discretization of the semi-discrete problems obtained in the previous section. To this end, we construct finite dimensional subspaces $\hat{V}_h \subset \hat{V}$, $\hat{V}_h^0 \subset \hat{V}^0$, $\hat{L}_h^0 \subset \hat{L}^0$. For a Galerkin approximation, the specific form of the basis functions does not matter. A concrete realization can be performed in terms of a Galerkin finite element method (in short FEM).

6.2.2 Finite element spaces

As basis functions, we choose piecewise polynomial functions up to order l. The spatial terms are computed in a fixed reference configuration. This is the characteristic feature of the ALE_{fx} approach. The computational domain $\widehat{\Omega}$ is partitioned into open cells $\hat{K}$ that depend on the spatial dimension d. A mesh consists of quadrilateral or hexahedron cells $\hat{K}$. They perform a non-overlapping cover of the computation domain $\widehat{\Omega} \subset \mathbb{R}^d$,

$d = 2, 3$. The mesh $\hat{\mathcal{T}}_h = \{\hat{K}\}$ of $\widehat{\Omega}$ is formed by taking all cells. The cell parameter $\hat{h}$ is given as a cell-wise constant function $\hat{h}_K := \text{diam}(\hat{K})$ (where $\text{diam}(\hat{K})$ denotes the diameter $\hat{h}_K$ of a cell $\hat{K}$). The maximum diameter is denoted by $\hat{h} := \max_{\hat{K} \in \mathcal{T}_h} \hat{h}_k$.

We follow the standard literature ([43, 44, 57]) to formulate the following statements:

Definition 6.8 (Regularity). *A mesh $\hat{\mathcal{T}}_h = \{\hat{K}\}$ is called regular if the following conditions are fulfilled:*

1) *$\overline{\widehat{\Omega}} = \bigcup_{\hat{K} \in \hat{\mathcal{T}}_h} \overline{\hat{K}}$.*

2) *$\hat{K}_1 \cap \hat{K}_2 = \emptyset$ for all cells $\hat{K}_1, \hat{K}_2 \in \hat{\mathcal{T}}_h$ with $\hat{K}_1 \neq \hat{K}_2$.*

3) *Any face of any cell $\hat{K}_1 \in \hat{\mathcal{T}}_h$ is either a subset of the boundary $\partial\widehat{\Omega}$ or a face of another cell $\hat{K}_2 \in \hat{\mathcal{T}}_h$.*

◇

The last condition is too restrictive for our purposes and is weakened for the following reason. To facilitate adaptive mesh refinement and to avoid connecting elements, we use the concept of *hanging nodes*. Cells are allowed to have nodes that lie on the midpoints of the faces or edges of neighboring cells. At most, one hanging node is allowed on each face or edge. In three dimensions, this concept is generalized to subplanes and faces because we must deal with two types of lower manifolds.

We define continuous H^1-conforming finite element spaces $\hat{V}_h^l$ by (see [44, 57, 150]):

$$\hat{V}_h^l := \left\{ \hat{v}_h \in C(\overline{\widehat{\Omega}}) \mid \hat{v}_h|_{\hat{K}} \in \mathcal{Q}(\hat{K}) \quad \forall \hat{K} \in \hat{\mathcal{T}}_h \right\} \subseteq H^1(\widehat{\Omega}).$$

Here, $\mathcal{Q}(\hat{K})$ denotes the space of polynomial-like functions on $\hat{K} \in \hat{\mathcal{T}}_h$. In the following, we introduce the space $\mathcal{Q}_l(\hat{K})$ of tensor product polynomials up to degree l. On the reference cell $\hat{K}_{\text{unit}} = (0, 1)^d$ they are defined as

$$\hat{\mathcal{Q}}_l(\hat{K}_{\text{unit}}) := \text{span} \left\{ \prod_{i=1}^{d} \hat{x}_i^{\alpha_i} \mid \alpha_i \in \{0, 1, \dots, l\} \right\}.$$

We consider for each $\hat{K} \in \hat{\mathcal{T}}_h$ the bilinear transformation $\hat{\sigma}_K : \hat{K}_{\text{unit}} \to \hat{K}$. Then, the Q_1^c element is defined as

$$Q_1^c(\hat{K}) = \{\hat{q} \circ \hat{\sigma}_K^{-1} : \hat{q} \in \text{span} < 1, \hat{x}, \hat{y}, \hat{x}\hat{y} >\} \qquad (d = 2),$$
$$Q_1^c(\hat{K}) = \{\hat{q} \circ \hat{\sigma}_K^{-1} : \hat{q} \in \text{span} < 1, \hat{x}, \hat{y}, \hat{z}, \hat{x}\hat{y}, \hat{x}\hat{z}, \hat{y}\hat{z}, \hat{x}\hat{y}\hat{z} >\} \qquad (d = 3),$$

with dim $Q_1^c = 4$ (in 2D) and $Q_1^c = 8$ (in 3D) in which the dimension denotes the local degrees of freedom on a single cell. The Q_2^c element (in two dimensions) is defined as

$$Q_2^c(\hat{K}) = \{\hat{q} \circ \hat{\sigma}_K^{-1} : \hat{q} \in \text{span} < 1, \hat{x}, \hat{y}, \hat{x}\hat{y}, \hat{x}^2, \hat{y}^2, \hat{x}^2\hat{y}, \hat{y}^2\hat{x}, \hat{x}^2\hat{y}^2 >\},$$
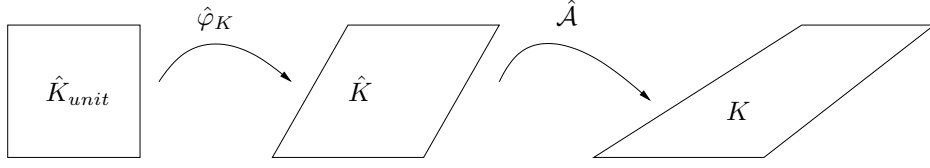
Figure 43: Transformation $\hat{\varphi}_K$ from the unit cell $\hat{K}_{unit}$ to the ALE cell $\hat{K}$ and from that cell via the ALE mapping $\hat{\mathcal{A}}$ to the physical cell K.

with dim $Q_2^c = 9$. Finally, the P_1^{dc} element is defined with the help of linear functions and it reads

$$P_1^{dc}(\hat{K}) = \{\hat{q} \circ \hat{\sigma}_K^{-1} : \hat{q} \in \text{span}, <1, \hat{x}, \hat{y}>\}$$

with dim $P_1^{dc}(\hat{K}) = 3$. If the transformation $\hat{\sigma}_K$ itself is an element of $\hat{\mathcal{Q}}_l(\hat{K})^d$, the corresponding finite element space is called *isoparametric*.

Extending these concepts to finite element spaces in the case of hanging nodes requires some remarks. To enforce global continuity (i.e., global conformity), the degrees of freedom located on the interface between different refinement levels have to satisfy additional constraints. They are determined by interpolation of neighboring degrees of freedom. Therefore, hanging nodes do not carry any degrees of freedom. For more details on this, we refer to [53].

To ensure the approximation properties of the finite element spaces, additional conditions on the geometry of the cells are required. The two classical assumptions from the literature ([43, 44]) are the so-called *uniformity* and the weaker *quasi-uniformity*:

Definition 6.9 (Quasi-Uniformity). *A family of meshes $\{\hat{\mathcal{T}}_h | h \searrow 0\}$ is called quasi-uniform if there is a constant κ such that the following two conditions are fulfilled:*

1) For each transformation $\hat{\sigma}_K : \hat{K}_{unit} \to \hat{K}$ it holds

$$\frac{\sup\{||\nabla\hat{\sigma}_K(\hat{x})\hat{x}|| \, |\hat{x} \in \hat{K}, ||\hat{x}|| = 1\}}{\inf\{||\nabla\hat{\sigma}_K(\hat{x})\hat{x}|| \, |\hat{x} \in \hat{K}, ||\hat{x}|| = 1\}} \leq \kappa, \qquad \hat{K} \in \bigcup_h \hat{\mathcal{T}}_h. \tag{150}$$

2) It holds

$$\frac{\hat{h}_K}{\hat{\rho}_K} \leq \kappa \quad \forall \hat{K} \in \bigcup_h \hat{\mathcal{T}}_h.$$

$\diamond$

6.2.3 Spatial discretization of fluid-structure interaction

To compute fluid-structure interactions problems, we prefer the biquadratic, discontinuous-linear Q_2^c/P_1^{dc} element. The definitions of the spaces for the unknowns $\hat{v}_h$, $\hat{u}_f$ and $\hat{p}_h$

read:

$$\hat{V}_h := \{\hat{v}_h \in [C(\hat{\Omega}_h)]^d, \hat{v}_h|_{\hat{K}} \in [Q_2(\hat{K})]^d \quad \forall \hat{K} \in \hat{\mathcal{T}}_h, \hat{v}_h|_{\hat{\Gamma}\setminus\hat{\Gamma}_i} = 0\},$$

$$\hat{W}_h := \{\hat{u}_h \in [C(\hat{\Omega}_h)]^d, \hat{u}_h|_{\hat{K}} \in [Q_2(\hat{K})]^d \quad \forall \hat{K} \in \hat{\mathcal{T}}_h, \hat{u}_h|_{\Gamma_0} = 0\},$$

$$\hat{P}_h := \{\hat{p}_h \in [\hat{L}^2(\hat{\Omega}_h)], \hat{p}_h|_{\hat{K}} \in [P_1(\hat{K})] \quad \forall \hat{K} \in \hat{\mathcal{T}}_h\}.$$

Defining the displacement variables $\hat{u}_h$ and $\hat{w}_h$ is straightforward.

Remark 6.10. *Other choices for inf-sub stable elements would be the classical Taylor-Hood element Q_2^c/Q_1^c or also Q_2^c/P_0^{dc}.* $\diamond$
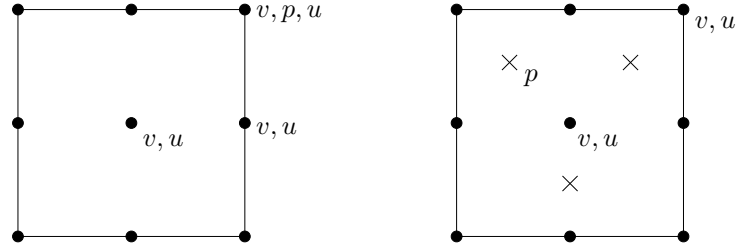

Figure 44: Taylor Hood element Q_2^c/Q_1^c (left) and Q_2^c/P_1^{dc} element (right).

The continuity of the velocity values across different mesh cells is one property of the Q_2^c/P_1^{dc} element. In contrast, the pressure is allowed to be discontinuous across faces because it is defined utilizing discontinuous test functions. In addition, this element preserves local mass conservation, is of low order, gains the *inf-sup stability*, and it is therefore an optimal choice for both fluid problems and fluid-structure interaction problems. Because there is no relationship between fluid and structure pressure (beyond the fact that there is no physical meaning of pressure for compressible materials), the Q_2^c/P_1^{dc} is a good choice for fluid-structure interactions.

Bearing the three mesh motion models in mind, the computation of fluid-structure interaction with biharmonic mesh motion incurs a greater computational cost at each time step than using only a harmonic model or the equations of linear elasticity because an additional equation is added to the problem (see Problem 5.20). In the context of a Galerkin finite element scheme, the spatial discretization of the mixed biharmonic equation is stable for equal-order discretization on polygonal domains, which is one of our assumptions. In this lecture notes, we work with Q_2^c elements for $\hat{u}_h$ and $\hat{\eta}_h$.

For the next statement, let $\hat{v}_{f,h}^D$, $\hat{u}_{f,h}^D$, and $\hat{v}_{s,h}^D$ be suitable extensions of Dirichlet inflow data. Having these preparations, the spatially (and temporal) discretized problem of (120) reads:

Problem 6.11. *Let the semi-linear form be composed as shown in Problem 6.4. Find $\hat{U}_h^n = \{\hat{v}_{f,h}^n, \hat{v}_{s,h}^n, \hat{u}_{f,h}^n, \hat{u}_{s,h}^n, \hat{p}_{f,h}^n, \hat{p}_{s,h}^n\} \in \hat{X}_{h,D}^0$, where $\hat{X}_{h,D}^0 := \{\hat{v}_{f,h}^D + \hat{V}_{f,\hat{v},h}^0\} \times \hat{L}_{s,h} \times \{\hat{u}_{f,h}^D + \hat{V}_{f,\hat{u},h}^0\} \times \{\hat{u}_{s,h}^D + \hat{V}_{s,h}^0\} \times \hat{L}_{f,h}^0 \times \hat{L}_{s,h}^0$, for all $n = 1, 2, \ldots, N$ such that*

$$\hat{A}(\hat{U}_h^n)(\hat{\Psi}_h) = \widehat{F}(\hat{\Psi}_h) \quad \forall \hat{\Psi}_h \in \widehat{X}_h,$$

113

with $\hat{\Psi}_h = \{\hat{\psi}^v_{f,h}, \hat{\psi}^v_{s,h}, \hat{\psi}^u_{f,h}, \hat{\psi}^u_{s,h}, \hat{\psi}^p_{f,h}, \hat{\psi}^p_{s,h}\}$ and $\widehat{X}_h = \hat{V}^0_{f,\hat{v},h} \times \hat{L}_{s,h} \times \hat{V}^0_{f,\hat{u},\widehat{\Gamma}_i,h} \times \hat{V}^0_{s,h} \times \hat{L}^0_{f,h} \times \hat{L}^0_{s,h}$.

6.2.4 Stabilization for convection-dominated flows

In the case of higher Reynolds numbers the flow becomes convection dominated and needs to be stabilized. Residual based stabilization is first introduced in Brooks and Hughes [46] and is intensively analyzed in Wall [243]. Our method of choice is a rough simplification of the streamline upwind Petrov-Galerkin (SUPG) method.

We start with a consistent formulation for the fluid problem that is given on the continuous level in a time-dependent domain Ω_f. Then, the stabilization term reads (in which we omit for the moment the subscripts 'h' and 'n' in the equations):

$$S_{\text{stab}}(U^n_h)(\Psi) := \sum_{K \in \mathcal{T}_h} (\rho_f \hat{\partial}_t v_f + \rho_f (v_f - w) \cdot \nabla v_f - \text{div} \sigma_f, \delta_{K,n}(v_f \cdot \nabla) \psi^v_f)_K$$

with

$$\delta_{K,n} = \delta_0 \frac{h_K^2}{6\nu_f + h_K \|v^n_h\|_K}, \quad \delta_0 = 0.1.$$

For more details on the choice of these parameters, we refer the reader to [39].

From the computational point of view, the major disadvantage comes from the necessity of computing second derivatives contained in the stress tensor σ_f, because we must consider the strong formulation. Specifically, in the case of fluid-structure interaction problems, this formulation is a serious drawback. To this end, we only use a nonconsistent simplified version (in Ω_f):

$$S_{\text{stab}}(U^n_h)(\Psi) := \sum_{K \in \mathcal{T}_h} (\rho_f v_f \cdot \nabla v_f, \delta_{K,n}(v_f \cdot \nabla)\psi^v_f)_K.$$

This term can be rewritten in the reference configuration $\widehat{\Omega}_f$ and reads:

$$\hat{S}_{\text{stab}}(\hat{U}^n_h)(\hat{\Psi}) := \sum_{\widehat{K} \in \mathcal{T}_h} (\hat{\rho}_f (J\widehat{F}^{-1}\hat{v}_f \cdot \widehat{\nabla})\hat{v}_f, \delta_{K,n}(\widehat{F}^{-1}\hat{v}_f \cdot \widehat{\nabla})\hat{\psi}^v_f)_{\widehat{K}}. \tag{151}$$

Problem 6.12. *Let the semi-linear form be composed as shown in Problem 6.4. Find $\hat{U}^n_h = \{\hat{v}^n_{f,h}, \hat{v}^n_{s,h}, \hat{u}^n_{f,h}, \hat{u}^n_{s,h}, \hat{p}^n_{f,h}, \hat{p}^n_{s,h}\} \in \widehat{X}^0_{h,D}$, where $\widehat{X}^0_{h,D} := \{\hat{v}^D_{f,h} + \hat{V}^0_{f,\hat{v},h}\} \times \hat{L}_{s,h} \times \{\hat{u}^D_{f,h} + \hat{V}^0_{f,\hat{u},h}\} \times \{\hat{u}^D_{s,h} + \hat{V}^0_{s,h}\} \times \hat{L}^0_{f,h} \times \hat{L}^0_{s,h}$, for all $n = 1, 2, \ldots, N$ such that*

$$\hat{A}(\hat{U}^n_h)(\hat{\Psi}_h) + \hat{S}_{stab}(\hat{U}^n_h)(\hat{\Psi}) = \widehat{F}(\hat{\Psi}_h) \quad \forall \hat{\Psi}_h \in \widehat{X}_h,$$

with $\hat{\Psi}_h = \{\hat{\psi}^v_{f,h}, \hat{\psi}^v_{s,h}, \hat{\psi}^u_{f,h}, \hat{\psi}^u_{s,h}, \hat{\psi}^p_{f,h}, \hat{\psi}^p_{s,h}\}$ and $\widehat{X}_h = \hat{V}^0_{f,\hat{v},h} \times \hat{L}_{s,h} \times \hat{V}^0_{f,\hat{u},\widehat{\Gamma}_i,h} \times \hat{V}^0_{s,h} \times \hat{L}^0_{f,h} \times \hat{L}^0_{s,h}$.

Remark 6.13. *An elegant alternative has been investigated in [159] (and further references of the same author) in recent years. This scheme belongs to flux-corrected transport algorithms and can be applied to convection-dominated transport problems.*
◇

6.3 Newton's method

6.3.1 Classical Newton's method

Let $f \in C^1[a, b]$ and $x_0 \in [a, b]$ be an intial value. The tangent (based for instance on a Taylor expension) of f is given by

$$t(x) = f(x_k) + (x - x_k)f'(x_k), \quad k = 0, 1, 2, \ldots.$$

A root is then given by:

$$x_{k+1} = x_k - \frac{f(x_k)}{f'(x_k)}, \quad k = 0, 1, 2, \ldots. \tag{152}$$

This is iteration terminates if a stopping criterium

$$\frac{|x_{k+1} - x_k|}{|x_k|} < TOL, \tag{153}$$

or

$$|f(x_k)| < TOL. \tag{154}$$

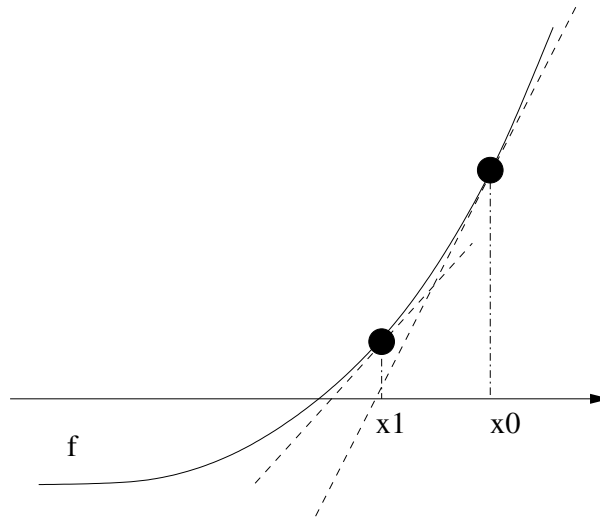is fulfilled. This iteration is possible as long as $f'(x_k) \neq 0$.

Figure 45: Geometrical interpretation of Newton's method.

Remark 6.14. *Newton's method belongs to fix-point iteration schemes with the iteraction function:*

$$F(x) := x - \frac{f(x)}{f'(x)}. \tag{155}$$

For a fix-point $\hat{x} = F(\hat{x})$ it holds: $f(\hat{x}) = 0$ $\diamond$

The main results is given by:

Theorem 6.15 (Newton's method). *The function $f \in C^2[a,b]$ has a root $\hat{x}$ in the interval $[a,b]$ and*

$$m := \min_{a \le x \le b} |f'(x)| > 0, \quad M := \max_{a \le x \le b} |f''(x)|.$$

Let $\rho > 0$ such that

$$q := \frac{M}{2m}\rho < 1, \quad K_\rho(\hat{x}) := \{x \in \mathbb{R} : |x - \hat{x}| \le \rho\} \subset [a,b].$$

Then, for any starting point $x_0 \in K_\rho(\hat{x})$, the sequence of iterations $x_k \in K_\rho(\hat{x})$ converges to the root $\hat{x}$. Furthermore, we have the a priori estimate

$$|x_k - \hat{x}| \le \frac{2m}{M}q^{2^k}, \quad k \in \mathbb{N},$$

and a posteriori estimate

$$|x_k - \hat{x}| \le \frac{1}{m}|f(x_k)| \le \frac{M}{2m}|x_k - x_{k+1}|^2, \quad k \in \mathbb{N}.$$

Often (and in particular for higher-dimensional problems such as fluid-structure interaction), Newton's method is formulated in terms of a defect-correction scheme.

Definition 6.16 (Defect). *Let $\tilde{x} \in \mathbb{R}$ an approximation of the solution $f(x) = y$. The defect (or similarly the residual) is defined as*

$$d(\tilde{x}) = y - f(\tilde{x}).$$

◇

For the sake of presentation, let the right hand side be $y = 0$. For the approximation x_k, the defect $d_k := 0 - f(x_k)$ is given by and we write:

Definition 6.17 (Newton's method as defect-correction scheme).

$$f'(x_k)\delta x = d_k, \quad d_k := -f(x_k),$$
$$x_{k+1} = x_k + \delta x, \quad k = 0, 1, 2, \ldots.$$

The iteration is finished with the same stopping criterium as for the classical scheme.
◇

6.3.2 Extension to higher-dimensional problems

Time and spatial discretization end at each single time step in a nonlinear quasi-stationary problem

$$\hat{A}(\hat{U}_h^n)(\hat{\Psi}) = \hat{F}(\hat{\Psi}) \quad \forall \hat{\Psi} \in \hat{X}_h,$$

which is solved with a Newton-like method. As done in the previous section, we can express this relation in terms of the defect:

$$d := \hat{F}(\hat{\Psi}) - \hat{A}(\tilde{U}_h^n)(\hat{\Psi}) = 0 \quad \forall \hat{\Psi} \in \hat{X}_h,$$

where $\tilde{U}_h^n$ denotes an approximate solution at time step t^n. Given an initial Newton guess $\hat{U}_h^{n,0}$, find for $j = 0, 1, 2, \ldots$ the update $\delta \hat{U}_h^n$ of the linear defect-correction problem

$$\hat{A}'(\hat{U}_h^{n,j})(\delta \hat{U}_h^n, \hat{\Psi}) = -\hat{A}(\hat{U}_h^{n,j})(\hat{\Psi}) + \hat{F}(\hat{\Psi}), \tag{156}$$

$$\hat{U}_h^{n,j+1} = \hat{U}_h^{n,j} + \lambda \delta \hat{U}_h^n. \tag{157}$$

In this algorithm, $\lambda \in (0, 1]$ is used as damping parameter for line search iterations. A crucial role for (highly) nonlinear problems includes the appropriate determination of λ. A simple strategy is to modify the update step in (156) as follows: For given $\lambda \in (0, 1)$ determine the minimal $l^* \in \mathbb{N}$ via $l = 0, 1, \ldots, N_l$, such that

$$R(\hat{U}_{h,l}^{n,j+1}) < R(\hat{U}_{h,l}^{n,j}), \tag{158}$$

$$\hat{U}_{h,l}^{n,j+1} = \hat{U}_h^{n,j} + \lambda^l \delta \hat{U}_h^n. \tag{159}$$

For the minimal l, we set

$$\hat{U}_h^{n,j+1} := \hat{U}_{h,l^*}^{n,j+1}.$$

In this context, the nonlinear residual $R(\cdot)$ is defined as

$$R(\hat{U}_h^n) := \max_i \left\{ \hat{A}(\hat{U}_h^n)(\hat{\Psi}_i) - \hat{F}(\hat{\Psi}_i) \right\} \quad \forall \hat{U}_h^n \in \hat{X}_h,$$

where $\{\hat{\Psi}_i\}$ denotes the nodal basis of $\hat{X}_h$.

The directional derivative $\hat{A}'(\hat{U})(\delta \hat{U}, \hat{\Psi})$ that is utilized previously, is defined in the same fashion as Gâteaux derivative. The definition of the directional derivative in terms of a semi-linear form reads:

$$\hat{A}'(\hat{U})(\delta \hat{U}, \hat{\Psi}) := \lim_{\varepsilon \to 0} \frac{1}{\varepsilon} \left\{ \hat{A}(\hat{U} + \varepsilon \delta \hat{U})(\hat{\Psi}) - \hat{A}(\hat{U})(\hat{\Psi}) \right\} = \frac{d}{d\varepsilon} \hat{A}_h(\hat{U} + \varepsilon \delta \hat{U})(\hat{\Psi}) \Big|_{\varepsilon=0}.$$

Remark 6.18. *If the directional derivative exists for all directions, we call the derivative Gateaux-derivative. Moreover, the Fréchet-derivative is a stronger concept of derivatives; consequently, each Fréchet derivative is also a Gateaux-derivative.* ⋄

Let us explain the concepts in a bit more detail in the following. Given a function $f : X \to Y$ and $f'(a) \in L(X, Y)$ where L is as usually the space of linear and continuous operators. Recall that $L(X, \mathbb{R}) =: X'$ is the dual space. The derivative $f'(a)$ is computed as action on vectors of X (see definition of the directional derivative), i.e.,

$$f'(a)\delta a = \lim_{\varepsilon \to 0} \frac{f(a + \varepsilon \delta a) - f(a)}{\varepsilon} = \frac{d}{d\varepsilon} f(a + \varepsilon \delta a)|_{\varepsilon=0} \in Y.$$

The element $f'(a)\delta a \in Y$ is called the directional derivative. In a Hilbert space, we the special case:

$$f'(a)(\delta a) = (\nabla f(a), \delta a) \quad \forall \delta a \in X$$

where we denote $\nabla f(a)$ as the gradient.

6.4 Evaluation of the directional derivatives

Due to the large size of the Jacobian matrix and the strongly nonlinear behavior of fluid-structure interaction problems in the monolithic ALE framework, the calculation of the Jacobian matrix can be cumbersome. Nevertheless, in this context, we use the exact Jacobian matrix to identify the optimal convergence and accuracy properties of the Newton method. The derivation of directional derivatives is also illustrated by means of several examples presented elsewhere [81, 205, 250]. For more details on the computation of the directional derivatives on the interface, we refer the reader to [70, 207]. Evaluation of the directional derivatives for fluid-structure interaction with help of *automatic differentiation* is demonstrated by Dunne [70].

6.4.1 First some simple examples

Recall that we need to differentiate in each direction.

Example 6.19. *Let u be the solution variable for*

$$A(u)(\varphi) = (\nabla u, \nabla \varphi)$$

be the residual. Then, the directional derivative in direction δu is given by:

$$A'(u)(\delta u, \varphi) = (\nabla \delta u, \nabla \varphi).$$

Example 6.20. *Let p and u solution variables for*

$$A(p, u)(\varphi) = (-pI + \rho\nu(\nabla u + \nabla u^T), \nabla \varphi)$$

be the residual. Then, the directional derivative in direction $\{\delta p, \delta u\}$ is given by:

$$A'(p, u)(\{\delta p, \delta u\}, \varphi) = (-\delta p I + \rho\nu(\nabla \delta u + \nabla \delta u^T), \nabla \varphi).$$

Remark 6.21. *Hopefully you noticed that everything was linear so far.* ⋄

Example 6.22. *Let v and u solution variables for*

$$A(v, u)(\varphi) = (v\nabla u, \nabla \varphi)$$

be the residual. Then, the directional derivative in direction $\{\delta v, \delta u\}$ is given by:

$$A'(v, u)(\{\delta v, \delta u\}, \varphi) = (\delta v \nabla u + v \nabla \delta u, \nabla \varphi)$$

using the chain rule.

Despite the fact that we later account on block system, let us explain what we mean by *taking all directional derivatives in the context of finite elements*. Let $V_h := \{\varphi_1, \ldots, \varphi_N\}$ a finite element space. The relation between derivatives and linear equation system is as follows. Given $u \in V_h$, the residual reads:

$$A(u_h)(\varphi_h) = (\nabla u_h, \nabla \varphi_h) \quad \forall \varphi_h \in V_h.$$

Now we build the derivative in direction δu_h:

$$A'(u_h)(\delta u_h, \varphi_h) = (\nabla \delta u_h, \nabla \varphi_h) \quad \forall \varphi_h \in V_h.$$

Recall that $\delta u_h = \sum_{j=1}^{N} u_j \varphi_j$. Now, we replace δu_h by all test functions using its property being a linear combination and for all test functions:

$$A'(u_h)(\varphi_i, \varphi_j) = \sum_j u_j (\nabla \varphi_j, \nabla \varphi_i)$$

Then, we obtain $Ax = b$ with

$$A = \begin{pmatrix} (\nabla \varphi_1, \nabla \varphi_1) & \dots & (\nabla \varphi_N, \nabla \varphi_1) \\ & \vdots & \\ (\nabla \varphi_1, \nabla \varphi_N) & \dots & (\nabla \varphi_N, \nabla \varphi_N) \end{pmatrix} \tag{160}$$

and $x = (u_1, \dots, u_N)^T$.

Remark 6.23. *Do not forget: the test function dictates the row! In symmetric problems like for Poisson problems this does not matter, but in non-symmetric problems (transport, Navier-Stokes) this is important.* $\diamond$

6.4.2 Directional derivatives of fluid-structure

In this section, we apply the previous concepts to the evaluation of the directional derivatives for fluid-structure interaction. We examin term by term. As before, let the solution $\hat{U}_h^n = \{\hat{v}_{f,h}^n, \hat{v}_{s,h}^n, \hat{u}_{f,h}^n, \hat{u}_{s,h}^n, \hat{p}_{f,h}^n, \hat{p}_{s,h}^n\} \in \widehat{X}_h$ be given. Further, let $\delta \hat{U}_h^n = \{\delta\hat{v}_{f,h}^n, \delta\hat{v}_{s,h}^n, \delta\hat{u}_{f,h}^n, \delta\hat{u}_{s,h}^n, \delta\hat{p}_{f,h}^n, \delta\hat{p}_{s,h}^n\} \in \widehat{X}_h$. In the following, we omit explicit notation of 'h' and 'n'.

The Jacobian $\hat{A}'(\hat{U})(\delta\hat{U}, \hat{\Psi})$ is split up into fluid contributions and structure terms:

$$\hat{A}'(\hat{U})(\delta\hat{U}, \hat{\Psi}) := \hat{A}_f'(\hat{U}_f)(\delta\hat{U}_f, \hat{\Psi}_f) + \hat{A}_s'(\hat{U})(\delta\hat{U}_s, \hat{\Psi}_s).$$

Using the previous arrangement (134), we deal with

$$\hat{A}_f'(\hat{U}_f)(\delta\hat{U}_f, \hat{\Psi}_f) \tag{161}$$
$$= \hat{A}_{f,T}'(\hat{U}_f)(\delta\hat{U}_f, \hat{\Psi}_f) + \hat{A}_{f,I}'(\hat{U}_f)(\delta\hat{U}_f, \hat{\Psi}_f) + \hat{A}_{f,E}'(\hat{U}_f)(\delta\hat{U}_f, \hat{\Psi}_f) + \hat{A}_{f,P}'(\hat{U}_f)(\delta\hat{U}_f, \hat{\Psi}_f), \tag{162}$$

and

$$\hat{A}_s'(\hat{U}_s)(\delta\hat{U}_s, \hat{\Psi}_s) \tag{163}$$
$$= \hat{A}_{s,T}'(\hat{U}_s)(\delta\hat{U}_s, \hat{\Psi}_s) + \hat{A}_{s,I}'(\hat{U}_s)(\delta\hat{U}_s, \hat{\Psi}_s) + \hat{A}_{s,E}'(\hat{U}_s)(\delta\hat{U}_s, \hat{\Psi}_s) + \hat{A}_{s,P}'(\hat{U}_s)(\delta\hat{U}_s, \hat{\Psi}_s). \tag{164}$$

The concrete evaluation of each term on the fully discrete level is derived in the following.

Basic relations

In the sequel, we often use the short-hand-notation

$$\partial_b A(\delta z) := \frac{\partial A}{\partial b}(\delta z),$$

for the derivative of a tensor A w.r.t. b in direction δz. We begin with the basic relations that are required for each of the subproblems. For the deformation gradient $\widehat{F}$, it holds in a direction $\delta \hat{z} \in H^1(\widehat{\Omega})$:

$$\partial_z \widehat{F}(\delta \hat{z}) = \widehat{\nabla} \delta \hat{z}, \quad \partial_z \widehat{F}^T(\delta \hat{z}) = \widehat{\nabla} \delta \hat{z}^T. \tag{165}$$

In the following, we recall the evaluation of the inverse relations (see, e.g., [139])

$$\partial_z \widehat{F}^{-1}(\delta \hat{z}) = -\widehat{F}^{-1} \widehat{\nabla} \delta \hat{z} \widehat{F}^{-1}, \quad \partial_z \widehat{F}^{-T}(\delta \hat{z}) = -\widehat{F}^{-T} \widehat{\nabla} \delta \hat{z}^T \widehat{F}^{-T}.$$

Finally, the derivative of the determinant $\hat{J}$ can be expressed as

$$\partial_z \hat{J}(\delta z) = \hat{J} \mathrm{tr}(\widehat{F}^{-1} \widehat{\nabla} \delta z).$$

Fluid's Cauchy stress tensor

In the fluid part, we are concerned with the evaluation of directional derivatives in the three directions $\delta \hat{v}_f, \delta \hat{p}_f$ and $\delta \hat{u}_f$. We start with the Cauchy stress tensor $\widehat{\sigma}_f = \widehat{\sigma}_{f,vu} + \widehat{\sigma}_{f,p}$:

$$\partial_v \widehat{\sigma}_{f,vu}(\delta \hat{v}_f) = 2\hat{\rho}_f \nu_f (\widehat{\nabla} \delta \hat{v}_f \widehat{F}^{-1} + \widehat{F}^{-T} \widehat{\nabla} \delta \hat{v}_f^T),$$

$$\partial_p \widehat{\sigma}_{f,p}(\delta \hat{p}_f) = -\delta \hat{p}_f \hat{I},$$

$$\partial_u \widehat{\sigma}_{f,vu}(\delta \hat{u}_f) = 2\hat{\rho}_f \nu_f (\widehat{\nabla} \hat{v}_f(-\widehat{F}^{-1} \widehat{\nabla} \delta \hat{u} \widehat{F}^{-1}) + (-\widehat{F}^{-T} \widehat{\nabla} \delta \hat{u}^T \widehat{F}^{-T}) \widehat{\nabla} \hat{v}_f^T).$$

Summarizing these contributions yields

$$\partial_U \widehat{\sigma}_{f,vu}(\delta \hat{U}_f) = \partial_v \widehat{\sigma}_{f,vu}(\delta \hat{v}_f) + \partial_u \widehat{\sigma}_{f,vu}(\delta \hat{u}_f), \qquad \partial_U \widehat{\sigma}_{f,p}(\delta \hat{U}_f) = \partial_p \widehat{\sigma}_{f,p}(\delta \hat{v}_p).$$

Thus, the derivative of the transformed Cauchy stress tensor in the reference domain reads:

$$\partial_U (\hat{J} \widehat{\sigma}_f \widehat{F}^{-T})(\delta \hat{U}_f) = \hat{J} \mathrm{tr}(\widehat{F}^{-1} \widehat{\nabla} \delta \hat{u}_f) \widehat{\sigma}_f \widehat{F}^{-T} + \hat{J} \partial_U \widehat{\sigma}_f(\delta \hat{U}_f) \widehat{F}^{-T} + \hat{J} \widehat{\sigma}_f(-\widehat{F}^{-T} \widehat{\nabla} \delta \hat{u}_f^T \widehat{F}^{-T}).$$

The Cauchy stress tensor is decomposed by reason motivated in Problem 6.4. It is obvious that this decomposition must be considered in the linearization process, too.

Fluid's convection term

For the treatment of the convection term (also including the ALE convection term), we use the relation $\hat{u}_f \cdot \widehat{\nabla} \hat{v}_f = \widehat{\nabla} \hat{v}_f \hat{u}_f$ and decompose the convection term as

$$\hat{\rho}_f \hat{J}(\widehat{F}^{-1}(\hat{v}_f - \hat{w}) \cdot \widehat{\nabla}) \hat{v}_f = \hat{\rho}_f \hat{J}(\widehat{\nabla} \hat{v}_f \widehat{F}^{-1}) \hat{v}_f - \hat{\rho}_f \hat{J}(\widehat{\nabla} \hat{w} \widehat{F}^{-1}) \hat{v}_f.$$

With the help of the previously introduced basic relations, the derivative of the first part reads:

$$\partial_U(\hat{\rho}_f\hat{J}(\widehat{\nabla}\hat{v}_f\widehat{F}^{-1})\hat{v}_f)(\delta\hat{U}_f) = \hat{\rho}_f\hat{J}\mathrm{tr}(\widehat{F}^{-1}\widehat{\nabla}\delta\hat{u}_f)(\widehat{\nabla}\hat{v}_f\widehat{F}^{-1})\hat{v}_f \tag{166}$$

$$+ \hat{\rho}_f\hat{J}(\widehat{\nabla}\delta\hat{v}_f\widehat{F}^{-1})\hat{v}_f \tag{167}$$

$$+ \hat{\rho}_f\hat{J}(\widehat{\nabla}\hat{v}_f(-\widehat{F}^{-1}\widehat{\nabla}\delta\hat{u}_f\widehat{F}^{-1})\hat{v}_f \tag{168}$$

$$+ \hat{\rho}_f\hat{J}(\widehat{\nabla}\hat{v}_f\widehat{F}^{-1})\delta\hat{v}_f. \tag{169}$$

In the second part, we cannot directly differentiate the fluid domain velocity $\hat{w}$. As previously discussed this term is constructed (linear in time) with the help of the displacements $\hat{u}_f$. Thus, in Equation (166), we only must replace the second term. Using the construction of $\hat{w} = \frac{1}{k}(\hat{u}_f - \hat{u}_f^{n-1})$ in which $\hat{u}_f^{n-1}$ denotes the solution of the previous time step, we readily get

$$\partial_u\hat{w}(\delta\hat{u}_f) := \partial_u\frac{1}{k}(\hat{u}_f - \hat{u}_f^{n-1})(\delta\hat{u}_f) = \frac{1}{k}\delta\hat{u}_f. \tag{170}$$

With this, we obtain for the second equation on the right-hand-side in (166)

$$\frac{1}{k}\hat{\rho}_f\hat{J}(\widehat{\nabla}\delta\hat{u}_f\widehat{F}^{-1})\hat{v}_f.$$

In the remaining terms of (166), we replace $\widehat{\nabla}\hat{v}_f$ with $\widehat{\nabla}\hat{w}$.

Fluid's time derivative

We continue with the time derivative of the fluid term:

$$\hat{\rho}_f\hat{J}\partial_t\hat{v}_f \approx \hat{\rho}_f\hat{J}^{n,\theta}\frac{\hat{v}_f - \hat{v}_f^{n-1}}{k},$$

where we employ (137) for the temporal discretization. First, we obtain

$$\partial_u\hat{J}^{n,\theta}(\delta\hat{u}_f) = \partial_u(\theta\hat{J} + (1-\theta)\hat{J}^{n-1})(\delta\hat{u}_f) = \theta\hat{J}\mathrm{tr}(\widehat{F}^{-1}\widehat{\nabla}\delta\hat{u}_f). \tag{171}$$

Next, we get

$$\partial_v\frac{1}{k}(\hat{v}_f - \hat{v}_f^{n-1})(\delta\hat{v}_f) = \frac{1}{k}\delta\hat{v}_f.$$

With this equation, we compute for (171):

$$\partial_U\left(\hat{\rho}_f\frac{1}{k}\hat{J}^{n,\theta}(\hat{v}_f - \hat{v}_f^{n-1})\right)(\delta\hat{U}_f) = \hat{\rho}_f\frac{\theta}{k}\hat{J}\mathrm{tr}(\widehat{F}^{-1}\widehat{\nabla}\delta\hat{u}_f)(\hat{v}_f - \hat{v}_f^{n-1}) + \hat{\rho}_f\frac{1}{k}\hat{J}^{n,\theta}(\delta\hat{v}_f).$$

Fluid's incompressibility

We proceed with the incompressibility term of the fluid. To compute the derivative, we utilize a byproduct of the divergence relation of the Piola transformation:

$$\widehat{\mathrm{div}}(\hat{J}\widehat{F}^{-1}\hat{v}_f) = \hat{J}\mathrm{tr}(\widehat{\nabla}\hat{v}_f\widehat{F}^{-1}).$$

Then, we get

$$\partial_v \hat{J} \text{tr}(\widehat{\nabla}\hat{v}_f \widehat{F}^{-1})(\delta\hat{v}_f) = \hat{J}\text{tr}(\widehat{\nabla}\delta\hat{v}_f \widehat{F}^{-1}),$$

$$\partial_u \hat{J} \text{tr}(\widehat{\nabla}\hat{v}_f \widehat{F}^{-1})(\delta\hat{u}_f) = \hat{J}\text{tr}(\widehat{F}^{-1}\widehat{\nabla}\delta\hat{u}_f)\text{tr}(\widehat{\nabla}\hat{v}_f \widehat{F}^{-1}) - \hat{J}\text{tr}(\widehat{\nabla}\hat{v}_f \widehat{F}^{-1}\widehat{\nabla}\delta\hat{u}_f \widehat{F}^{-1}).$$

Fluid's mesh motion

It remains to consider the derivative of the mesh motion equation. Using the harmonic mesh motion model (see definition of $\widehat{\sigma}_{\text{mesh}}$ in (35)), we readily obtain

$$\partial_u(\alpha_u \widehat{\nabla}\hat{u}_f)(\delta\hat{u}_f) = \alpha_u \widehat{\nabla}\delta\hat{u}_f.$$

Using the linear-elastic mesh motion model (see definition of $\widehat{\sigma}_{\text{mesh}}$ in (38)), we get

$$\partial_u(\alpha_\lambda(\text{tr}\,\hat{\epsilon})\hat{I} + 2\alpha_\mu\hat{\epsilon})(\delta\hat{u}_f) = \alpha_\lambda \frac{1}{2}(\text{tr}\,(\widehat{\nabla}\delta\hat{u}_f + \widehat{\nabla}\delta\hat{u}_f^T)\hat{I} + \alpha_\mu(\widehat{\nabla}\delta\hat{u}_f + \widehat{\nabla}\delta\hat{u}_f^T).$$

Fluid's do-nothing condition

Next, we consider the derivative of the boundary term $\hat{g}_f := -\hat{\rho}_f\nu_f\widehat{F}^{-T}\widehat{\nabla}\hat{v}_f^T$ on $\widehat{\Gamma}_{f,N}$ (see (31)):

$$\partial_U(-\hat{\rho}_f\nu_f\widehat{F}^{-T}\widehat{\nabla}\hat{v}_f^T)(\delta\hat{U}_f) = \hat{\rho}_f\nu_f(\widehat{F}^{-T}\widehat{\nabla}\delta\hat{u}_f^T\widehat{F}^{-T})\widehat{\nabla}\hat{v}_f^T + \hat{\rho}_f\nu_f\widehat{F}^{-T}\widehat{\nabla}\delta\hat{v}_f^T.$$

Fluid's stabilization

Finally, we explain the differentiation of the stabilization term. In this expression, we only differentiate the first argument although the second argument also depends on the solution variable. Using the derivative of the convection term, we readily obtain

$$\hat{S}'_{\text{stab}}(\hat{U}_f)(\delta\hat{U}_f, \hat{\Psi}_f) = (\partial_U(\hat{\rho}_f\hat{J}(\widehat{\nabla}\hat{v}_f\widehat{F}^{-1})\hat{v}_f)(\delta\hat{U}_f), \delta_{K,n}(\widehat{F}^{-1}\hat{v}_f \cdot \widehat{\nabla})\hat{\psi}_f^v)_{\widehat{K}_f}, \quad (172)$$

on each cell $\widehat{K}_f \in \mathcal{T}_h$.

Structure's constitutive tensors

We continue with the description for the derivatives of the structure subproblem. Using standard elasticity (i.e., the damping terms are omitted) with the STVK model, we only must compute the derivatives with respect to $\hat{u}_s$. In the presence of incompressible materials, we also account for the pressure $\hat{p}_s$. Finally, the consideration of strong damping makes it necessary to compute derivatives with respect to $\hat{v}_s$.

Let us begin with the Green-Lagrange tensor (defined in (73)) that is employed to formulate the STVK material:

$$\partial_u \widehat{E}(\delta\hat{u}_s) = \frac{1}{2}(\widehat{\nabla}\delta\hat{u}_s^T\widehat{F} + \widehat{F}^T\widehat{\nabla}\delta\hat{u}_s).$$

Then, the constitutive tensor $\widehat{\Sigma} := \widehat{\Sigma}(\hat{u}_s)$ reads

$$\partial_u \widehat{\Sigma}(\delta\hat{u}_s) = \lambda_s \frac{1}{2}\text{tr}(\widehat{\nabla}\delta\hat{u}_s^T\widehat{F} + \widehat{F}^T\widehat{\nabla}\delta\hat{u}_s)\hat{I} + \mu_s(\widehat{\nabla}\delta\hat{u}_s^T\widehat{F} + \widehat{F}^T\widehat{\nabla}\delta\hat{u}_s).$$

For the incompressible IMR material, we obtain

$$\partial_p \widehat{\sigma}_{\mathrm{IMR}}(\delta \hat{p}_s) = -\delta \hat{p}_s \hat{I},$$
$$\partial_u \widehat{\sigma}_{\mathrm{IMR}}(\delta \hat{u}_s) = \mu_1(\delta \hat{u}_s \widehat{F}^T + \widehat{F} \delta \hat{u}_s^T) - \mu_2(\widehat{F}^{-T} \widehat{\nabla} \delta \hat{u}_s^T \widehat{F}^{-T} \widehat{F}^{-1} + \widehat{F}^{-T} \widehat{F}^{-1} \widehat{\nabla} \delta \hat{u}_s \widehat{F}^{-1}),$$

and from this, we readily deduce

$$\partial_p \widehat{\sigma}_{\mathrm{INH}}(\delta \hat{p}_s) = -\delta \hat{p}_s \hat{I},$$
$$\partial_u \widehat{\sigma}_{\mathrm{INH}}(\delta \hat{u}_s) = \mu_1(\delta \hat{u}_s \widehat{F}^T + \widehat{F} \delta \hat{u}_s^T).$$

Structure's damping terms

Finally, using strong damping, we compute the derivatives in the direction $\delta \hat{v}_s$ of $\hat{\epsilon}(\hat{v}_s)$. Then,

$$\partial_v \hat{\epsilon}(\hat{v}_s)(\delta \hat{v}_s) = \frac{1}{2}(\widehat{\nabla} \delta \hat{v}_s + \widehat{\nabla} \delta \hat{v}_s^T).$$

Proposition 6.24. *At each Newton step* (156)*, we solve a linear system, where (an example of) its residual $\hat{A}(\hat{U})(\hat{\Psi}) - \widehat{F}(\hat{\Psi})$ on the continuous level is defined in Problem 6.1. The Jacobian of this problem is split into*

$$\hat{A}'(\hat{U})(\delta \hat{U}, \hat{\Psi}) := \hat{A}'_f(\hat{U}_f)(\delta \hat{U}_f, \hat{\Psi}_f) + \hat{A}'_s(\hat{U}_s)(\delta \hat{U}_s, \hat{\Psi}_s).$$

Using the arrangements (161) *and* (163)*, we deal with the following expressions:*

$$\hat{A}'_{f,T}(\hat{U}_f)(\delta \hat{U}_f, \hat{\Psi}_f) = \rho_f \frac{\theta}{k}(\hat{J} tr(\widehat{F}^{-1} \widehat{\nabla} \delta \hat{u}_f)(v_f - \hat{v}_f^{n-1}), \hat{\psi}_f^v)_{\widehat{\Omega}_f} + \rho_f \frac{1}{k}(\hat{J}^{n,\theta}(\delta \hat{v}_f), \hat{\psi}_f^v)_{\widehat{\Omega}_f}$$
$$+ \rho_f(\hat{J}(\widehat{\nabla} \hat{v}_f \widehat{F}^{-1})(\delta \hat{v}_f - k^{-1}\delta \hat{u}_f), \hat{\psi}_f^v)_{\widehat{\Omega}_f},$$

$$\hat{A}'_{f,E}(\hat{U}_f)(\delta \hat{U}_f, \hat{\Psi}_f) = \rho_f(\hat{J} tr(\widehat{F}^{-1} \widehat{\nabla} \delta \hat{u}_f)(\widehat{\nabla} \hat{v}_f \widehat{F}^{-1})(\hat{v}_f - \hat{w}), \hat{\psi}_f^v)_{\widehat{\Omega}_f}$$
$$+ \rho_f(\hat{J}(\widehat{\nabla} \delta \hat{v}_f \widehat{F}^{-1})(\hat{v}_f - \hat{w}), \hat{\psi}_f^v)_{\widehat{\Omega}_f}$$
$$+ \rho_f(\hat{J}(\widehat{\nabla} \hat{v}_f(-\widehat{F}^{-1} \widehat{\nabla} \delta \hat{u}_f \widehat{F}^{-1})(\hat{v}_f - \hat{w}), \hat{\psi}_f^v)_{\widehat{\Omega}_f}$$
$$+ (\partial_U(\hat{J}\hat{\sigma}_{f,vu} \widehat{F}^{-T})(\delta \hat{U}_f), \hat{\psi}_f^v)_{\widehat{\Omega}_f} + \langle \partial_U g_f(\delta \hat{U}), \hat{\psi}_f^v \rangle_{\widehat{\Gamma}_N}$$
$$- (\rho_f \hat{J} tr(\widehat{F}^{-1} \widehat{\nabla} \delta \hat{u}_f) \hat{f}_f, \hat{\psi}_f^v)_{\widehat{\Omega}_f},$$

$$\hat{A}'_{f,I}(\hat{U}_f)(\delta \hat{U}_f, \hat{\Psi}_f) = (\alpha_u \widehat{\nabla} \delta \hat{u}_f, \widehat{\nabla} \hat{\psi}_f^u)_{\widehat{\Omega}_f}$$
$$+ (\hat{J} tr(\widehat{\nabla} \delta \hat{v}_f \widehat{F}^{-1}), \hat{\psi}_f^p)_{\widehat{\Omega}_f} + (\hat{J} tr(\widehat{F}^{-1} \widehat{\nabla} \delta \hat{u}_f) tr(\widehat{\nabla} \hat{v}_f \widehat{F}^{-1}), \hat{\psi}_f^p)_{\widehat{\Omega}_f}$$
$$- (\hat{J} tr(\widehat{\nabla} \hat{v}_f \widehat{F}^{-1} \widehat{\nabla} \delta \hat{u}_f \widehat{F}^{-1}), \hat{\psi}_f^p)_{\widehat{\Omega}_f},$$

$$\hat{A}'_{f,P}(\hat{U}_f)(\delta \hat{U}_f, \hat{\Psi}_f) = (\partial_U(\hat{J}\hat{\sigma}_{f,p} \widehat{F}^{-T})(\delta \hat{U}_f), \widehat{\nabla} \hat{\psi}_f^v)_{\widehat{\Omega}_f},$$

$$\hat{S}'_{stab}(\hat{U}_f)(\delta \hat{U}_f, \hat{\Psi}_f) = (\partial_U(\rho_f \hat{J}(\widehat{\nabla} \hat{v}_f \widehat{F}^{-1}) \hat{v}_f)(\delta \hat{U}_f), \delta_{K,n}(\widehat{F}^{-1} \hat{v}_f \cdot \widehat{\nabla}) \hat{\psi}_f^v)_{\widehat{K}_f},$$

123

and

$$\hat{A}'_{s,T}(\hat{U}_s)(\delta\hat{U}_s, \hat{\Psi}_s) = k^{-1}(\hat{\rho}_s\delta\hat{v}_s, \hat{\psi}^v_s)_{\widehat{\Omega}_s} + k^{-1}(\hat{\rho}_s\hat{u}_s, \hat{\psi}^u_s)_{\widehat{\Omega}_s} - (\hat{\rho}_s\delta\hat{v}_s, \hat{\psi}^u_s)_{\widehat{\Omega}_s}$$
$$+ (\partial_U\hat{P}(\delta\hat{U}_s, \hat{\psi}^p_s)_{\widehat{\Omega}_s},$$
$$\hat{A}'_{s,E}(\hat{U}_s)(\delta\hat{U}_s, \hat{\Psi}_s) = (\partial_u(\widehat{F}\widehat{\Sigma})(\delta\hat{u}_s), \widehat{\nabla}\hat{\psi}^v_s)_{\widehat{\Omega}_s}$$
$$+ \gamma_w(\delta\hat{v}_s, \hat{\psi}^v_s)_{\widehat{\Omega}_s} + \gamma_s(\partial_v\hat{\epsilon}(\hat{v}_s)(\delta\hat{v}_s), \hat{\psi}^v_s)_{\widehat{\Omega}_s},$$
$$\hat{A}'_{s,I}(\hat{U}_s)(\delta\hat{U}_s, \hat{\Psi}_s) = (\partial_U\hat{P}(\delta\hat{U}_s), \hat{\psi}^p_s)_{\widehat{\Omega}_s},$$
$$\hat{A}'_{s,P}(\hat{U}_s)(\delta\hat{U}_s, \hat{\Psi}_s) = (\partial_U(\hat{J}\hat{\sigma}_{s,p}\widehat{F}^{-T})(\delta\hat{U}_s), \widehat{\nabla}\hat{\psi}^v_s)_{\widehat{\Omega}_f}.$$

6.5 Solution of linear equations

In this final subsection, we discuss solution methods for fluid-structure interaction problems. Specific realizations are closely related to the FSI coupling algorithms depending a partitioned or monolithic approach is employed.

- Monolithic solution [11, 15, 16, 63, 104, 128, 129, 141, 231, 238, 263];

- Partitioned: [10, 67, 155, 158, 160, 165, 230].

Let us briefly show the structure. For spatial discretization, we use the previously introduced spaces $V_h \times W_h \times L_h$ with vector valued basis

$$\{\psi_i \,|\, i = 1, \ldots, N\},$$

where the basis functions are primitive (they are only non-zero in one component), so we can separate them into velocity, displacement, and pressure basis functions and sort them accordingly:

$$\psi_i = \begin{pmatrix} \chi_i^v \\ 0 \\ 0 \end{pmatrix}, \text{ for } i = 1, \ldots, N_v,$$

$$\psi_{(N_v+i)} = \begin{pmatrix} 0 \\ \chi_i^u \\ 0 \end{pmatrix}, \text{ for } i = 1, \ldots, N_u,$$

$$\psi_{(N_v+u+i)} = \begin{pmatrix} 0 \\ 0 \\ \chi_i^p \end{pmatrix}, \text{ for } i = 1, \ldots, N_p,$$

where $N_v + N_u + N_p = N$. This is now used to transform into a system of the form

$$Mx = F, \tag{173}$$

where M is a block matrix (the Jacobian) and F the right hand side consisting of the residuals. The block structure for ALE-FSI with harmonic or linear-elastic mesh motion is

$$M = \begin{pmatrix} M^{vv} & M^{vu} & M^{vp} \\ M^{uv} & M^{uu} & M^{up} \\ M^{pv} & M^{pu} & M^{pp} \end{pmatrix}, \qquad F = \begin{pmatrix} F^v \\ F^u \\ F^p \end{pmatrix},$$

In the matrix, the degrees of freedom that belong to Dirichlet conditions (here only displacements since we assume Neumann conditions for the phase-field) are strongly enforced by replacing the corresponding rows and columns as usual in a finite element code.

6.6 A useful example of finite-difference-in-time, Galerkin-FEM-in-space-discretization and linearization in a Newton setting

I believe that the discretization of nonlinear time-dependent partial differential equations is finally very similar to solving Poisson's problem. Hopefully, I convince the reader in this section.

We are given the following example:

Problem 6.25. *Let the following PDE be given (we omit any 'hats'): Find v and u, for allmost all times, such that*

$$\partial_t^2 u - J\nabla \cdot \sigma(v)F^{-T} = f, \quad in \ \Omega, \quad plus \ bc. \ and \ initial \ cond.,$$

and where (as before) $J := J(u), F := F(u)$ and $\sigma(v) = (\nabla v + \nabla v^T)$.

6.6.0.1 Time discretization We aim to apply a One-Step-θ scheme applied to the mixed problem:

$$\partial_t v - J\nabla \cdot \sigma(v)F^{-T} = f,$$
$$\partial_t u - v = 0.$$

One-Step-θ discretization with time step size k, and $\theta \in [0,1]$, leads to

$$\frac{v - v^{n-1}}{k} - \theta J\nabla \cdot \sigma(v)F^{-T} - (1-\theta)J^{n-1}\nabla \cdot \sigma(v^{n-1})(F^{-T})^{n-1} = \theta f + (1-\theta)f^{n-1},$$

$$\frac{u - u^{n-1}}{k} - \theta v - (1-\theta)v^{n-1} = 0.$$

6.6.0.2 Spatial pre-discretization: weak form on the continuous level We multiply by the time step k, apply with test functions from suitable spaces V and W and obtain the weak formulations

$$(v - v^{n-1}, \varphi) + k\theta(J\sigma(v)F^{-T}, \nabla\varphi) + k(1-\theta)(J^{n-1}\sigma(v^{n-1})(F^{-T})^{n-1}, \varphi)$$
$$= k\theta(f, \varphi) + k(1-\theta)(f^{n-1}, \varphi) \quad \forall \varphi \in V,$$
$$(u - u^{n-1}, \psi) + k\theta(v, \psi) + k(1-\theta)(v^{n-1}, \psi) = 0 \quad \forall \psi \in W.$$

Sorting terms on left and right hand sides:

$$(v, \varphi) + k\theta(J\sigma(v)F^{-T}, \nabla\varphi)$$
$$= (v^{n-1}, \varphi) - k(1-\theta)(J^{n-1}\sigma(v^{n-1})(F^{-T})^{n-1}, \varphi)$$
$$+ k\theta(f, \varphi) + k(1-\theta)(f^{n-1}, \varphi) \quad \forall \varphi \in V,$$
$$(u, \psi) + k\theta(v, \psi) = (u^{n-1}, \psi) - k(1-\theta)(v^{n-1}, \psi) \quad \forall \psi \in W.$$

6.6.0.3 A single semi-linear form - first step towards Newton solver Now, we build a single semi-linear form $A(\cdot)(\cdot)$ and right hand side $F(\cdot)$. Let[21] $U := \{v, u\} \in V \times W$ and $\Psi := \{\varphi, \psi\} \in V \times W$: Find $U \in V \times W$ such that:

$$A(U)(\Psi) = (v, \varphi) + k\theta(J\sigma(v)F^{-T}, \nabla\varphi) + (u, \psi) + k\theta(v, \psi)$$
$$F(\Psi) = (v^{n-1}, \varphi) - k(1-\theta)(J^{n-1}\sigma(v^{n-1})(F^{-T})^{n-1}, \varphi) + k\theta(f, \varphi)$$
$$+ k(1-\theta)(f^{n-1}, \varphi)(u^{n-1}, \psi) - k(1-\theta)(v^{n-1}, \psi)$$

for all $\Psi \in V \times W$.

6.6.0.4 Evaluation of directional derivatives - second step for Newton solver We follow Section 6.4.1. Let $\delta U := \{\delta v, \delta u\} \in V \times W$. Then the directional derivative of $A(U)(\Psi)$ is given by:

$$A'(U)(\delta U, \Psi) = (\delta v, \varphi) + k\theta\Big(J'(\delta u)\sigma(v)F^{-T} + J\sigma'(\delta v)F^{-T} + J\sigma(v)(F^{-T})'(\delta u), \nabla\varphi\Big)$$
$$+ (\delta u, \psi) + k\theta(\delta v, \psi),$$

where we applied the chain rule for the term $J\sigma(v)F^{-T}$. Here, in the 'non-prime' terms in the nonlinear part; namely J, F^{-T} and $\sigma(v)$, the previous Newton solution is inserted. We have now all ingredients to perform the Newton step (156).

6.6.0.5 Spatial discretization in finite-dimensional spaces and linear system In the final step, we assume conforming finite-dimensional subspaces $V_h \subset V$ and $W_h \subset W$ with $V_h := \{\varphi_1, \ldots, \varphi_N\}$ and $W_h := \{\psi_1, \ldots, \psi_M\}$. Then, the update solution variables in each Newton step are given by:

$$\delta v_h := \sum_{j=1}^{N} v_j \varphi_j, \quad \text{and} \quad \delta u_h := \sum_{j=1}^{M} u_j \psi_j.$$

For the linearized semi-linear form $A'(U)(\delta U, \Psi)$, we have:

$$A'(U_h)(\delta U_h, \Psi_h)$$

and with this (A_{ij} representing the entries of the Jacobian):

$$A_{ij} := A'(U_h)(\Psi_j, \Psi_i) = \sum_{j=1}^{N} v_j(\varphi_j, \varphi_i)$$

$$+ k\theta\Big(\sum_{j=1}^{M} u_j J(\psi_j)\sigma(v)F^{-T} + J(\sum_{j=1}^{N} v_j\sigma'(\varphi_j))F^{-T} + J\sigma(v)(\sum_{j=1}^{M} u_j(F^{-T})'(\psi_j)), \nabla\varphi_i\Big)$$

$$+ \sum_{j=1}^{M} u_j(\psi_j, \psi_i) + k\theta \sum_{j=1}^{N} v_j(\varphi_j, \psi_i)$$

for all test functions running through $i = 1, \ldots, N, N+1, \ldots, M$.

---

[21]Of course, the solution spaces for ansatz- and test functions might differ.

6.7 Hands-on: implementation of benchmark examples in ANS/deal.II and DOpElib; based on C++

To supplement our algorithmic discussion with some practical aspects, the reader is invited to test him/her-self some concepts presented so far. Implementations are present in two software packages deal.II [13] (source code [256] in ANS[22]) and DOpElib [115, 116]:

- ALE-FSI in deal.II (ANS) with biharmonic mesh motion
  http://www.archnumsoft.org/ [256] solving FSI benchmark problems [142]

- Nonstationary Navier-Stokes benchmark problems [217] at
  http://www.dopelib.uni-hamburg.de/ `Examples/PDE/InstatPDE/Example1`

- ALE-FSI benchmark problems [142] with biharmonic mesh motion at
  http://www.dopelib.uni-hamburg.de/ `Examples/PDE/InstatPDE/Example2`

- Biot-Lame-Navier system: augmented Mandel's benchmark at
  http://www.dopelib.uni-hamburg.de/ `Examples/PDE/InstatPDE/Example6`

- Stationary FSI optimization at
  http://www.dopelib.uni-hamburg.de/ `Examples/OPT/StatPDE/Example9`

We notice that the implementation is performed in a *very practical* monolithic way that has two assumptions; namely, displacements and velocity are taken from globally-defined Sobolev spaces rather than restricting them to the sub-domains and one (major) limitation (the development of an iterative linear solver and preconditioners might be challanging since we do not distuingish the sub-problems in the system matrix). Putting these two limitations aside, the idea results in a fascinating easy way to implement multiphysics problems in non-overlapping domains.

Remark 6.26. *It has been appeared that the basic program structure could be easily generalized and extended to other complex multiphysics problems such as moving boundary problems with chemical reactions as well as pressure-elasticity-phase-field coupling.* ⋄

---

[22]ANS = Archive of Numerical Software, http://www.archnumsoft.org/
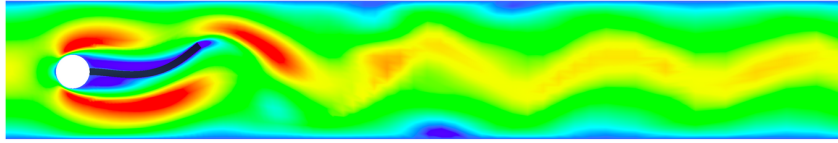
Solving Monolithic Fluid-Structure Interaction Problems in Arbitrary Lagrangian Eulerian Coordinates with the deal.II Library

Thomas Wick

We describe a setting of a nonlinear fluid-structure interaction problem and the corresponding solution process in the finite element software package deal.II. The fluid equations are transformed via the ALE mapping (Arbitrary Lagrangian Eulerian framework) to a reference configuration and these are coupled with the structure equations by a monolithic solution algorithm. To construct the ALE mapping, we use a biharmonic equation. Finite differences are used for temporal discretization. The derivation is realized in a general manner that serves for different time stepping schemes. Spatial discretization is based on a Galerkin finite element scheme. The nonlinear system is solved by a Newton method. Using this approach, the Jacobian matrix is constructed by exact computation of the directional derivatives. The implementation using the software library package deal.II serves for the computation of different fluid-structure configurations. Specifically, our geometry data are taken from the fluid-structure benchmark configuration that was proposed in 2006 in the DFG project Fluid-Structure Interaction I: Modelling, Simulation, Optimisation. Our results show that this implementation using deal.II is able to produce comparable findings.
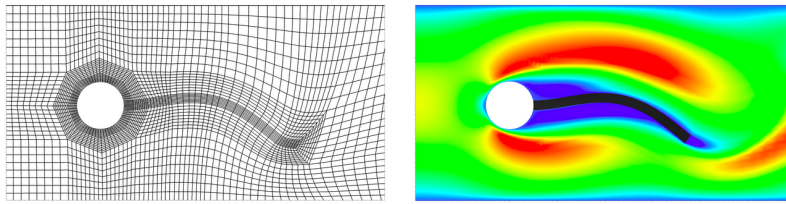

Figure 46: Reference [256] at http://www.archnumsoft.org/

The structure of such a program for time-dependent nonlinear problems is as follows:

- Input of all data: geometry, material parameters, right hand side values

- Sorting and associating degrees of freedom

- Assembling the Jacobian

- Assembling the right hand side residual

- Newton's method

- Solution of linear equations

- Postprocessing (output, a posteriori error estimation, mesh refinement)

- Main routine including time step loop

7 Sensitivity Analysis

In this final chapter, we leave forward modeling and concentrate on further aspects beyond:

- Error estimation and mesh adaptivity;

- Sensitivity analysis;

- Optimization.

All these topics have in common that either implicitly or explicitly, a quantity of interest J is subject of our investigation. Often, this quantity of interest is associated with calculating derivatives of solutions to FSI problems with respect to the given data. Such derivatives with respect to given data such as volume forces or boundary values have been used excessively in numerical papers concerned with sensitivity calculations or derivative based minimization problems, see, e.g., [4, 171, 193, 208, 216, 239]. In addition, sensitivity calculations are required for certain a posteriori error estimation techniques, such as the DWR-method [14, 26, 27]. Studies with a particular emphasize on FSI problems are carried out, for instance in [71, 118, 205, 242, 252]. Steps of optimization-related problems subject to FSI have been tackled in, e.g., [32, 47, 193, 208].

7.1 A differentiable solution map for stationary FSI

We discuss a result from theoretical fluid-structure interaction; namely the proof that there is at least one locally unique solution that is Fréchet-differentiable with respect to the boundary data and volume forces. Consequently, the following result is an extension of [117].

Proposition 7.1. *Suppose, we are given Problem 5.22. Let* $\hat{g}_f \in W^{2-1/p,p}(\Gamma)/R$, *and* $\hat{f}_s \in L^p(\widehat{\Omega}_s)$ *be given with* $3 < p < \infty$. *Assuming that* $\hat{g}_f$, *and* $\hat{f}_s$ *are small enough, then there exists a solution* $\hat{U} = (\hat{v}_f, \hat{p}_f, \hat{u}_s) \in W^{2,p} \cap H_0^1 + (g_f, 0, 0) \times W^{1,p} \times W^{2,p} \cap H_0^1$ *to the coupled Problem* (5.22). *Furthermore, there is a constant* M, *such that there is a locally unique solution satisfying the additional condition:*

$$\|(\hat{v}_f, \hat{p}_f)\|_F + \|\hat{u}_s\|_S \leq M. \tag{174}$$

In addition, the herewith defined mapping $S \colon W^{2-1/p,p}(\Gamma)/R \times L^p(\widehat{\Omega}_s) \to W^{2,p} \cap H_0^1 + (\hat{g}_f, 0, 0) \times W^{1,p} \times W^{2,p} \cap H_0^1$

$$(\hat{g}_f, \hat{f}_s) \mapsto (\hat{v}_f, \hat{p}_f, \hat{u}_s),$$

is continuously differentiable in a neighborhood of $(0, 0)$.

Proof. See [258]. $\square$

130

7.2 Dynamic-in-time interface-oriented mesh adaptivity applied to Eulerian-ALE coupling

Before we go into more detail on accurate a posteriori error estimation, we discuss dynamic-in-time mesh adaptivity according to the FSI interface. Our goal is explained in Figure 47 in which we consider a growing interface (in fact a discontinuity) and we wish to have a fine mesh around this discontinuity.
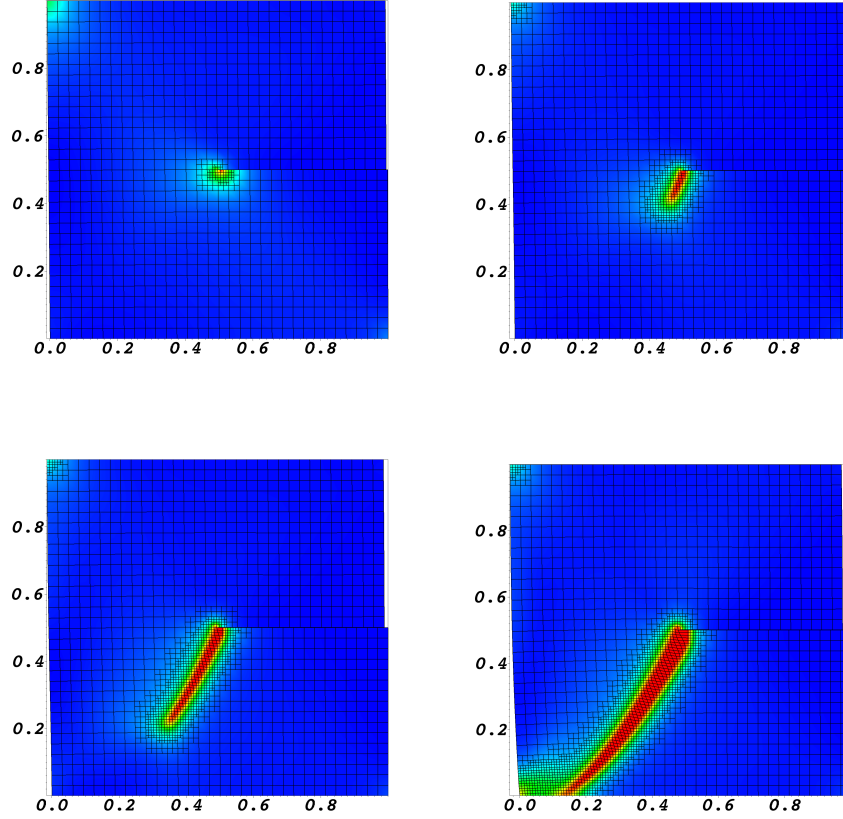

Figure 47: Dynamic-in-time mesh refinement with hanging nodes around a propagating discontinuity/interface.

As demonstration, we apply the EALE (FSITICT) technique to compute valve flapping. To enhance the quality of the numerical approximation, a sufficiently high mesh resolution is required in particular in the neighborhood of the FSI-interface; specifically for FSI formulated in fully Eulerian coordinates using a non-fitted finite element

131

method. It is clear that we are not interested in global mesh refinement since this is too expensive. The easiest way is, to locally refine the mesh at the beginning of the simulation. This however, requires a priori knowledge about the movement of the elastic structure. Imagine that we have a ball that moves throughout the whole domain (for example like Richter [204]). This would finally result in global mesh refinement. Even in less drastic cases, a priori refinement is quite unsatisfactory. Here, a big portion of the domain has to be refined in the region where we expect the beam to move. A much better idea is proposed in this study using interface-oriented mesh refinement. Not only does this procedure perform mesh refinement around the interface but it does also coarsen the mesh if the interface moved further. Illustrations are provided in Figure 47 and 49.

In fact, the second step is important to control the computational cost. It would be very easy to set all times new refinement flags. Without any coarsening, we would end up in a very fine mesh even in regions where the interface moved away (recall Richter's moving ball). Summarizing, the mesh adaptation algorithm consists of two major steps:

- Mesh refinement and

- Mesh coarsening,

leading to

Algorithm 7.2 (Interface-oriented mesh adaptivity). *In detail, the following steps are performed:*

- *Set maximum number of (total) refinement levels L_{max}*

- *Set minimum number of (total) refinement levels L_{min}*

- *At each time $t^n, n = 1, 2, 3, \ldots$: Identification of the interfaces*
  - *Mesh refinement:*
    * *Mark all interface cells (as shown in [255], Figure 6). On each of those cells:*
    * *Check if maximum refinement level L_{max} is already reached*
    * *If present level $L < L_{max}$, then set refinement flag*
  - *Mesh coarsening:*
    * *Mark all refined cells (with $L > L_{min}$) without interface. On each of those cells:*
    * *If present level $L > L_{min}$, then set coarsening flag*

With the help of an example, let us briefly explain the meaning of L_{max} and L_{min}. Set $L_{max} = 5$ and $L_{min} = 1$. A two-times globally refined mesh corresponds to $L = 2$. Then, the regions including the interface are three times locally refined, leading to the maximal refinement level $L_{max} = 5$. Regions without interface are coarsend once,

because we start with $L = 2$ and the minimum level is $L_{min} = 1$. To illustrate the outcome of Algorithm 7.2, resulting meshes are shown in Figure 49.

The data for the material parameters and the geometry are partially based on experimental data 1 (in collaboration with the cardiologist Mizerski [178]) and are supplemented with literature values [97, 197].
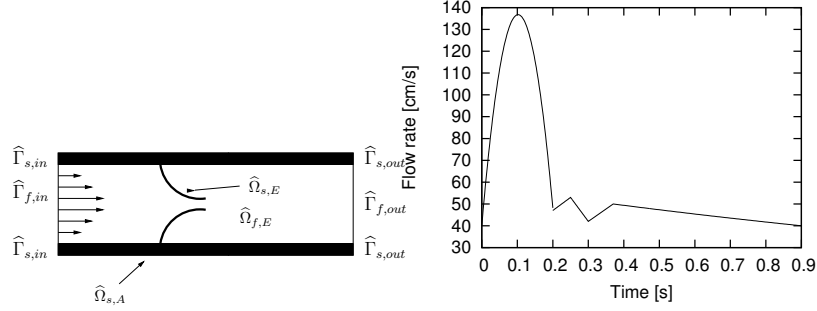

Figure 48: Configuration and inflow profile of the flap test with contact.
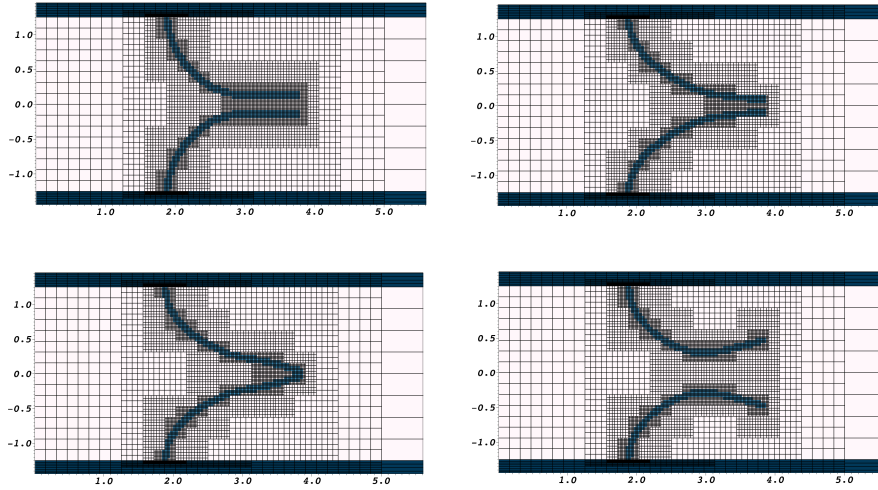

Figure 49: Flap dynamics with contact: Local mesh adaptivity for the closing and opening of the flaps. Cells indicated in blue denote elastic structures and interface elements.
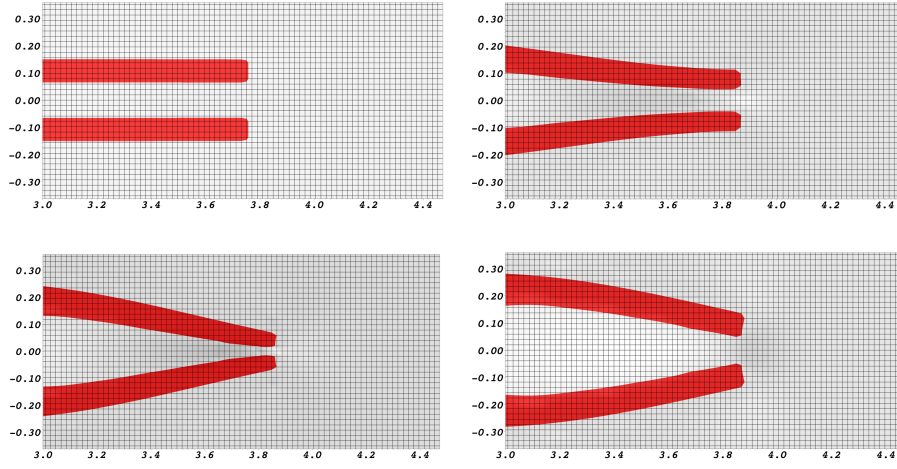
133

Figure 50: Flap dynamics with contact: Zoom-in to the tips of the two flaps. Development of the contact and re-opening for a sequence of four time steps. A minimal distance of one mesh cell is observed when the two flaps meet (bottom left). This is reasonable because otherwise the fluid equations would become invalid.
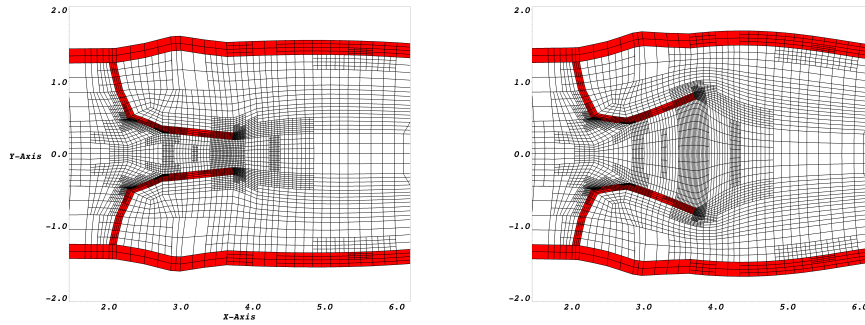

Figure 51: Flap dynamics with contact: ALE computation to highlight its drawback. Achieving contact is very sophisticated because too many mesh cells are located between both flaps in the moment of closing (top). Very large deformations cause the fluid mesh to distort at the tips of the flaps as shown in the bottom figure.

134

7.3 A partition-of-unity-based variational localization technique for a posteriori error estimation with the dual-weighted residual method

The goal of this section is

- To introduce a novel variational localization technique [210, 211][23] for the dual-weighted residual (DWR) method and highlighting why this formulation is preferrable (at least for coupled multiphysics problems such as fluid-structure interaction) compared to the classical method [26].

The DWR method goes back to Becker & Rannacher [26, 27] and is based on pioneering work by Eriksson, Estep, Hansbo and Johnson [75]. It has been further developed in [2, 108, 192]. A summary is provided in [14]. Applications include fluid-dynamics [24, 148], structural dynamics [201, 202], and further to complex multiphysics problems like chemically reactive flows [40]. We are specifically interested in fluid-structure interaction references [84, 118, 205, 252, 264].

The DWR method allows for estimating the error $u - u_h$ between the exact solution $u \in V$ (for a function space V) to the PDE and the Galerkin solution $u_h \in V_h \subset V$ in general functionals $J : V \to \mathbb{R}$. These functionals can be norms but also more general expressions, like point-values, (local) averages or technical expressions like (in the case of fluid dynamics) lift- or drag-coefficients. Error estimators based on the DWR method always consist of residual evaluations, that are weighted by adjoint sensitivity measures. These sensitivities are the solution to adjoint problems that measure the influence of the error functional J. For adaptive mesh refinement, we need to localize the error estimator $\eta(u_h, z_h) \approx J(u) - J(u_h)$ (for its definition see Equation (183)). The quality of this approximation procedure can be measured by the *effectivity index* eff_h, defined as

$$\text{eff}_h := \frac{\eta(u_h, z_h)}{J(u) - J(u_h)}. \tag{175}$$

Similar to the effectivity index (175), we define the *indicator index* to measure the quality of the localization process:

$$\text{ind}_h := \frac{\sum_i |\eta_i|}{|J(u) - J(u_h)|}. \tag{176}$$

It is not possible to reach strict effectivity with $\text{ind}_h \to 1$ in the context of goal-oriented errors. The functional error $J(u) - J(u_h)$ has a sign, and hence the error can vanish, although the solution shows a very large approximation error, e.g. by symmetry reasons. The local estimator values η_i may have changing sign, such that $\sum_i |\eta_i|$ may be a strong over-estimation. However, we will aim at strategies, where ind_h is uniformly bounded in h.

Let us again concentrate on stationary formulations in order to learn the techniques. The Galerkin approximation to Equation (120) (neglecting the time derivatives and stabilization terms), reads: Find $\hat{U}_h = \{\hat{v}_{f,h}, \hat{v}_{s,h}, \hat{u}_{f,h}, \hat{u}_{s,h}, \hat{p}_{f,h}\} \in \widehat{X}_{h,D}^0$,

---

[23]Another variational technique based on filtering was introduced in [41].

where $\widehat{X}^0_{h,D} := \{\hat{v}^D_{f,h} + \hat{V}^0_{f,\hat{v},h}\} \times \hat{\mathcal{L}}_{s,h} \times \{\hat{u}^D_{f,h} + \hat{V}^0_{f,\hat{u},h}\} \times \{\hat{u}^D_{s,h} + \hat{V}^0_{s,h}\} \times \hat{L}^0_{f,h}$, such that

$$\hat{A}(\hat{U}_h)(\hat{\Psi}_h) = \hat{F}(\hat{\Psi}_h) \quad \forall \hat{\Psi}_h \in \widehat{X}_h. \tag{177}$$

The solution $\hat{U}_h$ is used to calculate an approximation $J(\hat{U}_h)$ of the goal-functional $J(\hat{U}) : \widehat{X} \to \mathbb{R}$. This functional is assumed to be sufficiently differentiable. Concretely, it is used for the evaluation of point values (the deflection of the valve), line integrals (the computation of the stresses), or domain integrals (L^2-norm of the velocity).

Example 7.3. *The error of a deflection $\hat{u}_s$ in y-direction at some point $\hat{p} \in \widehat{\Omega}$ can be estimated using the following (regularized) functional:*

$$J(\hat{u}_{s,y}) := |B_\varepsilon|^{-1} \int_\varepsilon \hat{u}_{y,s} \, d\hat{x} = \hat{u}_{y,s}(\hat{p}) + O(\varepsilon^2),$$

where B_ε is the ε-ball around the point $\hat{p}$.

Example 7.4. *The error of mean normal fluxes over lower-dimensional manifolds. For example, we compute the error of wall stresses in y-direction along the interface between the fluid and the structure, which can be estimated with*

$$J(\hat{U}) := \int_{\hat{S}} \hat{J} \hat{\sigma}_f \widehat{F}^{-T} \hat{n}_f \, \hat{d} \, d\hat{s},$$

where $\hat{d}$ is a unit vector perpendicular to the mean flow direction. Later, we compute the wall stresses along the interface of the aorta $\hat{S} := \widehat{\Gamma}_{aorta}$. In particular, accurate wall stress measurement is important for clinical applications.

We use the (formal) Euler-Lagrange method, to derive a computable representation of the approximation error $J(\hat{U}) - J(\hat{U}_h)$. Concretely, the task is

$$\min\{J(\hat{U}) - J(\hat{U}_h)\} \quad \text{s.t.} \quad \hat{A}(\hat{U})(\hat{\Psi}) = \hat{F}(\hat{\Psi}) \quad \forall \hat{\Psi} \in \widehat{X}.$$

As usual for optimization problems, we introduce a dual variable $\hat{Z}$ (usually referred to as *sensitivity*) to formulate the Lagrangian functional

$$\mathcal{L}(\hat{U}, \hat{Z}) = J(\hat{U}) + \hat{F}(\hat{Z}) - \hat{A}(\hat{U})(\hat{Z}).$$

We obtain the optimality system

$$\mathcal{L}'_{\hat{Z}}(\hat{U}, \hat{Z})(\delta\hat{Z}) = \widehat{F}(\delta\hat{Z}) - \hat{A}(\hat{U})(\delta\hat{Z}) = 0 \quad \delta\hat{Z} \in \widehat{X},$$
$$\mathcal{L}'_{\hat{U}}(\hat{U}, \hat{Z})(\delta\hat{U}) = J'(\hat{U})(\delta\hat{U}) - \hat{A}'_{\hat{U}}(\hat{U})(\delta\hat{U}, \hat{Z}) = 0 \quad \delta\hat{U} \in \widehat{X}.$$

In this context, we deal with a *primal* problem and a *dual* problem. The primal problem corresponds to the original equation. In an appropriate discrete space $\widehat{X}_h \subset \widehat{X}$, the discrete problem reads:

$$\mathcal{L}'_{\hat{Z}}(\hat{U}_h, \hat{Z}_h)(\delta\hat{Z}_h) = \widehat{F}(\hat{Z}_h) - \hat{A}(\hat{U}_h)(\delta\hat{Z}_h) = 0 \quad \delta\hat{Z}_h \in \widehat{X}_h, \tag{178}$$
$$\mathcal{L}'_{\hat{U}}(\hat{U}_h, \hat{Z}_h)(\delta\hat{U}_h) = J'(\hat{U}_h)(\delta\hat{U}_h) - \hat{A}'_{\hat{U}}(\hat{U}_h)(\delta\hat{U}_h, \hat{Z}_h) = 0 \quad \delta\hat{U}_h \in \widehat{X}_h. \tag{179}$$

For given solutions $\{\hat{U}, \hat{Z}\}$ and $\{\hat{U}_h, \hat{Z}_h\}$ we obtain the following identity for the approximation error:

$$J(\hat{U}) - J(\hat{U}_h) = \mathcal{L}(\hat{U}, \hat{Z}) - \mathcal{L}(\hat{U}_h, \hat{Z}_h).$$

To *compute* this relation, we use the results of [27] and we obtain:

Theorem 7.5. *For any solution of the Problem 177, we obtain the error representation*

$$J(\hat{U}) - J(\hat{U}_h) = \frac{1}{2}\rho(\hat{U}_h)(\hat{Z} - \hat{\Psi}_h) + \frac{1}{2}\rho^*(\hat{U}_h, \hat{Z}_h)(\hat{U} - \hat{\Phi}_h) + \mathcal{R}_h^{(3)}, \tag{180}$$

for all $\{\hat{\Phi}_h, \hat{\Psi}_h\} \in \widehat{X}_h \times \widehat{X}_h$ and with the primal and dual residuals:

$$\rho(\hat{U}_h)(\hat{Z} - \hat{\Psi}_h) := -A(\hat{U}_h)(\cdot), \tag{181}$$

$$\rho^*(\hat{U}_h, \hat{Z}_h)(\hat{U} - \hat{\Phi}_h) := J'(\hat{U}_h)(\cdot) - A'(\hat{U}_h)(\cdot, \hat{Z}_h). \tag{182}$$

The remainder term is $\mathcal{R}_h^{(3)}$ is cubic in the primal and the dual errors. This error identity can be used to drive an automatic mesh refinement process and/or can be adopted to estimate the error.

Proof. We refer to [27] for a proof of this theorem. □

Neglecting the remainder results in the error estimator

$$\eta(u_h, z_h) = \frac{1}{2}\rho(\hat{U}_h)(\hat{Z} - \hat{\Psi}_h) + \frac{1}{2}\rho^*(\hat{U}_h, \hat{Z}_h)(\hat{U} - \hat{\Phi}_h). \tag{183}$$

The dual variable $\hat{Z} = \{\hat{z}_f^v, \hat{z}_s^v, \hat{z}_f^u, \hat{z}_s^u, \hat{z}_f^p\}$ is computed with the corresponding (linearized) dual problem (obtained as first equation in (178))

$$A'(\hat{U}_h)(\hat{\Psi}_h, \hat{Z}_h) = J'(\hat{\Psi}_h), \quad \forall \hat{\Psi}_h \in \tilde{X}_h, \tag{184}$$

where not necessarily $\tilde{X}_h = \widehat{X}_h$. The matrix $\hat{A}'$ denotes the transposed matrix of the primal problem and it is assembled as one further Newton Jacobian in the nonlinear solution process; we refer to [14]. The dual Problem (184) can be solved with a global higher approximation or local higher interpolation. With these solutions, we obtain approximations of the differences $\hat{Z} - \hat{\Psi}_h$ in the error representation (180). The solvability of the primal problem and the dual problem is not for granted, we refer for a deeper discussion to [71].

7.3.1 The classical DWR localization for simplified fluid-structure interaction

Proposition 7.6. *With the previous assumptions, we have for stationary fluid-structure interaction the error representation*

$$J(\hat{U}) - J(\hat{U}_h) \approx \eta_h^f + \eta_h^s + \eta_h^i, \tag{185}$$

where we split the local error indicators into fluid η_h^f, structure η_h^s, and interface contributions η_h^i. In detail, we have

$$\eta_h^f := \sum_{\hat{K} \in \hat{\mathcal{T}}_h} \Big\{ (-\hat{\rho}_f \hat{J}(\widehat{F}^{-1}\hat{v}_f \cdot \widehat{\nabla})\hat{v}_f + \widehat{\nabla} \cdot \widehat{\sigma}_{appr} - \widehat{\nabla}\hat{p}_f, \hat{z}_f^v - \hat{\psi}_h^v)_{\hat{K}_f} \tag{186}$$

$$+ \frac{1}{2}([\hat{J}\widehat{\sigma}_f\widehat{F}^{-T}\hat{n}_f], \hat{z}_f^v - \hat{\psi}_h^v)_{\partial\hat{K}_f\backslash\partial\widehat{\Omega}\cup\widehat{\Gamma}_i} + (\widehat{div}(\hat{J}\widehat{F}^{-1}\hat{v}_f), \hat{z}_f^p - \hat{\psi}_h^p)_{\hat{K}_f} \tag{187}$$

$$+ (\widehat{\nabla} \cdot \widehat{\sigma}_{mesh}, \hat{z}_f^u - \hat{\psi}_h^u)_{\hat{K}_f} + \frac{1}{2}([\widehat{\sigma}_{mesh}\hat{n}_f], \hat{z}_f^u - \hat{\psi}_h^u)_{\partial\hat{K}_f\backslash\partial\widehat{\Omega}\cup\widehat{\Gamma}_i} \Big\} \tag{188}$$

$$\tag{189}$$

and

$$\eta_h^s := \sum_{\hat{K} \in \hat{\mathcal{T}}_h} \Big\{ (\widehat{\nabla} \cdot \widehat{\Sigma}_{appr}, \hat{z}_s^v - \hat{\psi}_h^v)_{\hat{K}_s} + \frac{1}{2}([\widehat{F}\widehat{\Sigma}_{appr}\hat{n}_s], \hat{z}_s^v - \hat{\psi}_h^v)_{\partial\hat{K}_s\backslash\partial\widehat{\Omega}\cup\widehat{\Gamma}_i} \Big\}, \tag{190}$$

and

$$\eta_h^i := \sum_{\hat{K} \in \hat{\mathcal{T}}_h} \Big\{ \frac{1}{2}([\hat{J}\widehat{\sigma}_f\widehat{F}^{-T}\hat{n}_f], \hat{z}_f^v - \hat{\psi}_h^v)_{\widehat{\Gamma}_i} + \frac{1}{2}([\widehat{\sigma}_{mesh}\hat{n}_f], \hat{z}_f^u - \hat{\psi}_h^u)_{\widehat{\Gamma}_i} \tag{191}$$

$$+ \frac{1}{2}([\widehat{F}\widehat{\Sigma}_{appr}\hat{n}_s], \hat{z}_s^v - \hat{\psi}_h^v)_{\widehat{\Gamma}_i} \Big\}, \tag{192}$$

where $\widehat{\sigma}_{mesh}$ was defined in Section 5.3.4 and where $[\cdot]$ denotes the jump across intercell boundaries.

The previous declared error representation consists of the *cell residuals* (measuring the consistency of the discrete solution $\hat{U}_h$) and the edge terms $[\cdot]$ (measuring the discrete smoothness). The latter one has similar properties to the smoothness-based refinement indicators as introduced before. The residuals terms are weighted with so-called *sensitivity factors*

$$\hat{z}_{f,s}^v - \hat{\psi}_h^v, \quad \hat{z}_{f,s}^u - \hat{\psi}_h^u, \quad \hat{z}_f^p - \hat{\psi}_h^p,$$

that are obtained by solving the dual Problem (184).

Proposition 7.7. *From the previous error representation, we derive the following approximate error estimate*

$$|J(\hat{U}) - J(\hat{U}_h)| \approx \sum_{\hat{K} \in \hat{\mathcal{T}}_h} \eta_{\hat{K}}, \quad \eta_{\hat{K}} := \sum_{i=1}^{8} \rho_K^{(i)} \omega_K^{(i)},$$

with the residual terms and the weights

$$\rho_K^{(1)} := || - \hat\rho_f \hat{J}(\widehat{F}^{-1}\hat{v}_f \cdot \widehat\nabla)\hat{v}_f + \widehat\nabla \cdot \hat\sigma_{appr} - \widehat\nabla \hat{p}_f ||_{\hat{K}}, \qquad \omega_K^{(1)} := ||\hat{z}_f^v - \hat\psi_h^v||_{\hat{K}},$$

$$\rho_K^{(2)} := ||\widehat\nabla \cdot \widehat\Sigma_{appr}||_{\hat{K}}, \qquad \omega_K^{(2)} := ||\hat{z}_s^v - \hat\psi_h^v||_{\hat{K}},$$

$$\rho_K^{(3)} := ||\widehat\nabla \cdot \hat\sigma_{mesh}||_{\hat{K}}, \qquad \omega_K^{(3)} := ||\hat{z}_f^u - \hat\psi_h^u||_{\hat{K}},$$

$$\rho_K^{(4)} := ||\widehat{div}(\hat{J}\widehat{F}^{-1}\hat{v}_f)||_{\hat{K}}, \qquad \omega_K^{(4)} := ||\hat{z}_f^p - \hat\psi_h^p||_{\hat{K}},$$

$$\rho_K^{(5)} := \frac{1}{2}\hat{h}_K^{-1/2}||[\hat{J}\hat\sigma_f \widehat{F}^{-T}\hat{n}_f]||_{\partial\hat{K}\cup\widehat\Gamma_i}, \qquad \omega_K^{(5)} := \frac{1}{2}\hat{h}_K^{1/2}||\hat{z}_f^v - \hat\psi_h^v||_{\partial\hat{K}\cup\widehat\Gamma_i},$$

$$\rho_K^{(6)} := \frac{1}{2}\hat{h}_K^{-1/2}||[\widehat{F}\widehat\Sigma_{appr}\hat{n}_s]||_{\partial\hat{K}\cup\widehat\Gamma_i}, \qquad \omega_K^{(6)} := \frac{1}{2}\hat{h}_K^{1/2}||\hat{z}_s^v - \hat\psi_h^v||_{\partial\hat{K}\cup\widehat\Gamma_i},$$

$$\rho_K^{(7)} := \frac{1}{2}\hat{h}_K^{-1/2}||[\hat\sigma_{mesh}\hat{n}_f]||_{\partial\hat{K}\cup\widehat\Gamma_i}, \qquad \omega_K^{(7)} := \frac{1}{2}\hat{h}_K^{1/2}||\hat{z}_f^u - \hat\psi_h^u||_{\partial\hat{K}\cup\widehat\Gamma_i}.$$

The weights $\omega^{(i)}$ are approximated by post-processing of the discrete dual solution.

A mesh adaptation algorithm

Let an error tolerance TOL be given. Local error indicators from an a posteriori error estimate on the mesh $\hat{\mathcal{T}}_h$ are extracted to realize the mesh adaption:

$$|J(\hat{U}) - J(\hat{U}_h)| \le \eta := \sum_{\hat{K}\in\mathbb{T}_h} \eta_{\hat{K}} \quad \text{for all cells } \hat{K} \in \hat{\mathcal{T}}_h.$$

This information is used to adapt the mesh using the following strategy:

1. Compute the primal solution $\hat{U}_h$ and the dual solution $\hat{Z}_h$ on the present mesh $\hat{\mathcal{T}}_h$.

2. Determine the cell indicator $\eta_{\hat{K}}$ at each cell $\hat{K}$.

3. Compute the sum of all indicators $\eta := \sum_{\hat{K}\in\hat{\mathcal{T}}_h} \eta_{\hat{K}}$.

4. Check, if the stopping criterion is satisfied: $|J(\hat{U}) - J(\hat{U}_h)| \le \eta \le TOL$, then accept $\hat{U}_h$ within the tolerance TOL. Otherwise, proceed to the following step.

5. Mark all cells $\hat{K}_i$ that have values $\eta_{\hat{K}_i}$ above the average $\frac{\alpha\eta}{N}$ (where N denotes the total number of cells of the mesh $\mathbb{T}_h$ and $\alpha \approx 1$).

Other mesh adaption strategies are discussed in [14, 27].

Remark 7.8 (Drawbacks of the classical approach)**.** *Partial integration (similar to [40]) is not required. Consequently, we neither need to evaluate a strong form nor face terms in the inner part of the domain. Consequently, lengthy terms and computational costly evaluations are avoided.* ⋄

7.3.2 A new PUM-based localization for fluid-structure interation

What are now the key features?

- In addition to Remark 7.8, it is the ease of implementation and accuracy (in particular for situations as shown before: fluid-structure solid growth, reactive flow coupled to Navier-Stokes);

- this is achieved by keeping the weak form and introducing a partition-of-unity (PU), which can be of lowest order (e.g., Q_1 elements);

- Straightforward to employ;

- Does not require patched meshes.

7.3.2.1 Formulation for Poisson's problem Let the PU be denoted by $V_h^{(1)}$ (without restrictions on Dirichlet boundaries) and with its usual nodal basis $\{\psi_h^i, \ i = 1, \ldots, N^{(1)}\}$. The local error indicator for Poisson's problem,

$$(\nabla u, \nabla \varphi) = (f, \varphi) \quad \forall \varphi \in V,$$

is then given by [211]

$$\eta_i^{\mathrm{PU}} = \sum_{j=1}^{N^{(r)}} \left\{ (f, (\phi_{2h}^{(2),j} - \phi_h^j)\psi_h^i)_\Omega - \left(\nabla u_h, \nabla((\phi_{2h}^{(2),j} - \phi_h^j)\psi_h^i)\right)_\Omega \right\} \vec{z}_j, \qquad (193)$$

and it can be efficiently computed in an element-wise manner, as only few test-functions ϕ_h^j, $\phi_{2h}^{(2),j}$ and ψ_h^i overlap on every element $K \in \Omega_h$.

For the application, we only need evaluations of the right hand side and the residual with modified test-function. This localization technique can be readily applied to general meshes in two and three dimensions. In contrast to the filtering approach, we do not require special mesh structures, such as patches. In particular for three dimensional simulations, the use of patched meshes can substantially increases the problem size. However, the problem of obtaining good approximations to the weights $z - i_h z$ and $u - i_h u$ remains and here, using reconstruction of patches still is one of the most efficient strategies.

7.3.2.2 Formulation for FSI   Extending from Poisson's to FSI, the primal DWR estimator for stationary fluid-structure interaction reads [210]:

Proposition 7.9.

$$\eta_i^{PU} = \sum_{j=1}^{N^{(r)}} -(\hat{\rho}_f \hat{J}(\widehat{F}^{-1}\hat{v}_f \cdot \widehat{\nabla})\hat{v}_f), \hat{\psi}^v)_{\widehat{\Omega}_f} - (\hat{J}\hat{\sigma}_f\widehat{F}^{-T}, \widehat{\nabla}\hat{\psi}^v)_{\widehat{\Omega}_f} + \langle \hat{g}_f, \hat{\psi}^v \rangle_{\widehat{\Gamma}_N}$$
$$- (\widehat{F}\widehat{\Sigma}, \widehat{\nabla}\hat{\psi}^v)_{\widehat{\Omega}_s} - (\hat{\sigma}_{mesh}, \widehat{\nabla}\hat{\psi}^u)_{\widehat{\Omega}_f} - (\widehat{div}(\hat{J}\widehat{F}^{-1}\hat{v}_f), \hat{\psi}^p)_{\widehat{\Omega}_f}$$

where the weighting functions are defined as

$$\hat{\psi}^v := (\phi_{2h,v}^{(2),j} - \phi_{h,v}^j)\psi_h^i,$$
$$\hat{\psi}^u := (\phi_{2h,u}^{(2),j} - \phi_{h,u}^j)\psi_h^i,$$
$$\hat{\psi}^p := (\phi_{2h,p}^{(2),j} - \phi_{h,p}^j)\psi_h^i$$
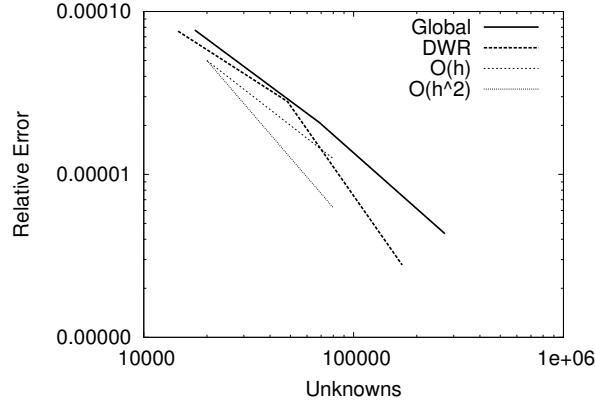

Figure 52: FSI 1-benchmark: Error plots for point value u_y error estimation.
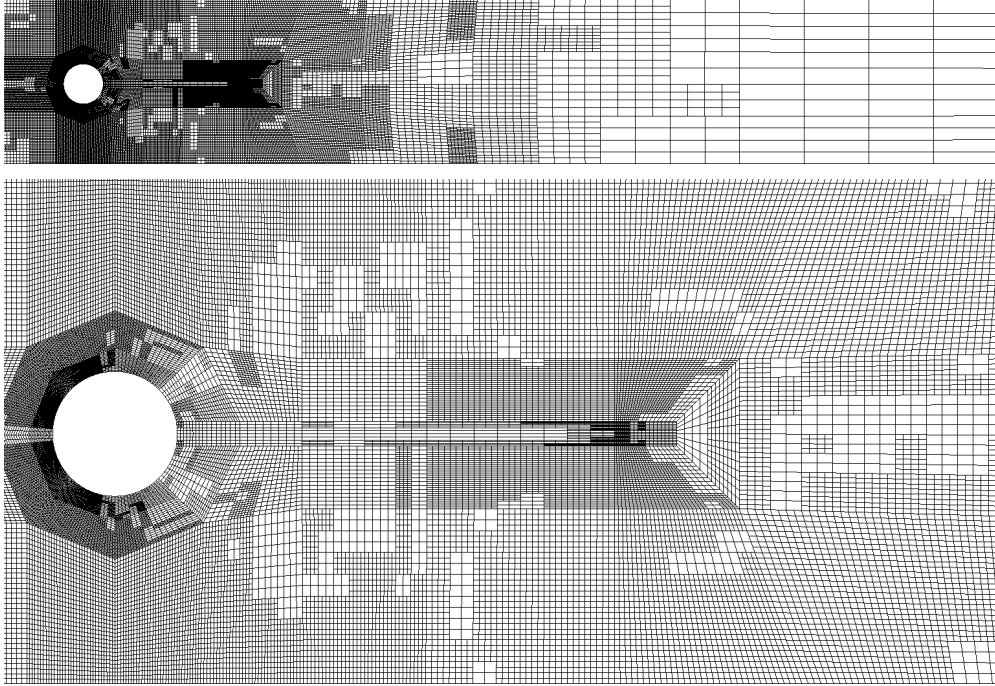
141

Figure 53: FSI 1-benchmark: locally-refined meshes. Whole mesh and zoom-in to the point estimation u_y.

Table 2: Effectivity indices: FSI 1-benchmark

DoF	u_y	Eff(global)	DoF	u_y	Eff(dwr)
17504	$8.96e-04$	$2.92e-1$	14572	$8.95e-4$	$3.43e-1$
68736	$8.40e-04$	$3.70e-1$	48420	$8.47e-4$	$3.13e-1$
272384	$8.24e-04$	$6.06e-1$	170416	$8.22e-4$	$9.55e-1$

7.4 Gradient-based optimization

Likewise to Section 7.3, we concentrate on stationary FSI-problems. We first describe general concepts and then proceed with optimal control and parameter estimation problems for Navier-Stokes and FSI. General and nicely-written introductions can be found e.g., in [136, 186, 236, 241].

- For optimization we consider the following setting: by $J : \mathcal{X} \to \mathbb{R}$ we denote a given functional of interest. We assume, that J is two times continuously Fréchet differentiable.

Example 7.10. *Such a functional can be the measurement of wall-stresses, flow rates or a bending moment.*

Furthermore, by Q_d we denote a finite dimensional set of control parameters that enter the state problem. We notice that the developed algorithms of this study could also be used for infinite control spaces; for optimization with parabolic equations we refer the reader to [175]. Among endless possibilities for the control $q \in Q_d$, common examples are material parameters, inflow rates or pressure-drops. For a given $q \in Q_d$, the controlled state-equation is split into the (nonlinear) state part and a control term which linearly depends on the control $q \in Q_d$:

$$U \in v_D + \mathcal{X} : \quad A(U)(\Phi) + B(U)(q, \Phi) = 0 \quad \forall \Phi \in \mathcal{X}, \tag{194}$$

where the exact definition of the control form $B(\cdot)(\cdot, \cdot)$ depends on the particular choice of the control type. To keep the notation easy in the present section, we combine the state operator and the control operator into one common semi-linear form:

$$A(q, U)(\Phi) := A(U)(\Phi) + B(U)(q, \Phi).$$

The goal of our optimization problem is to determine the optimal parameters $q \in Q_d$ such that the functional of interest $J(\cdot)$ gets minimal. This quantity of interest is completed by a regularization term of Tikhonov type, which involves a corresponding regularization parameter α. Then, the cost functional reads:

$$J(q, U) := J(U) + \frac{\alpha}{2}||q - \bar{q}||_Q^2, \tag{195}$$

with a reference control $\bar{q} \in Q_d$ and a suitable norm $|| \cdot ||_Q$ in the control-space. We consider the following optimization problem:

Problem 7.11 (Constrained optimization)**.** *Minimize the cost functional $J(q, U)$ subject to the state equation $A(q, U)(\Phi) = 0$ (as defined in (194)) for $(q, U) \in Q \times \{v_D + \mathcal{X}\}$.*

The constrained optimization problem on the space $Q_d \times \mathcal{X}$ is reformulated into an unconstrained optimization problem on the space Q_d. Therefore, we assume the existence of the solution operator $S : Q_d \to v_D + \mathcal{X}$ with a unique solution $U = S(q)$. Herewith, we define the reduced cost functional $j : Q_d \to \mathbb{R}$ by

$$j(q) := J(q, S(q)). \tag{196}$$

Thus, the constrained optimization problem can be formulated by means of

143

Problem 7.12 (Unconstrained optimization)**.** *Minimize $j(q)$ for $q \in Q_d$.*

Remark 7.13. *Because of the nonlinear structure of the state equation (194), the reduced cost functional is in general not convex (even if the cost functional $J(q, U)$ would be so).* ⋄

Using the reduced formulation of Problem 7.12, the existence of the optimization problem could be shown with the help of calculus of variations (see, e.g., [167]). A detailed analysis of theoretical results discussing the well-posedness of this general optimality system as well as the existence and uniqueness of possible optimal solutions are found in the literature, see e.g. [136, 236].

Then:

Problem 7.14.

$$j(q) := J(q, S(q)) \rightarrow \min, \quad A(q, S(q))(\Psi) = 0 \quad \forall \Psi \in V. \tag{197}$$

The local existence and sufficient regularity of S is assumed.

The solution to the unconstrained Problem 7.14 is characterized by the first-order necessary-optimality condition:

$$j'(q)(\delta q) = 0 \quad \forall \delta q \in Q_d. \tag{198}$$

The second-order necessary-optimality which guarantees a (local) minimum reads:

$$j''(q)(\delta q, \delta q) \geq 0 \quad \forall \delta q \in Q_d. \tag{199}$$

In the following, we concentrate on the (formal) computation of the optimality conditions that are employed for the implementation. The most easy way to express them is done by means of the Lagrangian $\mathcal{L} : Q_d \times \mathcal{X} \times \mathcal{X} \to \mathbb{R}$:

$$\mathcal{L}(q, U, Z) := J(q, U) - A(q, U)(Z). \tag{200}$$

With the help of the Lagrangian, we derive the optimality system (Karush-Kuhn-Tucker - KKT system) for a triple $(q, U, Z) \in Q_d \times \mathcal{X} \times \mathcal{X}$:

$$\begin{aligned}
\mathcal{L}'_Z(q, U, Z)(\Phi) = 0 \quad &\forall \Phi \in \mathcal{X} \qquad \text{(State Equation)}, \\
\mathcal{L}'_U(q, U, Z)(\Phi) = 0 \quad &\forall \Phi \in \mathcal{X} \qquad \text{(Adjoint Equation)}, \\
\mathcal{L}'_q(q, U, Z)(\delta q) = 0 \quad &\forall \delta q \in Q_d \qquad \text{(Gradient Equation)},
\end{aligned}$$

or equivalently

$$\begin{aligned}
A(q, U)(\Phi) &= 0 &&\forall \Phi \in \mathcal{X}, \\
A'_U(q, U)(\Phi, Z) &= J'_U(q, U)(\Phi) &&\forall \Phi \in \mathcal{X}, \\
A'_q(q, U)(\delta q, Z) &= J'_q(q, U)(\delta q) &&\forall \delta q \in Q_d.
\end{aligned} \tag{201}$$

Remark 7.15. *The KKT system is equivalent to the first-order necessary-optimality condition stated before, if the linearization of the semi-linear form is regular enough. We note that this system could be directly discretized with a Galerkin finite element method. Another approach (see [22, 25, 175]) that uses the reduced formulation is discussed in the following.* ⋄

7.4.1 Solution process of the reduced formulation

In the following, we discuss the solution process of the unconstrained optimization problem. The philosophy of this section follows [22, 25, 175]; their results have been built upon the earlier studies elsewhere [135, 235]. The algorithms are still general enough to be independent from fluid-structure interaction.

We use the standard Newton method to solve the optimization problem. On this level, because we need to work with the discretized control space Q_d, we introduce its basis

$$\left\{ \tau q_i \,|\, i = 1, 2, 3, \ldots, \dim Q_d \right\}.$$

Specifically, the control space Q_d in this work is always finite dimensional with one or two parameters:

$$\mathrm{span}\{q_1, q_2\} =: Q_d = \mathbb{R}^2,$$

i.e., $\dim Q_d = 2$.

With these preliminaries, Newton's method to solve Problem 7.12 reads: For $l = 0, 1, \ldots$, solve

$$\begin{aligned}
j''(q^l)(\delta q, \tau q) &= -j'(q^l)(\delta q) \quad \forall \tau q \in Q_d, \\
q^{l+1} &= q^l + \omega \delta q,
\end{aligned} \tag{202}$$

with a line search parameter $\omega \in (0, 1]$ which will be specified in Algorithm 7.18. Specifically, the residual and the Hessian of Newton's method (202) can be computed with the help of the following two results:

Proposition 7.16 (Residual of Newton's method)**.** *Let $q \in Q_d, U = S(q) \in \mathcal{X}$ and $Z \in \mathcal{X}$ the dual solution be obtained after solving the first and second equation of the KKT system (201). Then the residual of Newton's method (202) is defined as*

$$j'(q)(\delta q) := \mathcal{L}'_q(q, U, Z)(\delta q),$$

i.e., in explicit representation

$$j'(q)(\delta q) := \alpha_T(q, \tau q)_Q - A'_q(q, U)(\tau q, Z).$$

Proof. The proof uses standard techniques. Details can be found in [25]. $\qquad\square$

Proposition 7.17 (Hessian of Newton's method)**.** *Let $q \in Q_d, U = S(q) \in \mathcal{X}$ and $Z \in \mathcal{X}$ and $\delta q \in Q_d$ be given. Further, let $\delta U \in \mathcal{X}$ be the solution of the tangent problem*

$$\delta U \in \mathcal{X}, \quad A'_U(q, U)(\delta U, \Phi) = -A'_q(q, U)(\delta q, \Phi) \quad \forall \Phi \in \mathcal{X},$$

and $\delta Z \in \mathcal{X}$ the solution of the adjoint Hessian problem

$$A'_U(q, U)(\Phi, \delta Z) = J''_{UU}(q, U)(\delta U, \Phi) - A''_{UU}(q, U)(\delta U, \Phi, Z) - A''_{qU}(q, U)(\delta q, \Phi, Z) \quad \forall \Phi \in \mathcal{X}.$$

Then it holds for all $\tau q \in Q_d$:

$$j''(q)(\delta q, \tau q) := \alpha_T(\delta q, \tau q)_Q - A''_{qq}(q, U)(\delta q, \tau q, Z) - A''_{Uq}(q, U)(\delta U, \tau q, Z) - A'_q(q, U)(\tau q, \delta Z).$$

145

This is equivalent to

$$j''(q)(\delta q, \tau q) = \mathcal{L}''_{qq}(q, U, Z)(\delta q, \tau q)$$
$$+ \mathcal{L}''_{Uq}(q, U, Z)(\delta U, \tau q)$$
$$+ \mathcal{L}''_{Zq}(q, U, Z)(\delta Z, \tau q) \quad \text{for } \tau q \in Q.$$

Proof. For the proof this statement (including its time-dependent version), we refer to Becker et al. [25]. The stationary version of this proposition is easily derived by neglecting all time derivatives, which concludes the assertion. □

Let us summarize the important equations.

Lagrangian
$$\mathcal{L}(q, u, z) = J(q, u) - A(q, u)(z)$$

State Equation

$$a(q, u)(\phi) = 0$$

Dual Equation

$$\mathcal{L}'_u(q, u, z)(\phi) = 0$$
$$\Leftrightarrow a'_u(q, u)(\phi, z) = J'_u(q, u)(\phi)$$

Tangent Equation

$$\mathcal{L}''_{qz}(q, u, z)(\delta q, \phi) + \mathcal{L}''_{uz}(q, u, z)(\delta u, \phi) = 0$$
$$\Leftrightarrow a'_u(q, u)(\delta u, \phi) + a'_q(q, u)(\delta q, \phi) = 0$$

Dual Hessian Equation

$$\mathcal{L}''_{qu}(q, u, z)(\delta q, \phi) + \mathcal{L}''_{uu}(q, u, z)(\delta u, \phi)$$
$$+ \mathcal{L}''_{zu}(q, u, z)(\delta z, \phi) = 0$$
$$\Leftrightarrow a'_u(q, u)(\phi, \delta z) + a'_{uu}(q, u)(\delta u, \phi, z)$$
$$+ a'_{qu}(q, u)(\delta q, \phi, z) = J''_{uu}(q, u)(\cdot, \cdot)$$

Newton left hand side: first derivative

$$j'(q)(\delta q) = \mathcal{L}'_q(q, u, z)(\delta q) \quad \text{(Gradient equation)}$$
$$\Leftrightarrow j'(q)(\delta q) = -a'_q(q, u)(\delta q, z) + J'_q(q, u)(\delta q)$$

Newton right hand side: second derivative

$$j''(q)(\delta q, \delta r) = \mathcal{L}''_{qq}(q, u, z)(\delta q, \delta r) + \mathcal{L}''_{uq}(q, u, z)(\delta u, \delta r)$$
$$+ \mathcal{L}''_{zq}(q, u, z)(\delta z, \delta r)$$
$$\Leftrightarrow j''(q)(\delta q, \delta r) = J''_{qq}(q, u)(\delta q, \delta r) - a''_{qq}(q, u)(\delta q, \delta r, z)$$
$$- a''_{uq}(q, u)(\delta u, \delta r, z) - a'_q(q, u)(\delta r, \delta z).$$

The two previously mentioned propositions form the basis of the following optimization algorithm:

Algorithm 7.18 (Optimization loop). *Given an initial control $q^0 \in Q_d$ iterate for $l = 0, 1, \ldots$:*

1. *Compute the state solution $U^l = \{v^l, p^l, u^l\}$:*

$$U^l \in v_D + \mathcal{X}, \quad A(q^l, U^l)(\Phi) = 0 \quad \forall \Phi \in \mathcal{X}.$$

2. *Compute adjoint solution $Z^l = \{z_v^l, z_p^l, z_u^l\}$:*

$$Z^l \in \mathcal{X}, \quad A'_U(q^l, U^l)(\Phi, Z^l) = J'_U(q^l, U^l)(\Phi) \quad \forall \Phi \in \mathcal{X}.$$

3. *Evaluate Newton's right hand side (Proposition 7.16) for $Q_d \ni \tau q = \tau q_i$, $(i = 1, 2, \ldots \dim Q_d)$:*

$$j'(q^l)(\delta q_i) := \alpha_T(q^l, \tau q_i)_Q - A'_q(q^l, U^l)(\tau \hat{q}_i, Z^l), \quad i = 1, 2, \ldots \dim Q_d.$$

4. *Assemble the coefficient vector $f \in \mathbb{R}^{\dim Q_d}$ (as representation for the right hand side $\nabla j(q^l) \in Q_d$ of Newton's method):*

$$Gf = (j'(q^l)(\tau q_i))_{i=1}^{\dim(Q_d)}, \quad G_{ij} = (\tau q_j, \tau q_i)_Q,$$

where $j'(q^l)(\tau q_i) = (\nabla j(q^l), \tau q_i) = \sum_{j=1}^{\dim Q_d} f_j(\tau q_j, \tau q_i)_Q$.

5. *Compute the tangent solution $\delta U^l = \{\delta v^l, \delta p^l, \delta u^l\}$:*

$$\delta U^l \in \mathcal{X}, \quad A'_U(q^l, U^l)(\delta U^l, \Phi) = -A'_q(q^l, U^l)(\delta q, \Phi) \quad \forall \Phi \in \mathcal{X}.$$

6. *Compute the adjoint for Hessian solution $\delta Z^l = \{\delta z_v^l, \delta z_p^l, \delta z_u^l\}$:*

$$\delta Z^l \in \mathcal{X}, \quad A'_U(q^l, U^l)(\Phi, \delta Z^l) = J''_{UU}(q^l, U^l)(\delta U^l, \Phi)$$
$$- A''_{UU}(q^l, U^l)(\delta U^l, \Phi, Z^l) - A''_{qU}(q^l, U^l)(\delta q, \Phi, Z^l) \quad \forall \Phi \in \mathcal{X}.$$

7. *Evaluate Newton's left hand side (Proposition 7.17) for $Q_d \ni \tau q = \tau q_i$, $(i = 1, 2, \ldots \dim Q_d)$:*

$$j''(q^l)(\delta q, \tau q_i) := \alpha_T(\delta q, \tau q_i)_Q - A''_{qq}(q^l, U^l)(\delta q, \tau q_i, Z^l)$$
$$- A''_{Uq}(q^l, U^l)(\delta U^l, \tau q_i, Z^l) - A'_q(q^l, U^l)(\tau q_i, \delta Z^l) \quad \forall \delta q \in Q_d.$$

8. *Assemble the coefficient vector $h \in \mathbb{R}^{\dim(Q_d)}$ (as representation of the left hand side $j''(q^l)(\delta q, \tau q_i)$ of Newton's method):*

$$Gh = (j''(q^l)(\delta q, \tau q_i))_{i=1}^{\dim(Q_d)}$$

where $j''(q^l)(\delta q, \tau q_i) = (\nabla^2 j(q^l)(\delta q, \tau q_i)_Q)_{i=1}^{dimQ_d} = \sum_{j=1}^{dimQ_d} h_j(\tau q_j, \tau q_i)_Q.$

9. *Solve: $j''(q^l)(\delta q, \tau q_i) = -j'(q^l)(\tau q_i)$ with $\tau q_i \in Q_d$ via*

$$\text{Minimize} \quad j(q^l) + \langle f, d \rangle + \frac{1}{2}\langle Hd, d \rangle,$$

with $\langle a, b \rangle := a^T Gb$ and $H := G^{-1}K$. Furthermore, $K_{ij} = \nabla^2 j(q^l)(\delta q_j, \tau q_i)_Q)_Q$ denotes the coefficient matrix of the Hessian $\nabla^2 j(q^l)$ and $d \in \mathbb{R}^{dimQ_d}$ represents the coefficient vector of δq. The solution is obtained by a CG-solver that requires matrix-vector products only.

10. *Correction step:*
$$q^{l+1} = q^l + \omega \delta q,$$

with $\omega \in (0, 1]$ as large as possible, such that

$$j(q^l + \delta q) \leq j(q^l) + \omega \cdot \nabla j(q^l)\delta q.$$

The parameter ω is determined via the Armijo-backtracking strategy. For details we refer the reader to [185, 186].

11. *Increment $l \to l + 1$.*

12. *Repeat all steps until: $|f| = \|\nabla j(q^l)\| < TOL.$*

This section is devoted to the application of the presented scheme to fluid-structure interaction systems. First, we need to evaluate all derivatives necessary to assemble the systems required to carry out Algorithm 7.18. While an approximation of the derivatives would in principle be possible by using finite differences [118] or by automatic differentiation, see [70] in the context of fluid-structure interaction, we analytically calculate all these derivatives as shown in Section 6.4.

7.4.1.1 State and adjoint equations In steps 1, 2, 5 and 6 of the algorithm, we need to solve problems given in a variational formulation using the test- and trial-space $\mathcal{X}$. These infinite dimensional problems will be discretized using the finite element method. All these variational problems are surface-coupled problems with different equations in the fluid and the structure domain. All four problems include balancing conditions on the common interface Γ_i, where in the case of the state-equation in Step 1 these balancing conditions are standard conditions of continuous velocity and the dynamic coupling conditions of the interface stresses:

$$v_f = 0 \quad \text{on } \Gamma_i.$$
$$J\hat{\sigma}_f F^{-T} n_f + F\Sigma_s n_s = 0 \quad \text{on } \Gamma_i. \tag{203}$$

In [208] we provide details on all derived variational formulations appearing in Algorithm 7.18. For solving the nonlinear state equation, we employ a Newton method that requires the Jacobian of the semilinear-form $A(\cdot)(\cdot)$. This linearized equation utilizes the same bilinear form as the tangent equation in Step 5 of the algorithm. The coupling condition given by variational manners are the linearization of (203). Let $W = \{w_v, w_p, w_u\} \in \mathcal{X}$ be the unknown solution. Then, it holds on Γ_i:

$$
J \left\{ \frac{d\hat{\sigma}_f}{dv_f}(w_v) + \frac{d\hat{\sigma}_f}{dp_f}(w_p) + \frac{d\hat{\sigma}_f}{du}(w_u) + \mathrm{tr}(F^{-1}\nabla w_u)\hat{\sigma}_f - \hat{\sigma}_f F^{-1}\nabla w_u \right\} n_f
$$
$$
+ \left\{ \nabla w_u \Sigma_s + F\frac{d\Sigma_s}{du}(w_u) \right\} n_s = 0, \quad w_f = 0. \quad (204)
$$

Once the Jacobian is implemented, the adjoint form is given by transposing the system matrix. Hence, the effort for solving the adjoint equations is comparable to an additional step of the state equation's Newton scheme. The balancing condition inherent in the adjoint equation is given by variational principles and is of Robin-type coupling all three adjoint variables z_v, z_p and z_u. The derivation of the strong formulation of this coupling condition is cumbersome. In Figure 54 we show the velocity, displacement and pressure of the optimal state solution and their corresponding adjoint solutions. These visualizations are taken from [208].
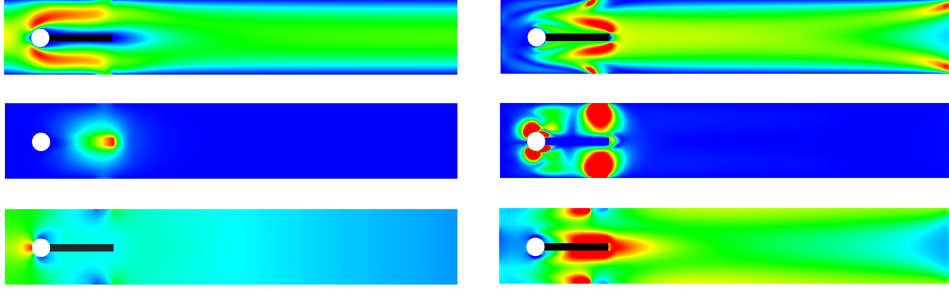

Figure 54: FSI-1 optimal control benchmark problem taken from [208]. Left: primal solutions of the optimal state for velocity, displacement, and pressure. Right: adjoint solutions for velocity, displacement and pressure at the right. Note, that velocity and pressure components are defined in the fluid domain only.

7.4.2 Implementation structure in DOpElib

The implementation is based on DOpElib and was initially inspired [24] by Gascoigne [23] and RoDoBo [212].

$$
\begin{aligned}
\text{CellEquation (state)} &\Leftrightarrow A(q,u)(\phi) & (205) \\
\text{CellEquationU (adjoint)} &\Leftrightarrow A'_u(q,u)(\phi,z) & (206) \\
\text{CellEquationUT (tangent)} &\Leftrightarrow A'_u(q,u)(\delta u,\phi) & (207) \\
\text{CellEquationUTT (adjoint hessian)} &\Leftrightarrow A'_u(q,u)(\phi,\delta z) & (208) \\
\text{CellEquationQ (gradient)} &\Leftrightarrow A'_q(q,u)(\delta q,z) & (209) \\
\text{CellEquationQT (tangent)} &\Leftrightarrow A'_q(q,u)(\delta q,\phi) & (210) \\
\text{CellEquationQTT (hessian)} &\Leftrightarrow A'_q(q,u)(\delta q,\delta z) & (211) \\
\text{CellEquationUU (adjoint hessian)} &\Leftrightarrow A''_{uu}(q,u)(\delta u,\phi,z) & (212) \\
\text{CellEquationQU (adjoint hessian)} &\Leftrightarrow A''_{qu}(q,u)(\delta q,\phi,z) & (213) \\
\text{CellEquationUQ (hessian)} &\Leftrightarrow A''_{uq}(q,u)(\delta u,\delta r,z) & (214) \\
\text{CellEquationQQ (hessian)} &\Leftrightarrow A''_{qq}(q,u)(\delta q,\delta r,z) & (215) \\
\text{CellRightHandSide (state)} &\Leftrightarrow f(\phi) & (216) \\
\text{CellMatrix (all)} &\Leftrightarrow A'(q,u)(\delta u) & (217) \\
\text{ControlCellEquation (gradient or hessian)} &\Leftrightarrow \mathcal{L}'_q(q,u,z)(\delta q) & (218) \\
\text{ControlCellMatrix (all)} &\Leftrightarrow A(q,u)(\phi) & (219)
\end{aligned}
$$

Functionals

$$
\begin{aligned}
\text{Value (all)} &\Leftrightarrow J(q,u) & (220) \\
\text{ValueU (all)} &\Leftrightarrow J'_u(q,u)(\phi) & (221) \\
\text{ValueQ (all)} &\Leftrightarrow J'_q(q,u)(\phi) & (222) \\
\text{ValueUU (all)} &\Leftrightarrow J''_{uu}(q,u)(\psi,\phi) & (223) \\
\text{ValueQU (all)} &\Leftrightarrow J''_{qu}(q,u)(\psi,\phi) & (224) \\
\text{ValueUQ (all)} &\Leftrightarrow J''_{uq}(q,u)(\psi,\phi) & (225) \\
\text{ValueQQ (all)} &\Leftrightarrow J''_{qq}(q,u)(\psi,\phi) & (226) \\
& & (227)
\end{aligned}
$$

---

[24] Actually in the years 2009/2010 when the project started.

7.4.3 Boundary control of stationary fluid flow

Let us see whether we understood the concepts and compute a numerical test. The following example has been proposed by Roland Becker [21, 22].
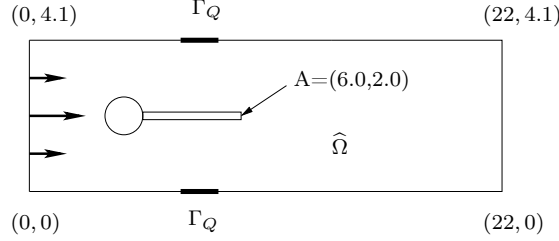

Figure 55: Flow around cylinder with elastic flag with circle-center $(2, 2)$ and radius $r = 0.5$. Structure material: 'compressible St. Venant-Kirchhoff'.

7.4.3.1 Configuration Goal of optimization is drag minimization around the cylinder:

$$(J_{\text{Drag}}(U), 0) := (F_D, 0) = \int_S \sigma_f \cdot n_f\, e_1\, ds. \tag{228}$$

As usually, the stress tensor is given by

$$\sigma_f = -pI + \rho\nu(\nabla v + \nabla v^T).$$

The Neumann control acts at the boundary Γ_Q and is given by a piecewise constant control $q = \{q_1, q_2\} \in \mathbb{R}^2$. The initial values can be chosen as $q = 0.0$ or $q = 0.1$ for both components. The physical unknowns are a vector-velocity field v and as scalar pressure field p. The semi-linear form of the problem reads:

Find $u = \{v, p\} \in \{v^{in} + V\} \times L^2$ and $q \in \mathbb{R}^2$ such that

$$A(q, u)(\phi) = \rho\nu(\nabla v + \nabla v^T, \nabla\phi^v)_{\Omega_f} + (\nabla v\, v, \phi^v)_{\Omega_f} - (p, \nabla \cdot \phi^v)_{\Omega_f} + (\nabla \cdot v, \phi^p)_{\Omega_f}$$
$$- (q, n \cdot \phi^v)_{\Gamma_Q} = 0.$$

for all test functions $\phi = \{\phi^v, \phi^p\} \in V$. Please note that the convection term differs from standard notation:

$$\nabla v\, v := (\nabla v)v = v \cdot \nabla v.$$

Further the pressure term can be rewritten as

$$-(p, \nabla \cdot \phi^v)_{\Omega_f} = -(pI, \nabla\phi^v)_{\Omega_f}$$

where I denotes the identity matrix in 2D.

The target functional is considered as

$$j(v, p) = \int_{\Gamma_O} n \cdot \sigma(v, p) \cdot d\, ds,$$

151

where Γ_O denotes the cylinder boundary, and d is a vector in the direction of the mean flow. For theoretical and numerical reasons, this functional needs to be regularized, including the control variable q, such that

$$J(q, v, p) = j(v, p) + \frac{\alpha}{2}||q - q_0||,$$

where α is the Tikhonov parameter and q_0 some reference control.

The rest of the program is similar to the previous optimization problems where we formulate the state equation in a weak form $a(v, p)(\phi)$ such that the final problem reads

$$J(q, v, p) \to \min \quad \text{s.t.} \quad A(q, v, p)(\phi) = 0.$$

7.4.3.2 Equations for gradient-based optimization
The following terms are required for the optimization process:

CellEquation (state): Compute

$$A(q, u)(\phi) = \rho\nu(\nabla v + \nabla v^T, \nabla \phi^v)_{\Omega_f} + (\nabla v \, v, \phi^v)_{\Omega_f}$$
$$- (p, \nabla \cdot \phi^v)_{\Omega_f} + (\nabla \cdot v, \phi^p)_{\Omega_f}.$$

CellMatrix (all): Compute

$$A(q, u)(\phi_i, \phi_j) = \rho\nu(\nabla \phi_j^v + \nabla(\phi_j^v)^T, \nabla \phi_i^v)_{\Omega_f} + (\nabla \phi_j^v \, v + \nabla v \, \phi_j^v, \phi_i^v)_{\Omega_f}$$
$$- (\phi_j^p, \nabla \cdot \phi_i^v)_{\Omega_f} + (\nabla \cdot \phi_j^v, \phi_i^p)_{\Omega_f}$$

where the velocity v of fluid's convection term depends the type of equation under investigation:

$$v = v^{n-1} \quad \text{(Previous Newton step for state matrix)}$$
$$v = v^{state} \quad \text{(Actual state solution for adjoint, gradient, etc.)}$$

CellEquationU (adjoint): Compute

$$a_u'(q, u)(\phi, z) = \rho\nu(\nabla \phi^v + \nabla(\phi^v)^T, \nabla z^v)_{\Omega_f} + (\nabla \phi^v \, v^{state} + \nabla v^{state} \phi^v, z^v)_{\Omega_f}$$
$$- (\phi^p I, \nabla z^v)_{\Omega_f} + (\nabla \cdot \phi^v, z^p)_{\Omega_f}$$

CellEquationUT (tangent): Compute

$$a_u'(q, u)(\delta u, \phi) = \rho\nu(\nabla \delta u^v + \nabla(\delta u^v)^T, \nabla \phi^v)_{\Omega_f} + (\nabla \delta u^v \, v^{state} + \nabla v^{state} \delta u^v, \phi^v)_{\Omega_f}$$
$$- (\delta u^p I, \nabla \phi^v)_{\Omega_f} + (\nabla \cdot \delta u^v, \phi^p)_{\Omega_f}$$

CellEquationUTT (adjoint hessian): Compute

$$a_u'(q, u)(\phi, \delta z) = \rho\nu(\nabla \phi^v + \nabla(\phi^v)^T, \nabla \delta z^v)_{\Omega_f} + (\nabla \phi^v \, v^{state} + \nabla v^{state} \phi^v, \delta z^v)_{\Omega_f}$$
$$- (\phi^p I, \nabla \delta z^v)_{\Omega_f} + (\nabla \cdot \phi^v, \delta z^p)_{\Omega_f}$$

CellEquationUU (adjoint hessian): Compute

$$a''_{uu}(q, u)(\delta u, \phi, z) = (\nabla \phi^v \, \delta u^{v,state} + \nabla \delta u^{v,state} \phi^v, z^v)_{\Omega_f}$$

Here: z^v are the adjoint values as already shown before, and $\delta u^{v,state}$ are the tangent values which are already computed.

BoundaryEquation (state): Compute

$$A(q, u)(\phi) = -\rho \nu (\nabla v^T \cdot n, \phi^v)_{\Gamma_{out}} - (q_0, n \cdot \phi^v)_{\Gamma_{q0}} - (q_1, n \cdot \phi^v)_{\Gamma_{q1}}$$

BoundaryMatrix (all): Compute

$$A(q, u)(\phi_i, \phi_j) = -\rho \nu (\nabla(\phi_j^v)^T \cdot n, \phi_i^v)_{\Gamma_{out}}$$

BoundaryEquationQ (gradient): Compute

$$A'_q(q, u)(\delta q, z)[0] = -(1, n \cdot z^v)_{\Gamma_{q0}}$$
$$A'_q(q, u)(\delta q, z)[1] = -(1, n \cdot z^v)_{\Gamma_{q1}}$$

where $\delta q = 1$ since q has been chosen constant.

BoundaryEquationQT (tangent): Compute

$$A'_q(q, u)(\delta q, \phi) = -(\delta q_0, \phi^v \cdot n)_{\Gamma_{q0}} - (\delta q_1, \phi^v \cdot n)_{\Gamma_{q1}}$$

BoundaryEquationQTT (hessian): Compute

$$A'_q(q, u)(\delta q, \delta z)[0] = -(1, n \cdot z^v)_{\Gamma_{q0}}$$
$$A'_q(q, u)(\delta q, \delta z)[1] = -(1, n \cdot z^v)_{\Gamma_{q1}}$$

where $\delta q = 1$ since q has been chosen constant.

BoundaryEquationU (adjoint): Compute

$$A'_u(q, u)(\phi, z) = -\rho \nu (\nabla(\phi^v)^T \cdot n, z^v)_{\Gamma_{out}}$$

BoundaryEquationUT (tangent): Compute

$$A'_u(q, u)(\delta u, \phi) = -\rho \nu (\nabla(\delta u^v)^T \cdot n, \phi^v)_{\Gamma_{out}}$$

BoundaryEquationUTT (adjoint hessian): Compute

$$A'_u(q, u)(\phi, \delta z) = -\rho \nu (\nabla(\phi^v)^T \cdot n, \delta z^v)_{\Gamma_{out}}$$

ControlCellEquation (gradient or hessian):
ControlCellMatrix (all):
We turn now to the computation of the cost functional including the regularization term.

BoundaryValue:

$$J(q, u) = c_D \int_S \sigma_f(v, p) \cdot n \, e_1 \, ds + \frac{\alpha}{2} ||q||^2_{\Gamma_q}$$

where $c_D = 500$ and $\alpha > 0$

BoundaryValueU:

$$J'_u(q, u)(\phi) = c_D \int_S \sigma_f(\phi^v, \phi^p) \cdot n e_1 \, ds$$

BoundaryValueQ:

$$J'_q(q, u)(\phi) = \alpha(q, \phi)_{\Gamma_q}$$

BoundaryValueQQ:

$$J''_{qq}(q, u)(\delta q, \phi) = \alpha(\delta q, \phi)_{\Gamma_q}$$

7.4.3.3 Numerical results We consult our source code from [116]
`Examples/OPT/StatPDE/Example3` (in version dopelib-2.0).

As starting values for q we choose in a first run $q = 0$ and also $q = 0.1$ in order to
see if we converge to the same optimal solution.

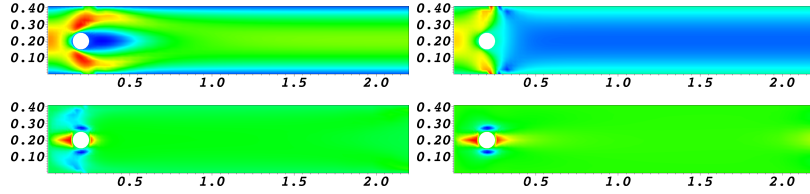| DoF	q_{start}	q_{top}	q_{bottom}	J_{opt}	Drag_{opt}	J_{start}	$\text{Drag}_{\text{start}}$
6000	0.0	0.312	0.309	2.5595	2.46292	4.144	4.1443
6000	0.1	0.312	0.309	2.5595	2.46292	3.083	3.0731

Figure 56: Stationary flow control: primal solution at the beginning and end of the
optimization (top) and corresponding adjoint solution (bottom). For all
solutions, we plot the x-velocity field.

7.4.4 FSI-1 parameter estimation benchmark

This second test is taken from [208] and we consider another extension of the FSI-
1 benchmark problem and define a parameter identification test-case. We aim at
identifying the Lamé coefficient μ_s in such a way, that the tip of the beam undergoes
a given deformation $u_y(A) = 8.2 \cdot 10^{-4}$ (i.e., close to the solution of the uncontrolled
configuration in the original FSI-1 benchmark problem). All material parameters as
well as the boundary data is chosen as in the previous section. For identifying the
parameter we choose the following regularized functional:

$$J(q, U) = \|u_y - \bar{u}_y\|^2 + \frac{\alpha}{2} \|q - \bar{q}\|^2,$$

154

DoF	$u_x(A)$	$u_y(A)$	q
5 032	$2.38095e-05$	0.000920281	471742
19 488	$2.37664e-05$	0.000844817	477626
76 672	$2.35301e-05$	0.000837236	481284
Uncontrolled			
76 672	$218.332e-05$	0.001999470	500
FSI-1 benchmark results (without any control)			
76 672	$2.27036e-05$	0.000822894	500000

Table 3: FSI-1 parameter estimation problem. Initial control $q_{\text{initial}} = 500$, $\bar{q} = 5 \cdot 10^5$ and $\alpha = 10^{-5}$.

with $q = \mu_s$ (the Lamé coefficient) and $\bar{u}_y = 8.2 \cdot 10^{-4}$. Furthermore, we choose $\bar{q} = 5 \cdot 10^{-5}$ and a small Tikhonov parameter $\alpha = 10^{-5}$.

The initial control value is given by $q_{\text{initial}} = \mu_{\text{initial}} = 500$, far away from the optimal state. In Table 3 we indicate the results of the optimization algorithm. In Figure 57 we show plots of the state and adjoint solution for this optimization problem.
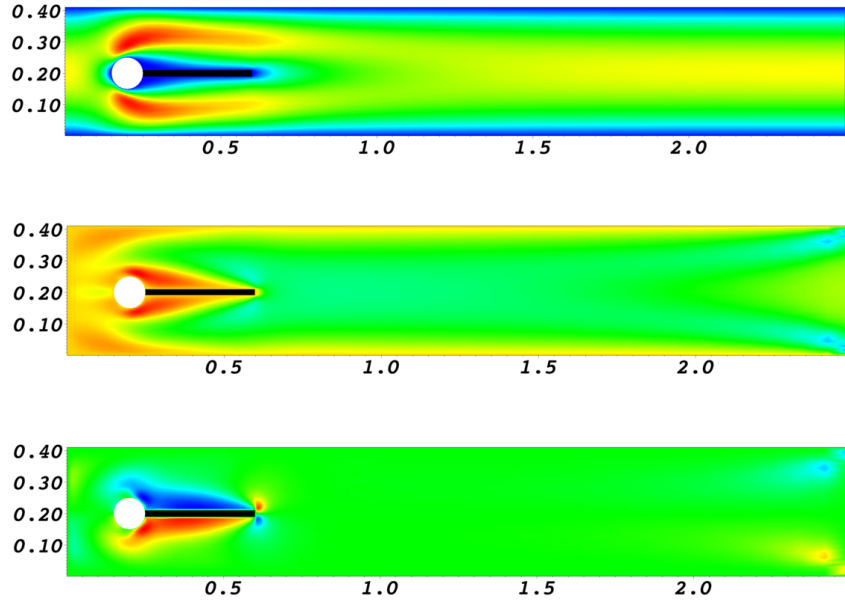

Figure 57: FSI parameter estimation: x-velocity profile (top) and corresponding adjoint solution in v_x direction (middle) and adjoint solution in v_y direction (bottom).

7.4.5 Monolithic versus partitioned coupling in Newton's optimization loop

We want to draw our attention to an interesting study in comparing monolithically-coupled fluid-structure interaction and partitioned coupling on the level of the outer optimization loop. This is achieved by neglecting the ALE-transformation in the adjoint, tangent and additional Hessian. Then, we clearly observe that monolithic coupling allows for higher accuracy as shown in Figure 7.4.5. This is in perfect agreement with partitioned (weak and strong) coupling and a monolithic approach for the forward problem. If you wish to satisfy a good tolerance for the coupling conditions, you either need to use a partitioned algorithm with strong coupling (i.e., possibly many subiterations in each time step) or you should use a monolithically-coupled scheme.
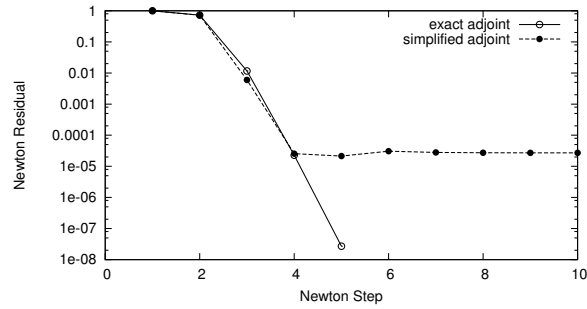

Figure 58: Convergence of the Newton iteration considering exact adjoint equations and a simplification neglecting the adjoint coupling conditions.

8 Acknowledgments

References

[1] R. A. Adams. *Sobolev Spaces.* Academic Press, 1975.

[2] M. Ainsworth and J. T. Oden. A posteriori error estimation in finite element analysis. *Computer Methods in Applied Mechanics and Engineering*, 142(1-2):1–88, 1997.

[3] J. E. Akin, T. Tezduyar, and M. Ungor. Computation of flow problems with the mixed interface-tracking/interface-capturing technique (MITICT). *Comp. Fluids*, 36:2–11, 2007.

[4] M. Allen and K. Maute. Reliability-based shape optimization of structures undergoing fluid-structure interaction phenomena. *Comput. Methods Appl. Mech. Engrg.*, 194(30-33):3472–3495, 2005.

[5] M. Asterino, F. Chouly, and F. Fernández. An added-mass free semi-implicit coupling scheme for fluid-structure interaction. *C. R. Acad. Sci. Paris, Sér. I.*, 347(1-2):99–104, 2009.

[6] M. Asterino and C. Grandmont. Convergence analysis of a projection semi-implicit coupling scheme for fluid-structure interaction problems. *Numer. Math.*, 116(4):721–767, 2008.

---

[25] This is an ironic statement. To clarify: in fact, it was a great pleasure to design such a code and honestly I benefit myself having a clean code because from time to time I also download it to test new things or for verification.

[7] G. Avalos, I. Lasiecka, and R. Triggiani. Beyond lack of compactness and lack of stability of a coupled parabolic-hyperbolic fluid-structure system. In K. Kunisch, J. Sprekels, G. Leugering, and F. Tröltzsch, editors, *Optimal Control of Coupled Systems of Partial Differential Equations*, volume 158 of *International Series of Numerical Mathematics*, pages 1–33. Birkhäuser Basel, 2009.

[8] F. Baaijens. A fictitious domain/mortar element method for fluid-structure interaction. *Int. J. Num. Methods Fluids*, 35(7):743–761, 2001.

[9] I. Babuska and U. Banerjee. Stable generalized finite element method (sgfem). *Computer Methods in Applied Mechanics and Engineering*, 201-204(0):91 – 111, 2012.

[10] S. Badia, F. Nobile, and C. Vergara. Robin-robin preconditioned krylov methods for fluid-structure interaction problems. *Computer Methods in Applied Mechanics and Engineering*, 198(33-36):2768 – 2784, 2009.

[11] S. Badia, Q. Quaini, and A. Quarteroni. Modular vs. non-modular preconditioners for fluid-structure interaction systems with large added-mass effect. *Comput. Methods. Appl. Mech. Engrg.*, 197:4216–4232, 2008.

[12] W. Bangerth, M. Geiger, and R. Rannacher. Adaptive Galerkin finite element methods for the wave equation. *Comput. Methods Appl. Math.*, 10:3–48, 2010.

[13] W. Bangerth, T. Heister, and G. Kanschat. *Differential Equations Analysis Library*, 2012.

[14] W. Bangerth and R. Rannacher. *Adaptive Finite Element Methods for Differential Equations*. Birkhäuser, Lectures in Mathematics, ETH Zürich, 2003.

[15] A. Barker and X. Cai. Two-level newton and hybrid schwarz preconditioners for fluid-structure interaction. *SIAM Journal on Scientific Computing*, 32(4):2395–2417, 2010.

[16] A. T. Barker and X.-C. Cai. Scalable parallel methods for monolithic coupling in fluid-structure interaction with application to blood flow modeling. *Journal of Computational Physics*, 229(3):642 – 659, 2010.

[17] S. Basting and M. Weissmann. A hybrid level set-front tracking finite element approach for fluid-structure interaction and two-phase flow applications. *J. Comp. Physics*, 255:228–244, 2013.

[18] K.-J. Bathe and G. Ledezma. Benchmark problems for incompressible fluid flows with structural interactions. *Comput. Struct.*, 85:628–644, 2007.

[19] Y. Bazilevs, V. M. Calo, T. Hughes, and Y. Zhang. Isogeometric fluid-structure interaction: theory, algorithms, and computations. *Comput. Mech.*, 43:3–37, 2008.

[20] Y. Bazilevs, K. Takizawa, and T. Tezduyar. *Computational Fluid-Structure Interaction: Methods and Applications.* Wiley, 2013.

[21] R. Becker. Mesh adaptation for stationary flow control. *J. Math. Fluid Mech.*, 3(4):317–341, 2001.

[22] R. Becker. Adaptive finite elements for optimal control problems. University of Heidelberg, 2004. Habilitationsschrift.

[23] R. Becker, M. Braack, D. Meidner, T. Richter, and B. Vexler. The finite element toolkit GASCOIGNE. HTTP://WWW.GASCOIGNE.UNI-HD.DE.

[24] R. Becker, V. Heuveline, and R. Rannacher. An optimal control approach to adaptivity in computational fluid mechanics. 40:105–120, 2002.

[25] R. Becker, D. Meidner, and B. Vexler. Efficient numerical solution of parabolic optimization problems by finite element methods. *Optim. Methods Softw.*, 22(5):813–833, 2007.

[26] R. Becker and R. Rannacher. A feed-back approach to error control in finite element methods: basic analysis and examples. *East-West J. Numer. Math.*, 4:237–264, 1996.

[27] R. Becker and R. Rannacher. *An optimal control approach to error control and mesh adaptation in finite element methods*, pages 1–102. Acta Numerica 2001, Cambridge University Press, a. iserles edition, 2001.

[28] T. Belytschko, J. Kennedy, and D. Schoeberle. Quasi-eulerian finite element formulation for fluid-structure interaction. Proceedings of Joint ASME/CSME Pressure Vessels and Piping Conference, page p.13. ASME paper 78-PVP-60, 1978.

[29] A. Bensoussan, J. Lions, and G. Papanicolaou. *Asymptotic Analysis for Periodic Structures.* North-Holland, 1978.

[30] J. Berenger. A perfectly matched layer for the absorption of electromagnetic waves. *J. Comput. Phys.*, 114, 1994.

[31] C. Bernardi and E. Süli. Time and space adaptivity for the second-order wave equation. *Math. Models Methods Appl. Sci.*, 15(2):199–225, 2005.

[32] C. Bertoglio, P. Moireau, and J.-F. Gerbeau. Sequential parameter estimation for fluid-structure problems: Application to hemodynamics. *International Journal for Numerical Methods in Biomedical Engineering*, 28(4):434–455, 2012.

[33] M. Besier. *Adaptive Finite Element methods for computing nonstationary incompressible Flows.* PhD thesis, University of Heidelberg, 2009.

[34] M. Besier and R. Rannacher. Goal-oriented space-time adaptivity in the finite element galerkin method for the computation of nonstationary incompressible flow. *Int. J. Num. Meth. Fluids*, accepted 2011.

[35] M. Biot. Consolidation settlement under a rectangular load distribution. *J. Appl. Phys.*, 12(5):426–430, 1941.

[36] M. Biot. General theory of three-dimensional consolidation. *J. Appl. Phys.*, 12(2):155–164, 1941.

[37] M. Biot. Theory of elasticity and consolidation for a porous anisotropic solid. *J. Appl. Phys.*, 25:182–185, 1955.

[38] J. Bonet and R. Wood. *Nonlinar Continuum Mechanics for Finite Element Analysis*. Cambridge University Press, Cambridge, 1997.

[39] M. Braack, E. Burman, V. John, and G. Lube. Stabilized finite element methods for the generalized Oseen equations. *Comput. Methods Appl. Mech. Engrg.*, 196(4-6):853–866, 2007.

[40] M. Braack and A. Ern. Adaptive computation of reactive flows with local mesh refinement and model adaptation. In e. a. M. Feistauer, editor, *Numerical Mathematics and Advanced Applications, ENUMATH 2003*, pages 159–168. Springer, 2004.

[41] M. Braack and A. Ern. Coupling multimodeling with local mesh refinement for the numerical solution of laminar flames. 8(4):771–788, 2004.

[42] M. Braack and P. Mucha. Directional do-nothing condition for the navier-stokes equations. *J. Comp. Math.*, 32:507–546, 2014.

[43] D. Braess. *Finite Elemente*. Springer-Verlag Berlin Heidelberg, Berlin, Heidelberg, vierte, überarbeitete und erweiterte edition, 2007.

[44] S. C. Brenner and L. R. Scott. *The mathematical theory of finite element methods*. Number 15 in Texts in applied mathematics ; 15 ; Texts in applied mathematics. Springer, New York, NY, 3. ed. edition, 2008.

[45] M. Bristeau, R. Glowinski, and J. Periaux. Numerical methods for the Navier-Stokes equations. *Comput. Phys. Rep.*, 6:73–187, 1987.

[46] A. Brooks and T. Hughes. Streamline upwind/Petrov-Galerkin formulations for convection dominated flows with particular emphasis on the incompressible Navier-Stokes equations. *Comput. Methods Appl. Mech. Engrg.*, 32(1-3):199–259, 1982.

[47] F. Bucci and I. Lasiecka. Optimal boundary control with critical penalization for a pde model of fluid-solid interactions. *Calc. Var. Partial Differential Equations*, 37(1-2):217–235, 2010.

[48] C. J. Budd, W. Huang, and R. D. Russell. Adaptivity with moving grids. *Acta Numerica*, 18:111–241, 5 2009.

[49] M. Bukac, S. Canic, R. Glowinski, J. Tambaca, and A. Quaini. Fluid-structure interaction in blood flow capturing non-zero longitudinal structure displacement. *J. Comput. Phys.*, 2012. http://dx.doi.org/10.1016/j.jcp.2012.08.033.

[50] H.-J. Bungartz, M. Mehl, and M. Schäfer. *Fluid-Structure Interaction II: Modelling, Simulation, Optimization.* Lecture Notes in Computational Science and Engineering. Springer, 2010.

[51] H.-J. Bungartz and M. Schäfer. *Fluid-Structure Interaction: Modelling, Simulation, Optimization*, volume 53 of *Lecture Notes in Computational Science and Engineering*. Springer, 2006.

[52] E. Burman and M. Fernandez. Stabilization of explicit coupling in fluid-structure interaction involving fluid incompressibility. *Comput. Methods. Appl. Mech. Engrg.*, 198:766–784, 2009.

[53] G. F. Carey and J. T. Oden. *Finite Elements. Volume III. Compuational Aspects.* The Texas Finite Element Series, Prentice-Hall, Inc., Englewood Cliffs, 1984.

[54] P. Causin, J.-F. Gerbeau, and F. Nobile. Added-mass effect in the design of partitioned algorithms for fluid-structure problems. *Comput. Methods Appl. Mech. Engrg.*, 194:4506–4527, 2005.

[55] P. G. Ciarlet. *Lectures on Three Dimensional Elasticity.* Springer Berlin Heidelberg New York, 1983.

[56] P. G. Ciarlet. *Mathematical Elasticity. Volume 1: Three Dimensional Elasticity.* North-Holland, 1984.

[57] P. G. Ciarlet. *The finite element method for elliptic problems.* North-Holland, Amsterdam [u.a.], 2. pr. edition, 1987.

[58] R. Codina, G. Houzeaux, H. Coppola-Owen, and J. Baiges. The fixed-mesh {ALE} approach for the numerical approximation of flows in moving domains. *Journal of Computational Physics*, 228(5):1591 – 1611, 2009.

[59] G.-H. Cottet, E. Maitre, and T. Mileent. Eulerian formulation and level set models for incompressible fluid-structure interaction. *Math. Modell. Numer. Anal.*, 42:471–492, 2008.

[60] O. Coussy. *Poromechanics.* Wiley, 2004.

[61] D. Coutand and S. Shkoller. Motion of an elastic solid inside an incompressible viscous fluid. *Arch. Rational Mech. Anal.*, pages 25–102, 2005.

[62] D. Coutand and S. Shkoller. The interaction between quasilinear elastodynamics and the Navier-Stokes equations. *Arch. Rational Mech. Anal.*, 179:303–352, 2006.

[63] P. Crosetto, S. Deparis, G. Fourestey, and A. Quarteroni. Parallel algorithms for fluid-structure interaction problems in haemodynamics. *SIAM J. Sci. Comp.*, 33(4):1598–1622, 2011.

[64] C. D'Angelo and P. Zunino. Robust numerical approximation of coupled Stokes' and Darcy's flows applied to vascular hemodynamics and biochemical transport. *M2AN*, 45:447–476, 2011.

[65] H. Darcy. *Les Fontaines de la Ville de Dijon.* Dalmont, Paris, 1856.

[66] R. Dautray and J.-L. Lions. *Mathematical Analysis and Numerical Methods for Science and Technology*, volume 5. Springer-Verlag, Berlin-Heidelberg, 2000.

[67] S. Deparis, M. Discacciati, G. Fourestey, and A. Quarteroni. Fluid-structure algorithms based on Steklov-Poincaré operators. *Comp. Methods Appl. Mech. Engrg*, 195(41-43):5797–5812, 2006.

[68] J. Donea, S. Giuliani, and J. Halleux. An arbitrary lagrangian-eulerian finite element method for transient dynamic fluid-structure interactions. *Comput. Methods Appl. Mech. Engrg.*, 33:689–723, 1982.

[69] T. Dunne. An Eulerian approach to fluid-structure interaction and goal-oriented mesh adaption. *Int. J. Numer. Methods in Fluids*, 51:1017–1039, 2006.

[70] T. Dunne. *Adaptive Finite Element Approximation of Fluid-Structure Interaction Based on Eulerian and Arbitrary Lagrangian-Eulerian Variational Formulations.* PhD thesis, University of Heidelberg, 2007.

[71] T. Dunne, T. Richter, and R. Rannacher. *Numerical simulation of fluid-structure interaction based on monolithic variational formulations*, pages 1–75. Comtemporary Challenges in Mathematical Fluid Mechanics. Springer, World Scientific, Singapore, 2010.

[72] G. Duvaut and J. L. Lions. *Inequalities in Mechanics and Physics.* Springer, Berlin-Heidelberg-New York., 1976.

[73] A. S. Dvinsky. Adaptive grid generation from harmonic maps on riemannian manifolds. *Journal of Computational Physics*, 95(2):450 – 476, 1991.

[74] C. Eck, H. Garcke, and P. Knabner. *Mathematische Modellierung.* Springer, 2008.

[75] K. Eriksson, D. Estep, P. Hansbo, and C. Johnson. Introduction to adaptive methods for differential equations. In A. Iserles, editor, *Acta Numerica 1995*, pages 105–158. Cambridge University Press., 1995.

[76] L. C. Evans. *Partial differential equations.* American Mathematical Society, 2000.

[77] C. Farhat, P. Geuzaine, and C. Grandmont. The discrete geometrical conservation law and the nonlinear stability of the ALE schemes for the solution of flow problems on moving grids. *J. Comp. Phys.*, 174:669–694, 2001.

[78] C. Fefferman. Existence and smoothness of the Navier-Stokes equations. Millenium Prize, -.

[79] M. Feistauer, J. Hasnedlová-Prokopová, J. Horacek, A. Kosik, and V. Kucera. {DGFEM} for dynamical systems describing interaction of compressible fluid and structures. *Journal of Computational and Applied Mathematics*, 254(0):17 – 30, 2013. Nonlinear Elliptic Differential Equations, Bifurcation, Local Dynamics of Parabolic Systems and Numerical Methods.

[80] Z. Feng and E. Michaelides. The immersed boundary-lattice Boltzmann method for solving fluid-particles interaction problems. *J. Comp. Phys.*, 195:602–628, 2004.

[81] F. Fernández and M. Moubachir. A Newton method using exact Jacobians for solving fluid-structure coupling. *Comput. Struct.*, 83:127–142, 2005.

[82] M. Fernández and J.-F. Gerbeau. *Algorithms for fluid-structure interaction problems*, pages 307–346. Volume 1 of Formaggia et al. [87], 2009.

[83] M. Fernandez, J.-F. Gerbeau, and C. Grandmont. A projection semi-implicit scheme for the coupling of an elastic structure with an incompressible fluid. *Int. J. Numer. Meth. Engng.*, 69:794–821, 2007.

[84] P. Fick, E. Brummelen, and K. Zee. On the adjoint-consistent formulation of interface conditions in goal-oriented error estimation and adaptivity for fluid-structure interaction. *Computer Methods in Applied Mechanics and Engineering*, 199:3369–3385, 2010.

[85] L. Formaggia and F. Nobile. A stability analysis for the arbitrary Lagrangian Eulerian formulation with finite elements. *East-West Journal of Numerical Mathematics*, 7:105 – 132, 1999.

[86] L. Formaggia and F. Nobile. Stability analysis of second-order time accurate schemes for ALE-FEM. *Comp. Methods Appl. Mech. Engrg.*, 193(39-41):4097 – 4116, 2004.

[87] L. Formaggia, A. Quarteroni, and A. Veneziani. *Cardiovascular Mathematics: Modeling and simulation of the circulatory system*. Springer-Verlag, Italia, Milano, 2009.

[88] L. Formaggia and A. Veneziani. Reduced and multiscale models for the human cardiovascular system. Technical Report 21, Lecture notes VKI Lectur Series, 2003.

[89] L. Formaggia, A. Veneziani, and C. Vergara. Flow rate boundary problems for an incompressible fluid in deformable domains: formulations and solution methods. *Comp. Methods Appl. Mech. Engrg.*, 199:677–688, 2010.

[90] R. Franck and R. Lazarus. *Mixed Eulerian-Lagrangian method*, volume In Methods in Computational Physics, pages 47–67. Academic Press: New York, 1964.

[91] S. Frei and T. Richter. A locally modified parametric finite element method for interface problems. *SIAM Journal on Numerical Analysis*, 52(5):2315–2334, 2014.

[92] S. Frei and T. Richter. Second order time-stepping for parabolic interface problems with moving interfaces. submitted, 2014.

[93] S. Frei, T. Richter, and T. Wick. Eulerian techniques for fluid-structure interactions - part i: Modeling and simulation. accepted in ENUMATH Proceedings, Lausanne 2013, Springer, 2014.

[94] S. Frei, T. Richter, and T. Wick. Eulerian techniques for fluid-structure interactions - part ii: Applications. accepted in ENUMATH Proceedings, Lausanne 2013, Springer, 2014.

[95] S. Frei, T. Richter, and T. Wick. Solid growth and clogging in fluid-structure interaction using ale and fully eulerian coordinates. in review, 2014.

[96] T.-P. Fries and T. Belytschko. The extended/generalized finite element method: An overview of the method and its applications. *Int. J. Numer. Meth. Engrg.*, 84:253–304, 2010.

[97] Y. Fung. *Biodynamics: Circulation*. Springer-Verlag, first ed. edition, 1984.

[98] C. FÃ¶rster, W. A. Wall, and E. Ramm. Artificial added mass instabilities in sequential staggered coupling of nonlinear structures and incompressible viscous flows. *Computer Methods in Applied Mechanics and Engineering*, 196(7):1278 – 1293, 2007.

[99] X. Gai. *A coupled geomechanics and reservoir flow model on parallel computers*. PhD thesis, The University of Texas at Austin, 2004.

[100] S. Ganesan and L. Tobiska. A coupled arbitrary lagrangian-eulerian and lagrangian method for computation of free surface flows with insoluble surfactants. *Journal of Computational Physics*, 228(8):2859 – 2873, 2009.

[101] S. Ganesan and L. Tobiska. Arbitrary lagrangian-eulerian finite-element method for computation of two-phase flows with soluble surfactants. *Journal of Computational Physics*, 231(9):3685 – 3702, 2012.

[102] E. S. Gawlik and A. J. Lew. High-order finite element methods for moving boundary problems with prescribed boundary evolution. *Computer Methods in Applied Mechanics and Engineering*, 278(0):314 – 346, 2014.

[103] F. Gazzola and M. Squassina. Global solutions and finite time blow up for damped semilinear wave equations. *Ann. I. H. Poincaré*, 23:185–207, 2006.

[104] M. Gee, U. Küttler, and W. Wall. Truly monolithic algebraic multigrid for fluid–structure interaction. *International Journal for Numerical Methods in Engineering*, 85(8):987–1016, 2011.

[105] J.-F. Gerbeau. Direct and inverse modeling in hemodynamics. Talk at the ENUMATH Conference in Leicester, 2011.

[106] A. Gerstenberger and W. A. Wall. An extended finite element method/lagrange multiplier based approach for fluid-structure interaction. *Computer Methods in Applied Mechanics and Engineering*, 197(19-20):1699–1714, 2008.

[107] A. J. Gil, A. A. Carreno, J. Bonet, and O. Hassan. The immersed structural potential method for haemodynamic applications. *J. Comp. Physics*, 229:8613–8641, 2010.

[108] M. Giles and E. Süli. Adjoint methods for pdes: a posteriori error analysis and postprocessing by duality. *Acta Numerica 2002*, pages 145–236, 2002. A. Iserles, ed.

[109] V. Girault, G. Pencheva, M. F. Wheeler, and T. Wildey. Domain decomposition for poroelasticity and elasticity with dg jumps and mortars. *Mathematical Models and Methods in Applied Sciences*, 21(1):169–213, 2011.

[110] V. Girault and P.-A. Raviart. *Finite Element method for the Navier-Stokes equations.* Number 5 in Computer Series in Computational Mathematics. Springer-Verlag, 1986.

[111] R. Glowinski, T. Pan, T. Hesla, D. Joseph, and J. PÃ©riaux. A fictitious domain approach to the direct numerical simulation of incompressible viscous flow past moving rigid bodies: Application to particulate flow. *Journal of Computational Physics*, 169(2):363 – 426, 2001.

[112] R. Glowinski, T.-W. Pan, T. Hesla, and D. Joseph. A distributed lagrange multiplier/fictitious domain method for particulate flows. *International Journal of Multiphase Flow*, 25(5):755 – 794, 1999.

[113] R. Glowinski, T.-W. Pan, and J. Periaux. A fictitious domain method for dirichlet problem and applications. *Computer Methods in Applied Mechanics and Engineering*, 111(3-4):283 – 303, 1994.

[114] R. Glowinski and J. Periaux. Numerical methods for nonlinear problems in fluid dynamics. In *Proc. Intern. Seminar on Scientific Supercomputers*. North Holland, Feb. 2-6 1987.

[115] C. Goll, T. Wick, and W. Wollner.

[116] C. Goll, T. Wick, and W. Wollner. *DOpElib: Differential Equations and Optimization Environment*, 2009.

[117] C. Grandmont. Existence for a three-dimensional steady state fluid-structure interaction problem. *Journal of Mathematical Fluid Mechanics*, 4:76–94, 2002.

[118] T. Grätsch and K.-J. Bathe. Goal-oriented error estimation in the analysis of fluid flows with structural interactions. *Comp. Methods Appl. Mech. Engrg.*, 195:5673–5684, 2006.

[119] P. Grisvard. *Elliptic Problems in Nonsmooth Domains*, volume 24. Pitman Advanced Publishing Program, Boston, 1985.

[120] C. Groß mann and H.-G. Roos. *Numerische Behandlung partieller Differentialgleichungen.* Teubner-Studienbücher Mathematik ; Lehrbuch Mathematik. Teubner, Wiesbaden, 3., völlig überarb. und erw. aufl. edition, 2005.

[121] H. Guzman. *Domain Decomposition Methods in Geomechanics*. PhD thesis, The University of Texas at Austin, 2012.

[122] A. Hansbo and P. Hansbo. An unfitted finite element method based on nitsche's method for elliptic interface problems. *Comput. Meth. Appl. Mech. Engrg.*, 191(47-48):5537–5552, 2002.

[123] P. Hansbo and J. Hermansson. Nitsche's method for coupling non-matching meshes in fluid-structure vibration problems. *Comp. Mech.*, 32:134–139, 2003.

[124] P. Hansbo, J. Hermansson, and T. Svedberg. Nitsche's method combined with space-time finite elements for ALE fluid-structure interaction problems. *Comput. Meth. Appl. Mech. Engrg.*, 193:4195–4206, 2004.

[125] J. D. Hart, F. Baaijens, G. Peters, and P. Schreuers. A computational fluid-structure interaction analysis of a fiber-reinforced stentless aortic valve. *Journal of Biomechanics*, 36(5):699–712, 2003.

[126] J. Hasnedlová, M. Feistauer, J. Horacek, A. Kosik, and V. Kucera. Numerical simulation of fluid-structure interaction of compressible flow and elastic structure. *Computing*, 95(1):343–361, 2013.

[127] P. He and R. Qiao. A full-Eulerian solid level set method for simulation of fluid-structure interactions. *Microfluid Nanofluid*, 11:557–567, 2011.

[128] M. Heil. An efficient solver for the fully coupled solution of large-displacement fluid-structure interaction problems. *Comput. Methods Appl. Mech. Engrg.*, 193:1–23, 2004.

[129] M. Heil, A. L. Hazel, and J. Boyle. Solvers for large-displacement fluid-structure interaction problems: segregated versus monolithic approaches. *Comput. Mech.*, 43:91–101, 2008.

166

[130] B. Helenbrook. Mesh deformation using the biharmonic operator. *Int. J. Numer. Methods Engrg.*, pages 1–30, 2001.

[131] L. Heltai and F. Costanzo. Variational implementation of immersed finite element methods. *Computer Methods in Applied Mechanics and Engineering*, 229-232(0):110 – 127, 2012.

[132] C. Hesch, A. Gil, A. A. Carreno, J. Bonet, and P. Betsch. A mortar approach for fluid-structure interaction problems: Immersed strategies for deformable and rigid bodies. *Computer Methods in Applied Mechanics and Engineering*, 278(0):853 – 882, 2014.

[133] J. G. Heywood and R. Rannacher. Finite-element approximation of the nonstationary Navier-Stokes problem part iv: Error analysis for second-order time discretization. *SIAM Journal on Numerical Analysis*, 27(2):353–384, 1990.

[134] J. G. Heywood, R. Rannacher, and S. Turek. Artificial boundaries and flux and pressure conditions for the incompressible Navier-Stokes equations. *International Journal of Numerical Methods in Fluids*, 22:325–352, 1996.

[135] M. Hinze and K. Kunisch. Second order methods for optimal control of time-dependent fluid flows. *SIAM J. Control Optim.*, 40:925–946, 2001.

[136] M. Hinze, R. Pineau, M. Ulbrich, and S. Ulbrich. *Optimization with PDE constraints.* Mathematical Modelling: Theory and Applications, Vol. 23. Springer, 2009.

[137] C. Hirt, A. Amsden, and J. Cook. An arbitrary Lagrangian-Eulerian computing method for all flow speeds. *J. Comput. Phys.*, 14:227–253, 1974.

[138] J. HOFFMAN, J. JANSSON, and M. STöCKLI. Unified continuum modeling of fluid-structure interaction. *Mathematical Models and Methods in Applied Sciences*, 21(03):491–513, 2011.

[139] G. Holzapfel. *Nonlinear Solid Mechanics: A continuum approach for engineering.* John Wiley and Sons, LTD, 2000.

[140] J. Hron. *Fluid structure interaction with applications in biomechanics.* PhD thesis, Charles University Prague, 2001.

[141] J. Hron and S. Turek. *A monolithic FEM/Multigrid solver for ALE formulation of fluid structure with application in biomechanics*, volume 53, pages 146–170. Springer-Verlag, 2006.

[142] J. Hron and S. Turek. *Proposal for numerical benchmarking of fluid-structure interaction between an elastic object and laminar incompressible flow*, volume 53, pages 146 – 170. Springer-Verlag, 2006.

[143] T. Hughes. *The finite element method.* Dover Publications, 2000.

[144] T. Hughes, J. Cottrell, and Y. Bazilevs. Isogeometric analysis: Cad, finite elements, nurbs, exact geometry and mesh refinement. *Computer Methods in Applied Mechanics and Engineering*, 194(39-41):4135 – 4195, 2005.

[145] T. Hughes, W. Liu, and T. Zimmermann. Lagrangian-Eulerian finite element formulation for incompressible viscous flows. *Comput. Methods Appl. Mech. Engrg.*, 29:329–349, 1981.

[146] J. Humphrey. *Cardiovascular Solid Mechanics: Cells, Tissues, and Organs.* Springer-Verlag New York, 2002.

[147] M. Ignatova, I. Kukavica, I. Lasiecka, and A. Tuffaha. On well-posedness and small data global existence for an interface damped free boundary fluid-structure model. *Nonlinearity*, 27(3):467, 2014.

[148] C. D. J. H. J. Jansson, J. Spuhler. Automated error control in finite element methods with applications in fluid flow. Technical Report at KTH, 2014.

[149] W. Jaeger, A. Mikelic, and M. Neuss-Radu. Homogenization limit of a model system for interaction of flow, chemical reactions, and mechanics in cell tissues. *SIAM J. Math. Anal.*, 43(3):1390–1435, 2011.

[150] C. Johnson. *Numerical solution of partial differential equations by the finite element method.* Cambridge University Press, Campridge, 1987.

[151] N. Kikuchi and J. Oden. *Contact problems in elasticity.* Studies in Applied Mathematics. Society for Industrial and Applied Mathematics (SIAM), Philadelphia, PA, 1988.

[152] D. Kinderlehrer and G. Stampacchia. *An Introduction to Variational Inequalities and Their Applications.* Classics in Applied Mathematics. Society for Industrial and Applied Mathematics, 2000.

[153] P. Knabner, C. J. v. Duijn, and S. Hengst. An analysis of crystal dissolution fronts in flows through porous media. part 1: Compatible boundary conditions. *Adv. Water Resour.*, 18:171–185, 1995.

[154] K. Königsberger. *Analysis 2.* Springer Lehrbuch. Springer, Berlin – Heidelberg – New York, 2., korrigierte und erw. auflage edition, 1997.

[155] P. Kuberry and H. Lee. A decoupling algorithm for fluid-structure interaction problems based on optimization. *Computer Methods in Applied Mechanics and Engineering*, 267(0):594 – 605, 2013.

[156] K. Kumar, T. van Noorden, M. Wheeler, and T. Wick. An ale-based method for reaction-induced boundary movement towards clogging. ENUMATH 2013, Switzerland, Aug 2013.

[157] K. Kumar, M. Wheeler, and T. Wick. Reactive flow and reaction-induced boundary movement in a thin channel. accepted in SIAM J. Sci. Comput., 2013.

[158] U. Küttler and W. A. Wall. *The dilemma of domain decomposition approaches in fluid-structure interactions with fully enclosed incompressible fluids*, volume 60 of *Domain decomposition methods in science and engineering XVII*, pages 575–582. Springer, Berlin, 2008.

[159] D. Kuzmin. Explicit and implicit fem-fct algorithms with flux linearization. *Journal of Computational Physics*, 228(7):2517 – 2534, 2009.

[160] U. KÃ¼ttler and W. Wall. Fixed-point fluid-structure interaction solvers with dynamic relaxation. *Computational Mechanics*, 43(1):61–72, 2008.

[161] A. Laadhari, R. Ruiz-Baier, and A. Quarteroni. Fully eulerian finite element approximation of a fluid-structure interaction problem in cardiac cells. *Int. J. Numer. Methods Engrg.*, 96:712–738, 2013.

[162] A. Ladd. Numerical simulations of particulate suspensions via a discretized Boltzmann equation. part i: theoretical foundations. *Journal of Fluid Mechanics*, 271, 1994.

[163] A. Ladd. Numerical simulations of particulate suspensions via a discretized Boltzmann equation. part ii: numerical results. *Journal of Fluid Mechanics*, 271, 1994.

[164] O. Ladyzhenskaya. *The mathematical theory of viscous incompressible flows.* Gordon and Breach, New York, 1969.

[165] U. Langer and H. Yang. Partitioned solution algorithms for fluid-structure interaction problems with hyperelastic models. *Journal of Computational and Applied Mathematics*, 276(0):47 – 61, 2015.

[166] A. Legay, J. Chessa, and T. Belytschko. An eulerian-lagrangian method for fluid-structure interaction based on level sets. *Computer Methods in Applied Mechanics and Engineering*, 195(17-18):2070 – 2087, 2006. Fluid-Structure Interaction.

[167] J.-L. Lions. *Optimal Control of Systems Governed by Partial Differential Equations*, volume 170 of *Grundlehren Math. Wiss.* Springer, Berlin, 1971.

[168] R. Liu. *Discontinuous Galerkin Finite Element Solution for Poromechanics.* PhD thesis, The University of Texas at Austin, 2004.

[169] R. Liu, M. Wheeler, C. Dawson, and R. Dean. A fast convergent rate preserving discontinuous galerkin framework for rate-independent plasticity problems. *Comp. Methods Appl. Mech. Engrg.*, 199:3213–3226, 2010.

[170] M. Lukacova-Medvidova, G. Rusnakova, and A. Hundertmark-Zauskova. Kinematic splitting algorithm for fluid-structure interaction in hemodynamics. *Computer Methods in Applied Mechanics and Engineering*, 265(0):83 – 106, 2013.

[171] E. Lund, H. Moller, and L. A. Jakobsen. Shape design optimization of stationary fluid-structure interaction problems with large displacements and turbulence. *Struct. Multidisc. Optim.*, 25:383–392, 2003.

[172] M. Luskin and R. Rannacher. On the soothing property of the Crank-Nicolson scheme. *Applicable Analysis*, 14(2):117 – 135, 1980.

[173] J. Mandel. Consolidation des sols (étude mathémathique. *Geotechnique*, 3:287–299, 1953.

[174] A. Marciniak-Czochra and M. Ptashnyk. Derivation of a macroscopic receptor-based model using homogenization techniques. *SIAM J. Math. Anal.*, 40(1):215–237, 2008.

[175] D. Meidner. *Adaptive Space-Time Finite Element Methods for Optimization Problems Governed by Nonlinear Parabolic Systems*. PhD thesis, University of Heidelberg, 2008.

[176] A. Mikelić, M. Wheeler, and T. Wick. A phase-field method for propagating fluid-filled fractures coupled to a surrounding porous medium. ICES Report 14-08, in revised review, April/Nov 2014.

[177] A. Mikelić and M. F. Wheeler. On the interface law between a deformable porous medium containing a viscous fluid and an elastic body. *M3AS: Mathematical Models and Methods in Applied Sciences*, 22(11), 2012.

[178] J. Mizerski. Modeling heart valve dynamics. Personal Correspondance, 2010.

[179] M. E. Moghadam, Y. Bazilevs, T.-Y. Hsia, I. E. Vignon-Clementel, and A. L. Marsden. A comparison of outlet boundary treatments for prevention of backflow divergence with relevance to blood flow simulations. *Comput. Mech.*, 48:277–291, 2011.

[180] A. Moura. *The Geometrical Multiscale Modelling of the Cardiovascular System: Coupling 3D FSI and 1D Models*. PhD thesis, Instituto Superior Técnico, Technical University of Lisbon, 2007.

[181] W. Mulder, S. Osher, and J. Sethian. Computing interface motion in compressible gas dynamics. *J. Comput. Phys.*, 100(2):209–228, 1992.

[182] J. Nitsche. über ein Variationsprinzip zur lösung von dirichlet-problemen bei verwendung von teilräumen, die keinen randbedingungen unterworfen sind. *Abh. Math. Sem. Univ. Hamburg*, 36:9–15, 1971.

[183] F. Nobile. *Numerical Approximation of Fluid-Structure Interaction Problems with Applications to Haemodynamics*. PhD thesis, École Polytechnique Fédérale de Lausanne, 2001.

[184] F. Nobile and C. Vergara. An effective fluid-structure interaction formulation for vascular dynamics by generalized Robin conditions. *SIAM J. Sci. Comput.*, 30(2):731–763, 2008.

[185] J. Nocedal and S. J. Wright. *Numerical Optimization*. Springer, New York, 1999.

[186] J. Nocedal and S. J. Wright. *Numerical optimization*. Springer Ser. Oper. Res. Financial Engrg., 2006.

[187] W. Noh. *A time-dependent two-space-dimensional coupled Eulerian-Lagrangian code*, volume 3 of *Methods Comput. Phys.*, pages 117–179. Academic Press, New York, 1964.

[188] T. L. v. Noorden. Crystal precipitation and dissolution in a thin strip. *European J. Appl. Math.*, 20(1):69–91, 2009.

[189] T. L. v. Noorden, I. S. Pop, A. Ebigbo, and R. Helmig. An upscaled model for biofilm growth in a thin strip. *Water Resour. Res.*, 46(W06505), 2010.

[190] E. Onate, S. Idelsohn, F. Delpin, and R. Aubry. The particle finite element method, an overview. *Int. J. Comput. Methods*, pages 1–43, 2004.

[191] S. Osher and J. Sethian. Fronts propagating with curvature-dependent speed: algorithms based on Hamiltonian-Jacobi formulations. *J. Comput. Phys.*, 79(1):12–49, 1988.

[192] J. Peraire and A. Patera. Bounds for linear-functional outputs of coercive partial differential equations: local indicators and adaptive refinement. In P. Ladeveze and J. Oden, editors, *Advances in Adaptive Computational Methods in Mechanics*, pages 199–215. Elsevier, Amsterdam, 1998.

[193] M. Perego, A. Veneziani, and C. Vergara. A variational approach for estimating the compliance of the cardiovascular tissue: An inverse fluid-structure interaction problem. *SIAM Journal on Scientific Computing*, 33(3):1181–1211, 2011.

[194] C. Peskin. *The immersed boundary method*, pages 1–39. Acta Numerica 2002, Cambridge University Press, 2002.

[195] S. Piperno and C. Farhat. Paritioned procedures for the transient solution of coupled aeroelastic problems - part ii: energy transfer analysis and three-dimensional applications. *Comput. Methods Appl. Mech. Engrg.*, 190:3147–3170, 2001.

[196] A. Quaini, S. Canic, R. Glowinski, S. Igo, C.J.Hartley, W. Zoghbi, and S. Little. Validation of a 3d comoputational fluid-structure interaction model simulating flow through elastic aperature. *Journal of Biomechanics*, 45:310–318, 2012.

[197] A. Quarteroni. What mathematics can do for the simulation of blood circulation. Technical report, MOX Institute, Milano, 2006.

[198] R. Rannacher. Finite element solution of diffusion problems with irregular data. *Numer. Math.*, 43:309–327, 1984.

[199] R. Rannacher. On the stabilization of the Crank-Nicolson scheme for long time calculations. Preprint, August 1986.

[200] R. Rannacher. Numerische methoden der Kontinuumsmechanik (Numerische Mathematik 3). Vorlesungsskriptum, 2001.

[201] R. Rannacher and F.-T. Suttmeier. A posteriori error control in finite element methods via duality techniques: Application to perfect plasticity. *Computational Mechanics*, 21(2):123–133, 1998.

[202] R. Rannacher and F.-T. Suttmeier. A posteriori error estimation and mesh adaptation for finite element models in elasto-plasticity. *Computer Methods in Applied Mechanics and Engineering*, 176(1-4):333 – 361, 1999.

[203] R. Rannacher and F.-T. Suttmeier. Error estimation and adaptive mesh design for FE models in elasto-plasticity. In E. Stein, editor, *Error-Controlled Adaptive FEMs in Solid Mechanics*. John Wiley, 2000.

[204] T. Richter. A fully Eulerian formulation for fluid-structure interaction problems. *J. Comput. Phys.*, 233:227–240, 2012.

[205] T. Richter. Goal-oriented error estimation for fluid-structure interaction problems. *Comp. Methods Appl. Mech. Engrg.*, 223-224:38–42, 2012.

[206] T. Richter. FSI Book. in preparation, 2014.

[207] T. Richter and T. Wick. Finite elements for fluid-structure interaction in ALE and fully Eulerian coordinates. *Comp. Methods Appl. Mech. Engrg.*, 199:2633–2642, 2010.

[208] T. Richter and T. Wick. Optimal control and parameter estimation for stationary fluid-structure interaction. *SIAM J. Sci. Comput.*, 35(5):B1085–B1104, 2013.

[209] T. Richter and T. Wick. On time discretizations of fluid-structure interactions. In *Multiple Shooting and Time Domain Decomposition Methods*, Contributions in Mathematical and Computational Science, 2014.

[210] T. Richter and T. Wick. Pum-based localization for dwr a posteriori error estimation applied to fluid-structure interaction. in preparation, 2014.

[211] T. Richter and T. Wick. Variational localizations of the dual weighted residual estimator. accepted for publication in Journal for Computational and Applied Mathematics, Preprint online http://www.numerik.uni-hd.de/ richter/, 2014.

[212] RoDoBo: A C++ library for optimization with stationary and nonstationary PDEs. `http://www.rodobo.uni-hd.de`.

[213] P. A. Sackinger, P. R. Schunk, and R. R. Rao. A Newton-Raphson pseudo-solid domain mapping technique for free and moving boundary problems: a finite element implementation. *J. Comput. Phys.*, 125(1), 2005.

[214] P. Sagaut. *Large Eddy Simulation for incompressible flows*. Springer, 2006.

[215] N. D. D. Santos, J.-F. Gerbeau, and J. Bourgat. A partitioned fluid-structure algorithm for elastic thin valves with contact. *Comp. Methods Appl. Mech. Engrg.*, 197(19-20):1750–1761, 2008.

[216] M. Schäfer, D. Sternel, G. Becker, and P. Pironkov. *Efficient Numerical Simulation and Optimization of Fluid-Structure Interaction*, volume 53, pages 133–160. Springer-Verlag, 2010.

[217] M. Schäfer and S. Turek. *Flow Simulation with High-Performance Computer II*, volume 52 of *Notes on Numerical Fluid Mechanics*, chapter Benchmark Computations of laminar flow around a cylinder. Vieweg, Braunschweig Wiesbaden, 1996.

[218] M. Schmich and B. Vexler. Adaptivity with dynamic meshes for space-time finite element discretizations of parabolic equations. *SIAM J. Sci. Comput.*, 30(1):369 – 393, 2008.

[219] J. Sethian and P. Smereka. Level set methods for fluid interface. Annual Review, 2003.

[220] J. Simo and T. Hughes. *Computational Inelasticity*. Springer, 2000.

[221] K. Stein, T. Tezduyar, and R. Benney. Mesh moving techniques for fluid-structure interactions with large displacements. *J. Appl. Mech.*, 70:58–63, 2003.

[222] K. Sugiyama, S. Li, S. Takeuchi, S. Takagi, and Y. Matsumato. A full Eulerian finite difference approach for solving fluid-structure interacion. *J. Comp. Phys.*, 230:596–627, 2011.

[223] P. Sun, J. Xu, and L. Zhang. Full eulerian finite element method of a phase field model for fluid-structure interaction problem. *Computers & Fluids*, 90(0):1 – 8, 2014.

[224] S. Takagi, K. Sugiyama, and Y. Matsumato. A review of full Eulerian mehtods for fluid structure interaction problems. *J. Appl. Mech.*, 79(1):010911, 2012.

[225] K. Takizawa and T. Tezduyar. Computational methods for parachute fluid-structure interactions. *Archives of Computational Methods in Engineering*, 19:125–169, 2012.

[226] P. L. Tallec and S. Mani. Numerical analysis of a linearised fluid-structure interaction problem. *Numer. Math.*, 87:317–354, 2000.

[227] T. Tezduyar. Finite element methods for flow problems with moving boundaries and interfaces. *Archives of Computational Methods in Engineering*, 8(2):83–130, 2001.

[228] T. Tezduyar, M. Behr, and J. Liou. A new strategy for finite element computations involving moving boundaries and interfaces - the deforming-spatial-domain/space-time procedure: I. the concept and the preliminary numerical tests. *Comp. Methods Appl. Mech. Engrg.*, 94:339–351, 1992.

[229] T. Tezduyar, M. Behr, S. Mittal, and J. Liou. A new strategy for finite element computations involving moving boundaries and interfaces - the deforming-spatial-domain/space-time procedure: II. Computation of free-surface flows, two-liquid flows, and flows with drifting cylinders. *Comp. Methods Appl. Mech. Engrg.*, 94:353–371, 1992.

[230] T. Tezduyar and S. Sathe. Modeling of fluid-structure interactions with the space-time finite elements: solution techniques. *Int. J. Numer. Meth. Fluids*, 54:855–900, 2007.

[231] T. Tezduyar, S. Sathe, and K. Stein. Solution techniques for the fully discretized equations in computation of fluid-structure interaction with space-time formulations. *Comp. Methods Appl. Mech. Engrg.*, 195(41-43):5743–5753, 2006.

[232] T. Tezduyar, K. Takizawa, C. Moorman, S. Wright, and J. Christopher. Space-time finite element computation of complex fluid-structure interaction. *Int. J. Numer. Meth. Fluids*, 64:1201–1218, 2010.

[233] T. E. Tezduyar, M. Behr, S. Mittal, and A. A. Johnson. *Computation of Unsteady Incompressible Flows With the Finite Element Methods Space-Time Formulations, Iterative Strategies and Massively Parallel Implementations*, volume 143 of *New Methods in Transient Analysis, PVP-Vol. 246, AMD-Vol. 143*, pages 7–24. ASME, New York, 1992.

[234] R. Trémolières, J. Lions, and R. Glowinski. *Numerical Analysis of Variational Inequalities*. Studies in Mathematics and its Applications. Elsevier Science, 2011.

[235] F. Tröltzsch. On the Lagrange-Newton-SQP method for the optimal control of semilinear parabolic equations. *SIAM J. Control Optim.*, 38:294–312, 1999.

[236] F. Tröltzsch. *Optimale Steuerung partieller Differentialgleichungen - Theorie, Verfahren und Anwendungen*. Vieweg und Teubner, Wiesbaden, 2nd edition, 2009.

[237] S. Turek. *Efficient solvers for incompressible flow problems*. Springer-Verlag, 1999.

[238] S. Turek, J. Hron, M. Madlik, M. Razzaq, H. Wobker, and J. Acker. Numerical simulation and benchmarking of a monolithic multigrid solver for fluid–structure interaction problems with application to hemodynamics. Technical

report, Fakultät für Mathematik, TU Dortmund, Feb. 2010. Ergebnisberichte des Instituts für Angewandte Mathematik, Nummer 403.

[239] S. Turek, J. Hron, M. Razzaq, H. Wobker, and M. Schäfer. *Numerical benchmarking of fluid-structure interaction: a comparison of different discretization and solution approaches*, pages 413–424. Fluid Structure Interaction II: modelling, simulation, optimization. Springer, Heidelberg, 2010.

[240] S. Turek, L. Rivkind, J. Hron, and R. Glowinski. Numerical analysis of a new time-stepping θ-scheme for incompressible flow simulations. Technical report, TU Dortmund and University of Houston, 2005. Dedicated to David Gottlieb on the occasion of his 60th anniversary.

[241] M. Ulbrich and S. Ulbrich. *Nichtlineare Optimierung*. Birkhäuser Verlag, 2012.

[242] K. van der Zee, E. van Brummelen, and R. de Borst. Goal-oriented error estimation for Stokes flow interacting with a flexible channel. *International Journal of Numerical Methods in Fluids*, 56:1551–1557, 2008.

[243] W. A. Wall. *Fluid-Struktur-Interaktion mit stabilisierten Finiten Elementen*. PhD thesis, University of Stuttgart, 1999.

[244] W. A. Wall, A. Gerstenberger, U. Küttler, and U. Mayer. *An XFEM based fixed-grid approach for 3D fluid-structure interaction*, pages 327–349. Fluid Structure Interaction II: modelling, simulation, optimization. Springer, Heidelberg, 2010.

[245] H. Wang and T. Belytschko. Fluid-structure interaction by the discontinuous-Galerkin method for large deformations. *Int. J. Numer. Methods Engrg.*, 77:30–49, 2009.

[246] F. Weller. *Modeling, Analysis, and Simulation of Thrombosis and Hemostasis*. PhD thesis, Universität Heidelberg, Institut für Angewandte Mathematik, Heidelberg, 2008.

[247] T. Wick. *Untersuchung von Kopplungsmechanismen von Fluid-Struktur-Interaktion*. PhD thesis, University of Siegen, 2008.

[248] T. Wick. *Adaptive Finite Element Simulation of Fluid-Structure Interaction with Application to Heart-Valve Dynamics*. PhD thesis, University of Heidelberg, 2011.

[249] T. Wick. Adaptive finite elements for fluid-structure interactions on a prolongated domain: Applied to valve simulations. In *Comput. Methods Mech.*, Warsaw in Poland, May 9-12 2011.

[250] T. Wick. Fluid-structure interactions using different mesh motion techniques. *Comput. Struct.*, 89(13-14):1456–1467, 2011.

[251] T. Wick. Coupling of fully Eulerian with arbitrary Lagrangian-Eulerian coordinates for fluid-structure interaction. Preprint, 2012.

[252] T. Wick. Goal-oriented mesh adaptivity for fluid-structure interaction with application to heart-valve settings. *Arch. Mech. Engrg.*, 59(6):73–99, 2012.

[253] T. Wick. Coupling of fully Eulerian and arbitrary Lagrangian-Eulerian methods for fluid-structure interaction computations. *Comput. Mech.*, 2013.

[254] T. Wick. Flapping and contact fsi computations with the fluid-solid interface-tracking/interface-capturing technique and mesh adaptivity. *Comp. Mech.*, 2013.

[255] T. Wick. Fully Eulerian fluid-structure interaction for time-dependent problems. *Comp. Methods Appl. Mech. Engrg.*, 255(0):14–26, 2013.

[256] T. Wick. Solving monolithic fluid-structure interaction problems in arbitrary Lagrangian Eulerian coordinates with the deal.ii library. *Archive of Numerical Software*, 1:1–19, 2013.

[257] T. Wick, G. Singh, and M. Wheeler. Fluid-filled fracture propagation using a phase-field approach and coupling to a reservoir simulator. ICES Preprint 14-20, 2014.

[258] T. Wick and W. Wollner. On the differentiability of fluid-structure interaction problems with respect to the problem data. RICAM report 2014-16, http://www.ricam.oeaw.ac.at/publications/reports/, Oct 2014.

[259] A. M. Winslow. Numerical solution of the quasilinear poisson equation in a nonuniform triangle mesh. *Journal of Computational Physics*, 1(2):149 – 172, 1966.

[260] J. Wloka. *Partielle Differentialgleichungen*. B. G. Teubner Verlag, Stuttgart, 1982.

[261] W. Wood. A unified set of single step algorithms. *Int. J. Numer. Meth. Eng.*, 20:2303–2309, 1984.

[262] W. Wood. *Practical time-stepping schemes*. Clarendon Press, 1990.

[263] H. Yang and U. Langer. Numerical simulation of fluid-structure interaction problems with hyperelastic models: A monolithic approach. Technical report, 2014. RICAM preprint 2014-09, http://www.ricam.oeaw.ac.at/publications/reports/.

[264] K. Zee, E. Brummelen, I. Akkerman, and R. Borst. Goal-oriented error estimation and adaptivity for fluid-structure interaction using exact linearized adjoints. 200:2738–2757, 2011.

[265] L. Zhang, A. Gerstenberger, X. Wang, and W. K. Liu. Immersed finite element method. *Computer Methods in Applied Mechanics and Engineering*, 193(21-22):2051 – 2067, 2004. Flow Simulation and Modeling.

[266] S. Zhang and Z. Zhang. Invalidity of decoupling a biharmonic equation to two Poisson equations on non-convex polygons. *Int. J. Numer. Anal. Modeling*, 5(1):73–76, 2008.

[267] H. Zhao, J. Freund, and R. Moser. A fixed-mesh method for incompressible flow-structure systems with finite solid deformations. *J. Comput. Phys.*, 227(6):3114–1340, 2008.